

**Investigating the origins of
macroscopic variation in differential
ethnic hair types**

Matthew Wade

**Submitted in partial fulfilment of the requirements of the
degree of Doctor of Philosophy**

School of Optometry and Vision Sciences

Cardiff University

May 2013

Dedicated with all my love to my Mum and Dad

Acknowledgements

I gratefully acknowledge the financial support provided by Unilever R&D, Port Sunlight and Cardiff University during the course of my studies.

I am greatly indebted to Professor Tim Wess for providing me with the opportunity to undertake this study and also for providing me with the guidance, support and supervision needed for me to complete this PhD project. I am also indebted to Dr Ian Tucker for his technical advice, support and encouragement throughout the course of my tenure and Dr Linda Wess for proofreading.

Throughout the period of this study I have worked with a number of people who have contributed through their advice and assistance. I would like to thank Colin Berry, John Harwood, Irina Guschina, Valerie O' Donnell, Madhav Mondhe, Victoria Hammond, Pangiota Manti, and Clair Baldock.

Technical assistance and support was provided by the beamline scientists and technical staff at the ID18F beamline at the ESRF, the X33 beamline at DESY, the P12 beamline at PETRA III and the I22 beamline at Diamond. I wish to extend my gratitude to all those that helped me at these institutions.

I would finally like to thank Dr Kate Patten and Dr Lee Gonzalez. I would like to thank Kate for her constant analytical and administrative assistance and I would like to thank Lee for his humour, wisdom and motivational support, without which I almost certainly would not have completed this PhD.

Table of Contents

DECLARATION	2
ACKNOWLEDGEMENTS	3
TABLE OF CONTENTS	4
LIST OF ABBREVIATIONS	11
LIST OF FIGURES	14
LIST OF TABLES	28
ABSTRACT	31
CHAPTER 1: INTRODUCTION	33
1.1 Hair structure overview	33
1.2 Forces	34
1.2.1 Covalent bonding	36
1.2.2 Hydrogen bonding	37
1.2.3 Coulombic interactions	38
1.2.4 Hydrophobic interactions	38
1.2.5 Van der Waals bonding	38
1.3 The ultrastructure of hair	39
1.3.1 Cuticle	39
1.3.2 Cortex	42
1.3.3 Medulla	42
1.4 Molecular Structures	44
1.4.1 Alpha Keratin	45
1.4.2 Coiled coils & dimers	47
1.4.3 Keratin intermediate filaments (KIFs)	49
1.4.4 Keratin associated proteins (KAPs)	52

1.5 Keratinous molecular assemblies	55
1.5.1 Macrofibrils & Cortical cells	55
1.5.2 Cell membrane complex (CMC)	60
1.5.3 Lipids	64
1.6 Ethnic variations in hair structure	67
1.7 Hypothesis	71
1.8 Summary	73
1.9 Project Aims	73
1.10 Project Objectives	74
CHAPTER 2: TECHNIQUES	75
2.1 Introduction	75
2.2 Electromagnetic radiation	75
2.3 X-ray scattering	76
2.3.1 Bragg's Law	78
2.3.2 Small angle X-ray scattering (SAXS)	83
2.3.3 Fibre diffraction	83
2.3.4 Small angle X-ray scattering of human hair fibres	84
2.3.5 Wide angle X-ray scattering of human hair fibres	86
2.4 Synchrotron radiation	87
2.4.1 Increasing synchrotron radiation	89
2.5 Infrared spectroscopy	89
2.6 High performance liquid chromatography (HPLC) and ultra performance liquid chromatography (UPLC)	91
2.7 Thin layer chromatography (TLC)	92
2.8 Gas chromatography (GC) and fire ionization detection (FID)	93
2.9 Mass spectrometry (MS)	94
2.10 Principal Component Analysis (PCA)	94

2.11 Summary	95
CHAPTER 3: MATERIALS & METHODS	97
3.1 Hair samples	97
3.2 X-ray scattering experimental setup	98
3.2.1 Synchrotron beamlines	98
3.2.2 ID18F - Microfocus X-ray fluorescence beamline at the ESRF	99
3.2.3 ID02 beamline at the ESRF	100
3.2.4 Data correction	102
3.2.5 Data analysis using Fibrefix	103
3.2.6 Data analysis using Fit2d	104
3.3 Attenuated total reflectance fourier transform infrared spectroscopy (ATR-FTIR)	104
3.3.1 Data analysis using Peakfit	106
3.4 Experimental procedure for the extraction of internal lipids	106
3.4.1 UPLC run conditions for the extraction of internal lipids	107
3.5 Extraction of endogenous and exogenous lipids from hair fibres	109
3.5.1 Hexane:diethyl ether washed lipids	110
3.5.2 Lipids extracted using chloroform:methanol	110
3.5.3 Hydrolysis of covalently bound lipids using potassium hydroxide solution	110
3.5.4 One-dimensional thin layer chromatography of individual lipid classes	111
3.5.5 Analysis of fatty acids by GC/FID	111
3.5.6 Analysis of hydrocarbons by GC/FID	112
3.5.7 Fatty acid and hydrocarbon analysis by GC/MS	112
3.6 Summary	113
CHAPTER 4: A BULK ANALYSIS OF ETHNIC HAIR FIBRES IN THE DRY AND WET STATES	114
4.1 Sample preparation	115
4.2 Data collection	115
4.2.1 Experimental X-ray scattering	116

4.3 Data processing	116
4.4 Results	119
4.4.1 Inter-ethnic observations in the dry and wet states in the WAXS region	119
4.4.2 Inter-ethnic observations in the dry and wet states in the SAXS region	120
4.4.2.1 Observations of the crystalline lipid	123
4.4.2.2 Inter-ethnic observations of the low angle diffuse scatter	127
4.4.2.3 Observations of the KIF inter-lateral packing	129
4.4.2.4 Observations of the 6.7 nm meridional arc reflection	131
4.4.3 PCA of the fibre diagrams	131
4.4.3.1 PCA of the WAXS region for dry and wet hair	132
4.4.3.2 PCA of the SAXS region for dry and wet hair	134
4.5 Discussion	136
4.6 Summary	139
CHAPTER 5: THE USE OF MICROFOCUS X-RAY DIFFRACTION TO STUDY DIFFERENTIAL ETHNIC HAIR TYPES	141
5.1 Sample Preparation	141
5.2 Data collection	141
5.3 Data processing	143
5.4 Results	147
5.4.1 Afro hair	147
5.4.2 Asian hair	150
5.4.3 Chinese hair	153
5.4.4 European hair	156
5.4.4.1 European type 1 hair	156
5.4.4.2 European type 2 hair	160
5.4.5 Japanese hair	162
5.5 Discussion	164
5.5.1 Interpretation and contextualisation of the specific sectors	164

5.5.2 Comparisons and variations observed intra and inter ethnically	167
5.5.3 Consideration of experimental conditions	170
5.6 Conclusions	173
CHAPTER 6: INVESTIGATION OF THE SURFACE STRUCTURE OF ETHNIC HAIR TYPES USING ATR-FTIR	175
6.1 Sample preparation	175
6.2 Data collection	176
6.3 Data analysis	176
6.4 Results	177
6.4.1 Analysis of the spectra arising from keratin across differential ethnic hair types	177
6.4.2 Principal component analysis (PCA) of the FTIR spectra	180
6.4.3 Second derivative analysis of the Amide bands in all hair types	187
6.4.4 Second derivative analysis of the polypeptide chain vibrational modes	188
6.4.5 Second derivative analysis of the amino acid side chain groups	189
6.4.6 Second derivative analysis of the higher harmonics	189
6.5 Discussion	190
7.6 Conclusions	192
CHAPTER 7: A BIOCHEMICAL ANALYSIS OF LIPIDS FROM DIFFERENTIAL ETHNIC HAIR TYPES	194
7.1 Sample preparation	195
7.2 Data collection	195
7.3 Data processing	195
7.4 Results	196
7.4.1 Results from TLC and GC/FID analysis	197
7.4.1.1 Total lipid content and contribution of different extraction groups	198
7.4.1.2 Composition and content of individual lipid classes in different extraction groups	201
7.4.1.2.1 Results from the hexane wash	202
7.4.1.2.2 Results from the solvent extraction	206

7.4.1.2.3 Results from the hydrolysed fraction	211
7.4.1.3 GC/FID analysis of fatty acid patterns in individual lipid classes extracted by different procedures from the hair types	215
7.4.1.3.1 Fatty acid profiles of the individual lipid classes from the hexane wash	219
7.4.1.3.2 Fatty acid profiles of the individual lipid classes from the solvent extraction	223
7.4.1.3.3 Fatty acid profile of the hydrolysed fraction	227
7.4.2 Summary of the results from the TLC and GC/FID analysis	229
7.4.2.1 Summary of the results from the hexane wash	229
7.4.2.1.1 Summary of the results of the fatty acid profiles from the WEs extracted	230
7.4.2.1.2 Summary of the results of the fatty acid profiles from the FFAs extracted	230
7.4.2.1.3 Summary of the results of the fatty acid profiles from the TAGs extracted	231
7.4.2.2 Summary of the results from the solvent extraction	231
7.4.2.2.1 Summary of the results of the fatty acid profiles from the PLs extracted	231
7.4.2.2.2 Summary of the results of the fatty acid profiles from the FFAs extracted	232
7.4.2.2.3 Summary of the results of the fatty acid profiles from the TAGs extracted	232
7.4.2.2.4 Summary of the results of the fatty acid profiles from the WEs extracted	232
7.4.2.3 Summary of the results for the fatty acid composition of the hydrolysed fraction	233
7.5 Discussion	233
7.6 Conclusions	245
CHAPTER 8: CONCLUSIONS & FUTURE WORK	247
8.1 Findings & Conclusions	247

8.2 Evaluation of the current work	251
8.3 Future work	252
REFERENCES	255
APPENDIX I: MICROFOCUS X-RAY DIFFRACTION SCANS	262
APPENDIX II: GAS CHROMATOGRAPHY MASS SPECTROMETRY PROFILES FOR LIPIDS	279
APPENDIX III: LIPID TABLES	288
PUBLICATIONS	298

List of Abbreviations

AFM	Atomic force microscopy
ARCCA	Advanced Research Computing @ Cardiff Facility
ATR-FTIR	Attenuated Total Reflection Fourier Transform Infrared Spectroscopy
BF	Base Function
CCCP13	Computational Project for Fibre Diffraction and Solution Scattering
CCD	Charge Coupled Device
cm	centimetres
CMC	Cell Membrane Complex
CRL	Compound Refractive Lenses
ESRF	European Synchrotron Radiation Facility
FA	Fatty Acid
FAME	Fatty Acid Methyl Ester
FFA	Free Fatty Acid
FID	Fire Ionization Detection
FWHM	Full Width Half Maximum
GC	Gas Chromatography
GeV	Gigaelectron Volts
HC	Hydrocarbons
HPLC	High Performance Liquid Chromatography
IF	Intermediate Filament

IMM	Intermacrofibrillar Matrix
IMS	Industrial Methylated Spirit
IR	Infrared
KAP	Keratin Associated Protein
keV	kiloelectron Volts
KIF	Keratin Intermediate Filament
Li	Lithium
m	metres
mm	millimetres
18-MEA	18-Methyl-Eicosanoic Acid
MS	Mass Spectrometry
nm	nanometres
PCA	Principal Component Analysis
PL	Polar Lipid
q	q range
SAXS	Small Angle X-ray Scattering
SEM	Scanning electron microscopy
Si	Silicon
SPR	Surface Plasmon Resonance
TAG	Triacylglycerols
TEM	Transmission Electron Microscopy
TLC	Thin Layer Chromatography

UPLC	Ultra Performance Liquid Chromatography
UV	Ultra violet
WAXS	Wide Angle X-ray Scattering
WE	Wax Esters
XRD	X-Ray Diffraction
XRF	X-Ray Fluorescence
°C	degrees Celsius
Å	Angstroms
λ	wavelength
μm	micrometres
μXRD	Microfocus X-Ray Diffraction

List of Figures

- Figure 1.1** – (A) Schematic of some of the structure found in hair; the pink region shows the cortex of the hair, the outer white region illustrates the cuticle cells enclosing the cortex and the central white region is the medulla of the hair. These three regions comprise the ultra structure of hair. (B) Scanning electron microscopy image of a human hair fibre which clearly shows the cuticle scales found on the outside of a fibre. Figures from (Bandli , Grooming 2007). 36
- Figure 1.2** – An energy versus displacement representation of the covalent bonds within alpha-keratin. The sharp, deep line represents the attractive force of the covalent bonds within the molecule and the arrow B indicates the small distance in Angstroms over which the bond force is effective. The shallow broader curve and the arrow A represent the energy and bond distance respectively for hydrogen bonding in an alpha helix. Image taken from (Feughelman 1997). 37
- Figure 1.3** – Schematic of a cuticle cell in a typical human hair fibre. The epicuticle is a thin membrane covering the outside edge of the cuticle scale. This is bound to the A-layer beneath it, the exocuticle lies bound beneath the A-layer via disulphide bonding and the endocuticle lies beneath the exocuticle. Figure adapted from (Wei, Bhushan et al. 2005). 40
- Figure 1.4** –Schematic showing a model for the structure of the epicuticle in human hair. The fatty acid layer consisting primarily of 18-MEA is covalently bound via thioester linkages to the proteolipid membrane below it. The proteolipid membrane in turn is bound to the A-layer below it via a process that is yet to be determined (Jones and Rivett 1997). Figure adapted from (Jones and Rivett 1997). 41
- Figure 1.5** – Two SEM images of longitudinally cryofractured human hair fibres which show the medulla. A shows an image of a thin type medulla, B shows the medulla of the hair fibre shown in A at higher magnification. In this image, globular structures as reported by (Wagner, Kiyohara et al. 2007) can be seen. Images taken from (Wagner, Kiyohara et al. 2007). 43

Figure 1.6 –Schematic showing the keratinous molecular structures which associate and aggregate to build up the larger molecular structures and the molecular assemblies found in hair. Figure taken from (Franbourg, Hallegot et al. 2003). 45

Figure 1.7 – Schematic of the alpha helix. The black lines represent covalent bonding between the peptide backbone of the helix. The dotted lines represent the hydrogen bonds between the amino acids of the amide groups (NH) and the carboxylic groups (CO). R represents the side chain groups; these may be neutral, basic or acidic depending on the type of keratin (type Ia or IIa). Figure taken from (Hoppe, Lohmann et al. 1983). 46

Figure 1.8 – The lateral Coulombic interactions between two alpha keratin helices to form a coiled coil arrangement. The e and g heptads are oppositely charged and the a and d heptads form ionic bonds. Figure taken from (Bouillon and Wilkinson 2005). 47

Figure 1.9 – The arrangement of a keratin dimer. Shown are the four central helical sections (1A, 1B, 2A, 2B) connected by three linker regions (L1, L12, L2) and a shift section (S). On either ends are the non-helical end regions N and C. These are known to show a non-helical structure and their length can vary (Parry and North 1998). Figure taken from (Bouillon and Wilkinson 2005) 48

Figure 1.10 – A keratin dimer (as shown in Figure 1.9) and the four subsequent modes of association to form keratin tetramers. Figure adapted from (Kreplak, Franbourg et al. 2002). 50

Figure 1.11 – One possible way in which the KIFs may be formed from the association of the smaller keratinous molecular structures which build a KIF (Davidson 2004). 51

Figure 1.12 – A SEM image of the cortex of human hair at magnification of x120,000. The image shows a high magnification of the macrofibrils found in the cortical cells of human hair fibres. The arrows point to the IMM found in the cortical cells which binds the macrofibrils. Within the macrofibrils themselves, the KIFs are present, showing variation in the way in which they are packed inter-laterally within the macrofibrils. There are differences seen in the packing of the KIFs from the centre of the macrofibril towards the edges. The bar indicates 0.1 μm . The inset image shows a higher

magnification image of the macrofibrils, the arrows in this image point towards the KIFs. The bar indicates a distance of 0.01 μm . Figure taken from (Takizawa, Takizawa et al. 1998). 56

Figure 1.13 – A SEM image of human hair in the cortex region. At the top of the image the outline of a cuticle cell can be seen. The white dotted line, annotated by ‘Ma’ encloses a macrofibril, the arrows point to the IMM which surrounds and binds the macrofibrils together in a cortical cell. ‘m’ denotes the melanin granules that are also found in cortical cells. The bar at the bottom of the image shows a scale of 0.1 μm . Figure taken from (Takizawa, Takizawa et al. 1998). 57

Figure 1.14 – Structure of the CMC between two cells. The two cells in the figure may indicate either cuticle or cortical cells. The δ -layer is defined by the black centre-most region and the β -layers lay either side of it, and include the epicuticle in this diagram. Figure adapted from (Bouillon and Wilkinson 2005). 61

Figure 1.15 – A SAXS fibre diagram for a Chinese hair sample in the dry state. The fibre diagram illustrates the first order of diffraction of the crystalline lipid bilayer. The q range of the image is 0.01 – 2.0 nm^{-1} . 66

Figure 2.1 – Schematic showing a part of the electromagnetic spectrum with the corresponding frequencies and energies of the radiation. 76

Figure 2.2 – A diagram outlining the basis of (a) constructive interference and (b) destructive interference from the theory of wave superposition. 79

Figure 2.3 - A diagram visually outlining the basis from which Bragg’s Law is drawn. 80

Figure 2.4 - Illustration of an X-ray diffraction setup. As the detector is moved further away from the sample only smaller angles are detected. The dotted lines show that the wide angle information is missed when the detector is placed at a longer distance from the sample. The small angle signal is compressed into a smaller space when the detector is at a shorter distance from the sample; this reduces the resolution of the small angle signal. The operational distance for wide angle X-ray scattering is between 7cm and 50 cm. The operational distance for small angle X-ray scattering is

between 1- 9.25 m. However, these distances are dependent on the instrumental setup and the wavelength of the light. 82

Figure 2.5 – An example of how biological materials with larger macromolecules present with partial crystalline order in the direction of fibre axis leads to fibre diffraction. The fibre diagram shown in this image is for the Chinese hair type in the dry state. The q range of the image is $0.01 - 2.0 \text{ nm}^{-1}$. 84

Figure 2.6 – Fibre diagram of the SAXS region highlighting the scattering features observed from a hair fibre. The image shown here is for the Chinese hair type in the dry state. The q range of the image is $0.01 - 2.0 \text{ nm}^{-1}$. 86

Figure 2.7 – Fibre diagram of the WAXS region highlighting the scattering features observed from a hair fibre. The image shown here is for the Asian hair type. The q range of the image is $0 - 20 \text{ nm}^{-1}$. 87

Figure 2.8 – Schematic of the layout of the synchrotron Soleil in France near Paris. The figure shows the initial linear accelerator where the electrons are initially accelerated. The electrons are then passed into the booster ring (the inner circle) where they are further accelerated. When the electrons have reached sufficient velocity they are passed into the storage ring (Synchrotron 2005). 88

Figure 2.9 – Some of the translational modes of a carbon dioxide molecule. The blue circle denotes the carbon atom and the black circles denote the oxygen atoms. 90

Figure 2.10 – Schematic of a gas chromatography setup coupled to a Fire ionization detector. 93

Figure 3.1 – Schematic showing the general layout of the ID18F beamline. The left hand side shows the experimental hutch containing the detectors, the sample mounting environment and the focussing optics and the right hand side shows the optics hutch containing the monochromator. The scale at the bottom shows the distance from the radiation source (storage ring). Not shown in the image is the control cabin. 100

Figure 3.2 – Schematic showing the layout of the ID02 beamline. The left hand side shows the optics hutch containing the monochromator and the toroidal mirror (not shown is the optional cylindrical mirror). The right hand side shows the experimental hutch containing the WAXS and SAXS detectors and the sample mounting environment. The scale at the bottom shows the distance from the radiation source (storage ring). Not shown in the image is the control cabin. 101

Figure 3.3 – Photograph showing the custom built five channel flow cell holder made by Unilever which was used to mount the samples at the ID02 beamline. 102

Figure 3.4 – A typical ATR-FTIR spectra for human hair. The spectra shown here is for the Chinese hair type. 105

Figure 3.5 - An example of TLC separation of the solvent-extracted lipid fraction (shown here is the Afro 4 sample – see Chapter 8 for further details) and the individual neutral lipid standards: TAG (tripalmitate), FFA (C17:0), WE (myristyl dodecanoate) and HC (heneicosane). 109

Figure 4.1 - A diagram showing how the 1-dimensional trace was obtained from the WAXS data. Seen in the figure is a wide angle diffraction pattern in the top left hand corner in a q range of $0 - 60 \text{ nm}^{-1}$ in the vertical direction. The red box highlights the meridional arc reflections that were captured by the WAXS detector at the ID02 beamline. The top left image in the figure has been adapted from (Fraser, MacRae et al. 1962). Figure shows the 2-dimensional diffraction pattern for the Chinese hair in the wet state in the WAXS region. The integration was made vertically from the bottom of the image to the top. This integration is used to form a 1-dimensional trace from the 2-dimensional fibre diagram. The 1-dimensional trace has units of intensity in arbitrary units on the y axis, and the x axis is in $q (\text{nm}^{-1})$. 117

Figure 4.2 - Some of the SAXS scans used in FibreFix to isolate specific areas of the 2-dimensional diffraction patterns to undergo PCA according to where the features lie in both q range and in angular region. The image on the left shows a scan of the entire region containing data. The middle image shows a scan isolating the meridional region capturing the low angle diffuse scatter and the diffuse 6.7 nm arc reflection but omitting the lipid reflection. The image on the right shows a scan isolating the equatorial region capturing

the low angle diffuse scatter and the reflection arising from the inter-lateral packing of the KIFs, it omits the lipid ring in this region. All images shown are for the Chinese hair type in the dry state. 118

Figure 4.3 –2-d fibre diagrams for each ethnic hair type in the dry state in the WAXS region. A: Afro Rubber, B: Afro Soft, C: Chinese, D: European and E: Mullato. All images are normalised and set to the same intensity scale and the q range of all the images is $5.0 - 60 \text{ nm}^{-1}$. 119

Figure 4.4 –2-d fibre diagrams for each ethnic hair type in the wet state in the WAXS region. A: Afro Rubber, B: Afro Soft, C: Chinese, D: European and E: Mullato. All images are normalised and set to the same intensity scale and the q range of all the images is $5.0 - 60 \text{ nm}^{-1}$. 120

Figure 4.5 –2-d fibre diagrams for each hair type in the dry state in the SAXS region. A: Afro Rubber, B: Afro Soft, C: Chinese, D: European and E: Mullato hair type. All images are normalised and set to the same intensity scale and the q range of all the images is $0.01 - 2.0 \text{ nm}^{-1}$. 121

Figure 4.6 –2-d fibre diagrams for each hair type in the wet state in the SAXS region. A: Afro Rubber, B: Afro Soft, C: Chinese, D: European E: Mullato hair type. All images are normalised and set to the same intensity scale and the q range of all the images is $0.01 - 2.0 \text{ nm}^{-1}$. 122

Figure 4.7 – Graphs showing the peaks arising from the inter-lateral packing of the KIFs in each hair type. The black line corresponds to the peak arising from the KIF inter-lateral packing and the red line corresponds to the peak arising from the crystalline lipid present in the hair. The dip in intensity between 40 and 80 degrees is a real effect due to the loss of data associated with the beamstop. The peaks seen here are from a full 360 degree azimuthal integration. The x axis is in degrees and the y axis is intensity in arbitrary units. A: Afro Rubber, B: Afro Soft, C: Chinese, D: Euro, E: Mullato. 124

Figure 4.8 - Bar chart displaying the relative total lipid content of each hair fibre as calculated from the integration of the lipid peaks corresponding to the 1-d traces of a full radial scan. 125

Figure 4.9 – The radial 1-d traces for each hair type in the dry state and the wet state respectively for an equatorial scan in the SAXS region. The arrows indicate what peak corresponds to which feature seen in the 2-d fibre diagram on the 1-d trace. The y axis is intensity measured in arbitrary units and the x axis is q (nm^{-1}). The graph shows $n=3$ for each hair type, thus creating three 1-d traces for each hair type.

127

Figure 4.10 –The equatorial radial 1-d traces for each hair type in the SAXS region. The black lines represent the dry hair state and the red lines represent the wet state. The difference in intensity between the dry and wet state 1-d traces is a real effect. The arrows indicate what peak corresponds to which feature seen in the 2-d fibre diagram on the 1-d trace. The horizontal axis is measured in q (nm^{-1}) and the vertical axis is measured in intensity (arbitrary units) for all graphs. The graph shows $n=3$ for each hair type, thus creating three 1-d traces for each hair type.

130

Figure 4.11 –The average eigenvalues coefficient weighting plots for the dry and wet state WAXS data and the dry and wet state SAXS data. The error bars indicate the standard error for the mean eigenvalue coefficient associated with each hair type for the respective base function. The averages are constructed from the corresponding 1-d radial traces of at least 3 different fibre diagrams in all cases. The horizontal axis is the base function number and the vertical axis is measured in intensity (arbitrary units) for all graphs.

133

Figure 4.12 –Multi-dimensional plots for the dry and wet state SAXS and WAXS regions. Top left shows a multi-dimensional plot for base function 1 on the x axis and base function 3 on the y axis for the dry state data in the WAXS region. Top right shows a multi-dimensional plot for base function 2 on the x axis and base function 3 for the y axis for the wet state data in the WAXS region. Bottom left shows a multi-dimensional plot for base function 1 on the x axis and base function 2 on the y axis for the full angular scan dry state data in the SAXS region. Bottom right shows a multi-dimensional plot for base function 1 on the x axis and base function 2 on the y axis for the full angular scan wet state data in the SAXS region. Both axes are in arbitrary units for all graphs.

134

Figure 4.13 –The average base function and the first five base functions outputted by the PCA for the WAXS and SAXS data in both the dry and wet state respectively. All vertical axes

are the intensity measured in arbitrary units and all horizontal axes are the respective q ranges measured in nm^{-1} . 136

Figure 5.1 – Figure detailing the basis of the skin-core experiments that were used for the data acquisition of the hair types under test at the ID18F beamline at the ESRF. Images taken at 5 micron increments across the hair fibre detail the textural variation of the structure of the hair fibre at different points. A typical scan involved collection of fifty 2-d fibre diagrams. Adapted from (Pierson and Gerts 2008). 142

Figure 5.2 – Figure details how one scattering feature in a 2-d fibre diagram is processed to form a 1-d linear trace for all the images taken in a scan across the hair fibre. The sample is horizontal and perpendicular to the X-ray beam. 144

Figure 5.3 – The eight sectors chosen by the in-house software from the 2-d fibre diagrams. Due to the inherent cylindrical symmetry of fibre diagrams, each image allows the opportunity to collect data from at least two equivalent diffraction regions. 145

Figure 5.4 – Small angle fibre diagram of the European type 1 hair sample showing crystalline lipid diffraction. The ring around the central small angle signal indicates presence of crystalline lipid structure in the sample. The hair sample is horizontal and therefore the equatorial reflections are vertical. The q range in this image extends out to 6 nm^{-1} . 146

Figure 5.5 - The integrated intensity plots for all of the sectors for the Afro hair type. 148

Figure 5.6 - Composite image of the fibre diagrams for the Afro hair type. The scan shows the fibre diagrams arranged in image order from left to right moving downwards in row. Some of the images which do not show scattering from the hair fibre have been omitted from the composite image. Each fibre diagram in the composite image represents an exposure taken in 5 micron incremental steps in the raster scan across the width of the hair fibre. Therefore every row in the above composite image represents 25 microns moved in the scan. 149

Figure 5.7 - The integrated intensity plots of the sectors for all the fibre diagrams for the Asian hair. 151

Figure 5.8 - Composite image of the fibre diagrams for the Asian hair type. Some of the images which do not show scattering from the hair fibre have been omitted from the composite image.	152
Figure 5.9 - The integrated intensity plots of the sectors outputted for the Chinese hair type.	154
Figure 5.10 - Composite image of all of the fibre diagrams for the Chinese hair type. Some of the images which do not show scattering from the hair fibre have been omitted from the composite image.	155
Figure 5.11 - The integral intensity plots for the sectors for the European type 1 hair.	157
Figure 5.12 - Composite image of all of the fibre diagrams for the European type 1 hair. Some of the images which do not show scattering from the hair fibre have been omitted from the composite image.	158
Figure 5.13 - Composite image of the lipid diffraction rings found in images 28 - 32 in the European type 1 hair. The intensity and q range of the images is the same in all images.	159
Figure 5.14 - The integrated intensity plots for the sectors for the European type 2 hair.	160
Figure 5.15 - Composite image of all of the fibre diagrams for European type 2 hair. Some of the images which do not show scattering from the hair fibre have been omitted from the composite image.	161
Figure 5.16 - The integrated intensity plots for the sectors for the Japanese hair.	162
Figure 5.17 - Composite image of all of the fibre diagrams for the Japanese hair. Some of the images which do not show scattering from the hair fibre have been omitted from the composite image.	163
Figure 6.1 – A typical spectra from a Chinese hair sample. Figure 7.1A shows all of the vibrational modes arising in the wavenumber region of 800 – 1750 cm ⁻¹ .A: cysteic acid stretch, B: cysteine monoxide stretch, C: cysteine dioxide stretch, D: Amide III band, E: CH ₃ symmetric deformation, F: anti-symmetric CH ₃ deformation mode, G: CH ₃ bending mode,	

H: CH₂ bending mode, I: CH deformation, J: Amide II band, K: Amide I band.

Figure 7.1B shows all of the vibrational modes arising in the wavenumber range of 2750 – 3550 cm⁻¹. L: CH₂ symmetric mode, M: CH₂ anti-symmetric mode, N: symmetric CH₃ mode, O: CH₃ anti-symmetric mode, P: Amide B band, Q: Amide A band. The vertical axis on both of the graphs is intensity measured in arbitrary units.

179

Figure 6.2 – Figure 6.2A: A multi-dimensional plot of the eigenvalues coefficients. The horizontal axis is BF 2 and the vertical axis is BF 3. Both axes represent the intensity measured in arbitrary units. The ellipses highlight the clustering seen by ethnic hair type. Figure 6.2B: The average base function eigenvalues coefficient weightings for each hair type in each base for the full spectral range. The hair types are arranged in the same order as indicated by the legend. The horizontal axis denotes the base function number and the vertical axis is the intensity measured in arbitrary units.

182

Figure 6.3 – Figure 6.3A: BF1 outputted by the PCA for the full spectral range for all hair types. Highlighted in the figure are all the vibrational modes seen in this base function across the entire spectral range. A: Amide III band, B: symmetric CH₃ deformation, C: CH deformation, D: Amide II band, E: Amide I band, F: symmetric CH₂ stretch, G: anti-symmetric CH₃ stretch, H: Amide B band. Figure 6.3B: BF2 outputted by the PCA for the full spectral range for all hair types. Highlighted in the figure are all the vibrational modes seen in this base function across the entire spectral range. I: cysteic acid stretch, J: Amide III band, K: CH₃ bending mode, L: Amide II band, M: Amide I band, N: Amide B band. The vertical axis is the intensity measured in arbitrary units on both graphs.

184

Figure 6.4 – Figure 6.4A: BF3 outputted by the PCA for the full spectral range for all hair types. Highlighted in the figure are all the vibrational modes seen in this base function across the entire spectral range. A: cysteic acid and cysteine monoxide stretches, B: cysteine dioxide stretch, C: Amide III band, D: CH₂ bending mode, E: Amide II band, F: carboxylate stretch, G: Amide I band, H: symmetric CH₂ stretching mode, I: anti-symmetric CH₂ stretching mode, J: Amide B band. Figure 6.4B: BF4 outputted by the PCA for the full spectral range for all hair types. Highlighted in the figure are all the vibrational modes seen in this base function across the entire spectral range.

K: Amide III band, L: CH₃ bending mode, M: Amide II band, N: Amide I band,
O: symmetric CH₂ stretch, P: anti-symmetric CH₂ stretching mode, Q: Amide B band.

The vertical axis is the intensity measured in arbitrary units on both graphs. 185

Figure 6.5 – Figure 6.5A: BF5 outputted by the PCA for the full spectral range for all hair types. Highlighted in the figure are all the vibrational modes seen in this base function across the entire spectral range. A: cysteine acid stretch, B: Amide III band, C: Amide II band, D: Amide I band. Figure 6.5B: the average base function outputted by the PCA for the full spectral range. Highlighted in the figure are all the vibrational modes seen in this base function across the entire spectral range. E: cysteine monoxide stretch, F: Amide III band, G: CH₃ deformation, H: CH₂ bending mode, I: CH deformation, J: Amide II band, K: Amide I band, L: CH₂ symmetric mode, M: CH₂ anti-symmetric mode, N: symmetric CH₃ mode, O: Amide B band, P: Amide A band. The vertical axis on both of the graphs is intensity measured in arbitrary units. 186

Figure 7.1 –Multi-dimensional plot of the lipids from the UPLC-MS analysis. The horizontal axis is the first principal component describing 37.27% of the variance in the data and the vertical axis is the second principal component which describes 9.89% of the variance in the data set. The codes on the diagram describe each sample that was used in the experiment and are labelled by ethnicity and sample number, for example EU1 is the first sample of the European hair type. The codes for ethnicities are; AFR=Afro, CN=Chinese, EU=European, JP=Japanese, MR=Mullato, SP=Spanish, TH=Thai, QC=Pooled sample and Sol=solvent. A pooled sample (QC) was created by combing an aliquot of all the samples used in the study and was run at the beginning following two runs of blank solvent (Sol) for column conditioning and quality control analysis. 196

Figure 7.2 - The total lipid content (µg of fatty acids/g biomass) for each hair type. Data as means ± SD (n=3-5). 199

Figure 7.3 - Relative lipid content (% of total lipids) extracted by each extraction procedure. Data as mean ± SD (n=3-5). 201

Figure 7.4 - Bar graph displaying the content of wax esters (WE), free fatty acids (FFA) and triacylglycerols (TAG) in the hexane wash ($\mu\text{g/g}$ biomass). Data as mean \pm SD (n=3-5). 203

Figure 7.5 - Bar graph displaying the relative content (% of total) of wax esters (WE), free fatty acids (FFA) and triacylglycerols (TAG) in the hexane wash. Data as mean \pm SD (n=3-5). 204

Figure 7.6 - Bar graphs of the individual lipid content of each class of lipid extracted from the hair using the chloroform:methanol procedure ($\mu\text{g/g}$ biomass). The bar graph at the top includes the values of FF and the graph at the bottom excludes the FFA. Data as mean \pm SD (n=3-5). 207

Figure 7.7 - Bar graph displaying the relative content (% of total) of polar lipids (PL), wax esters (WE), triacylglycerols (TAG) and free fatty acids (FFA) in the solvent- extractable fraction. Data as mean \pm SD (n=3-5). 209

Figure 7.8 - The concentrations of the hydrolysed fraction (in μg of fatty acids/g) for all hair types. Data as mean \pm SD (n=3-5). 211

Figure 7.9 - Spectra of Docosane ($\text{C}_{22}\text{H}_{46}$) run on the GC/MS. The x axis is the charge to mass ratio (m/z) and the y axis is abundance measured in arbitrary units. 213

Figure 7.10 - Spectra of tetracosane ($\text{C}_{24}\text{H}_{50}$) run on the GC/MS. The x axis is the charge to mass ratio (m/z) and the y axis is abundance measured in arbitrary units. 214

Figure 7.11 - GC/MS chromatogram of hydrocarbons from the AFRO4 hair sample. 1 – heneicosane $\text{C}_{20}\text{H}_{42}$, 2 – docosane $\text{C}_{22}\text{H}_{46}$, 3 – tricosane $\text{C}_{23}\text{H}_{48}$, 4 – tetracosane $\text{C}_{24}\text{H}_{50}$, 5 – heptacosane $\text{C}_{27}\text{H}_{56}$, 6- octacosane $\text{C}_{28}\text{H}_{58}$, 7 – nonacosane $\text{C}_{29}\text{H}_{60}$, 8 – Internal Standard (squalene). 215

Figure 7.12 - Chromatogram showing the fatty acid profile for the hydrolysed fraction for the Spanish 2 sample at the top and the Afro 2 sample at the bottom. The x axis on both

graphs is time (mins) and the y axis is intensity (arbitrary units). The C21A stands for the 18-MEA fatty acid and IS denotes the internal standard (C24:1). 216

Figure 7.13 - Chromatogram showing the fatty acid profile of the TAG lipid species from the solvent extraction (chloroform:methanol). The x axis on both graphs is time (mins) and the y axis is intensity (arbitrary units). The top chromatogram is the Mullato 3 sample. A denotes the C14:0 isomer, B - C14:1i, C - C15:0, D - C15:1, E - C15:1i, E - C16:0, F - C16:1, G - C16:1i, H - C17:0, I - C17:1, J - C17:1i, K - C18:0, L - C18:1, M - C24:0, N - C26:0. The bottom chromatogram shows the Spanish 2 sample. O shows the C12:0 isomer, P - C14:0, Q - C16:0, R - C16:1, S - C18:0, T - C18:1, U - C18:2. IS represents the internal standard on both chromatograms. The Mullato hair type shows a high proportion of C14 and C15 fatty acid isomers and C26:0 acid, the Spanish hair type shows large contents of C12:0 and C14:0 fatty acids. The internal standard is C24:1. 217

Figure 7.14 - Bar graphs showing the FA content of the WEs extracted from the hexane wash for all the hair types. Data as mean \pm SD (n=3-5). 219

Figure 7.15 - Bar graphs showing the relative fatty acid content (% of total FAs) of the FFAs extracted from the hexane wash for all hair types. Data as mean \pm SD (n=3-5). 220

Figure 7.16 - Bar graphs showing the fatty acid composition of the TAGs extracted from the hexane wash for the Chinese, European, Mullato, Spanish and Thai hair types. 222

Figure 7.17 - Bar graphs showing the fatty acid content (% of total FAs) of the PLs extracted for all hair types. Data as mean \pm SD (n=3-5). 223

Figure 7.18 - Bar graphs showing the relative content of fatty acids (% of total FAs) of the FFA fraction extracted with chloroform:methanol for all hair types. Data as mean \pm SD (n=3-5). 224

Figure 7.19 - Bar charts showing the FA content of the TAGs extracted with chloroform:methanol for all hair types. Data as mean \pm SD (n=3-5). 225

Figure 7.20 - Bar charts showing the FA content of the WEs extracted with the chloroform:methanol solvents from the Mullato, Spanish and Thai hair types.

Data as mean \pm SD (n=3-5).

226

Figure 7.21 - Bar charts showing the fatty acid composition of the hydrolysed fraction for the Mullato, Spanish and Thai hair types. Data as mean \pm SD (n=3-5).

228

List of Tables

Table 1.1 – The KAP families, their content, their approximate weight and the old nomenclature associated with them.	54
Table 1.2 – The differences in the geometric and morphologic properties between ethnic hair types. Table adapted from (Franbourg, Hallegot et al. 2003)	69
Table 3.1 – Information on the hair samples sourced from Unilever used in this thesis.	97
Table 3.2 - Gradient conditions for the UPLC run conditions for the lipid separation.	108
Table 4.1 – Real space dimensions for the crystalline lipid spacing in each hair sample in the dry state.	126
Table 4.2 - Value of the decay rate constant in the equatorial and meridional regions in the dry and wet states for each hair type.	128
Table 5.1 – Hair types used in this experiment and the details of the scans taken for each hair type.	146
Table 6.1 – Wavenumbers for all of the vibrational modes seen in human hair in the range 1000 - 4000 cm^{-1} . The Amide envelopes have a number of modes arising from several independent vibrations.	180
Table 6.2 – Average wavenumber value for each vibrational mode population in each respective Amide bandings across all hair types.	187
Table 6.3 – Average wavenumber value for the corresponding polypeptide vibrational modes in each hair type.	188
Table 6.4 – Average wavenumber value for the corresponding amino acid vibrational modes in each hair type.	189
Table 6.5 – Wavenumbers seen in second derivative analysis for all types of bonding in the wavenumber region 2850 – 3300 cm^{-1} for all ethnic hair types.	190

Table 7.1 - Total amount of lipids ($\mu\text{g/g}$ hair biomass) in different ethnic hair types and the relative (% of biomass) lipid content in hair; this provides an indication of how much of the hair fibre is lipid in each hair type.	199
Table 7.2 – Relative percentage of the total lipid content extracted from each extraction process.	200
Table 7.3 - Content of each lipid class extracted and the total lipid content extracted from the hexane wash. n.d. denotes that the lipid was not detected. Data as mean \pm SD (n=3-5).	202
Table 7.4 - Relative content (% of total in the hexane wash) of each individual lipid class in the hexane wash. Data as mean \pm SD (n=3-5).	204
Table 7.5 - Total lipid content extracted by lipid class expressed as a percentage of the total hair biomass used for extraction.	205
Table 7.6 - Content of polar lipids (PL), wax esters (WE), triacylglycerols (TAG) and free fatty acids (FFA) in the solvent- extractable fraction (μg of fatty acids/g biomass). Data as mean \pm SD (n=3-5).	206
Table 7.7 - Lipid content of each lipid class expressed as a percentage of the total lipid extracted in the solvent extraction.	208
Table 7.8 - Lipid classes expressed as a percentage of the total biomass of the hair used for the solvent extraction. Data as mean \pm SD (n=3-5).	210
Table 7.9 – Total lipid content in $\mu\text{g/g}$ of the lipids extracted from the hydrolysed fraction.	211
Table 7.10 - Content of the hydrolysed fraction expressed as a percentage of the total hair biomass. Data as mean \pm SD (n=3-5).	212

Table 7.11 - Relative contribution of each individual lipid class extracted in the hexane:diethyl ether wash expressed as a percentage of the total lipid extracted. Also given are the corresponding values as quoted in previous literature for the lipid classes from the sebaceous source. 237

Table 7.12 - Values for the relative content of each lipid class expressed as a percentage of the total hair biomass compared with values from literature. 240

Table 7.13 - Values for the relative content of each lipid class expressed as a percentage of the total lipid content compared with values from literature. 241

Abstract

In the modern world hair plays a cultural and aesthetic role. The hair care industry accounts for a large portion of the cosmetic and dermatological industry generating large financial sums in sales, and consequently research and development into hair care products is important for companies seeking to increase their market share and profits. Currently there are very few products which specifically target certain ethnicities as the basis of knowledge underlying what nanoscopic and molecular factors cause the variation seen at the macroscale of human hair is circumscribed. Therefore a need exists within this industry to expand the information available on the origins of macroscopic variation in differential ethnic hair types.

The work presented in this thesis is the embodiment of five different studies: a bulk X-ray scattering analysis of single hair fibres, a series of skin-core experiments utilising microfocus X-ray scattering, an attenuated total reflectance Fourier transform infrared spectroscopy study of the cuticle surface and a study of the lipids extracted from different spatial locations within hair fibres.

The bulk X-ray scattering analysis on single hair fibres showed that the non-keratinous materials; namely the lipids and the amorphous/disordered material and interfaces present are responsible for the largest source of variation seen inter-ethnically at the nanoscopic and supramolecular levels. The lipids were found to be different amongst hair types with respect to their crystalline spacing, the total intensity and thus volume present and also in the preferential structural orientation of the lipid arrangement. The low angle diffuse scatter which is thought to be related to the keratin associated proteins varied with respect to the extent in q range, the angular behaviour and the behaviour of the diffuse scatter under hydration conditions. The azimuthal spread of the reflection arising from the inter-lateral packing of the keratin intermediate filaments was also found to differ between hair types.

The skin-core experiments provide information on the textural variation of the hair fibre across the concentric subsections of hair enabling information to be sought on the structural components of the hair. The work presented shows that there are zonal differences in both the keratinous and non-keratinous structures present across the cross-section of the hair fibres both intra and inter-ethnically. The differences seen are in the size and location of specific hierarchical keratinous assembly structures and also in the ultra -structure of the hair fibre as whole.

Attenuated total reflectance Fourier transform infrared spectroscopy is a bench top technique that is widely available to investigate the surface structure of materials. The study presented has shown differences related to the keratin conformational structure and the hydrophilic properties of the hair fibres. There are also variations seen in the products of the cysteine containing structures due to weathering which may be due to a difference in the geographical location of the source.

Lipids that are present on either the surface of hair fibres or located within the hair fibre account for the largest non-proteinaceous component present in hair. An investigation characterising the lipids preferentially extracted from different spatial locations of the hair fibre has been performed. The work presented has revealed that there is significant variation both intra and inter-ethnically in the total lipid content present, the lipid classes and the fatty acid profiles. The variation in the fatty acid profiles may also possibly be related to the difference in signal seen in the X-ray diffraction study.

Chapter 1 – Introduction

There are four main types of structural bio materials from which the matrix of all multicellular living organisms are constructed; cellulose, collagen, chitin and keratin. These are fundamental to the function and structure of any living multicellular organism. Cellulose is an elementary material found in all plant matter and is vital in helping plants maintain stability to their structure. Collagen is found in all metazoan animals in their connective tissue, flesh and muscles; it is the most abundant protein found in animals and is fundamental to forming tissues and organs. Chitin is an important material for the development of exoskeletons in crustaceans and insects and is found in the cell walls of fungi. Keratin is a protein which forms an excellent protective barrier against chemical attack and environmental damage in animals, it is typically found in skin, hooves, quills, beaks, nails and hair and is characterised by mechanical properties of hardness and resilience. Although keratins were initially believed to have a common molecular structure, it was X-ray diffraction that revealed differences between some of the keratin based materials. This gave rise to two classes of keratin based on their characteristic diffraction patterns, with feather and claw being described as the beta pattern and mammalian quill, nail and hair as the alpha pattern. This distinction formed the basis for the description of the classical secondary structures in protein; the alpha helix and the beta sheet. This thesis focuses on the supramolecular hierarchies formed by the alpha helix based keratins, especially in hair.

Hair from various mammals has been extensively utilised by humans to their benefit; whether it is used for warm clothing, to use for tools such as paint brushes or to create other fabrications such as carpets or rugs. Wool which has many similar properties to human hair has been used for hundreds of years in a variety of applications, and continues to be a major commodity. In the early 20th century, research into the structure of wool and the way in which it could be manipulated started to become an important factor in industry and this led to research into keratinous materials.

In mammals, hair has essential physiological importance; it is a means of insulation, chemical and environmental protection, and an important factor in sensory perception. However, since humankind has evolved to depend less on its hair for physiological importance in the modern world, hair to humans takes on a very different role; mostly cultural and aesthetic.

In the 21st century many people are concerned about the appearance of their hair and pride themselves in having a particular style, this can involve a number of different products, chemicals or appliances to alter hair into the desired image of the consumer. Understanding the structure of hair and how it can be manipulated can lead to the development of new hair care products and appliances that can generate vast sums of money in sales. The hair care market for the UK alone was reported to be worth £1.2 billion in 2008 and reported to be one of the few markets to resist receding in the economic downturn (Elliot 2009). Many companies and businesses devote significant time and money into the research and development of new hair products and appliances in order to seek out increasing sales and a larger share of the market. With an increasing number of people in developing nations who can afford to spend more money on hair care, the size of the hair care market will increase and this in turn will lead to companies with a greater desire to increase their volume of sales.

There is now a focus in the hair care industry for research into different ethnic hair types and a need to understand genetic and phenotypic variations in hair. An increasing market in the developing nations needs a better understanding of specific hair types and the creation of corresponding products for successful product placement in this new niche market. Currently one of the biggest markets in the hair care industry is the black or African-American hair care market. In a 2009 a film investigated the black hair care market in the USA; it reported that this market was worth \$9 billion in the USA alone and documented the extreme lengths African-American women go to in order to fulfil a desired appearance (Stilson 2009).

1.1 Hair Structure Overview

Human hair is comprised of a number of discrete levels of molecular structure from the atomic to macroscopic scale which produce a structural hierarchy. It contains several levels of organisation of molecular structure that arise from the complex interplay of several forces that are common to all biological macromolecules. A human hair fibre is approximately 50 - 100 μm in diameter and can grow up to metres in length (Kreplak, Merigoux et al. 2001), the diameter of a hair fibre varies with age (Bogaty 1969) and race (Franbourg, Hallegot et al. 2003). Human hair is constructed from proteins, lipids and contains other trace materials. It is comprised of three distinct ultrastructural sections, moving inwards from the outside of the fibre these are; the cuticle, the cortex and the

medulla. The cuticle acts as a barrier or a sheath to the hair, protecting it from the environment (Kreplak, Merigoux et al. 2001). The cortex contains the most matter, typically 90%; this is where the highly organised keratinous hierarchical structure of the hair is found (Bertrand, Doucet et al. 2003). The medulla is a group of high porosity cells which provide a means of insulation for the organism. However, it should be noted that the medulla is not always present in human hair (Luell and Archer 1992). Hair is given a natural colour by the presence of melanin which is distributed in the cortex of the fibre (Bouillon and Wilkinson 2005).

There are two groups of proteins that comprise a hair fibre; keratin and keratin associated proteins (KAPs). The keratin found in hair is helical and constructed into filaments, keratin intermediate filaments (KIFs) which form the fibrous structure of the hair (Rafik, Doucet et al. 2004), KIFs are part of a super family of molecules; the intermediate filament family (IF), a comprehensive description of the formation and characteristics of IFs is presented by Parry and Steinert (Parry and Steinert 1995). The intermediate filaments were given their terminology due to the diameter of the structures that were observed in fibre diffraction studies; thicker than microfibrils but thinner than microtubules. IFs are defined to be 8-12 nm in diameter; KIFs are roughly 9 nm in diameter (Parry and Steinert 1995). There are two classes of keratins which are defined by their net charge; type Ia (acidic residues) and type IIa (neutral or basic residues). Keratins contain a high amount of cysteine in their sequence; this allows cross-linking in the form of disulphide bonds, this is what gives hair its characteristic high tensile strength (Bouillon and Wilkinson 2005). The KAPs are thought to have a globular conformation and are proposed to bind to each other and KIFs to form a continuous 'matrix' holding the fibrous structures in place (Fraser, MacRae et al. 1959).

Lipids are found within the hair fibre, some of which are in crystalline form, external lipids excreted from the sebaceous glands are found in the cuticle. Some trace elements such as the heavy metals iron and lead are also found in hair, these arise either from environmental sources (heavy metals) or excreted from the sebaceous glands and absorbed into the hair fibre (other trace elements) (Bertrand, Doucet et al. 2003). Figure 1.1 shows a schematic of some of the structures found in hair and a scanning electron microscopy (SEM) image of a hair fibre surface showing the cuticle scales on the outside of a hair fibre.

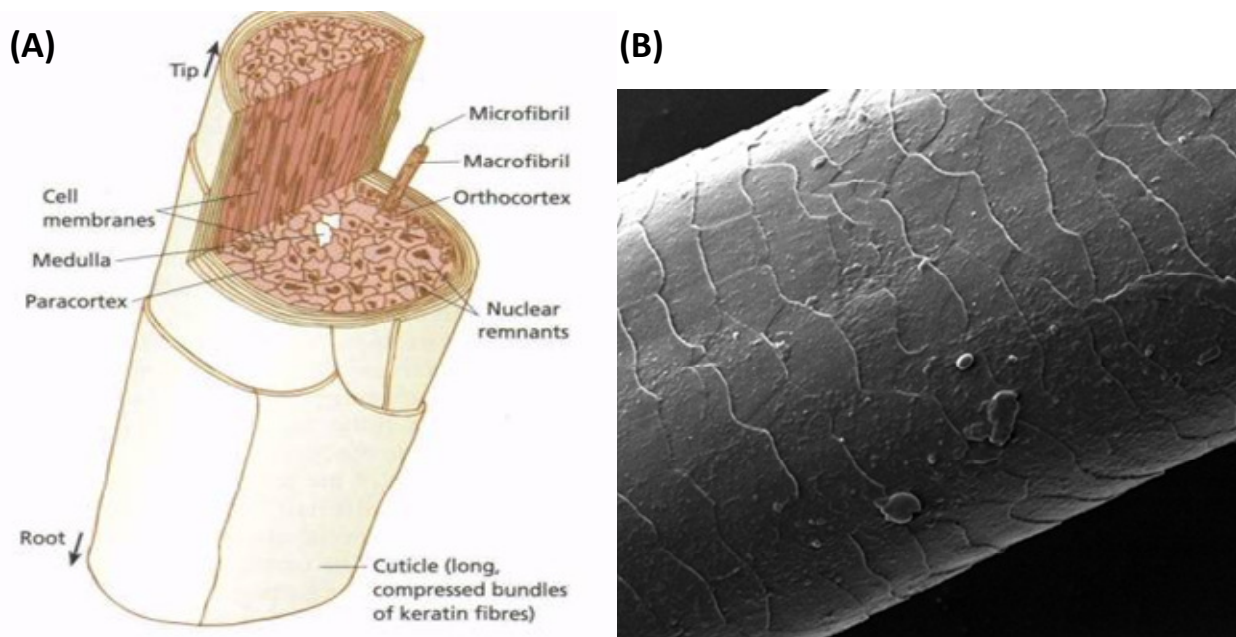


Figure 1.1 – (A) Schematic of some of the structure found in hair; the pink region shows the cortex of the hair, the outer white region illustrates the cuticle cells enclosing the cortex and the central white region is the medulla of the hair. These three regions comprise the ultra structure of hair. (B) Scanning electron microscopy image of a human hair fibre which clearly shows the cuticle scales found on the outside of a fibre. Figures from (Bandli , Grooming 2007).

The inter and intra molecular forces present in hair provide the fundamental basis to forming all of the molecular structures found; their specific interaction dictates the structures and assemblies created. An overview of the forces, molecular structures, molecular assemblies, ultrastructure and ethnic variations found in hair is presented in this chapter.

1.2 Forces

There are five principal forces found which govern the conformation in all biological macromolecules. These are:

- Covalent bonds
- Hydrogen bonds
- Coloumbic interactions
- Hydrophobic interactions
- Van der Waals bonding

Each of these forces play an essential role in macromolecular conformation and the basis of this is described below.

1.2.1. Covalent Bonding

Covalent bonds are very strong short range forces between two neighbouring atoms and are strongly directional as a result of the electrons being shared by two neighbouring atoms. The covalent bonds define the formal chemical structure of an organic compound which forms the peptide backbone of proteins, the side chains of amino acids and is the linkage between the sulphur atoms of the cysteine amino acids in the forming of disulphide bonds. Specific arrangements of amino acids joined by peptide bonds can lead to regular structures such as the alpha helix and beta sheet (Hoppe, Lohmann et al. 1983). As covalent bonds are strong and effective over a very short distance, it requires a large tensile force to stretch structures such as the alpha helix and deform it (Berg, Tymoczko et al. 2002); this property gives hair its high tensile strength (Bouillon and Wilkinson 2005).

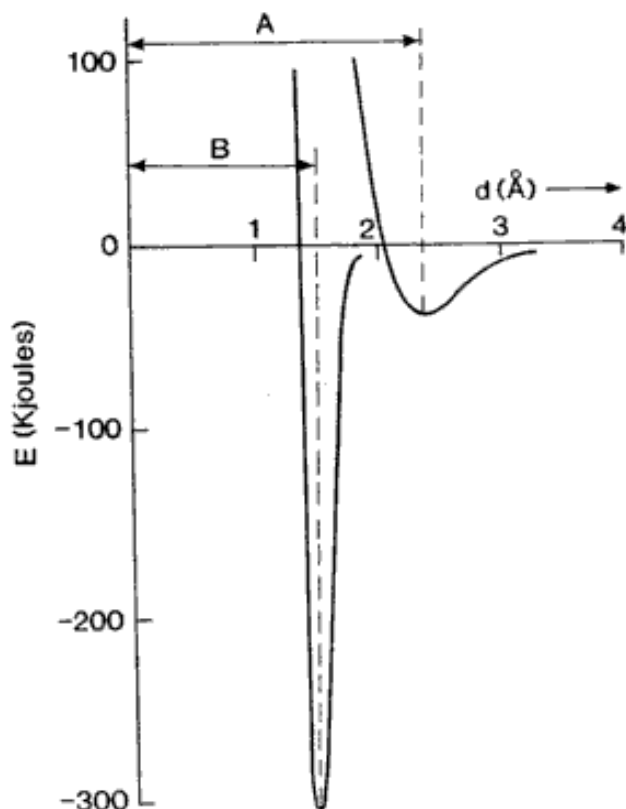


Figure 1.2 – An energy versus displacement representation of the covalent bonds within alpha-keratin. The sharp, deep line represents the attractive force of the covalent bonds within the molecule and the arrow B indicates the small distance in Angstroms over which the bond force is effective. The shallower broader curve and the arrow A represent the energy and bond distance respectively for hydrogen bonding in an alpha helix. Image taken from (Feughelman 1997).

1.2.2 Hydrogen Bonding

Hydrogen bonding arises from the attraction between the proton of hydrogen on the amide group and the pair of lone electrons from the oxygen atom on the carboxyl group (Hoppe, Lohmann et al. 1983). Hydrogen bonding in proteins occurs mostly between the carboxyl groups and amide groups of the main polypeptide chain and specific side chains (see Figure 1.7). The energy required to break a hydrogen bond is significantly lower than the covalent bond. A graphical comparison of the relative energies of hydrogen and covalent bonds is seen in Figure 1.2. Although covalent bonds define the formal chemical structure of all proteins, the hydrogen bonds contribute to defining the 3-dimensional secondary and tertiary structure of the protein.

1.2.3 Coulombic Interactions

Coulombic interactions occur between charged side chain groups on the polypeptide chains (Berg, Tymoczko et al. 2002). Oppositely charged side chains such as lysine (positive) and glutamate (negative) result in an attractive force forming an ionic bond. Such interactions can occur within and between polypeptide chains. In keratin, the hierarchical interaction of alpha helices is in part directed by the ionic bonds of charged amino acid side chains. Here, coulombic interactions between two alpha-helices allows them to form coiled coil structures, these also require contribution from hydrophobic interactions (see Sections 1.2.4 and 1.3.2).

1.2.4 Hydrophobic Interactions

Hydrophobic interactions arise from the tendency of non-polar entities to associate in the presence of water. For proteins this happens where the amino acid side chains are non-polar (the R group in Figure 1.7). The exposure of non-polar side chains to water would lead to the increased ordering of water molecules. Burying non-polar groups inside a protein reduces the interactions with the water molecules allowing the interaction of water molecules amongst themselves which in turn lowers the ordering of the solvent, water (Hoppe, Lohmann et al. 1983, Berg, Tymoczko et al. 2002). The net effect in a protein-solvent system is for the proteins to fold and become ordered as the solvent becomes disordered.

1.2.5 Van der Waals Bonding

Van der Waals bonding arises due to the dipole interaction between two neighbouring atoms (Young, Freedman et al. 2007). The dipole interaction may be permanent, induced or fluctuating. Van der Waals bonding is very weak; individually it does not make a major contribution to the mechanical integrity of structures. However, due to the sheer number of Van der Waals bonds formed inside a molecule, it makes a noticeable contribution.

Together, each of these forces makes a contribution to the structural function and integrity of hair and dictates which structures and assemblies can be created; these are reviewed in Sections 1.4 and 1.5.

1.3 The Ultrastructure of Hair

The ultrastructure of hair is the three concentric sections of a fibre; the cuticle, cortex and medulla.

1.3.1 Cuticle

The cuticle is the barrier of defence of a hair fibre to environmental damage and its contact interface with the external environment; its properties and function are therefore important. It is comprised of layers of cells bound to each other much like the configuration of roof tiles on a house. There may be 5 – 10 layers of cuticle, and these are bound to each other by the cell membrane complex (CMC), typically a cuticle cell is 0.5 μm thick and may be up to 60 μm in length (Orfanos, Montagna et al. 1981). The cuticle gives rise to characteristic mechanical and chemical properties that are of great interest to research and development in the hair care industry, specifically the shearing and bending properties of the fibre; it is hydrophobic, but it still allows water and other substances to pass through it into the cortex. At present the route for which water and other substances penetrates the cuticle into the cortex has not been fully characterised, but it is likely that it is a combination of diffusion across the cuticle cell via the

endocuticle layer which is porous and the CMC (see Section 1.5.2) (Potsch and Moeller 1996, Kelch, Wessel et al. 2000, Gummer 2001, Kreplak, Merigoux et al. 2001, Bouillon and Wilkinson 2005, Masukawa, Shimogaki et al. 2005, Formanek, Wilde et al. 2006, Inoue, Iwamoto et al. 2007, Chandrashekara and Ranganathaiah 2009).

The cuticle structure has mainly been studied using transmission electron microscopy (TEM) (Swift and Holmes 1965, King and Bradbury 1967, Bradbury and Leeder 1969, Orfanos, Montagna et al. 1981, Jones and Rivett 1997, Swift 1999, Robbins, Weigmann et al. 2004) although recent advances in microfocus X-ray diffraction (μ XRD) have allowed for some structural research to be carried out using this method (Kreplak, Merigoux et al. 2001, Ohta, Oka et al. 2005, Inoue, Iwamoto et al. 2007) and also atomic force microscopy (AFM) has made a contribution (Wei, Bhushan et al. 2005, Bhushan 2008) particularly in regards to its mechanical properties. It is comprised of distinct sections, moving inwards towards the cortex from the outer side these are; the epicuticle, the A-layer, the exo-cuticle and the endo-cuticle (Bouillon and Wilkinson 2005). Figure 1.3 shows a schematic of a cuticle cell highlighting the structural components that comprise it.

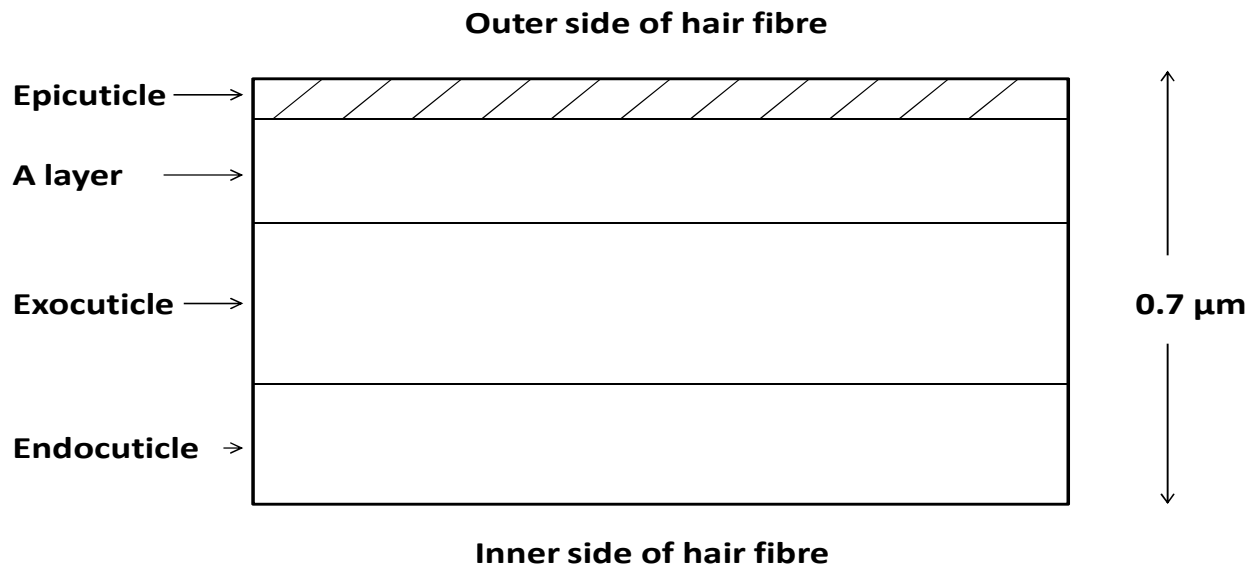


Figure 1.3 – Schematic of a cuticle cell in a typical human hair fibre. The epicuticle is a thin membrane covering the outside edge of the cuticle scale. This is bound to the A-layer beneath it, the exocuticle lies bound beneath the A-layer via disulphide bonding and the endocuticle lies beneath the exocuticle. Figure adapted from (Wei, Bhushan et al. 2005).

The outermost layer of the cuticle cell is the epicuticle; this fine membrane layer comes into contact with the surrounding atmosphere and gives rise to the surface chemical properties. It is approximately 5 – 7 nm thick (Bouillon and Wilkinson 2005) and is composed of lipids on the outermost edge bound to an inner proteinaceous matrix which is in turn bound to the A-layer below it (Jones and Rivett 1997). This layer functions as a highly resistant, hydrophobic layer protective to water, chemical and biological agents (Jones and Rivett 1997). The lipids found here are mostly free fatty acids with 18-methyl-eicosanoic acid (18-MEA) being the most prominent which is covalently bound via thioester linkages to the proteinaceous layer below (Bertrand, Doucet et al. 2003). Figure 1.4 details the structure of the epicuticle.

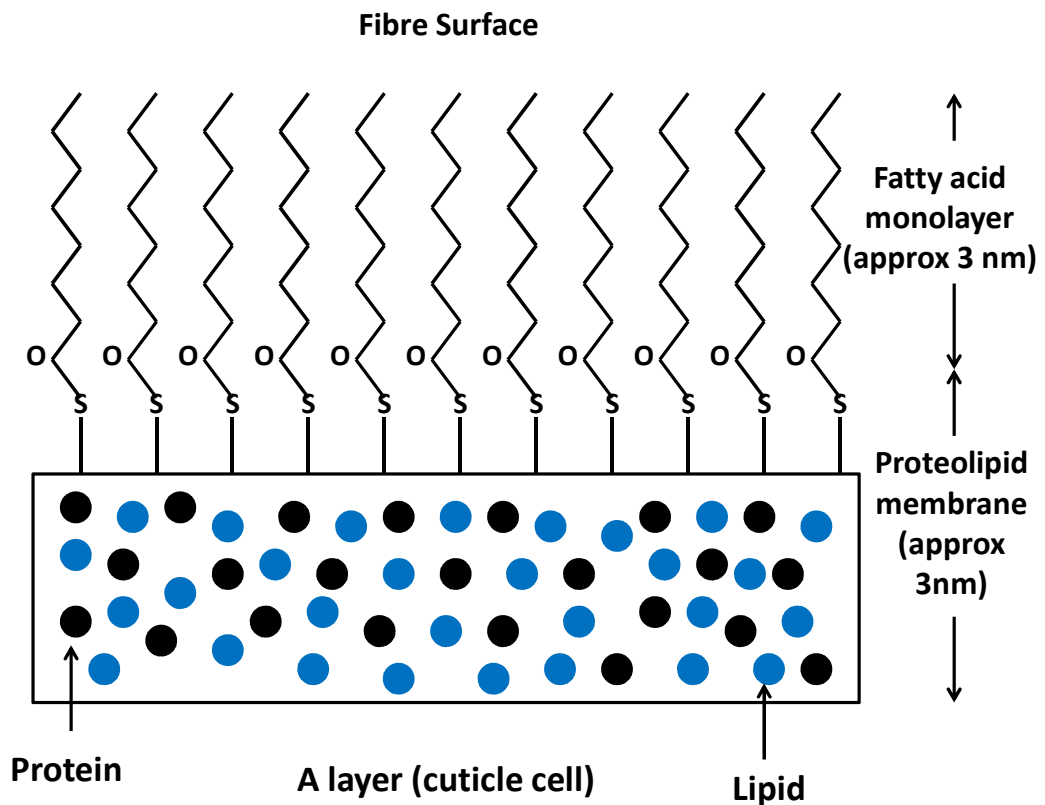


Figure 1.4 –Schematic showing a model for the structure of the epicuticle in human hair. The fatty acid layer consisting primarily of 18-MEA is covalently bound via thioester linkages to the proteolipid membrane below it. The proteolipid membrane in turn is bound to the A-layer below it via a process that is yet to be determined (Jones and Rivett 1997). Figure adapted from (Jones and Rivett 1997).

The A-layer lies beneath the epicuticle layer, it is composed entirely of proteins that show a high cysteine and thus sulphur content. This allows for the A-layer to form disulphide bonds which creates a high level of cross-linking between the A-layer and the exocuticle that lies below it (Bouillon and Wilkinson 2005). This part of the cuticle has low solubility due to the disulphide bonds and is highly resistant to abrasion and chemical attack (Orfanos, Montagna et al. 1981).

The endocuticle is found below the exocuticle and lies at the interfaces between the cuticle cells that are stacked or between the cuticle and cortex cells separated by the CMC (see Section 1.5.2) (Bouillon and Wilkinson 2005). It is composed of low sulphur proteins (Fraser, MacRae et al. 1972) that are weakly cross linked and forms a readily porous structure as determined by AFM experiments (O'Connor, Komisarek et al. 1995).

1.3.2 Cortex

The cortex is where the bulk of both the keratinous and non-keratinous molecular structures are located in the hair fibre; the cortex makes up to 90% of the hair fibre mass (Bertrand, Doucet et al. 2003). A comprehensive description of the way in which the molecular structures associate and produce the hierarchical structures which make up the assemblies found in the cortex, along with a description of the molecular components such as the lipids is given in Sections 1.4 – 1.6.

1.3.3 Medulla

The medulla is normally located in the centre of the hair fibre, however, in human hair it is variably present and may take on an intermittent form if found (Luell and Archer 1992). The medulla is composed of various types of cells loosely packed (Bouillon and Wilkinson 2005). A study on medullary cells found in porcupine quill reported that the cells contained virtually no cysteine content, a low amount of hydroxy and acidic amino acids (Rogers 1964). Infrared spectroscopy (IR) studies have shown that in some ethnic hair types the medulla contains a high concentration of lipids of a fatty acid composition (Kreplak, Briki et al. 2001) while other hair types show no presence of lipid in the medulla. An electron microscopy study reported that there may be two types of medullary classification based on observations using both SEM and TEM

techniques. The report proposed that there was a thin type medulla and a thick type medulla. The study also reported three clear components in the medulla; globular structures, disorganised cortical cells and a thin smooth layer similar in composition to that of the CMC (see Section 1.5.2) (Wagner, Kiyohara et al. 2007). A figure showing the medulla and some of the features found in the medulla as observed by electron microscopy can be seen in Figure 1.5.

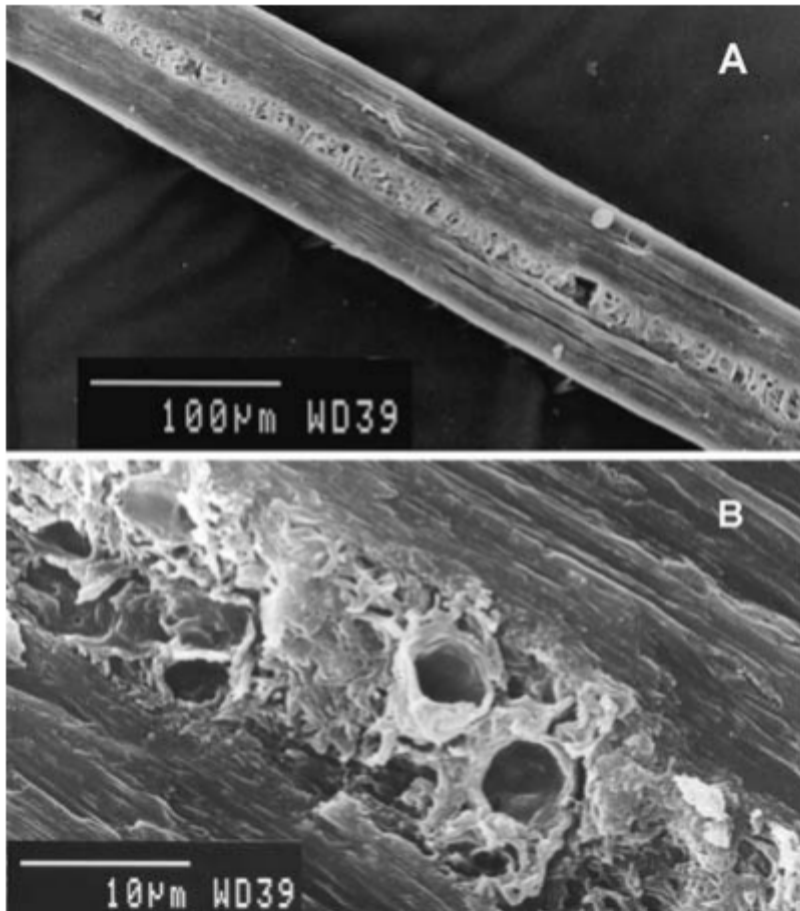


Figure 1.5 – Two SEM images of longitudinally cryofractured human hair fibres which show the medulla. A shows an image of a thin type medulla, B shows the medulla of the hair fibre shown in A at higher magnification. In this image, globular structures as reported by (Wagner, Kiyohara et al. 2007) can be seen. Images taken from (Wagner, Kiyohara et al. 2007).

1.4 Molecular structures

The modulation of organisation at different structural levels within keratin based tissues is reliant upon the interplay between different parts of KIF molecules and a variety of non-fibrous proteins. The complex interaction of both the non-keratinous and keratinous structures contributes to defining the structural properties of the hair fibre. Although, details of this interaction are relatively poorly understood, it is thought that it occurs at the terminal ends of KIFs. The KAPs form the non-keratinous molecular structures that are found in hair. In comparison to the keratinous molecules, these structures are relatively poorly understood despite their fundamental role in forming a hair fibre; the KAPs are proposed to bind the KIFs together in a continuous matrix. Figure 1.6 shows a schematic of the molecular structures found in hair. Starting from the smallest scale showing order; the alpha helix, this structure associates and axially aggregates to build larger molecular structures, the following is an account of all the keratinous molecular structures found in hair.

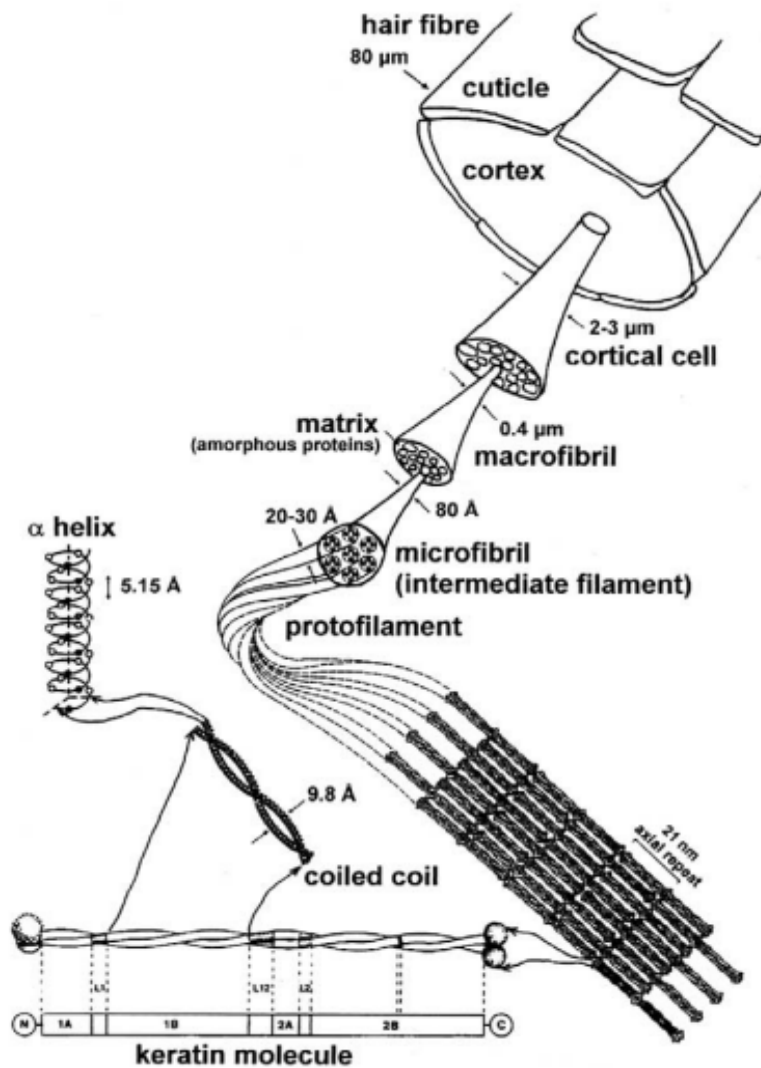
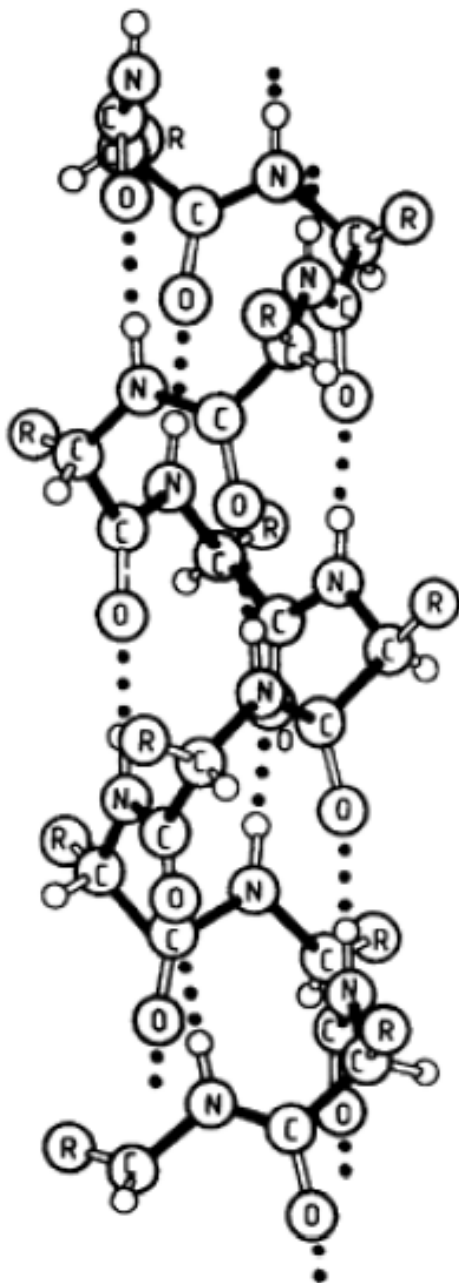


Figure 1.6 –Schematic showing the keratinous molecular structures which associate and aggregate to build up the larger molecular structures and the molecular assemblies found in hair. Figure taken from (Franbourg, Hallegot et al. 2003).

1.4.1 Alpha-Keratin

Alpha-keratin was first investigated by Lord Astbury in the 1930's when he used X-ray diffraction (XRD) methods to examine wool, nail, hair and other keratinous tissues under various conditions (Astbury and Street 1932, Astbury 1933, Astbury and Woods 1934, Astbury and Sisson 1935). These preliminary X-ray diffraction experiments showed that there were two types of keratins based on their characteristic diffraction patterns; alpha keratin and beta keratin. Building on this pioneering work, the structure of the alpha helix was described by Pauling in 1951 using fibre

diffraction techniques from the alpha-keratin based structures that Astbury used (Pauling, Corey et al. 1951). Pauling proved that the alpha helix is a fundamental protein structure conformation and it has since been shown that many proteins, at least in part, show alpha-helical structure (Hoppe, Lohmann et al. 1983).



The alpha helix conformation of keratin shown in Figure 1.7 is a biological polymer built from a covalently bonded polypeptide chain. Hydrogen bonding between the amide and carboxylate groups (NH and CO groups respectively) plays a crucial role in the stabilisation of the helix. One turn of an alpha-keratin helix is 5.15 Angstroms long; this is the repeat coiling distance or pitch for alpha keratin which corresponds to 3.6 amino acid residues per turn.

Figure 1.7 – Schematic of the alpha helix. The black lines represent covalent bonding between the peptide backbone of the helix. The dotted lines represent the hydrogen bonds between the amino acids of the amide groups (NH) and the carboxylic groups (CO). R represents the side chain groups; these may be neutral, basic or acidic depending on the type of keratin (type Ia or IIa). Figure taken from (Hoppe, Lohmann et al. 1983).

1.4.2 Coiled Coils & Dimers

Coiled coils are formed from two right-handed alpha-helices wrapping around each other to form a left-handed coiled coil structure. The bonds that dictate this are specific; coulombic and hydrophobic interactions are critical in the process. In each alpha helix, the turn of the helix (3.6 amino acids per turn) creates a repeating residue sequence which forms heptads (a-g) where residues a and d are apolar and residues e and g are oppositely charged groups. In hair, the moist environment of the cortical cell where the alpha-helices are found provides an environment that favours hydrophobic interactions. The hydrophobic interactions between heptads a and d 'shield' the heptads of e and g allowing them to form coulombic interactions between the two helices. For this to happen, the coiled coil must be composed of type Ia and type IIa keratin helices. Type Ia keratin helices have acidic side chain groups and type IIa keratin helices have neutral or basic side chain groups (Crewther and Parry 1977). Type Ia proteins have approximately 410 amino acids and weigh 47 kDa, type IIa proteins have approximately 500 amino acids in their sequence and weigh 54 kDa (Parry and Steinert 1995). Figure 1.8 shows a schematic of the coiled coil arrangement.

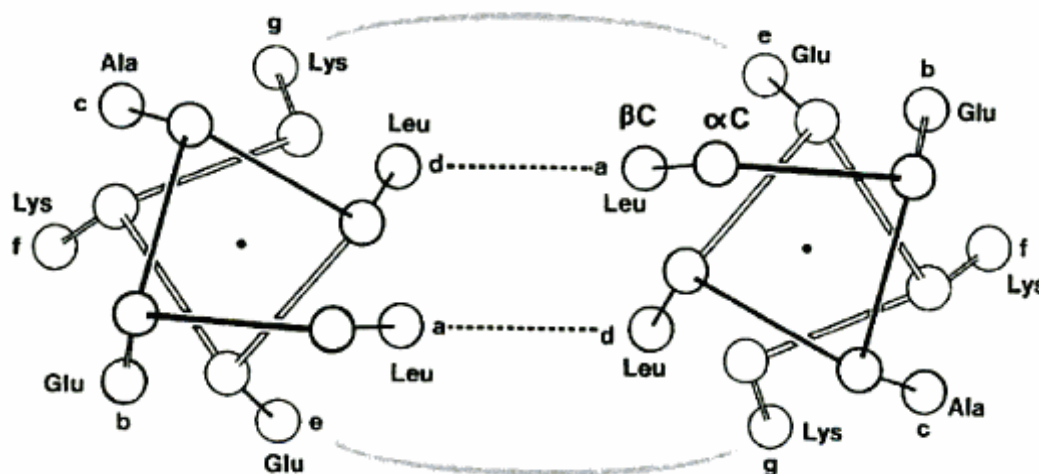


Figure 1.8 – The lateral Coulombic interactions between two alpha keratin helices to form a coiled coil arrangement. The e and g heptads are oppositely charged and the a and d heptads form ionic bonds. Figure taken from (Bouillon and Wilkinson 2005).

The keratin dimer is assembled from two alpha helices in a coiled coil arrangement. Figure 1.9 shows how a keratin dimer comprises two coiled coil arrangements lying parallel with each other. They are joined axially by four linker regions, a shift section (a disruption in the helical pattern) and two non-helical end regions, N and C. The complete length of a keratin dimer is approximately 45 nm and the coiled coil arrangements that constitute the dimer have a 21 nm axial repeat (Crewther and Parry 1977).

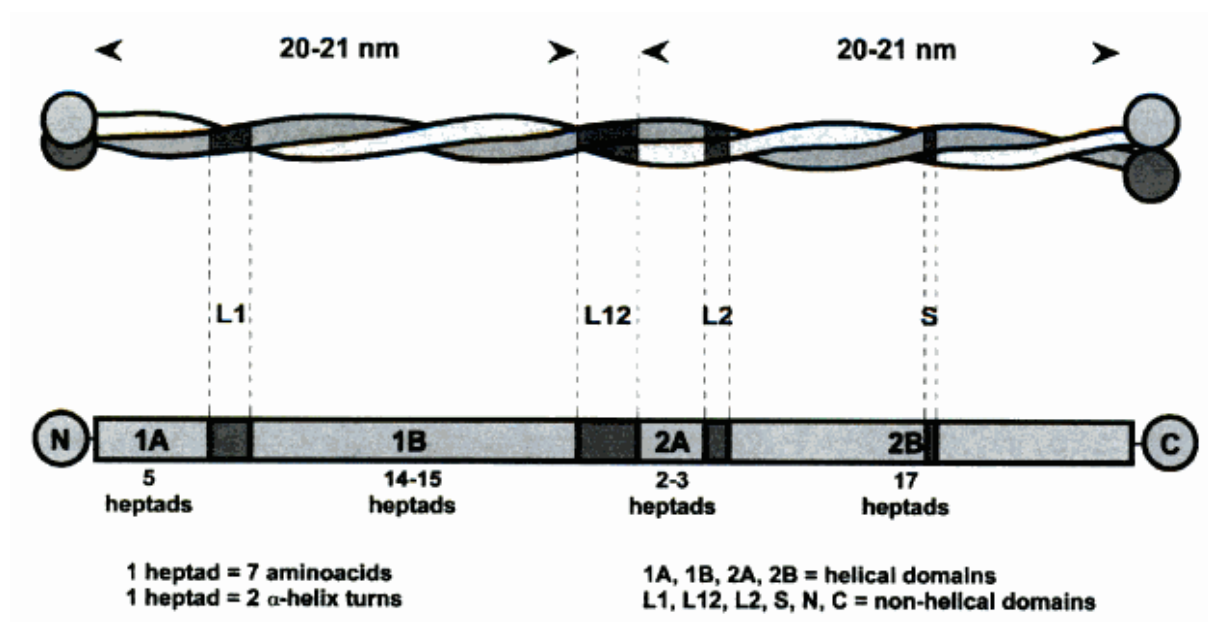


Figure 1.9 – The arrangement of a keratin dimer. Shown are the four central helical sections (1A, 1B, 2A, 2B) connected by three linker regions (L1, L12, L2) and a shift section (S). On either ends are the non-helical end regions N and C. These are known to show a non-helical structure and their length can vary (Parry and North 1998). Figure taken from (Bouillon and Wilkinson 2005).

The stability of this structure comes from the coulombic and apolar interactions between the heptads along the length of the coiled coil arrangement. Little structural information is known about the link regions although they are thought to be non-helical and lack a heptad substructure (Parry and Steinert 1995). Recent research has shown that the globular end regions exhibit characteristics of a domain containing beta sheet structures (Parry and North 1998, Parry, Strelkov et al. 2007).

1.4.3 Keratin Intermediate Filaments (KIFs)

After the pioneering work of Astbury in the 1930's, a significant portion of the next 80 years in this area of research was dedicated to characterising the structure of KIFs and the way in which they arrange themselves within various mammalian keratinous structures such as hooves, hair, nails and quills (Rafik, Doucet et al. 2004). This was mostly carried out using fibre diffraction and electron microscopy techniques to examine the packing (distribution within material) and physical structure of the KIFs. Pioneers in this field were Fraser and MacRae who have written many papers on the structure of KIFs and on keratin tissues (Fraser and MacRae 1958, Fraser, MacRae et al. 1959, Fraser, MacRae et al. 1962, Fraser, MacRae et al. 1964, Fraser, MacRae et al. 1972, Parry, Fraser et al. 1979, Fraser and MacRae 1983). There has also been research into the chemical composition of the KIFs (Langbein, Rogers et al. 1999, L, MA et al. 2001).

KIFs are constructed from the aggregation of keratin dimers; dimers associate to form tetramers, and tetramers aggregate to form KIFs. There are four different modes of interactions between dimers which can form tetramers (Crewther and Parry 1977). It is unclear if there is a specific order of assimilation, but they are all thought to occur. The modes of association of the dimers are dependent on what types of amino acids are found in the protein sequences (Parry and Steinert 1995). Figure 1.10 shows the four modes of assembly of a keratin dimer to a tetramer described below.

- The A_{12} mode; defined by the anti-parallel overlap of IF dimers.
- The A_{11} mode; a mode of assembly defined by the anti-parallel overlap of 1B segments.
- The A_{22} mode; defined by the anti-parallel overlap of 2B segments.
- The A_{CN} mode; defined by the parallel overlap between the C-terminal end of the rod domain of one dimer and the N-terminal end of the rod domain of another dimer.

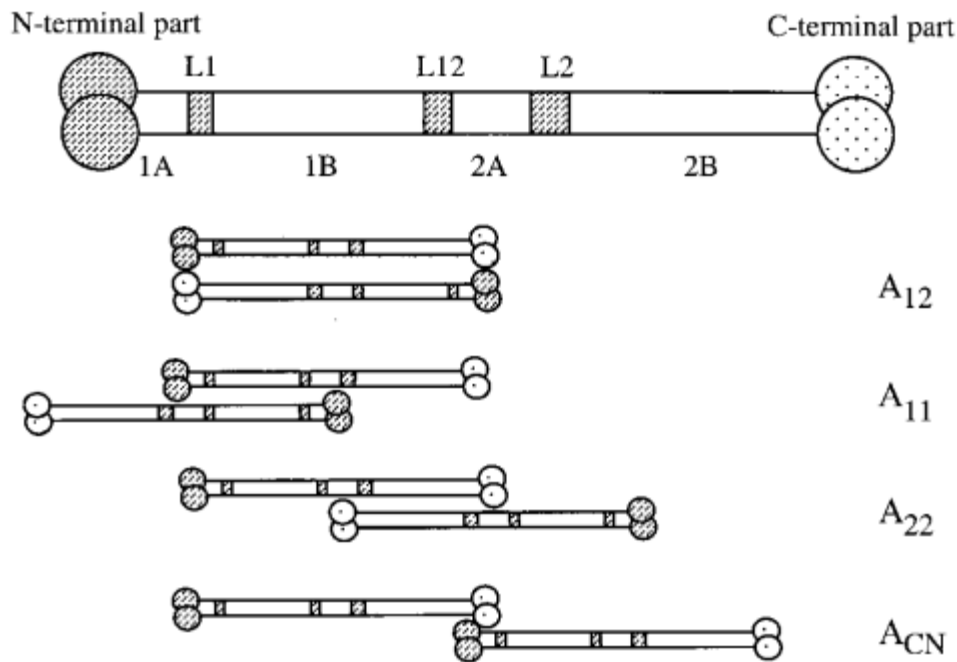


Figure 1.10 – A keratin dimer (as shown in Figure 1.9) and the four subsequent modes of association to form keratin tetramers. Figure adapted from (Kreplak, Franbourg et al. 2002).

Fraser & MacRae built a surface lattice model (Fraser and MacRae 1983) which described a way in which the tetramers arranged in a 2-d sheet are rolled up into a 3-D fibre to create a KIF (see Figure 1.11). This described the 6.7 nm meridional and 2.2 nm equatorial reflections seen in the small angle X-ray scattering (SAXS) images of KIF patterns. However, the 3-D structure of KIFs is still a matter of debate and other models to try and describe its structure including whether they form a ring or a ring + core structure have been formulated (Parry and Steinert 1995, Parry 1996, Briki, Busson et al. 1998).

The chemical signature of KIFs shows that the amino acid sequence of the central domain has a high homology (Geisler, Plessman et al. 1982, Dowling, Parry et al. 1983, Conway and Parry 1988). The differences between KIFs arise at the N and C terminal domains at either end of the central rod-like region in the form of the size and chemical nature of the domains.

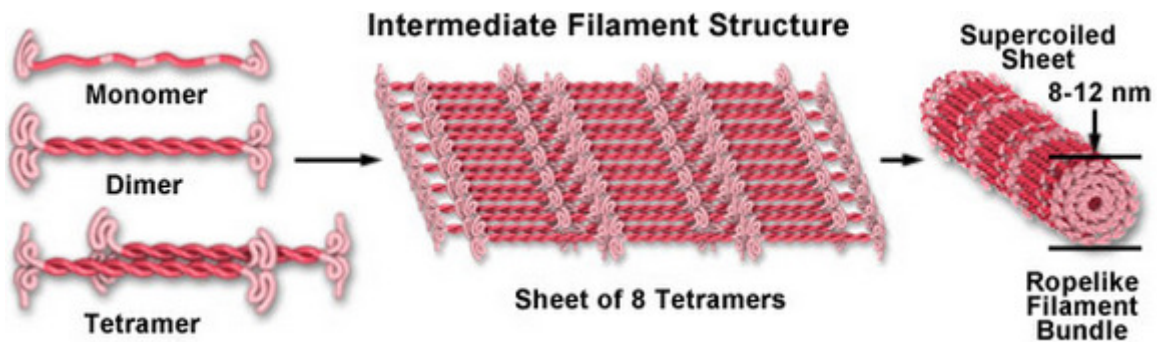


Figure 1.11 – One possible way in which the KIFs may be formed from the association of the smaller keratinous molecular structures which build a KIF (Davidson 2004) .

The central rod domain has a very low cysteine content (around 3%) whereas the N and C terminal domains in contrast show a high cysteine content (11-17%). This implies that the bonding between KIFs and/or KAPs is located at the terminal ends of the KIFs where disulphide bonding is more favourable (Parry and North 1998). Sequencing the N and C terminal domains has revealed repetitions in the amino acid sequences which led to the suggestion that the terminal domains have secondary structures which interact with both the rod domain and the matrix proteins (Parry and North 1998, Parry, Strelkov et al. 2007). The N terminal domains are proposed to have an alpha-helical structure whilst the C terminal exhibits a higher level of beta-sheet (Parry and North 1998).

The way in which KIFs are packed in hair (and other hard mammalian keratin tissues) has still not been fully characterised. Some models suggest KIFs laterally arrange themselves in a roughly quasi-hexagonal packing although this model does not seem to completely fit the experimental data (Rafik, Doucet et al. 2004). There is evidence for differences in the packing of the KIFs being dependent on the cysteine content of the KAPs found in the surrounding matrix (Fraser, MacRae et al. 1959). As such, there is still much research in this area to investigate KIFs and the way in which they arrange themselves and are distributed within hard mammalian tissues.

1.4.4 Keratin Associated Proteins (KAPs)

Keratin associated proteins (KAPs) are the non-fibrous proteins found in hair. There are a vast number of different KAPs grouped into various families (Langbein, Rogers et al. 1999). KAPs unlike keratin proteins are not highly ordered, they are thought to be globular in shape and have a high sulphur content and unpaired sulphur groups that allow them to construct disulphide bonds between other KAPs and KIFs (Parry and Steinert 1995).

When KAPs were discovered they were referred to as the matrix proteins, little information was known about either their structure or chemical composition. Advances in research have shown that the matrix proteins are a collection of a number of heterogeneous proteins which have now been grouped. They are divided into individual families based on their sequence and weight (Jolles, Zahn et al. 1997) and subdivided within their families based on their sequence homology and the nature of their repeat structures (Shimomura and Ito 2005).

The current nomenclature system proposed by Rogers and Powell (Jolles, Zahn et al. 1997) describes the KAPs as the following; KAPm.nxpL for the protein and KRTAPm.nxpL for the gene. 'm' denotes a family or unique protein, 'n' the component number, 'x' denotes a variant, 'p' corresponds to the pseudogene and 'L' stand for like. There has recently been a proposal to revise the nomenclature of the KAP proteins and genes due to advances in research on KAPs from other species and insight into genetic variation (Gong, Zhou et al. 2012). However, it is not yet clear whether the community has adopted the revised nomenclature.

There is limited information on the structure of KAPs, as there is no direct evidence on the native, isolated structure of any of the KAPs. They are thought to be globular in nature, deduced from the fact that it is unlikely that they are able to form alpha-helices as the amino acids they contain do not favour helix formation (Parry, Fraser et al. 1979). Due to the repeating nature of some of the amino acids present in their sequences, there is evidence that the KAPs form looped or folded structures, stabilised by intramolecular disulphide bonding (Parry, Fraser et al. 1979). Evidence has also been suggested that the KAPs may be roughly 2nm in size from XRD data of stained fibres (Fraser, MacRae et al. 1962) and from mechanical studies on wool (Spei 1975). It is not clear whether the signal from SAXS data corresponds to the amorphous nature of these proteins as there are contradictions in literature (Birbeck and Mercer 1956, Briki, Busson et al. 1998). Birbeck and Mercer (Birbeck and Mercer) proposed that the signal in the X-ray diffraction pattern came

from the cumulative effect of the filaments and matrix found in hair. However, Briki (Briki, Busson et al. 1998) later dismissed the concept of the small angle signal being related to the intermicrofibrillar origin and proposed that the signal contribution was from the intermacrofibrillar space and arises from randomly coiled polymers with a 3.3 nm dimension.

In contrast to the paucity of information on the structure of KAPs, the mechanical properties of KAPs as an interfibrillar matrix (i.e. not individually) are fairly well understood. KAPs found in hair behave much like a continuous hydrophilic gel (Shimomura and Ito 2005). In the presence of water, swelling of the matrix as a whole occurs giving rise to an increase in the inter-lateral spacing of the KIFs which has been observed and well documented (Feughelman 1959, Kreplak, Franbourg et al. 2002). The KAPs form up to 60% of the cortex volume while the KIFs make up the other 40% (Gillespie 1964). The majority of the bonds involved with KAPs are thought to be intramolecular (Parry, Fraser et al. 1979) although research shows that the KAPs are likely to have many disulphide bonds with the N and C terminal ends of the KIFs (Parry and North 1998, Parry, Strelkov et al. 2007).

Research regarding sequencing of the KAPs helped to develop information on some of their characteristics. There are many different KAPs that have been found and some are specific to the species of mammal (Jolles, Zahn et al. 1997). There are 27 KAP families at present with more than 100 different KAPs being isolated from sheep, mice, rabbits, rats and humans. Families 1 – 3, 10 – 16 and 23-27 are high sulphur KAPs; that is the KAPs found in these families contain 30% or less cysteine content and are typically 50 -75 kDa in weight. Families 4, 5, 9 and 17 represent the ultra-high sulphur KAPs (cysteine content above 30% and typical weight of 15-50 kDa) and families 6-8 and 19 – 22 are the high glycine-tyrosine KAPs (characterised by having a high quantity of tyrosine/glycine in their makeup and a typical weight of around 10 kDa). Of the 27 families of KAPs that have been discovered, 25 families of KAPs have been described in human hair (KAP 14 and 18 are only found in mice) (Rogers, Langbein et al. 2006).

Previous Classification	KAP families	Content	Weight (kDa)
High Sulphur	1,2,3,10, 11, 12, 13 14, 15, 16, 23, 24, 25, 26, 27	30% or less Cysteine content	50-75
Ultra -High Sulphur	4, 5, 9, 17	30% or more Cysteine content	15-50
High Tyrosine-Glycine	6, 7, 8, 19, 20, 21, 22	High quantities of Glycine and/or Tyrosine	~10

Table 1.1 – The KAP families, their content, their approximate weight and the old nomenclature associated with them.

Research has revealed there are genetic variations in three families of KAP genes; KAP1-n, KAP2-n and KAP4-n (where n denotes the component number) (Shimomura, Aoki et al. 2002, Kariya, Shimomura et al. 2005, Fujikawa, Fujimoto et al. 2012). The variations occur in the gene sequence which codes the cysteine-rich repeat sequences of the amino acids of some of the KAP proteins; these are size polymorphisms. Currently the size polymorphisms have only been studied in Japanese and Caucasian populations, and they may be due to intragenic deletion and/or duplication of sequences. The differences seen in the KAP genes between the two populations is thought to be a result of the divergence of the two populations during human evolution (Shimomura, Aoki et al. 2002). The KAP1-n family shows 7 size polymorphisms in the gene, the KAP2-n shows 5 and the KAP4-n family shows 13. It has been proposed that the size polymorphisms of KAPs may be a contributing factor in producing nanostructural variations inter-ethnically which may contribute to inter-ethnic macroscopic differences (Rogers and Schweizer 2005).

A number of *in-situ* hybridization studies have been carried out in order to identify where specific KAP gene families are expressed within the hair fibre (Rogers, Langbein et al. 2001, Rogers, Langbein et al. 2002, Rogers, L et al. 2004). Many of the KAP genes were found to be expressed in

different locations in the upper cortex of the hair fibre, with fewer being expressed in the cuticle and the matrix itself (Rogers, Langbein et al. 2001, Rogers, Langbein et al. 2002, Rogers, L et al. 2004, Rogers and Schweizer 2005). However, due to the difficulties associated with generating KAP specific anti-bodies for the proteins, at present it is unclear how accurately this method has mapped the location of specific KAP proteins in the hair fibre.

1.5 Keratinous molecular assemblies

Molecular assemblies found in human hair are built from the interaction of the keratinous and non-keratinous molecular structures (see Section 1.4.1 -1.4.4). Within these assemblies, both types of structures play a crucial role in creating the macroscopic properties of the fibre. The KAPs bind to themselves and the KIFs to create a matrix which holds the molecular structures together forming macrofibrils. In the cortex, the molecular structures combine to build macrofibrils, which in turn associate forming cortical cells. The cortical cells construct the cortex on the microscopic level, bound by the CMC. The cuticle has its own specific structure (see Section 1.3.1); cuticle cells are bound to each other and to cortical cells via the CMC. Structural lipids are present in the CMC and possess a bilayer arrangement; the lipids play an important role in the diffusion of water and other substances into the cortex of the hair fibre. The structural lipids are not a keratinous molecular assembly; they are a structural component that is present at the level of the keratinous assembly structures and shall be presented in this section.

1.5.1 Macrofibrils & Cortical Cells

Macrofibrils are formed from the aggregation of KIFs bound axially, immersed in the matrix of KAPs (Bouillon and Wilkinson 2005). These structures are approximately 0.1 – 0.4 µm in diameter and up to a few microns in length (Fraser, MacRae et al. 1972). They have a cylindrical structure and are bound together by a proteinaceous material sometimes referred to as the intermacrofibrillar matrix (IMM). The IMM is likely to be composed of remains from the initial cytoplasmic content of the cell before keratinisation, however there is very little information on the composition of the IMM available. The IMM also contains non-proteinaceous components such as nuclear residues and melanin pigments (Bouillon and Wilkinson 2005). Macrofibrils are

the primary components of cortical cells. Figure 1.12 shows an electron microscopy image of the cortex of the human hair highlighting the macrofibrils present and the IMM which binds them.

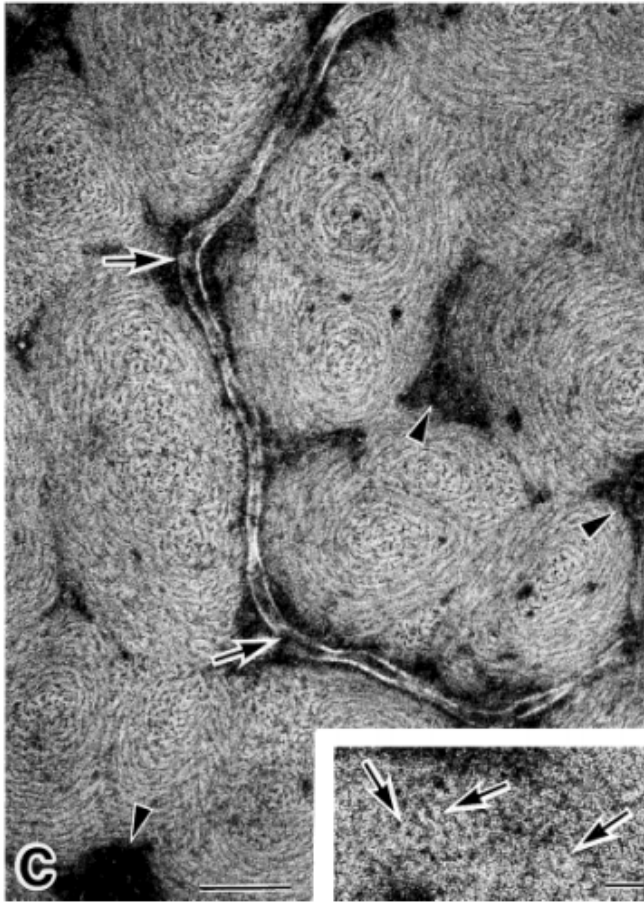


Figure 1.12 – A SEM image of the cortex of human hair at magnification of x120,000. The image shows a high magnification of the macrofibrils found in the cortical cells of human hair fibres. The arrows point to the IMM found in the cortical cells which binds the macrofibrils. Within the macrofibrils themselves, the KIFs are present, showing variation in the way in which they are packed inter-laterally within the macrofibrils. There are differences seen in the packing of the KIFs from the centre of the macrofibril towards the edges. The bar indicates 0.1 μm . The inset image shows a higher magnification image of the macrofibrils, the arrows in this image point towards the KIFs. The bar indicates a distance of 0.01 μm . Figure taken from (Takizawa, Takizawa et al. 1998).

Cortical cells make up the bulk of the cortex in the hair fibre, they are approximately 2 – 5 μm in diameter and can be 100 μm in length although there are large variations in the dimensions of cortical cells (Kidd 1965). Transmission electron microscopy (TEM) studies have revealed that

cortical cells are closely packed in the lateral plane, bound together by the CMC. In the axial direction they have a random phase distribution and are inter-locked through finger-like extensions protruding from them (Kassenbeck, Orfanos et al. 1981). They are held together by the CMC; the primary role of the CMC is to ensure cohesion between cortical cells but also for the cohesion of the cuticle cells to the cortical cells and the outside region of the cortex.

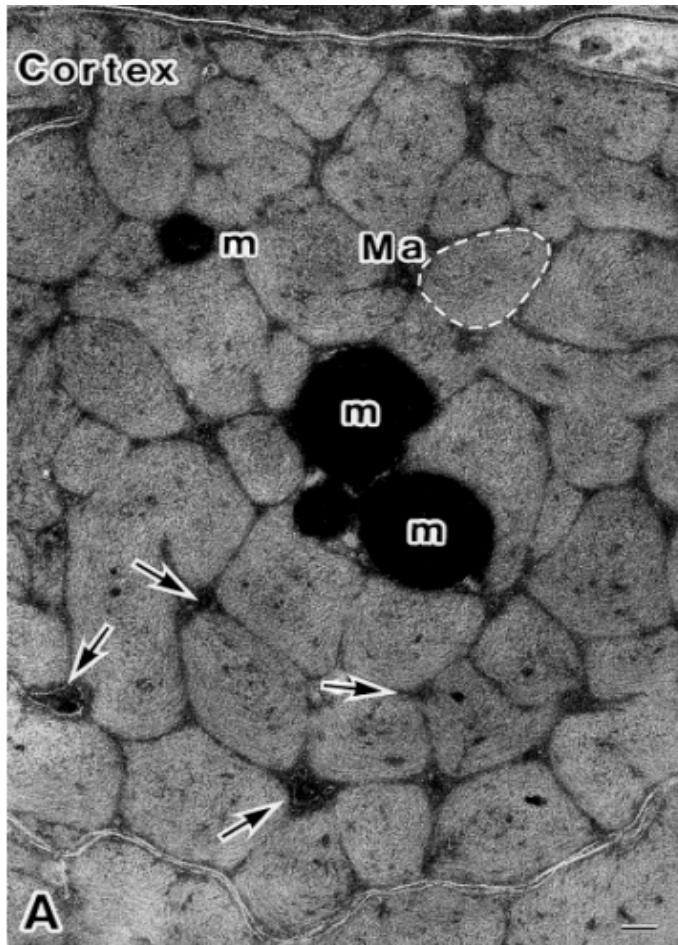


Figure 1.13 – A SEM image of human hair in the cortex region. At the top of the image the outline of a cuticle cell can be seen. The white dotted line, annotated by ‘Ma’ encloses a macrofibril, the arrows point to the IMM which surrounds and binds the macrofibrils together in a cortical cell. ‘m’ denotes the melanin granules that are also found in cortical cells. The bar at the bottom of the image shows a scale of 0.1 μm . Figure taken from (Takizawa, Takizawa et al. 1998).

The distribution of macrofibrils within cortical cells varies according to the type of cortical cell. This was first discovered by Swift (Kassenbeck, Orfanos et al. 1981) using TEM techniques. Swift reported that there are two types of cortical cells; the human orthocortical and human paracortical cell. The analogy of the orthocortical and paracortical cells arises from the comparatively well documented presence of these types of cortical cells in wool (Rogers 1959a, Rogers 1959b, Kaplin and Whiteley 1978, Orwin, Woods et al. 1984, Plowman, Bryson et al. 2000). In the human orthocortical cell, the macrofibrils are discretely observed, separated by the IMM. In contrast to this, the macrofibrils in human paracortical cells are closely packed, with very little IMM present (Kassenbeck, Orfanos et al. 1981).

In 2006 an X-ray scattering study was made using an X-ray beam of micron size to probe the cross section of different ethnic hair types containing curl (Kajiura, Watanabe et al. 2006), this also revealed information on some of the properties of the macrofibrils. Although, different ethnic hair types were used in the study for their different curl properties, it was reported that the cause of curl was the inhomogeneity of the nanostructure of the hair fibre, which was independent of the ethnic origin. The study reported that there were differences seen in the lateral packing of the KIFs across the hair fibre. The differences that were quantified in the study were the intensity profiles of the mean inter-lateral packing distance of the KIFs and the KIF radius. The orientation of the KIFs with respect to the fibre growth axis was determined using the Full Width HalfMaximum (FWHM) of the peak from an azimuthal integration of the equatorial intensity profile which gives information on the average tilt angle of the KIFs. They reported that the inter-lateral packing distance between KIFs was larger on the inside of the curl of a curly hair fibre than on the outside. They postulated that this provides evidence that the matrix component, i.e. the KAPs, have a larger volume on the inside of the curl than on the outside, thus increasing the inter-lateral distance of the KIFs. It was further reported that the curly hairs in the study showed a similar variation in the KIF inter-lateral packing dimensions as Merino wool (Kajiura, Watanabe et al. 2005) and helical tilt angles to that of Romney wool (Caldwell, Mastronarde et al. 2005).

A later study in 2009 using a combination of TEM, fluorescence microscopy and electron tomography confirmed the presence of different types of cortical cells present in hair samples from Japanese women (Bryson, Harland et al. 2009). Here, the study investigated the source of curl in hair fibres; they reported that lateral distribution of different types of cortical cells in the hair fibre make a significant contribution to the curl of the hair fibre. Four different types of

cortical cells, labelled A-D, were found in both the straight and curly hair samples; they are grouped based on the characteristics of the lateral distribution of the macrofibrils, the approximate volume of the IMM, presence of cytoplasmic remnants and the approximate KIF packing observed by TEM within the macrofibrils.

Type A cortical cells contain discrete, approximately circular macrofibrils well separated by a distinct and continuous layer of IMM. The lateral packing of the macrofibrils is described as relatively loose. The KIFs possess a hexagonal lateral packing arrangement and orientated approximately parallel to the hair fibre axis in the middle of the macrofibrils. Towards the edges of the macrofibrils, the KIFs are observed to have helical arrangements.

Type B cortical cells have closely packed macrofibrils with approximately circular or slightly elliptical shape; however, their size and shape shows more variation than type A cells. The macrofibrils appear as discrete structures separated by a thin layer of IMM and cytoplasmic remnants are present in approximately 15% of type B cortical cells. The KIF lateral packing is observed to be hexagonal near the centre of a macrofibril, then moving towards the peripheries of the macrofibril the KIF packing moves to a helical conformation and then towards a whorl-like arrangement.

Type C cortical cells are characterized by macrofibrils which are in direct contact or fused together without a separating layer of IMM, although IMM is observed at junctions between groups of macrofibrils. The macrofibrils are generally larger than those found in type A and B cells and a cytoplasmic remnant is centrally located in approximately 40% of the cells. The KIF arrangement in type C cells is diverse; they may contain hexagonally packed KIFs in helical arrangements, with whorl like outer regions as well which may also contain hexagonally packed KIFs with a close/loose formation.

Type D cortical cells were the least common cell types observed in the study. These cells were always observed to be adjacent to type C cells, contained large macrofibrils and large amounts of cytoplasmic remnants and IMM. Their KIF packing arrangement was reported to contain a similar mixture to that of the type C cortical cells.

Type A and type B cells produce the characteristics of the orthocortical cells and type C and D cortical cells the paracortical cells. In the cortex of the hair fibres, type B and C cells were

predominant over type A and D cells. In a straight hair fibre, the lateral distribution of ortho and paracortical cells was approximately even. However, in a curly hair fibre a predominance of orthocortical cells on the inside of the curl of the hair fibre was observed in combination with a predominance of paracortical cells observed on the outside of the curl. With reference back to the KIF arrangements found between the four types of cortical cells, this provides evidence for microfibrils containing helically arranged KIFs to be preferentially found on the inside of the curl of a hair fibre. Microfibrils with pseudo-hexagonal arrangements of KIFs are found on the outside of the curl of a hair fibre.

Using two different types of stains with preferential affinity to bind with specific KAPs, there were variations observed in the distribution of specific KAPs across the cross section of the cortex which is postulated to contribute to the hair fibre curl. KAPs with a high glycine/tyrosine content were observed with a higher frequency in the orthocortical cells, and KAPs with a high/ultra high sulphur content were observed more in the paracortical cells; this was similarly observed in wool (Plowman, Paton et al. 2007). Similarly a report on the amino acid content of curved human hair found higher amounts of cysteine on the outside of the curl and higher amounts of glycine on the inside of the curl (Nagase, Tsuchiya et al. 2008). It has therefore been postulated that KAPs may have a fundamental role in determining the KIF spatial arrangements in cortical cells (Bryson, Harland et al. 2009).

A review on the possible role KAPs play in determining the properties of cortical cells in wool and human hair fibres was presented in 2007 (Plowman, Paton et al. 2007). There has been subsequent work in Merino wool fibres which shows a preferential expression of high sulphur KAP in the paracortical cells which provides evidence for the notions inferred earlier (Plowman, Deb-Choudhury et al. 2009), however, at present, there has been no such study for human hair.

1.5.2 Cell membrane complex (CMC)

The cell membrane complex (CMC) consists of proteins and lipids and is distributed between the cortical cells, the cuticle cells and the cortex / cuticle cell interface (Swift and Holmes 1965). Its function is to allow cohesion between structures in the cortex and cuticle and is also postulated to play an important role in the chemical diffusion of substances into the cortex (Potsch and Moeller

1996, Kelch, Wessel et al. 2000, Gummer 2001, Masukawa, Shimogaki et al. 2005, Formanek, Wilde et al. 2006, Inoue, Iwamoto et al. 2007). Evidence on the structure of the CMC has mostly been obtained from electron microscopy (Swift and Holmes 1965, Leeder 1986, Masukawa, Shimogaki et al. 2005) although some XRD studies have been made (Kreplak, Merigoux et al. 2001, Inoue, Iwamoto et al. 2007). The CMC has been characterized between the cuticle cell layers; there are variations in the CMC within the cortex that make the CMC difficult to study in this region (Jolles, Zahn et al. 1997, Takizawa, Takizawa et al. 1998, Ohta, Oka et al. 2005). A comprehensive description of the CMC located in all regions of the hair was given by Robbins in 2009 (Robbins 2009). A basic schematic of the CMC of the cuticle interface has a sandwich like structure is seen in Figure 1.14; lipids of the β -layers are present on each side of the proteinaceous δ -layer.

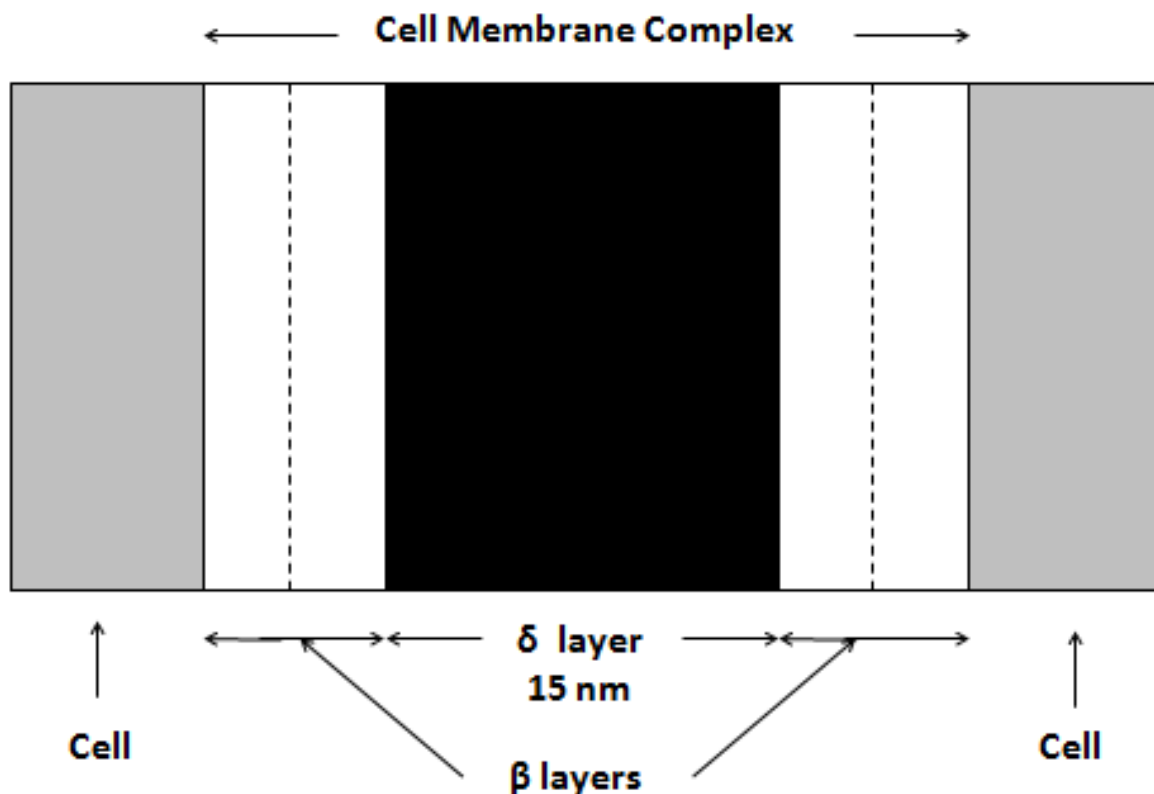


Figure 1.14 – Structure of the CMC between two cells. The two cells in the figure may indicate either cuticle or cortical cells. The δ -layer is defined by the black centre-most region and the β -layers lay either side of it, and include the epicuticle in this diagram. Figure adapted from (Bouillon and Wilkinson 2005).

The first X-ray study on the cuticle CMC (Kreplak, Merigoux et al. 2001) reported that the equatorial intensities attributed to the cuticle scattering from microbeam SAXS revealed a structure of approximately 20 nm in size and several other orders of 10, 7 and 5 nm respectively. By cross referencing the equatorial profile with TEM images of the hair taken from (Jolles, Zahn et al. 1997) the 20 nm structure was assigned to the CMC, with the other orders corresponding to the δ and two β layers. A later X-ray study on the CMC of the cuticle interface (Ohta, Oka et al. 2005) confirmed the previous findings and presented a more precise model for the estimation of the thickness of the δ and β layers. It also commented on how the variation in both the δ and β layers may affect the intensity modelling; the variation was proposed to be due to differences in cosmetic treatment or the lipids and protein composition present. A subsequent X-ray study on the effect of solvents on the CMC showed that solvents with hydrophilic characteristics had an effect on the δ layer and solvents with hydrophobic characteristics had an effect on the β layers (Inoue, Iwamoto et al. 2007). This provides evidence for the way in which hydrophilic molecules pass through the δ layer.

The lipids are thought to possess a bilayer structure based on evidence from the analysis of lipid extractions (Korner, Petrovic et al. 1995, Masukawa, Shimogaki et al. 2005). In the cuticle-cuticle CMC, the outer β layer (the layer on top of cuticle cells) contains 18-MEA (Jones and Rivett 1997, Kreplak, Merigoux et al. 2001, Robbins, Weigmann et al. 2004) and in the cortex-cortex CMC, this lipid is replaced by straight chain fatty acids (Robbins, Weigmann et al. 2004). The exact composition of the proteinaceous substance is still unknown; there are contradictions about its composition in literature. All literature reports its composition to be non-keratinous; some studies hypothesise it to exclusively contain glycoproteins (Allen, Ellis et al. 1991, Mitchell, Mifsud et al. 1992), however, other studies propose the δ layer to contain globular proteins (Robbins, Weigmann et al. 2004, Robbins 2009). The dimensions of the β -layers of the CMC are 2.5 – 4.0 nm thick and the δ -layer is 15-18 nm thick (Ohta, Oka et al. 2005) dependent on the origin of the source (Kreplak, Merigoux et al. 2001, Ohta, Oka et al. 2005).

The CMC in the cortex is continuous throughout this ultra structure (Jolles, Zahn et al. 1997) which is why it possibly plays such an important part in the diffusion processes of water and other substances in to the cortex of the hair fibre (Inoue, Iwamoto et al. 2007). A study using electron microscopy techniques showed that aqueous molecules were observed in the CMC and the cuticle at the same time, indicating different but complementary pathways of diffusion. Evidence was

found for a pathway from the CMC into the bulk of the cuticle, but not for a pathway across the bulk of the cuticle into the CMC (Gummer 2001).

Robbins presented a review which has given the most comprehensive description of the cortex and cuticle-cortex CMC to date (Robbins 2009), the cortex CMC, defined as the CMC layer between two cortical cells, has a different structure than the cuticle CMC. In the cortex CMC, the lipid 18-MEA is replaced by shorter chain fatty acids, which do not covalently bond with the cortical cell membrane. Instead, these fatty acids form salt linkages and polar bonds with the membrane and form bilayers. The bilayers are able to form because of the presence of cholesterol and cholesterol sulphates (Wertz, Abraham et al. 1986), there may also be ceramides present in the β layers. The δ layer is bound between the two β layers via the salt linkages and polar bonds at either side. It is likely that the δ layer composition is different to that of the cuticle CMC, due to the different bonding mechanisms (Robbins 2009).

A proposal for the structure of the cuticle-cortex CMC was also presented in Robbins' 2009 study (Robbins 2009). The structure is based on 'logic and supporting evidence'; currently there has been no experimental evidence to characterise this interface. The proposal for the structure is built from combining the models of the cuticle CMC interface with the cortex CMC interface. At present the only study that gives supporting evidence for this structure was a TEM study on the diffusion of uranyl dye (Leeder, Rippon et al. 1985). The study showed that two layers of dye were present in the cuticle-cuticle CMC, one layer was present in the cuticle-cortex CMC, and no dye was present in the cortex-cortex CMC, suggesting that the cuticle-cortex CMC is a composite of the cuticle and cortex CMC. In the model proposed by Robbins, the β layer which connects to the cuticle cell is thought to contain covalently bound fatty acids which are connected at their hydrophobic end to the δ layer below. The δ layer is proposed to contain a hydrophobic protein on the cuticle side in order for the cortex side to have a hydrophilic end which can form polar bonds and salt linkages with the fatty acids of the β layer below which would have the same characteristics as the cortex CMC; a fatty acid bilayer with ceramides and cholesterol sulfates present.

1.5.3 Lipids

The lipids found in hair originate from two different sources; cell membrane remains or sebum from the scalp. While some lipid is exclusively present in the cuticle region of the hair, there are other lipids within the cortex of the hair and in the medulla region (should this be present). Lipids compose two distinct groups in human hair; structural and surface lipids (Bertrand, Doucet et al. 2003), although they are sometimes grouped into endogenous and exogenous lipids. Endogenous lipids are defined as those present within the cortex of the hair fibre such as in the CMC. Exogenous lipids are those that have been secreted by the sebaceous glands (Coderch, Mendez et al. 2008).

Early work on the lipids present in human hair began with an approach into the chemical composition of the lipids that were extracted from hair and how it varies according to age, sex, individual and race (Nicolaidis and Rothman 1952, Nicolaidis and Rothman 1953, Krotoszynski, Gershbein et al. 1955). Later the development and realisation of infrared spectroscopy to analyse the chemical composition of lipids in specific zonal areas of the hair fibre (Akhtar, Edwards et al. 1997, Kreplak, Briki et al. 2001, Ackermann, Koster et al. 2008).

Lipids originating from the sebum excreted from the scalp contain a different composition; these lipids are comprised of triglycerides, fatty acids, wax esters and squalene (Downing, Strauss et al. 1969, Bertrand, Doucet et al. 2003). Initial studies on the lipids originating from sebum reported that the cholesterol content was over three times higher in young boys than in adult males, cholesterol content was similar between adult males and females and adults have a higher content of squalene than pre-pubescent boys (Nicolaidis and Rothman 1952). In a subsequent report on the chemical composition in regards to age, sex and race it was found that the largest differences in the percentage of fat per unit weight of hair was seen between pre-pubescent boys and men, and between white and black males. No significant differences were seen between sexes. It was reported that black males have up to 70% more hair fat per unit weight than white males and black women have up to 60% more hair fat per unit weight than white women. The composition of the hair fat (percentage of fatty acids and esterified acids) was shown to be very similar between white and black test subjects but the cholesterol content was found to be 25% lower in black subjects than in white subjects (Nicolaidis and Rothman 1953). This leads to

potential differences seen in the lipid content and composition between hair types of different ethnic origins.

The lipid present in the hair arising from the cell membrane source tends to be structural lipids that are found in the cell membrane complex (CMC) (see Section 1.5.2) and at the surface of cuticle cells (see Section 1.3.1). These lipids are free fatty acids, ceramides and cholesterol sulphates. The surface of the cuticle possesses a unique structural lipid; 18-MEA which is covalently bound to the outer layer of the cuticle (Wertz and Downing 1989, Bertrand, Doucet et al. 2003). In the cortex, 18-MEA is replaced by shorter chain fatty acids (Robbins, Weigmann et al. 2004, Robbins 2009).

The structural lipids found in the cortex of the hair appear in an organised state as observed from scattering experiments performed on hair (Fraser, MacRae et al. 1963). These lipids are present within the hair in a crystalline form and are thought to arise from the crystallisation of other molecules such as lipo-protein membranes and mitochondria after keratinisation (Fraser, MacRae et al. 1963). Scattering experiments performed on hair show that these lipid crystals have a periodicity within the cortex of approximately 4.5 nm (Bertrand, Doucet et al. 2003).

In 2003, Bertrand *et al* performed an experiment that stained the lipids present within hair with lead acetate (Bertrand, Doucet et al. 2003). By fixing heavy metal elements to the lipids in the hair, they conducted an X-ray diffraction (XRD) and X-ray fluorescence (XRF) experiment revealing higher orders of the lipid crystals in the samples. The higher orders of the lipids were revealed by the lead fixation to the lipid within the sample and gave rise to a number of lipid diffraction rings. They observed that the organised fraction of lipids within hair consisted mainly of fatty acid layers under a partial calcium soap form and that the first order of the 4.5 nm reflection corresponds to a C16 alkyl chain. The organised lipids in the hair had a preferential orientation; there was a strong orientation of the lipids to prevail around the hair axis.

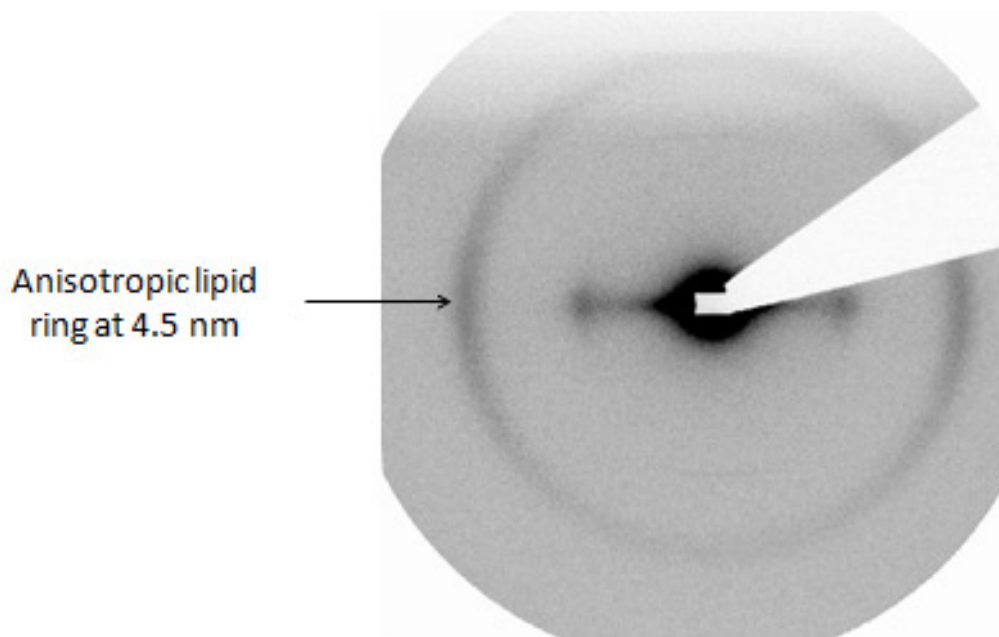


Figure 1.15 – A SAXS fibre diagram for a Chinese hair sample in the dry state. The fibre diagram illustrates the first order of diffraction of the crystalline lipid bilayer. The q range of the image is $0.01 - 2.0 \text{ nm}^{-1}$.

Advances in infrared micro-spectroscopy have allowed this technique to be utilised to probe across the cross section of a hair fibre to investigate the chemical composition. A study using this technique on Caucasian and Afro-American hairs reported that the Caucasian hair exhibited lipids localized inside the medulla and cuticle regions. It also reported that no lipid signal was seen for the Afro-American hair samples suggesting that this ethnic hair type showed no lipid across the cross section of the hair fibre. This is in contradiction to previous literature which reported that black males had 70% more hair fat per unit weight than white men (Nicolaidis and Rothman 1953). However, it should be noted that in the infrared study, the samples used came from girls and boys aged 8 and 10 years (Kreplak, Briki et al. 2001), and the biochemical study specifically detailed the differences among adults.

An X-ray study in 2008 used liposomes constructed from the lipids extracted from hair to create models for the lipid bilayers found in the CMC (Coderch, Mendez et al. 2008). They reported a 4.5 nm peak, which corresponded to a lamellar structure with second and third orders of 2.3 and 1.5 nm respectively. The structure did not show any capacity to retain water in its structure and therefore it is postulated that this bilayer is composed of non-polar lipid components. Considering

free fatty acids were the largest non-polar lipid components extracted from the endogenous source, it is suggested that this lamellar component is constructed from free fatty acids; this supports evidence from (Bertrand, Doucet et al. 2003). Another lipid structure was found with dimensions ranging from 7 – 10 nm. This structure was reported to be most likely composed from polar lipids such as ceramides, and possessed water retention capacity which may be the cause of the variation in its dimensions. It was also proposed that this lamellar structure is able to retain different amounts of water as a function of the lipid concentration. The evidence presented shows that the lipids found in hair at the CMC form two ordered lamellar structures depending on the type of lipid. The 4.5 nm lipid structure has hydrophobic properties and the 7 – 10 nm lipid structure has hydrophilic properties. The study also took data from the X-ray scattering of hair tresses under different humidity conditions; they reported that both the lamellar structures were found in the hair fibres with similar dimensions to that of the liposomes. The smaller lamellar structure had a 4.6 nm periodicity and was again reported to be unaffected by the relative humidity of the hair fibre. The larger lamellar structure also showed comparable characteristics within the hair fibre with respect to its liposomal form.

1.6 Ethnic variations in hair structure

Macroscopically, hair shows disparity between individuals, the most obvious is seen inter-ethnically. To date there have been very few studies into what causes this variation in hair structure at a nano and mesoscopic level. While there have been differences quantified between ethnic hair types, this has mainly focused on the chemical, geometric, morphologic and mechanical properties of the hair fibre as a bulk object (Menkart, Wolfram et al. 1966, Kamath, Hornby et al. 1984, Franbourg, Hallegot et al. 2003).

In 1966 a study made into the similarities and differences between wool, Caucasian and Negroid hair reported that the chemical composition between Negroid and Caucasian hair was very similar on the basis of amino acid analysis. The differences between the two hair types was only found to be in the hair fibre geometry with the Negroid hair showing a more twisted oval conformation compared to the cylindrical shape of the Caucasian hair (Menkart, Wolfram et al. 1966). A later study into the analysis of alkylated proteins extracted from various ethnic hair types reported that the amino acid composition was very similar between all hair types under test (Nappe and Kermici

1989). A study into the mechanical and fractographic behaviour (the way in which hair fibres fracture) of Negroid hair reported that the hair type had a lower tensile strength in comparison to other hair types and had a greater tendency to fracture at low levels of extension. This was postulated to be a consequence of poor cohesion between the cortical cells (Kamath, Hornby et al. 1984).

In 1988 a study of the composition of the low-sulphur fibrous keratinous proteins reported that the composition did not differ electrophoretically between ethnic hair types (Dekio and Jidoi 1998). A later study performed by the same group reported that the volume of fibrous proteins in relation to the volume of matrix proteins was found to differ between ethnic hair types. It was reported that on the basis of the ratio of fibrous protein to matrix substance or keratinous fibrous protein (KIF) to keratin associated protein (KAP) the Asian hair showed the largest ratio, the Caucasian the intermediate and the Negroid the lowest (Dekio and Jidoi 1990). There were few differences reported between the volumes of each respective proteinaceous substance extracted intra-ethnically. This implies that the macroscopic variation seen in ethnic hair types could be a direct cause of the volume of KAPs present within the hair type. The results also suggest that a hair type with more KIF proteins and less non-fibrous proteins (more KIFs, less KAPs) show a more cylindrical geometry and hair types that are more elliptical show the converse.

A study published in 2003 (Franbourg, Hallegot et al. 2003) on the geometric, morphologic and mechanical properties of hair quantified the differences seen in Asian, Caucasian and Afro hair types. This study mainly confirmed previous reports from earlier literature. It reported differences (or similarities) between these hair types on the diameter, cross section and shape of the hair fibre, the fibres mechanical properties, chemical composition and moisture content. In regards to the morphology of the hair fibre it reported that the Afro hair showed a high degree of heterogeneity in the diameter of the hair fibre and showed a high ellipticity in its shape which resembled a twisted oval rod. The Afro hair type also showed the greatest intra-ethnic variability in its ellipticity. The Asian hair had the largest hair fibre diameter and lowest ellipticity. The Caucasian hair was found to be an intermediate of the former hair types in regards to its diameter, cross-sectional shape and ellipticity, however, the Caucasian hair showed the largest intra-ethnic variability in its cross section. These findings are tabulated in Table 1.2.

Hair type	Diameter (μm)	Cross-sectional thickness	Ellipticity	Cross-sectional shape of hair fibre
Afro	45-120	Moderate to thick	1.75	Elliptical
Asian	35 – 125	Moderate to thick	1.25	Circular
Caucasian	30 – 100	Fine to moderate	1.35	Intermediate

Table 1.2 – The differences in the geometric and morphologic properties between ethnic hair types. Table adapted from (Franbourg, Hallegot et al. 2003)

The mechanical characteristics of each hair type reported in this study stated that the Afro hair had the lowest tensile strength, the Caucasian the highest and the Asian as an intermediate. The study also reported that the ethnic hair types showed negligible differences in their XRD patterns. However, it should be noted that no data was presented to support this and the analysis used to discriminate was not described. The study also made an investigation into the radial swelling, due to water, of the three hair types and reported that the Afro hair type showed a statistically significant lower swelling rate than the Asian and Caucasian hair types. They reported that the composition and structure of the hair types showed no inter-ethnic variation as determined by their X-ray analysis; they hypothesised that the difference in radial swelling may be due to the lipid content found in the hair.

In 2005 a TEM study into the distribution of the cysteine rich protein (KAP) distribution along the hair shaft in Asian, African and Caucasian hair reported that the distribution remained constant between all three hair types (Khumalo, Dawber et al. 2005).

In 2006 a study using microbeam SAXS techniques from lab and synchrotron sources were performed on Afro, Asian and Caucasian hair types to investigate the origin of curl in human hair. It was reported that the origin of curl, regardless of ethnic background, was found to arise from

the inhomogeneous distribution of the KIFs within the fibres. This variation is proposed to arise from different cortical cell regions; the ortho-like and para-like cortex arising from a similar analogy in wool where there are two types of cortical cells; ortho-cortical cells and para-cortical cells (Jolles, Zahn et al. 1997). More details on this study can be found in Section 1.5.1.

In 2013, a study into the lipids of differential ethnic hair types was published reporting the variation of lipid content on the basis of total extracted lipid content and composition, the X-ray diffraction signal from lipids present and confocal and fluorescence microscopy (Cruz, Fernandes et al. 2013). In addition to this the study also used molecular dynamics simulations to build models of the lipid interactions with keratin in the hair fibres. The study used three ethnic hair types; Asian, Caucasian and Afro. It reported that the overall content of extracted lipids from the Asian and Caucasian hair types were similar; 2.07% and 2.05% respectively, but the Afro hair type showed a larger quantity 3.5%. This corresponds to a 70% higher lipid content in the Afro than the Asian and Caucasian hair types in this study. This supports evidence from (Nicolaidis and Rothman 1953) which stated that black males had more hair fat than white males. The distribution of lipid composition was reported to be similar amongst the three hair types; the largest differences in distribution seen were in the content of cholesterol esters, ceramides and cholesterol sulphate content. The higher percentage of lipids found in the Afro hair type in this study was implied to be related to the lower hydration properties reported in (Franbourg, Hallegot et al. 2003).

The study also reported differences between the hair types based on the X-ray analysis. It was reported that the Afro hair type did not show reflections corresponding to the alpha-helical coils, or the coiled coil conformations. This contradicts (Franbourg, Hallegot et al. 2003) which stated that no structural differences were seen between the three hair types from X-ray diffraction analysis.

The study further reported that several orders of reflections were seen that must correspond to the lipids within the hair fibres, as they were absent after lipid extraction of non-covalently bound lipids using various chloroform:methanol solutions. These orders had spacings of; 3.7 Å, 4.1 Å, 5.0 Å and 15.0 Å; all of which indicate that the lipid signal arises at the inter-atomic scale. These are reported by the author to be related to the lipid present in the hair; however it should be noted that these do not correspond to lipid reflections observed or reported in any other previous literature. The absence of meridional reflections in the Afro hair type was suggested to be due to

the interference of free internal lipids with the keratin structure; this was enabled by the higher concentration of lipids found in the Afro hair type. Molecular dynamics simulations were used to model the interaction of a free fatty acid molecule with the keratin structure. In addition to this, both confocal and fluorescence microscopy were used to look for the lipid distribution in the three hair types. All three hair types showed a polar region around the cuticle corresponding to the high concentration of 18-MEA in this region. The absence of any other polar regions which would have been highlighted from the fluorescent dye, was implied to be an effect of the inability of the lipids to form polar aggregates in the cortex. It was stated that the lipids must be able to freely interact with the keratin structure which supports the X-ray diffraction data presented in this study.

1.7 Hypothesis

From the review presented in this chapter, it can be seen that there are certain areas of this research field that merit further investigation. It has been shown over many studies that the chemical composition of the KIFs in human hair fibres remains invariant, through both their electrophoretic patterns (Dekio and Jidoi 1998) and from biochemical analysis (Dowling, Parry et al. 1983, Conway and Parry 1988, Parry and Steinert 1995). It is therefore logical to assume that the origins of the macroscopic variations between ethnic hair types are not a result of gross compositional differences seen in the KIFs. From the evidence presented in Sections 1.4.4, 1.5.1, 1.5.3 and 1.6 it is likely that the cause of the macroscopic variation is due in part to the non-keratinous components of the hair fibre that modulate and augment the fibrous structure. It has been shown that there are differences in both the volume of KAPs inter-ethnically (Dekio and Jidoi 1990) and also the type of KAPs in the form of size polymorphisms (Shimomura, Aoki et al. 2002, Kariya, Shimomura et al. 2005, Fujikawa, Fujimoto et al. 2012). It has also been previously suggested that the size polymorphisms of KAPs may relate to inter-ethnic macroscopic variance (Rogers and Schweizer 2005). The studies presented in Section 1.5.1 show how variation in the volume of KAPs and the way in which they are distributed to augment the KIFs within cortical cells creates variation in the type of cortical cells found within the cortex and how this relates to the macroscopic properties (Kajiura, Watanabe et al. 2006, Bryson, Harland et al. 2009). The lipids are also suggested to make a significant contribution to the properties of the hair fibre. The studies presented in Section 1.5.3 discuss how the lipid types vary among age, sex and race (Nicolaidis

and Rothman 1952, Nicolaidis and Rothman 1953, Krotoszynski, Gershbein et al. 1955), and also in their structural form found within different locations within the hair fibre (Kreplak, Briki et al. 2001, Bertrand, Doucet et al. 2003, Coderch, Mendez et al. 2008, Cruz, Fernandes et al. 2013). Although there have been few studies which attempt to relate how the variation of lipids specifically relates to variation in the bulk fibre properties (Franbourg, Hallegot et al. 2003, Coderch, Mendez et al. 2008, Cruz, Fernandes et al. 2013), it should be pertinent that the lipids play a crucial role in the behaviour of hair fibres. Combining the above discussion points with that of the discussion points in the ethnic variation section (see Section 1.6), the following hypothesis can be made in regards to the origins of the structural differences found in ethnic hair.

The origins of the structural disparities lay at the nanostructural level beginning with the KAPs. As there is evidence that the KIFs are approximately homogeneous, but that the KAPs are heterogeneous and that they show size polymorphisms inter-ethnically, it is reasonable to suggest that this may be a basis for variation. The variation in distribution (Rogers, Langbein et al. 2001, Rogers, Langbein et al. 2002, Rogers, L et al. 2004, Rogers, Langbein et al. 2006), volume (Dekio and Jidoi 1990) and type of KAPs (Shimomura, Aoki et al. 2002, Kariya, Shimomura et al. 2005, Fujikawa, Fujimoto et al. 2012), which has been evidenced, contributes to producing a variation in the macrofibrils (Bryson, Harland et al. 2009), which in turn cumulates to produce variation in cortical cells (Kajiura, Watanabe et al. 2006, Bryson, Harland et al. 2009). This could be one way in which inter-ethnic variance may arise. Another way could be due to the difference in the lipid content of the hair fibre. It has been suggested in (Franbourg, Hallegot et al. 2003) that the radial swelling under hydration conditions is a direct result of the variation in the lipid content present between ethnic hair types. It has also been shown that different types of lipids present in hair have a different affinity for water (Coderch, Mendez et al. 2008) and that there are variations in the type and volume of lipids present among persons of differential age, sex and race (Nicolaidis and Rothman 1952, Nicolaidis and Rothman 1953, Krotoszynski, Gershbein et al. 1955).

In conclusion, I hypothesise the origins of inter-ethnic variation to be due, at least in part, to the non-keratinous components of the hair fibre. The project objectives found in the following section outline how this hypothesis shall be tested.

1.8 Project Aims

The work outlined in this thesis aims to investigate and develop the current knowledge of the structure of ethnic hair types. Ethnic hair types show a clear macroscopic difference in their appearance inter and intra-ethnically. Currently no studies have elucidated if this is due to the variation of the hair at the nano, molecular and sub-molecular levels. This study aims to examine the nano, molecular and sub-molecular structures found in ethnic hair types to investigate the basis for their macroscopic differences.

1.9 Project Objectives

This thesis sets out to qualify differences between ethnic hair types over several levels of scale using a combination of analytical techniques. The project objectives were to perform:

- a bulk fibre X-ray scattering analysis on ethnic hair types to determine if differences in the structure at the nano and supramolecular scales relate to the hair fibre as a whole.
- microfocus X-ray fibre diffraction to analyse and identify local structural variations across the hair fibre between ethnic hair types and quantify differences found.
- attenuated total reflection fourier transform infrared (ATR-FTIR) spectroscopy to identify and characterise the chemical composition of the hair types to reveal any variation seen between hair types at the cuticle surface of the hair fibre.
- a biochemical analysis of the lipids extracted from hair fibres to identify any variation in the lipid content between ethnic hair types.
- an X-ray solution scattering experiment to elucidate the shape, volume and tertiary structure of a keratin associated protein (KAP).

1.10 Summary

In this chapter an overview of the structure of hair and the methods and techniques used to analyse the structure has been presented. It has also provided a review of the current scientific research in regards to quantifying the structural variation of ethnic hair types. Although, there is a vast quantity of further scientific research being conducted on hair care and cosmetic science, it is

only the work that has been presented in this chapter that relates to this area of research exclusively in a structural context.

X-ray scattering techniques have proven to be a valuable resource in analysing the structure of hair at the nanoscopic scale. In subsequent studies the structural properties of hair will be analysed using an inter-disciplinary approach in an attempt to characterise various molecular components that contribute to the hair fibre.

Chapter 2 – Techniques

2.1 Introduction

This chapter gives an overview of the techniques used in this thesis. Both X-ray scattering and infrared spectroscopy exploit the interaction of electromagnetic radiation with matter in order to gain structural information on the sample. This chapter will examine how the techniques of X-ray scattering and infrared spectroscopy can be used to analyse the structure of hair. In addition to this, this chapter will present a basic overview on the concepts of high performance liquid chromatography (HPLC) and ultra performance liquid chromatography (UPLC), thin layer chromatography (TLC), gas chromatography (GC) and mass spectrometry (MS). These chromatography techniques have been used in this thesis to separate and analyse lipids extracted from hair.

2.2 Electromagnetic Radiation

Electromagnetic radiation is a form of energy that arises from the propagation of charged particles moving in a magnetic field, or the converse. Electromagnetic radiation has magnetic and electric charge components that oscillate in phase perpendicular to each other, and orthogonal to the direction of propagation. In a vacuum the speed of all electromagnetic radiation is equal to the speed of light. An overview of part of the electromagnetic spectrum with corresponding energies and frequencies is given in Figure 2.1.



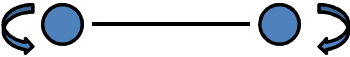
	Frequency (Hz)	Energy (kJ/mol)
γ-rays		
X-rays	10 ¹⁸	120000000
		
	Bond breaking & ionisation	12000
UV	10 ¹⁶	310
Visible		150
Near Infrared	10 ¹⁴	
Mid Infrared		
Far Infrared	10 ¹²	0.12
		
	Vibration	
Microwave	10 ¹⁰	0.0012
Radio	10 ⁶	
		
	Rotation	

Figure 2.1 – Schematic showing a part of the electromagnetic spectrum with the corresponding frequencies and energies of the radiation.

2.3 X-ray Scattering

X-ray scattering is an analytical technique which exploits the interaction of electromagnetic radiation of an X-ray wavelength (0.01 – 10 nanometres) with matter (i.e. the sample).

Information on the structures of materials can be obtained by analysing the resulting diffraction patterns arising from the re-emitted radiation from materials that have been subjected to X-ray radiation. A simple set of physical rules is applied to study all kinds of materials on a nanoscopic level with X-rays.

Most of the data has been collected using small angle X-ray scattering (SAXS) methods, this section contains the basis of the theory of both XRD and SAXS; XRD is the situation of scattering under specific conditions. SAXS has been used as the main technique for data acquisition as it is a non-invasive technique which is quick and easy to use and provides information on the structure of materials at the nanoscale. The X-ray sources used were generated from the 3rd generation synchrotron; European synchrotron radiation facility (ESRF) in Grenoble. An overview of the principles governing XRD, SAXS and the means of producing X-rays in synchrotron sources is presented.

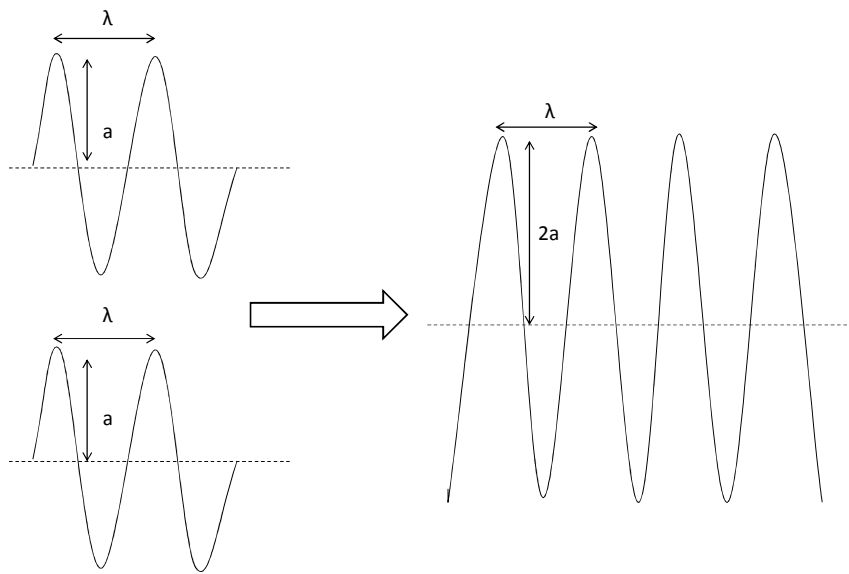
X-ray diffraction works on the principle that X-rays passing through a material will interact with the electrons in that material and excite them. For the electron to return to its unexcited state, it must release energy in the form of a photon. If the interaction between the X-rays and the electrons is elastic the emitted photons will have the same wavelength and frequency as the incident X-rays. The result is that no net energy is transferred to the electron itself. Therefore the emitted photons will have a phase relationship with other photons and can therefore interfere both constructively and destructively due to the path difference that they travel from the electrons which scatter them inside the material. This is referred to as coherent scattering. Incoherent scattering (inelastic scattering) occurs when the incident photons collide with electrons causing a loss of energy. The loss of energy in the photon causes the wavelength of the emitted photon to increase. In a crystal or crystalline materials, the cumulative effect of coherent scattering arising from the regular crystalline array gives rise to a much higher intensity than incoherent scattering, and so only coherent scattering shall be considered here. In crystals, the intensity of coherent scatter is so high due to the regular array that under these conditions scattering becomes diffraction; these conditions are given by Bragg's Law.

2.3.1 Bragg's Law

A crystal is a regular array of atoms within a material showing regular order in all three dimensions. Examples of common crystals are diamond, quartz and sodium chloride. Crystals can be described by a set of repeating unit cells that build up its structure. A unit cell is defined as the smallest possible volume that when repeated is representative of the entire crystal. A unit cell is defined by three dimensions and three angles; these are (a, b, c) and (α , β , γ) respectively. If a crystal can be described as an accumulation of unit cells then the structure of crystals can be described by associating lattice points with groups of atoms within the crystal. In crystallography, groups of atoms are called the basis, and the addition of the basis and the lattice points when repeated in real space forms the crystal structure. In the simplest case the crystal can be thought to possess rows of atoms, so there may be a row of atoms that lie below each other in the same plane; this is important when considering the principles for diffraction as explained by Bragg's Law.

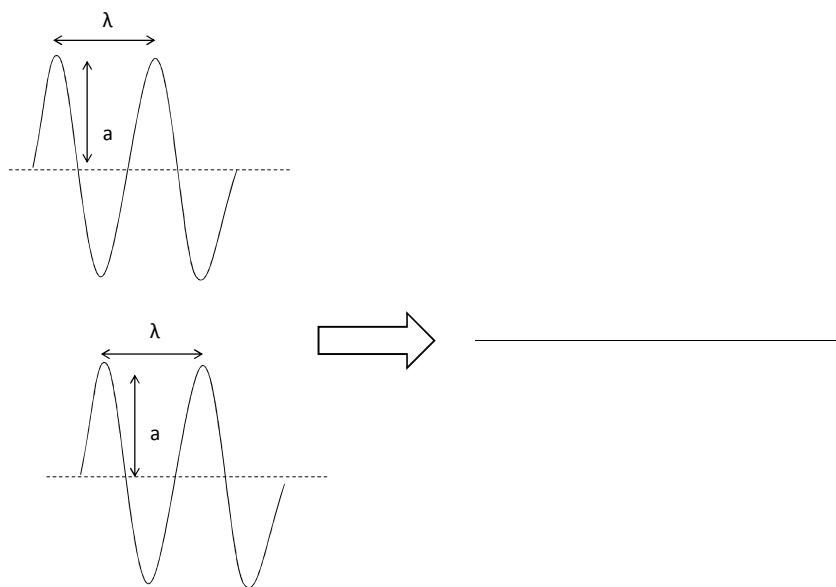
In a crystallography experiment a monochromatic beam of X-rays interacts with a crystal and the X-rays cause the electrons surrounding the atoms within the sample to become excited and oscillate. Not all of the electrons will be at the same distance from the X-ray source and therefore the photons emitted will not all be in phase with each other creating interference.

If the photons emitted from the material are out of phase they will undergo destructive interference. In the extreme case this causes no photons to be detected and so this contribution from the crystal goes undetected. This determines that the electrons in this part of the material show no degree of crystallinity. However, under very specific conditions, the photons emitted from the material will interfere constructively and will be detected contributing to the resulting diffraction pattern. This contribution to the diffraction pattern relates to regularity or crystallinity of the material under test. The specific conditions under which this happens are described by Bragg's Law. A diagram outlining the basis of constructive and destructive interference is seen in Figure 2.2.



(a) Constructive interference

Crests and troughs superpose



(b) Destructive interference

Crests and troughs cancel

Figure 2.2 – A diagram outlining the basis of (a) constructive interference and (b) destructive interference from the theory of wave superposition.

For all electrons in a row of the crystal, the path length from the source to the detector is the same, the angle of incident radiation is the same as the angle of scattered radiation resulting in

the waves both having the same path length. For scattered radiation in rows below to have the same path length to be in phase with each other, the path length must be equal to an integer number of wavelengths. From Figure 2.3, it is seen that the total path length difference that the wave has travelled when striking the electron on the second row is equal to $2d\sin\theta$. This is known as Bragg's condition for constructive interference.

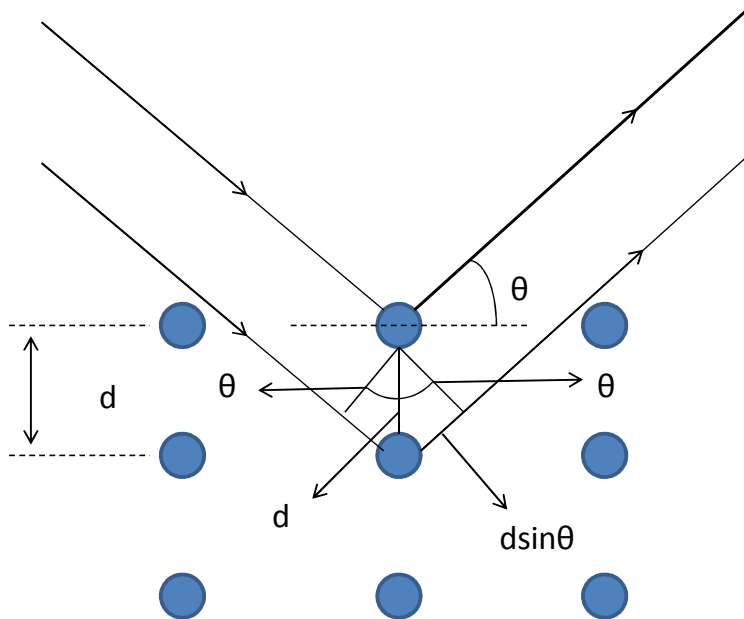


Figure 2.3 - A diagram visually outlining the basis from which Bragg's Law is drawn.

Figure 2.3 shows two separate X-ray waves arriving into different points of the crystal lattice. By using simple geometry it is seen that the path difference travelled for constructive interference must be equal to $2d\sin\theta$. Adapted from (Delta 2010).

$$2d\sin\theta = m\lambda$$

Where m is an integer ($m = 1, 2, 3, \dots$) λ is the wavelength, d is the spacing of the material and θ is the angle.

In three dimensions, Bragg's Law can be extended; for constructive interference to occur the planes of electrons found in the crystal must obey Bragg's Law to produce constructive interference.

When X-rays are scattered by an electron, diffraction patterns are observed if the photons that are emitted obey Bragg's Law. Diffraction patterns provide information on the structure of the material that the X-rays have interacted with. The position where the scattered X-ray hits a detector in relation to the incident X-ray beam can be used to calculate structural features of the sample. The X-rays that are generated hit a sample and are scattered at a variety of angles. As the detector is moved further away from the sample only X-rays with smaller angles of incidence are observed. This principle is used to see diffraction relating to different structural features of a sample. Figure 2.4 shows a simple illustration of an X-ray diffraction setup.

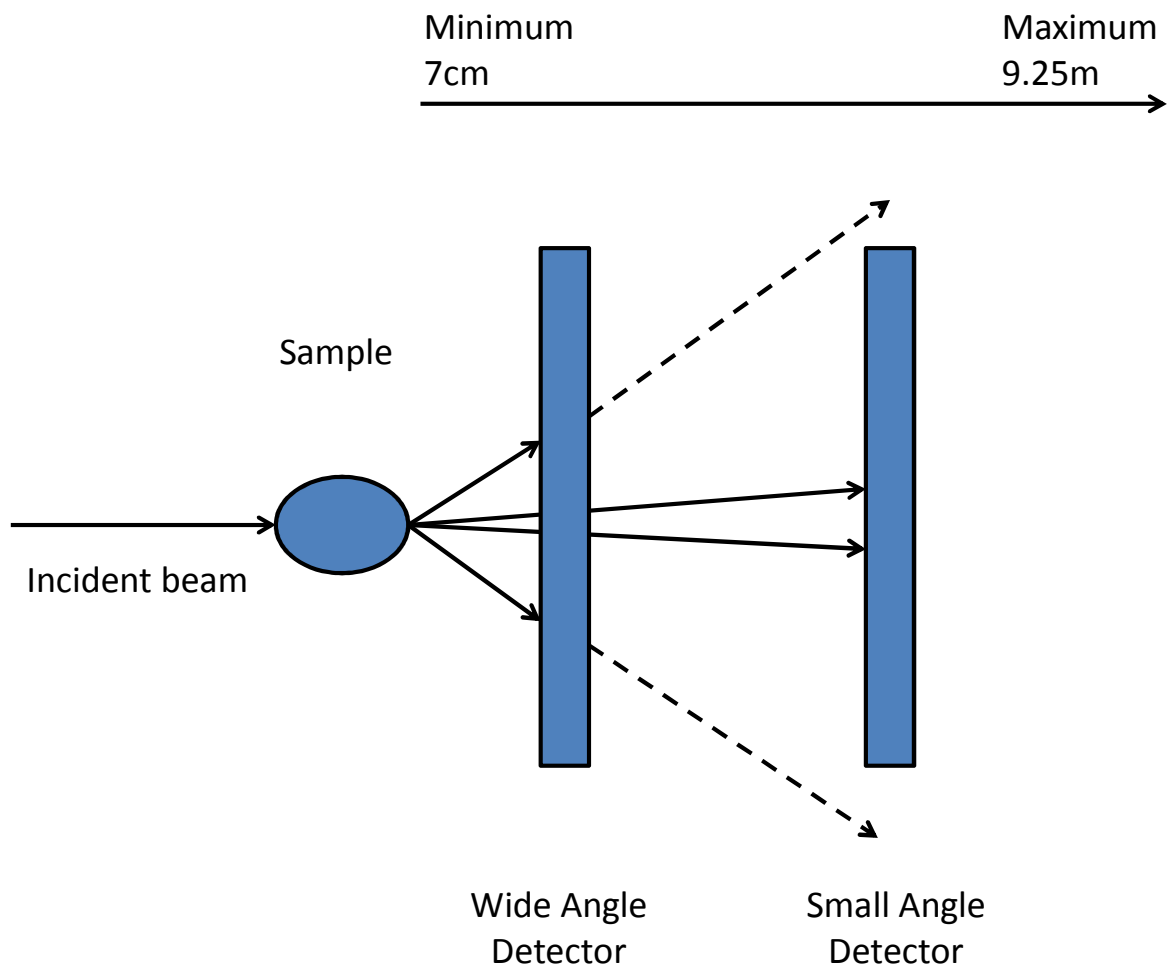


Figure 2.4 - Illustration of an X-ray diffraction setup. As the detector is moved further away from the sample only smaller angles are detected. The dotted lines show that the wide angle information is missed when the detector is placed at a longer distance from the sample. The small angle signal is compressed into a smaller space when the detector is at a shorter distance from the sample; this reduces the resolution of the small angle signal. The operational distance for wide angle X-ray scattering is between 7cm and 50 cm. The operational distance for small angle X-ray scattering is between 1- 9.25 m. However, these distances are dependent on the instrumental setup and the wavelength of the light.

Diffraction only occurs when the X-rays interact with materials that show some degree of crystallinity, however, all objects will scatter X-rays and scattering is thus the result of partial

phase relationships of the photons emitted from electrons in the sample. Scattering occurs when X-rays are scattered from non-perfect crystalline structures; these structures may have lost their crystallinity through increases or decreases in thermal motion or changes in atomic structure. Amorphous solids and liquids can give rise to X-ray scattering; these are referred to as disordered systems, structures with perfect crystallinity are called ordered systems. Large fibrous proteins often contain crystalline segments and can thus produce diffraction patterns. The molecules that build up these fibrous proteins often aggregate to form macromolecules that can be very large (of the order of hundreds of nanometres) and thus diffract X-rays at small angles. The intensity of diffraction is dependent on the degree of crystallinity in the material, and in many fibrous containing materials, there is often a greater degree of crystallinity in the axial direction parallel to the fibre axis, and a much smaller degree of crystallinity in the direction perpendicular to the fibre axis; this is referred to as partial order. There is therefore a preferred alignment in a fibre in order for certain diffraction features to be seen, a slight tilting of the fibre in a direction off axis (in the axial direction) will reduce the intensity of the diffraction features seen. Mounting the fibre perpendicular to the fibre growth axis reveals a different diffraction pattern altogether.

2.3.2 Small angle X-ray scattering (SAXS)

Small angle X-ray scattering (SAXS) is a well established technique for the investigation of non-periodic structures with colloidal dimensions; particles of dimensions 1-1000 nm. SAXS occurs when the dimensions within the sample become very large compared to the wavelength of the X-rays, the angle of incidence of the radiation becomes smaller until a small angle scattering situation is reached. The scattering process that takes place is due to electron density inhomogeneities within the sample. Any SAXS experiment can be defined by a reciprocity law; there is an inverse relationship between the particle size within the sample and the scattering angle (Glatter and Kratky 1982).

2.3.3 Fibre Diffraction

In biological science there are largely two distinct areas that involve the use of X-rays for material analysis; macromolecular crystallography and fibre diffraction. Protein crystallography subjects

crystalline proteins to X-rays for diffraction experiments. However, biological materials that contain larger biological macromolecules can be difficult to crystallise, thus it is often more useful to use SAXS. Where XRD is commonly used to study crystals, SAXS is commonly used to study materials that have larger constituent molecular structures (in the range 1-1000 nm) that often contain partially ordered crystalline structures. Figure 2.5 shows a schematic of the experimental setup of a fibre diffraction experiment.

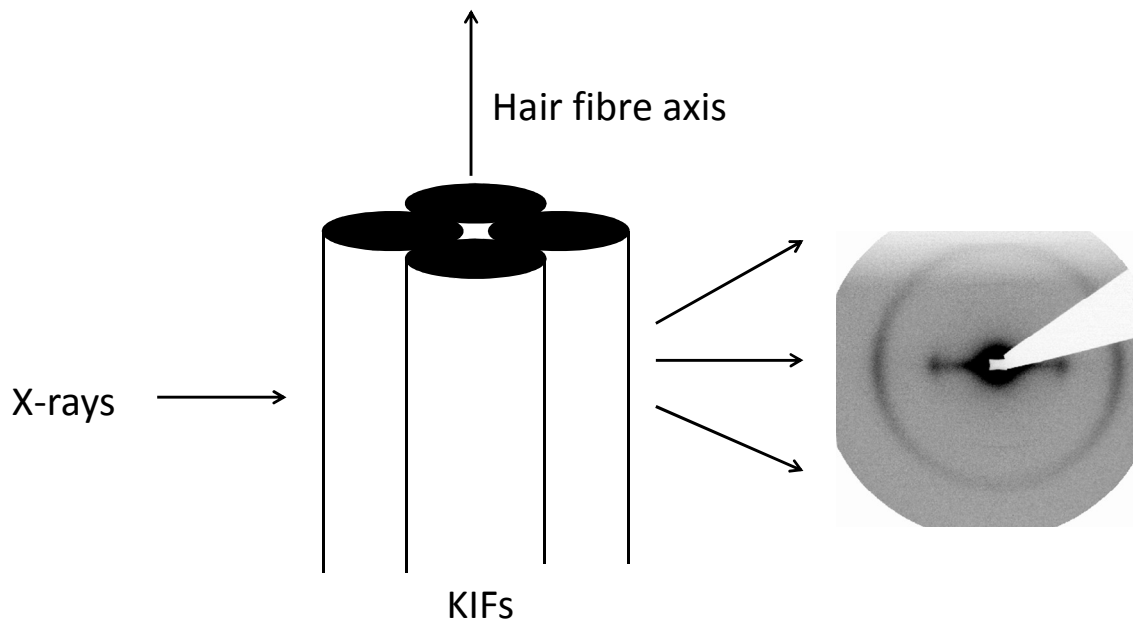


Figure 2.5 – Example of how biological materials with larger macromolecules present with partial crystalline order in the direction of fibre axis leads to fibre diffraction. The fibre diagram shown in this image is for the Chinese hair type in the dry state. The q range of the image is $0.01 - 2.0 \text{ nm}^{-1}$.

2.3.4 Small angle X-ray scattering of human hair fibres

Human hair fibres are partially ordered semi-crystalline fibre structures. They show crystalline order in the axial direction due to the aggregation of the hierarchical keratinous fibrous structures as described in Sections 1.4.1 –1.4.3. However in the direction perpendicular to fibre axis growth, human hair fibres show much less order, the lateral packing arising from the KIFs gives rise to the diffraction in the meridional orientation. In the small angle region (q range $0.01 - 2.0 \text{ nm}^{-1}$) information can be obtained on the supramolecular arrangements and the interfaces between the

structures. Order seen in the axial direction gives rise to reflections in the meridional region of a fibre diagram (diffraction pattern) and order seen in the lateral direction gives rise to reflections in the equatorial region of a fibre diagram. The scattering contributions to the fibre diagram arising from the fibrous structures within human hair are:

The broad equatorial interference peak that lies between $0.6 - 0.8 \text{ nm}^{-1}$ from the local interaction between the roughly cylindrical KIFs, this corresponds to an inter-lateral packing dimension of approximately 9 nm.

A low intensity but sharp meridional peak at $q = 0.93 \text{ nm}^{-1}$ corresponding to the 6.7 nm axial stagger of the 7th order of the 47 nm longitudinal axial pseudo-period resulting from the packing of keratin coiled coils into a KIF (Fraser and MacRae 1983). This is in part coupled to the 0.515 nm arc reflection in the wide angle region.

The low angle diffuse scatter in both the meridional and equatorial region in a q range of $0.01 - 1 \text{ nm}^{-1}$. High intensity diffuse scatter surrounding the beam stop is thought to correspond to the amorphous/disordered material found in hair fibres and the interfaces between the supramolecular structures.

There is also sometimes a contribution to the fibre diagram from lipids contained within the sample. An anisotropic lipid reflection is variably seen; this arises from the lipid crystals located in the hair fibre and gives rise to the intense reflection seen in Figure 2.6. The crystalline spacing of the lipid is approximately 4.5 nm (Bertrand, Doucet et al. 2003).

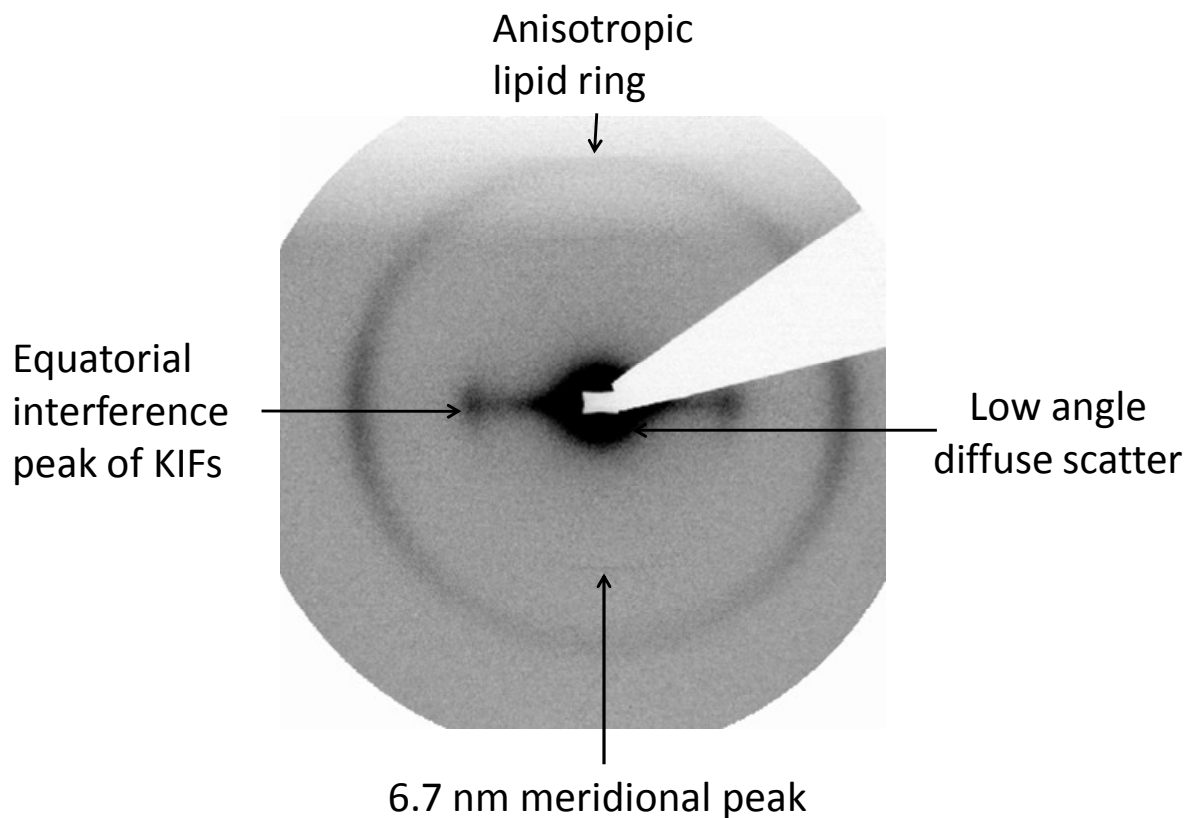


Figure 2.6 – Fibre diagram in the SAXS region highlighting the scattering features observed from a hair fibre. The image shown here is for the Chinese hair type in the dry state. The q range of the image is $0.01 - 2.0 \text{ nm}^{-1}$.

2.3.5 Wide angle X-ray scattering of human hair fibres

Wide angle X-ray scattering (WAXS) is where scattering occurs at a higher angle than that of SAXS. WAXS provides information on the sub-molecular structure of the sample. Human hair produces a fibre diagram characteristic of an alpha-helical protein coiled coil structural conformation modulated and augmented by other hierarchical and structural molecular associations in the wide angle region. Figure 2.7 shows a WAXS fibre diagram for human hair. In the wide angle region exhibited here (q range $0 - 20 \text{ nm}^{-1}$) there is an intense but narrow reflection on the meridian at 12.2 nm^{-1} which corresponds to a real space dimension of 0.515 nm .

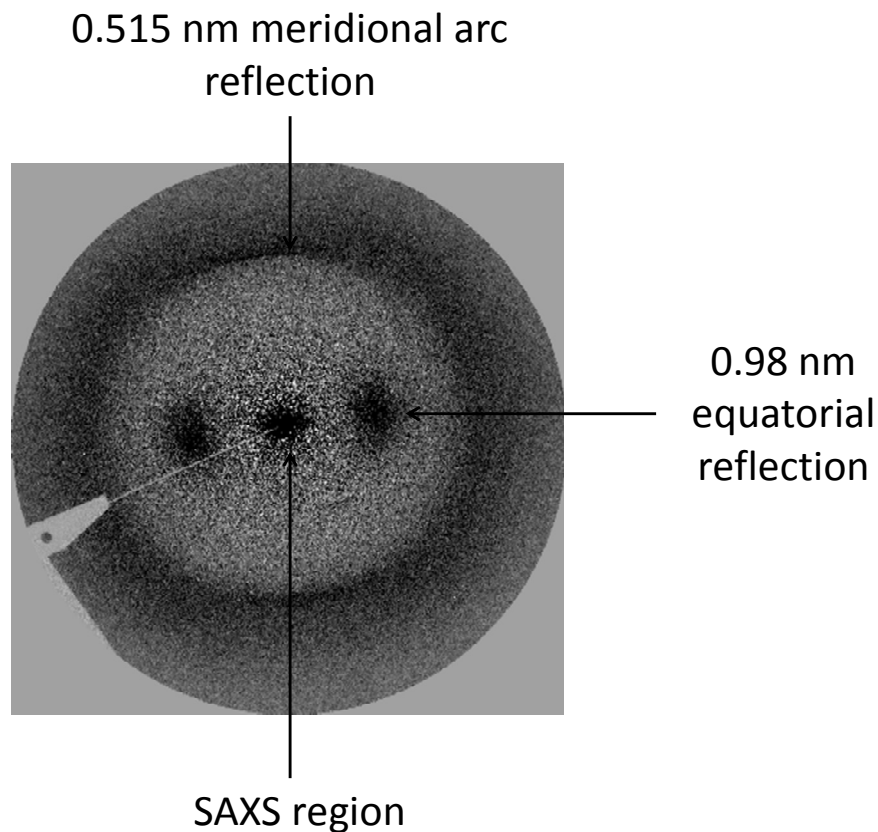


Figure 2.7 – Fibre diagram in the WAXS region highlighting the scattering features observed from a hair fibre. The hair sample used in this image was an Asian hair type. The q range of the image is $0 - 20 \text{ nm}^{-1}$.

2.4 Synchrotron Radiation

X-rays can be generated in a number of different ways for means of material analysis. One way in which X-rays can be generated is by accelerating particles to emit radiation; often these are electrons. Synchrotrons are particle accelerators (sometimes referred to as light sources) which produce vast amounts of high intensity radiation on a number of different wavelengths. By controlling the direction of the particles being accelerated, the radiation can be harnessed and utilised for experiments.

Synchrotron radiation works on the basis that charged particles moving in a magnetic field at relativistic speeds will emit radiation. Synchrotrons use powerful electromagnets to accelerate electrons round a cyclic accelerator to emit radiation.

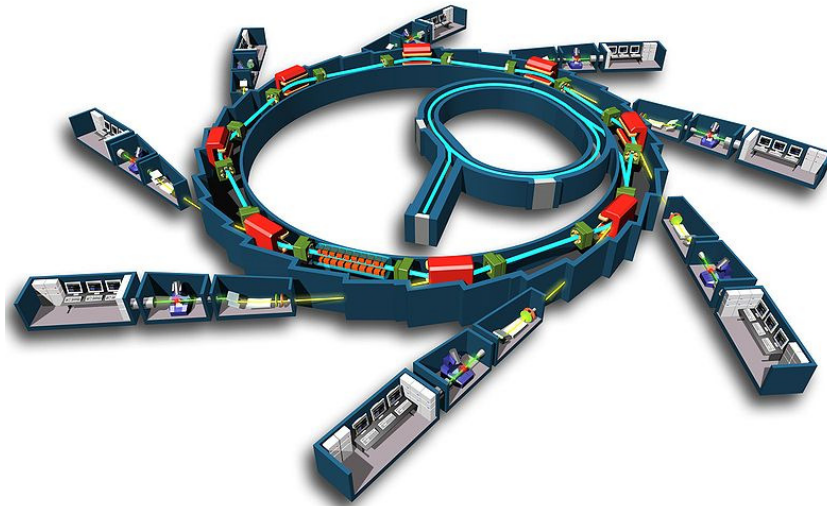


Figure 2.8 – Schematic of the layout of the synchrotron Soleil in France near Paris. The figure shows the initial linear accelerator where the electrons are initially accelerated. The electrons are then passed into the booster ring (the inner circle) where they are further accelerated. When the electrons have reached sufficient velocity they are passed into the storage ring (Synchrotron 2005).

Electrons are first emitted from an electron gun at A at the back of a linear accelerator. They then pass down the linear accelerator where electromagnets accelerate the electrons. The electrons are then passed through to the booster ring, B, where they undergo many rotations of the ring to accelerate them towards the speed of light. This is achieved by powerful electromagnets. When the electrons have reached a high enough velocity they are passed into the storage ring, C, where in 3rd generation synchrotrons, they also undergo further acceleration. Most 3rd generation storage rings are not truly circular; they are polygons with bending magnets in them, these are undulators or wigglers. These magnets in the storage ring cause the electrons to follow a helical path and by very precisely calculating the positions of the electrons, the intensities of the radiation they give off can be summed and increase the flux of the radiation further. Should the synchrotron start to lose intensity, 3rd generation synchrotrons can fill the storage ring back up

with newly accelerated electrons from the booster ring. This allows the synchrotron to emit continuous radiation. The electrons rotate around the storage ring at velocities close to the speed of light emitting radiation at a tangent to their position. Special openings in the storage ring allow this radiation to be passed down a beamline, D, where the radiation is passed through instrumentation and into the experimental beam hutch where experiments utilising the radiation can be performed safely. Synchrotron radiation is generally strongly polarised due to the regularity of the magnetic field direction within the emitting region, this leads to a high intensity, highly collimated radiation with very high energies. The radiation is widely tuneable to different wavelengths and sources can emit radiation anywhere from radio to X-ray energies. Synchrotron radiation is useful for a large amount of different analytical techniques, which has led to more people in the scientific community realising the potential usage of synchrotron radiation.

2.4.1 Increasing Synchrotron Radiation Intensity

Increasing the intensity of the radiation provided by synchrotrons enables shorter experimental time and greater experimental turnover. As discussed in Section 2.4 many 3rd generation synchrotrons are not truly circular; they are polygons with insertion devices placed in them at strategic points along the straight sections to allow for the radiation to be increased. The development of undulators and wigglers (bending magnets) maximises the brightness (number of photons per second in a narrow bandwidth per unit solid angle) of the synchrotron source. The increased intensity of the radiation is achieved by producing a series of deflections of the charged particle beam within its straight-line orbit around the storage ring.

2.5 Infrared Spectroscopy

Infrared (IR) radiation is of longer wavelength than visible radiation and covers the spectrum of wavelengths from 0.75 μm to 1000 μm . Infrared spectroscopy uses the bending, vibrational, stretching and rotational modes of molecules present in a sample to identify the chemical composition of the sample.

IR spectroscopy works on the basis that molecules exposed to IR radiation become excited; the electromagnetic radiation interacts with the dipoles of the molecules present in a sample and causes them to stretch, bend, vibrate or rotate around a common fixed position of the constituent atoms in the molecules. The dipoles have quantised energy states relating to their rotation, bending, vibration or stretching states. As the energy states of the molecules have quantised energies related to them, this means that they have specific frequencies related to them. By tabulating these frequencies, the corresponding modes to these frequencies can identify what molecules are present in the sample and thus the chemical composition. In IR spectroscopy these frequencies are wavenumbers.

Transitions between rotational states are generally of lower energy than between vibrational or stretching states, but there are numerous transitions, many of which involve combinations of changes to the rotational and vibrational states. These resonances can give rise to either emission or absorption of the IR radiation depending on the difference between the energy levels of the states. IR spectroscopy generally identifies the absorption of radiation as it passes through a medium. There are only a certain number of ways in which a molecule can be rotated or vibrated by the IR radiation. For a non-linear molecule composed of n atoms, the molecule has $3n$ degrees of freedom. These are divided up as 3 rotational motions, 3 translational motions and $3n-6$ vibrational motions. Some of the ways in which atoms can translate are shown below.

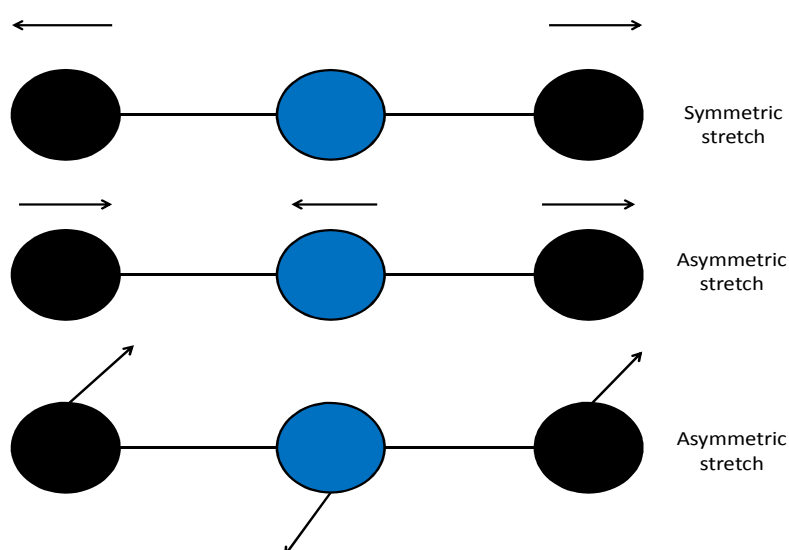


Figure 2.9 - Some of the translational modes of a carbon dioxide molecule. The blue circle denotes the carbon atom and the black circles denote the oxygen atoms.

In an IR experiment a sample is exposed to a source of IR radiation; the intensity of the source of IR radiation is measured before and after the interaction with the sample using a detector. The detector will show that there has been a net absorption of the IR radiation as it passes through the sample to the detector, but at certain frequencies, there will be sharp drops in the intensity of the radiation. These frequencies correspond to the vibrational or rotational modes of the molecules present in the sample; the energy of the radiation has been absorbed by the molecules to make them resonate at specific frequencies. Therefore IR spectroscopy can be used to detect how much radiation has been absorbed by the sample or transmitted through to the detector.

The IR region of spectroscopy in wavenumbers is normally quoted to be 100 – 10000 cm^{-1} , where a wavenumber is defined to be the reciprocal wavelength (Ferraro and Krishnan 1990).

wavenumber = $\frac{1}{\lambda}$ where λ is measured in cm and units in wavenumber are cm^{-1} .

The IR spectrum is split into three regions; the near infrared region (NIR), the mid infrared region (MIR) and the far infrared region (FIR). These regions correspond to the frequency of the radiation in relation to the visible frequencies of electromagnetic radiation. There are no definite wavenumber boundaries separating these regions, however the FIR region is normally quoted to be 100-400 cm^{-1} , the MIR 400-4000 cm^{-1} and NIR is 4000-14000 cm^{-1} (Ferraro and Krishnan 1990).

2.6 High performance liquid chromatography (HPLC) and ultra performance liquid chromatography (UPLC)

High performance liquid chromatography (HPLC) is a method of chromatography used to separate, purify and identify compounds in polydisperse solutions. HPLC uses solvents applied under high pressure to force the solution through a dense column. The molecules of the solution are differentially separated according to the interaction they have with the column. The column may possess different properties according to the desired separation; typically this is liquid-liquid partition, liquid-solid adsorption, ion-exchange, molecular exclusion, size exclusion and affinity chromatography. HPLC aims to separate and identify the composition of the sample under test as quickly and efficiently as possible.

Experimentally, HPLC utilises solvents (mobile phases) placed under high pressures via a pump to force the solvents and sample through the column (stationary phase). The retention time is the time taken for components of the sample to move through the stationary phase and be detected on the other side; it is dependent on the interaction of the sample with the stationary phase. The retention time is dependent on a number of different variables such as; the temperature of the column, the column dimensions, the flow rate, composition of the mobile phase and the basis of interaction between the sample and the stationary phase. HPLC can be used with a number of different types of detector to analyse components, the most common are UV or visible wavelength detectors or mass spectrometry detectors.

UPLC is the case of HPLC but utilising smaller columns with smaller stationary phase particle sizes and/or higher pressures which enables greater efficiency of the separation of eluents. A UPLC method was used in this thesis in combination with mass spectrometry in order to analyse lipids extracted from hair fibres.

2.7 Thin layer chromatography (TLC)

Thin layer chromatography (TLC) is a technique used to separate compounds using a thin layer of adsorbent material (stationary phase) placed in a solvent (mobile phase) and separated on the principle of capillary action. Separation is achieved due to the difference in the properties the components of the analyte have with the mobile phase.

The most common form of TLC uses a silica gel set onto a glass plate. The analyte is dissolved into a solvent before being blotted onto the gel and allowed to evaporate before being placed in a small amount of mobile phase in a sealed container. The sample moves up the stationary phase via capillary action, until an optimal separation has been achieved. The plates are then allowed to dry and sprayed with a fluorescence compound that allows visualisation of the analyte under UV light; typically this is a manganese zinc silicate.

The work presented in this thesis has used TLC to separate lipids extracted from hair samples.

2.8 Gas chromatography (GC) and Fire ionization detection (FID)

Gas chromatography (GC) and fire ionization detection (FID) are techniques that are used to separate and analyse components of a sample. GC uses an inert gas (such as nitrogen) as the mobile phase to move the analyte through a stationary phase of liquid which is typically held inside a column. The sample is injected onto the column where the mobile phase moves it through the column which contains the liquid stationary phase, separation is achieved by different retention times of the compounds which make up the sample. The different compounds are then detected and analysed. A common method of detection coupled with GC is FID; this method pyrolyzes the eluents exiting the GC column which are then detected between electrodes connected to an ammeter which reads a current that corresponds to the number of carbon ions per unit time. The eluents which exit the GC column are heated to ensure they remain in the gaseous phase and combined with hydrogen which is fed into the column. The eluents are then mixed with oxygen and travel up the column towards a positive voltage source which repels them into the flame which pyrolyzes the compounds in the eluents. The pyrolyzed eluents are repelled by the positive voltage source towards the collector plates which are coupled to an ammeter; this detects the number of ions as a current per unit time.

This thesis has utilised GC and FID to characterise the lipids extracted from hair.

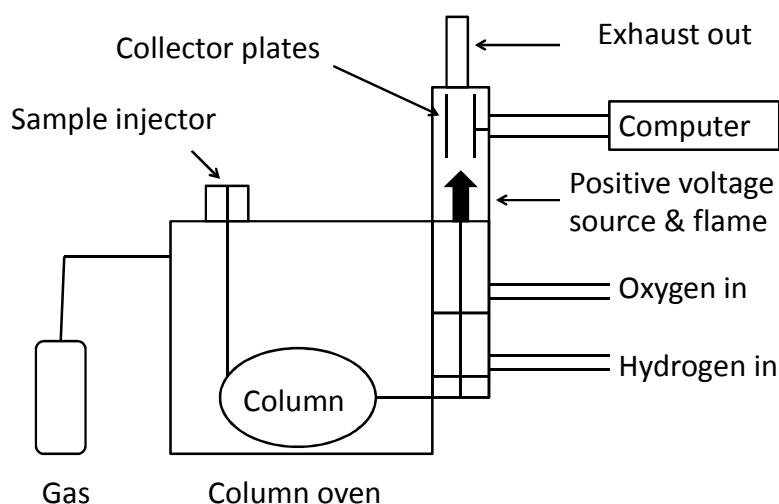


Figure 2.10 – Schematic of a Gas chromatography setup coupled to a fire ionization detector.

2.9 Mass spectrometry (MS)

Mass spectrometry (MS) is a technique capable of identifying the masses of molecules that comprise the material under test by measuring the mass-to-charge ratio. This is achieved by first ionizing the chemical compounds of the sample to generate charged molecules; these are then detected using a mechanism which can detect charged particles such as a magnetic sensor or a quadrupole. The signal from the detector is then interpreted into a spectra which contains all of the masses of the particles that were present in the sample.

In this thesis, MS has been used to identify the constituent components of lipids that have been extracted from hair fibres. This technique was coupled with PCA in order to investigate whether the lipids would cluster by ethnic hair type revealing if certain lipid species were exclusively found in specific ethnic origins.

2.10 Principal Component Analysis

Principal component analysis (PCA) is a mathematical technique used to identify underlying patterns within large data sets that may be hidden due to the large dimensionality of the data set. This technique is often used to highlight similarities and differences in the data set. PCA is a method which compresses the data set once the patterns have been established, thereby reducing the number of dimensions. PCA works by applying the following mathematical calculations to the data set; the following highlights the steps involved.

- After the data has been collected the mean of all the data points in each dimension needs to be subtracted. i.e. all the x values have the mean value of all the data points subtracted, and all the y values have the mean value of all the data points subtracted. This consequently produces a data set whose mean is zero.
- The covariance matrix is calculated. This is a plot of how much the dimensions vary from the mean with respect to each other. The covariance is always measured between two dimensions but can be used to show differences in three dimensional data.

- The eigenvalues and eigenvectors of the covariance matrix are calculated. The eigenvalues and eigenvectors provide information about the patterns of the data, similar to drawing a line of best fit. The eigenvector shows how data sets are related along a line and when extracted characterise the data.
- The data is compressed and the dimensionality is reduced. The eigenvector with the highest eigenvalue is known as the principal component of the data set. This means that this value describes the most significant relationship between the data dimensions once eigenvectors are found in the covariance matrix they are ordered from highest to lowest, which presents the components in order of significance. The first five components often describe the data to around 99% and so the remaining components are often discarded. By keeping only the first five components the final data set has five dimensions. The component data is then presented in a matrix of vectors, known as a feature vector, which is constructed by taking the eigenvectors you want to keep (i.e. the principle component eigenvectors) from the list of eigenvectors and forming a matrix.
- Once the components of the data set are formed in a feature vector, the transpose of the vector is taken and multiplied by the left of the original data set transposed. The data is then presented as a series of rows, where each row holds a separate dimension. This is the final step in the creation of a new data set.

PCA gives the original data set solely in terms of the vectors. The data has been transformed to be expressed as patterns between the vectors, whereby the patterns are the lines that describe the data. This is useful since the data has been classified as a combination of the contributions from each of the lines. The values of the data points tell us exactly where, above or below the trend line, the data point sits. The data is interpreted by plotting the rows of data (commonly known as base functions) against one another and against other sets of data.

2.11 Summary

In this chapter all of the techniques that have been used in this thesis have been discussed. The combination of inter-disciplinary techniques presented in this chapter complement each other in

order to investigate the structure of hair. For example, ATR-FTIR can be used to exclusively study the structural chemical composition of the hair fibres at the surface, whereas X-ray scattering techniques can be used to study the structure of the hair at the nanoscopic and submolecular scale. The various chromatography techniques also outlined in this chapter contribute to the analysis of different individual molecular components of hair.

Chapter 3 – Materials & Methods

This chapter provides a comprehensive description of all the materials and methods used in the experiments which contributed to this thesis.

3.1 Hair samples

All hair samples investigated in this thesis were provided by Unilever R&D, Port Sunlight, UK. Hair samples were all virgin hair types - i.e. had no chemical products or otherwise applied to them for the length of time that the hair samples were grown for; this had been ensured by a written contract between the sources and the suppliers. The samples were confidentially sourced from suppliers to Unilever and no details on the source were provided apart from the geographical location of the source. All samples are sourced from females. The samples were sourced from person's representative of specific ethnic backgrounds. The same hair fibres were not used in the same each experiment conducted; details of which hair fibres were used in the experiments can be found in the data collection sections of each results chapter. As human hair clippings are not classed as human tissue, the Human Tissue Act of 2004 does not apply to these samples. Table 3.1 provides information regarding the hair samples used.

Ethnicity	Number of sources
Afro	5
Asian	3
Chinese	3
European	4
Japanese	4
Mullato	5
Spanish	5
Thai	4

Table 3.1 – Information on the hair samples sourced from Unilever used in this thesis.

3.2 X-ray Scattering Experimental Setup

Chapter 2 described the theoretical basis for X-ray scattering and how it can be used to analyse the structure of biological materials and specifically hair fibres. This section describes the experimental setup and the equipment used to conduct the experiments at the two beamlines at the ESRF; ID18F and ID02.

3.2.1 Synchrotron Beamlines

At synchrotron sources radiation arising from the electrons moving at relativistic speeds within the storage ring of the synchrotron is emitted at tangents to the electron source (see Section 2.4). At these tangents, experimental stations are built along the beamline surrounding the storage ring that allow for this radiation to be harnessed and used in experiments. A typical beamline consists of three cabins; an optics cabin, an experimental cabin and a control cabin. The optics cabin contains the optical systems used to manipulate the incoming radiation beam to the required experimental characteristics. The experimental cabin contains the sample loading environment for the samples to be studied and the detectors which collect the resulting information produced from the interactions between the radiation and the sample. The control cabin is an environment where the researchers can control the experiment using computer control and collect and store the resulting data. The radiation beam enters the optical systems from the storage ring through an undulator. The main optical element(s) of a beamline is/are the monochromator which performs three main functions; wavelength selection, horizontal focusing and beam compression. Horizontal focusing from the monochromator allows for the beam to be given a specific size at a set point in space; usually at the sample loading position or the detector. The beam compression characteristics of the monochromator enable the beam diameter to become smaller via focussing. A monochromator is typically constructed from a crystal or set of crystals such as silicon. In many cases the general layout of beamlines is similar, however, each beamline has its own individual layout and characteristics tailored to capitalise for a specific experimental situation.

3.2.2 ID18F – Microfocus X-ray fluorescence beamline at the ESRF

The ID18F beamline was developed for simultaneous microfocus X-ray scattering and X-ray fluorescence experiments to be performed (Somogyi, Drakopoulos et al. 2001). The beamline provides radiation in a tuneable spectral range of 6 - 28 keV. The radiation passes through a set of primary slits and an attenuator into the monochromator which consists of two fixed exit double slit silicon crystals. To produce a microfocus beam parabolic compound refractive lenses (CRL) are used. The CRL is composed of a different number of individual Al lenses depending on the energy of the focussed beam (Snigirev, Kohn et al. 1996). The typical focal distance is between 0.5 – 1.2 m depending on the energy of the incoming beam and the size of the beam is 1 - 2 μm vertically x 12 - 15 μm horizontally providing a typical flux of 5×10^{10} photons/sec. Larger spot sizes can be obtained by defocussing the CRL lenses (Somogyi, Drakopoulos et al. 2001). This enables microfocus experiments to be performed which require a beam size of the micron scale. ID18F utilises a Si(Li) detector (GRESHAM) of 30 mm^2 active area and 3.5 mm thickness. The detector has an 8 μm thick Be window which is used to detect the characteristic X-ray line intensities generated in the excited micro-spot of the sample. The detector is connected to a charge coupled device (CCD) detector coupled via a fibre optic taper. The detector is a MAR CCD camera which is 2048 x 2048 pixels in size with 64.45 x 64.45 μm^2 pixel resolution with 16-bit encoding. A tungsten backstop 50 μm in diameter is placed a few millimetres before the camera entrance to absorb the direct beam. Figure 3.1 shows a schematic of the general layout of the ID18F beamline, full details of ID18F can be found at:

www.esrf.eu/UsersAndScience/Experiments/Imaging/ID18F

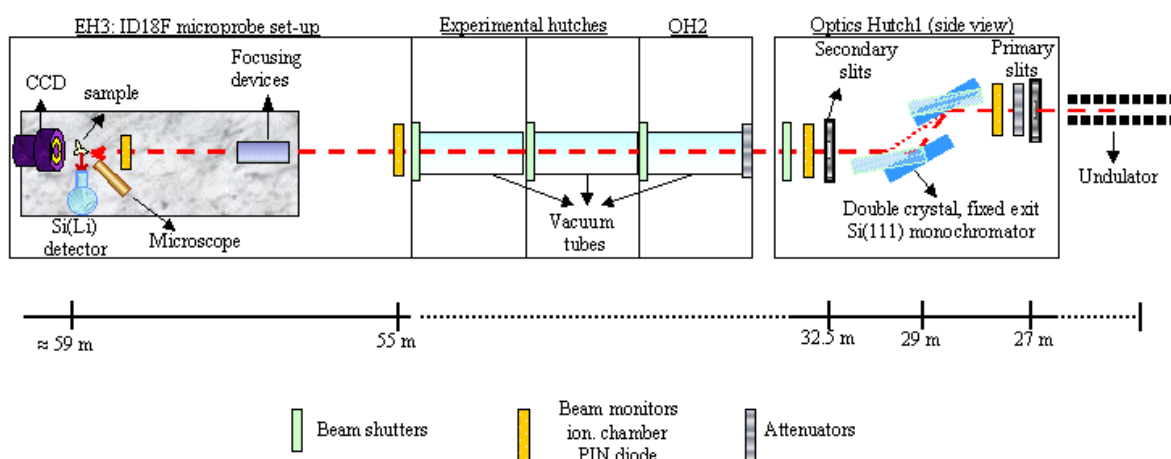


Figure 3.1 – Schematic showing the general layout of the ID18F beamline. The left hand side shows the experimental hutch containing the detectors, the sample mounting environment and the focussing optics and the right hand side shows the optics hutch containing the monochromator. The scale at the bottom shows the distance from the radiation source (storage ring). Not shown in the image is the control cabin.

Samples are mounted in ambient air conditions using a Huber goniometer head. The goniometer is mounted on a sample stage consisting of one rotation and three translation motor stages. The horizontal and vertical scanning range is 50 mm x 50 mm and the minimum step sizes of the translation are 1 μm horizontally and 0.1 μm vertically.

3.2.3 ID02 beamline at the ESRF

The ID02 beamline at the ESRF was developed to create a high brilliance beam with simultaneous time resolved acquisition for SAXS and WAXS experiments to be conducted. The beamline provides a tuneable spectral range of 8 – 17keV. A set of primary slits and an attenuator which adjusts the intensity of the beam and a silicon double crystal monochromator selects wavelengths in the range of $\lambda = 0.155 - 0.073 \text{ nm}$. The radiation is then passed through another set of slits and an optional attenuator and can interact with either a toroidal or a cylindrical shaped mirror. The photon flux at the detector is typically 4×10^{13} photons/sec. The combined use of SAXS and WAXS

detectors allows for a large q range of data acquisition; the largest q range obtainable is $0.01 - 40 \text{ nm}^{-1}$. The SAXS detector can be varied in distance from $1 - 10 \text{ m}$ from the sample mounting position and the WAXS detector is at a fixed distance of 0.4 m from the sample mounting position. The SAXS detector is a FReLoN (Fast Readout-Low Noise) Kodak CCD based detector. The detector has input field of $100 \text{ mm} \times 100 \text{ mm}$ and dynamic 16-bit range with a full frame rate of 3 frames/sec . The size of the CCD pixel array is 2048×2048 and the spatial resolution is $80 \mu\text{m}^2$. The size of the CCD pixel array is 3584×2048 with a nominal pixel size of $24 \mu\text{m}$ and the spatial resolution is $60 \mu\text{m}$. Figure 3.2 shows a schematic of the layout of the ID02 beamline.

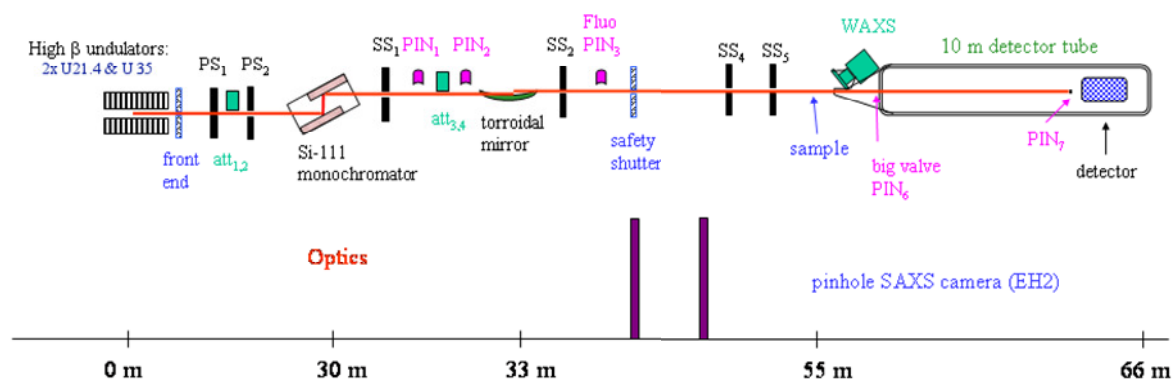


Figure 3.2 – Schematic showing the layout of the ID02 beamline. The left hand side shows the optics hutch containing the monochromator and the toroidal mirror (not shown is the optional cylindrical mirror). The right hand side shows the experimental hutch containing the WAXS and SAXS detectors and the sample mounting environment. The scale at the bottom shows the distance from the radiation source (storage ring). Not shown in the image is the control cabin.

In this thesis, the sample mounting equipment used was a custom built five channel flow cell holder provided by Unilever. The cell holder is constructed from stainless steel and comprises five isolated cells in series each with a syringe pump so that solutions can be pumped into the cells via computer control (see Figure 3.3). The cells take approximately 50 seconds to fill and 65 seconds to empty. The cells are built onto an optical bench and have mica windows for the X-rays to interact with the hair fibres inside of the cells. The size of the cell windows are 10 mm horizontally \times 32 mm vertically. The cells can be heated; this is controlled via computer through a heated PSU

system. Micro syringes at the top and bottom of each individual cell hold the single hair fibres steady, straight and under a small tension that does not affect the molecular structure of the hair. The cell holder is held on a goniometer stage which can be moved 390 mm horizontally and 140 mm vertically. Full details of ID02 can be found at:

www.esrf.eu/UsersAndScience/Experiments/SoftMatter/ID02/BeamlineDescription

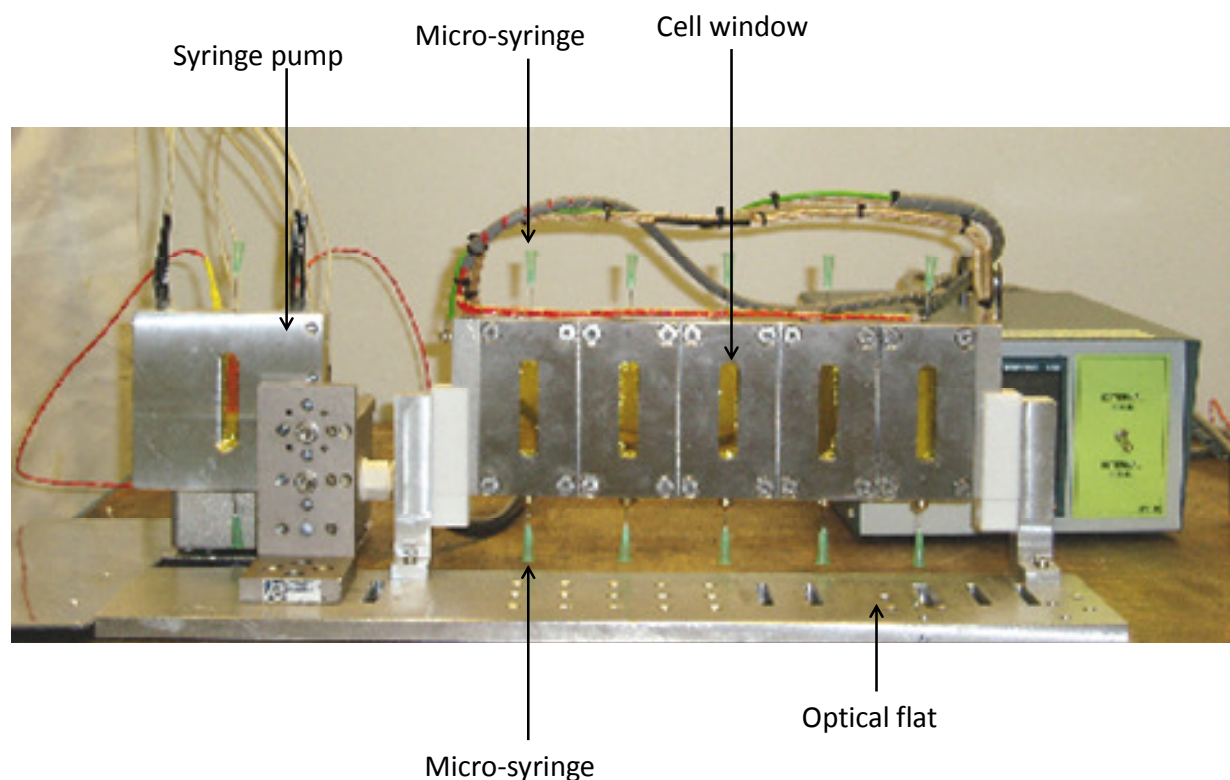


Figure 3.3 – Photograph of the custom built five channel flow cell holder made by Unilever which was used to mount the samples at the ID02 beamline.

3.2.4 Data Correction

For each detector at the synchrotron, there is a possibility of variation in the sensitivity of the detector across its active area. To account for this, correction techniques are employed to counter these effects. At the ID02 beamline, an online data correction package is automatically run on each sequential file in turn to correct the data. In detail the raw data is corrected for the dark current, readout noise, division by the flat-field and spatial distortion. A dark field image is collected; the detector runs without any synchrotron radiation present, this creates values for the

dark current, readout noise and allows flat-field file to be created which can be used to correct for the spatial distortion of the detector. Data files are normalised by the dark field image to produce corrected images. A similar method is employed at the ID18F beamline.

In addition to detector corrections, background images are taken. Background images correct for air and machine dependent scatter surrounding the sample; background subtraction is very important in solution scattering experiments where the scattering from the macromolecules in solution is very weak. A background image is a scattering image taken of the exact experimental conditions and for the same exposure time from which the sample information is collected but without the sample present. The background image is subtracted from all data files before further analysis.

3.2.5 Data Analysis using Fibrefix

FibreFix is a software program created by the collaborative computational project for fibre diffraction and solution scattering (CCP13). The software was developed to analyse non-crystalline materials. The patterns that can be analysed range from highly orientated fibre diffraction patterns to patterns with considerable disorientation such as those arising from solution scattering experiments.

It is often necessary to pre-process the 2-dimensional images before analysis can take place in FibreFix. Common practices may involve the optimal alignment of the 2-dimensional images if they show preferential orientation, thus it is necessary to manually align the individual exposures before further analysis. Another typical pre-analysis measure may involve the background subtraction of a blank diffraction pattern from the diffraction images using a suitable weighting. Other input parameters such as the pixel location of the beamstop on the diffraction images can be manually input in the parameters window. Additionally to this, if the diffraction pattern shows circular geometry, FibreFix has a function, 'Get Points' that can be used to calculate the centre point of the image which is the precursor requirement for functions such as azimuthal integration scans.

3.2.6 Data analysis using Fit2d

Fit2d is a software program developed in collaboration with users at the ESRF to process and analyse diffraction patterns of both crystalline and non-crystalline materials. Fit2d has a number of different functions for analysis of a number of different types of diffraction patterns.

Fit2d has a composite image function which enables multiple diffraction images to be processed and displayed at once. This is particularly useful for microfocus X-ray scattering where many diffraction images may be taken as the X-ray beam is scanned across a sample. This function allows the user to visually inspect the change in the diffraction patterns across the sample. Like FibreFix, Fit2d has functions which permits pre-processing of the diffraction images before analysis such as background subtraction and movement functions for optimal alignment of preferentially orientated diffraction images.

3.3 Attenuated Total Reflectance Fourier Transform Infrared spectroscopy (ATR-FTIR)

ATR-FTIR is an analytical technique exploiting the basis of infrared spectroscopy as described in Section 2.5 but exclusively applied to the surfaces of materials and allows for solids and liquids to be investigated without any prior sample preparation. ATR-FTIR works on the basis that radiation of infrared wavelengths is produced and is passed through a crystal where it is totally internally reflected at least once when in contact with a sample. Total internal reflection of the wave within the crystal creates an evanescent wave which can pass into the material under investigation. This evanescent wave passes through the material and at specific frequencies relating to the chemicals present in the sample, there will be absorptions. The evanescent wave is collected at a detector which provides information on the frequencies where absorptions have occurred so an interpretation of the chemical composition of the sample can be made. The penetration depth of the evanescent wave typically ranges from 0.5 – 2 micrometres into the sample; thus this technique is mainly used to probe the surface structure of materials (Coates and Reffner 1999). The exact penetration depth of the evanescent wave is dependent on the wavelength of the light, the angle of incidence of the radiation and the refractive indices of both the crystal and the sample. The evanescent wave can only be created if the refractive index of the crystal is higher

than that of the sample under test. Figure 3.4 shows an example of an ATR-FTIR spectra for human hair

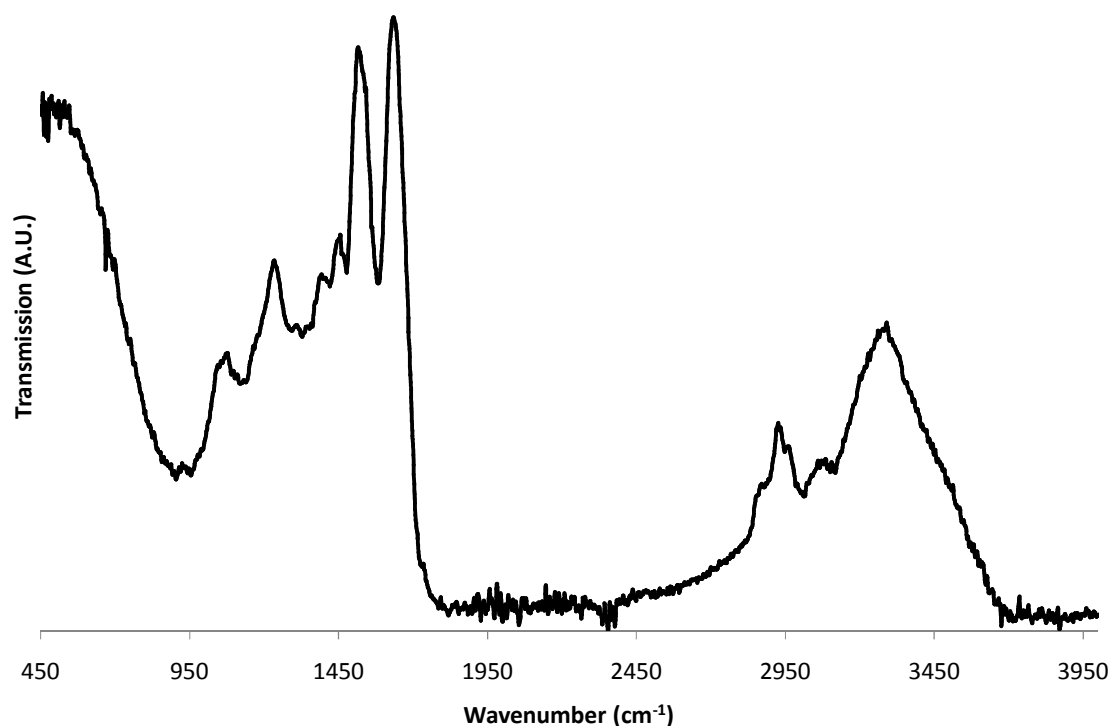


Figure 3.4 – A typical ATR-FTIR spectra for human hair. The spectra shown here is for the Chinese hair type.

All ATR-FTIR measurements were made on the Perkin Elmer Spectrum Spectrometer system using the Diamond Crystal ATR accessory. The software used was the Perkin Elmer Spectrum version 5.01. Sample analysis was performed on the surface of hair fibres with no pre-treatment.

The ATR attachment was used because it enables a study that only probes the surface structure of hair fibres, thus giving information exclusively on the cuticle structure. The ATR attachment uses an internal reflection element with a high refractive index, in the Perkin Elmer Spectrum one, this element is diamond. The FTIR spectra can be processed and analysed using the Peakfit Software program (see Section 3.3.1).

3.3.1 Data analysis using Peakfit

Peakfit is a software program that is designed to accurately determine peak parameters. The software enables such functions as peak fitting and baseline subtraction and can also be used to determine peak parameters such as the peak position, FWHM, integral area and amplitude. This software is capable of performing automated 2nd derivative analysis and has been used in this thesis to determine 2nd order derivatives of the vibrational modes for all the peaks present in the ATR-FTIR analysis of hair surface structure in Chapter 6.

3.4 Experimental procedure for the extraction of internal lipids

In this thesis, lipids were extracted from hair fibres to identify whether any variation could be detected in the amount of lipid present and/or in the biochemical structure of the lipids themselves. Two different methods for the extraction and analysis of the lipids extracted from hair were employed; the first as outlined here shall be called the extraction of internal lipids, and the latter the extraction of endogenous and exogenous lipids. The following is an account of the initial method that was used to extract the lipids and analyse them using UP-LC/MS (see Sections 2.6 and 2.10). This work was performed in collaboration with Valerie O' Donnell, Madhav Monde and Victoria Hammond. Madhav provided technical assistance to the extraction process and carried out the subsequent HPLC runs and data analysis.

10 mg of each hair type was weighed (KERN ALJ 160-4NM weighing scales) to undergo extraction. Each hair type was placed in a pestle and mortar along with a small amount of liquid nitrogen and the hair was ground into a fine powder. The powder was removed to glass tubes where 2.5 ml of an extracting solution was added, hexane:2-isopropanol:1M acetic acid 30:20:2 (v/v) along with 1 ml of HPLC grade water. The solution was vortexed for 2 mins, 2.5 ml of hexane was added and the solution was vortexed for a further 2 mins. The solution was centrifuged at 1,500 rpm at 4°C for 5 minutes to produce two phases and the upper hexane layer was removed to a clean glass tube. The original solution containing the finely ground hair was then re-extracted by adding an additional 2.5 ml of hexane and vortexed for 2 minutes and centrifuged at 1,500 rpm for 5 minutes at 4°C. The upper hexane layer was collected and combined with the previous collected

fraction. The fractions were dried in a speed vac for 2 hours (RapidVAP N2, Labconco). When the solutions were dried, 200 µl of mobile phase was added to the residue in preparation for UP-LC. The mobile phase solution added to the residue was a 50:50 (v/v) mix of mobile phase A and mobile phase B, where the mobile phases were:

Mobile phase A - acetonitrile:water (50:50), 1mM ammonium acetate, 0.1% glacial acetic acid

Mobile phase B – 2-Isopropanol:acetonitrile (70:30), 1mM ammonium acetate, 0.1% glacial acetic acid

3.4.1 UP-LC run conditions for the extraction of internal lipids

The separations of the lipids were made using a UP-LC technique. The column used was an RP Hypersil Gold (Thermo Scientific) C18 with dimensions; 150 mm x 2.1 mm with a 1.9 µm particle size.

Mobile Phase A – acetonitrile:water (50:50 v/v) + 10 mM ammonium acetate & 0.1% glacial acetic acid

Mobile Phase B – isopropanol:acetonitrile (90:10 v/v) + 10mM ammonium acetate & 0.1% glacial acetic acid

Extract samples were dissolved in 200 µl of mobile phase A and mobile phase B (50:50)

Flow rate = 400 µl/min

Column temperature = 25 °C

Injection volume = 16 µl

Run Time = 55 min

Auto-sampler temperature = 4 °C

The gradient was transformed linearly according to the conditions described in Table 3.3.

Time (min)	Mobile phase A (%)	Mobile phase B (%)	Flow rate (µl/min)
0.0	65.0	35.0	400
10.0	50.0	50.0	400
16.0	34.0	66.0	400
38.0	24.0	76.0	400
48.0	4.0	96.0	400
52.0	4.0	96.0	400
52.5	65.0	35.0	400
55.0	65.0	35.0	400

Table 3.2 - Gradient conditions for the UPLC run conditions for the lipid separation.

Global lipidomic analysis was performed in both positive and negative ion mode using UP- LC coupled to an Orbitrap Elite Mass Spectrometer (Thermo Scientific). A pooled sample (a 10 µl aliquot from all hair types) was run at the beginning following two runs of blank solvent for column conditioning and quality control analysis. All samples were run at random and a blank solvent was run after every 5th or 6th sample run.

The optimized MS conditions were as follows:

HESI temperature = 350 °C

sheath gas flow = 52 arbitrary units

auxiliary gas flow 17 units

capillary temperature = 320 °C

spray voltage = +/- 3.5 kV

S-lense RF level = 69.8/65.6 % respectively for positive and negative ion mode.

A high resolution (60000, full-width at half-maximum, FWHM) full scan MS data over 250 to 1400 m/z range was acquired in centroid mode. The UPLC-MS instrument was controlled by Xcalibur 2.1 software. The raw data files were analysed in SIEVE 2.0 (Vast Scientific) software for peak finding and alignment (i.e. to extract peak intensities for retention time matched accurate masses). One of the pooled sample runs was used as a reference run for global alignment.

3.5 Extraction of Endogenous and Exogenous lipids from hair fibres

This work was performed in collaboration with Irina Gushina and John Harwood. John Harwood provided methodology and Irina provided extensive technical assistance. Extraction of both endogenous and exogenous hair lipids was performed using the methods adapted from (Masukawa, Tsujimura et al. 2005). In detail 250 mg of each hair sample was weighed (using KERN ALJ 160-4NM weighing scales) and cut into smaller pieces using scissors and placed in glass tubes. The hair samples were first washed in a hexane:diethyl ether solution before being extracted using chloroform:methanol and were finally hydrolysed using potassium hydroxide. The lipids were initially separated into different lipid classes using TLC and then their quantification and fatty acid composition were evaluated using GC/FID. The lipids were identified on the TLC plates with reference to the authentic standard (see Figure 3.5). 30-50 μg of neuroic acid and 10-30 μg of squalene were used as internal standards for fatty acid/lipid and hydrocarbon quantification respectively, in GC/FID runs. All chemicals used were either analytical or HPLC reagent grade and sourced from Fisher and Sigma-Aldrich, UK. All abbreviations in this section and in Chapter 7 are defined as the following: TAG, triacylglycerols; FFA, free fatty acids; WE, wax esters; HC, hydrocarbons; PL, polar lipids.

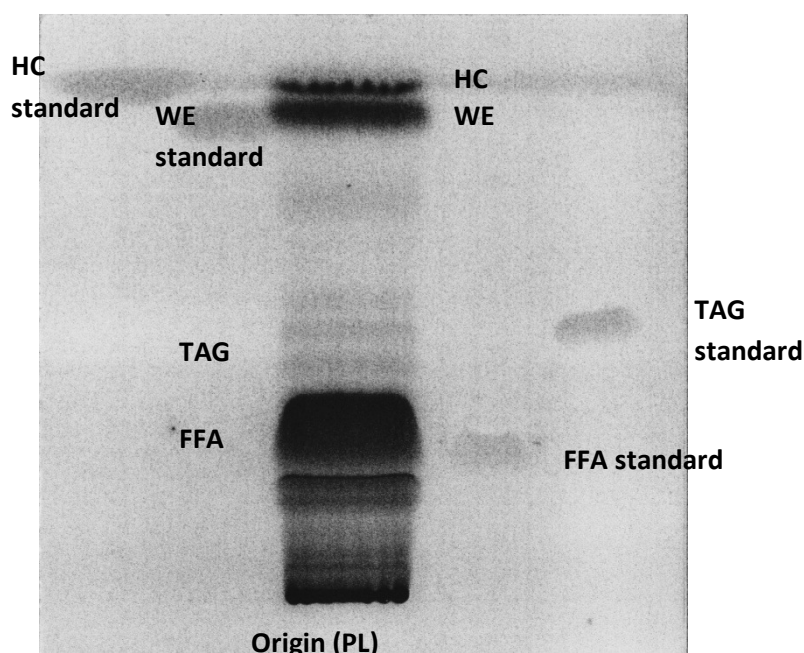


Figure 3.5 - An example of TLC separation of the solvent-extracted lipid fraction (shown here is the Afro 4 sample – see Chapter 8 for further details) and the individual neutral lipid standards: TAG (tripalmitate), FFA (C17:0), WE (myristyl dodecanoate) and HC (heneicosane).

3.5.1 Hexane:diethyl ether washed lipids

The surface lipids were extracted twice from the hair samples with a mixture of hexane:diethyl ether (1:1, v/v) (5 ml x 2). The hexane:diethyl ether solution was removed to a clean tube, and combined washes were dried under a stream of nitrogen. The surface lipids were re-dissolved in 200 µl of hexane and stored at -20°C prior to further analysis (see Sections 3.5.4, 3.5.5 and 3.5.6).

3.5.2 Lipids extracted using chloroform:methanol

When the surface lipids were washed, chloroform:methanol extraction was used to remove the lipids that are ionically bound to the hair fibre. The hair samples following the initial hexane wash were immersed in 5 ml of chloroform:methanol (1:2,v/v) for 24 hours at room temperature. After 24 hours, the solution was removed to a clean tube and a solution containing chloroform:methanol:water (18:9:1, v/v/v) was added to the hair clippings for 24 hours at room temperature. After 24 hours the solution was removed and combined with the other chloroform:methanol solution. To the combined fractions, 2 ml of Garbus solution (Garbus, Deluca et al. 1963) was added. This solution contained 2M potassium chloride in 0.5 M potassium phosphate buffer at pH 7.4. They were then vortexed for 1 min each and centrifuged at 1,500 rpm for 2 mins at room temperature to produce two phases. The upper layer was discarded and the lower layer containing the chloroform was removed to a clean tube where it was dried under a stream of nitrogen. The residue was re-dissolved in 300 µl of chloroform and stored at -20°C prior to further analysis (see Sections 3.5.4, 3.5.5 and 3.5.6).

3.5.3 Hydrolysis of covalently bound lipids using Potassium Hydroxide solution

The delipidated hair cuttings were saponified for 2 hours at 60 °C by adding 4 ml of 1M KOH in 90% aqueous methanol. To the resulting solution, 2 ml of water and 1 ml 6M HCl was added and the solutions were vortexed for 1 min each. The samples were then extracted twice using a solution containing 4 ml hexane:diethyl ether 1:1 (v/v). The samples were centrifuged at 1,500 rpm for 3 mins at room temperature and the upper aqueous phase was removed after each extraction step, the phases were combined and dried under a stream of nitrogen. The residue was

re-dissolved in 300 µl of hexane and stored at -20°C before further fatty acid analysis (see Section 3.5.5).

3.5.4 One-dimensional thin-layer chromatography of individual lipid classes

The whole volume (200 µl) of hexane wash lipids and aliquots (100 µl) of chloroform-methanol extracted lipids were used for the analysis of individual lipid classes. Individual lipid classes, namely PL, FFA, TAG, WE and HC were separated using one-dimensional TLC on silica gel G plates, 10 x 10 cm (Merck KGaA, Darmstadt, Germany) using hexane: diethyl ether: acetic acid 80:20:10 (v/v/v). The plates were placed in a sealed glass container with 35 ml of mobile phase for approximately 10 minutes, or until the samples had run the entire distance of the plate. After development the plates were allowed to dry, they were sprayed with a solution containing 0.05% of 8-anilino-4-naphthosulphonic acid in dry methanol and the lipid bands were revealed under UV light. These bands were circled using a pencil and were scraped from the plate manually. The lipids containing fatty acid residues (PL, FFA, TAG and WE) were further analysed by GC. These analyses allowed the individual fatty acid separation, identification and quantification.

Hydrocarbons were analysed as described in Section 3.5.6.

3.5.5 Analysis of fatty acids by GC/FID

Aliquots (100 µl) of hydrolysed lipids (see Section 3.5.3) or the lipid bands scraped from TLC plates (see Section 3.5.4) were used for methylation reaction. This methylation step converts the fatty acids to Fatty Acid Methyl Esters (FAMES). The samples were methylated by adding 3 ml of 2.5% sulphuric acid (H₂SO₄) in dry methanol:toluene (2:1, v/v) at 70°C for 2 h. A known amount of nervonic acid, C₂₄H₄₆O₂, (30-50 µg) was added as an internal standard. When the reaction terminated, 2 ml of 5% NaCl was added to the reaction mixture. FAMES were then extracted twice using 3ml of hexane, vortexed for 1 min, centrifuged at 1,500 rpm for 2 mins at room temperature, and the upper hexane phase was removed to a clean tube. The samples were then re-extracted using the same procedure; the two hexane phases were combined and dried under

nitrogen stream. The residue was dissolved in 50 μl of hexane and placed in vials for GC/FID analysis.

A Clarus 500 gas chromatograph with a flame ionizing detector (FID) (Perkin-Elmer 8500, Norwalk, CT, USA) and fitted with a 30 m x 0.25 mm internal diameter capillary column (Elite 225, Perkin Elmer) was used for separation and analysis of FAMEs. The oven temperature was 170 $^{\circ}\text{C}$ for the initial 3 minutes and then raised to 220 $^{\circ}\text{C}$ at 4 $^{\circ}\text{C min}^{-1}$ and held for 25 minutes for each run. The injection volume was 5 μl and the carrier gas used was nitrogen (at 20 psi flow rate). FAMEs were identified routinely by comparing retention times of peaks with those of N-15-A FA standards (Nu-Chek Prep. Inc., Elysian, MN, USA).

3.5.6 Analysis of hydrocarbons by GC/FID

Hydrocarbons separated by TLC (see Section 3.5.4) were eluted from silica gel using hexane:diethyl ether 1:1 (v/v) (3 ml x 2). The two hexane:diethyl ether phases were combined and dried under nitrogen stream. 100 μl of BSTFA, trimethylsilyl 2,2,2-trifluoro-N-(trimethylsilyl)acetimidate, and 10 μl pyridine (Sigma-Aldrich, UK) were used for conversion of hydrocarbons into their silylated derivatives (30 min at 70 $^{\circ}\text{C}$). 10-30 μg of squalene was used as an internal standard. The GC conditions used as they are described in the above paragraph, except the oven temperature: isothermal conditions at 230 $^{\circ}\text{C}$ were applied for the hydrocarbon silyl derivatives.

3.5.7 Fatty acid and hydrocarbon analysis by GC/MS

In order to identify the structures of individual hydrocarbons and to confirm the structural identification of the unusual FAs, selected samples were analysed by GC/MS. 1 μl of sample (FAME or silyl derivatives of hydrocarbons) was injected into the GC-MS (Agilent GC 6890N-MSD 5973N) at 200 $^{\circ}\text{C}$ in splitless mode and analysed over a 30 m x 0.25 mm internal diameter capillary column on 0.25 μm ZB5ms (Zebron Phenomenex). The column was operated under constant pressure of 13.34 psi Helium and the following temperature programme: initial temperature 85 $^{\circ}\text{C}$ for 3 min, 10 $^{\circ}\text{C/min}$ to 130 $^{\circ}\text{C}$, 3 $^{\circ}\text{C/min}$ to 300 $^{\circ}\text{C}$, 300 $^{\circ}\text{C}$ for 3 min. The mass spectrometer was operated at

a source temperature of 230 °C and an analyser temperature of 150 °C. Data were analysed using Chemstation (v D 00.00.38, Agilent) and identities of analytes were confirmed by AMDIS software (version 2.1, National Institute of Standards and Technology) and manually checked against reference spectra.

3.6 Summary

Chapter 3 has provided a comprehensive description of the parameters used for X-ray scattering and ATR-FTIR. A description of the methods used to analyse the data generated in this study has also been given. This multi-disciplinary approach enables analysis of different molecular components within the hair fibre which provides information contributing to the understanding of the hair fibre as a bulk object. It is essential that the results from one technique are validated with other techniques in order for there to be a more comprehensive study carried out.

Chapter 4 – A bulk analysis of ethnic hair fibres in the dry and wet states

Human hair exhibits obvious macroscopic variation between individuals of different ethnic backgrounds. However, it is unclear where the origins of the variation in structure lie at the nano, supramolecular and sub-molecular scales. While there have been studies into quantifying inter-ethnic differences such as the geometric, morphologic and mechanical properties, there have been very few studies into explaining qualitatively what causes these disparities on a nano and sub-molecular structural level (see Chapter 1). The aim of this experiment is to investigate the inter-ethnic variation and analyse which structures at which levels of scale show differences and relate this to the inter-ethnic macroscopic variation.

There are five hair types used in this study, two of which are Afro, providing four macroscopically distinct hair types. The Afro hair types are characterised by their high degree of curl, ellipticity and fragile nature; the fibres are very tightly coiled, short and stretching the fibres to unwind them can cause the fibres to break easily. There are two types used in this study; Afro Soft and Afro Rubber. The Afro Soft is defined as the type that is 'soft' to the touch, and the Afro Rubber type has a 'bounce' or 'rubber' like characteristic when touched by hand. Both hair types show typically have short length fibres; no more than 5cm long when stretched. The European type fibres are long (typically ranging from 15-30 cm), cylindrical in shape and straight. The Chinese hair type is very similar to that of the European but the hair fibres are visibly thicker. The Mullaato visually appears to be more similar to the European hair type but possesses a significant wave to each fibre suggesting a slightly more elliptical cross section, they are also shorter in length. All hair fibres are very dark brown in colour or black.

In this chapter an investigation combining Small angle X-ray scattering (SAXS) and Wide angle X-ray scattering (WAXS) data recorded simultaneously across several different ethnic hair types in the dry and wet states has been made. In this study SAXS and WAXS techniques have been utilised to investigate hair samples in a non-intrusive manner obtaining information on the structure of the hair fibres at the nano and supramolecular scale (SAXS) and the sub-molecular scale (WAXS). X-ray scattering techniques require minimal sample preparation and allows for samples to be studied *ex vivo*. Both techniques have been coupled with Principal component analysis (PCA) to

identify how the difference in fibre diagrams and hence the structure occurs between the differential ethnic hair types across several levels of scale.

4.1 Sample Preparation

Hair types used in this experiment are; Afro (two sources were used labelled Afro Soft and Afro Rubber), Chinese, European and Mullato. All measurements were taken from single hair fibres and three hair fibres were used for each source.

4.2 Data Collection

Each hair fibre was placed in a purpose built sealed cell holder which can be filled with liquids. The hair fibres were precisely aligned using micro-syringes at each end of the cell in which the hair was threaded through so as to hold it steady in the cell. The micro-syringes reduce any twisting motion by the hair and hold it straight. The hair fibres were bathed in the X-ray beam providing a bulk analysis of a single hair fibre – i.e. the fibre diagram is a result of the contribution of the scattering from all of the structures within the hair fibre. The hair fibre was vertical and perpendicular to the X-ray beam. For the dry state each experimental measurement involved taking four exposures at set incremental distances along the hair fibre axis with set exposure times which varied according to hair type. All incremental distances between exposures for both the dry and wet state were 400 microns. In order to examine the same hair samples in both the dry and wet state, the samples were wetted by filling the sample chambers with de-ionised water via a syringe pump. After the cells had been filled with de-ionised water the hair samples were left for 5 minutes to become sufficiently wet so as to be representative of a wet state. Three exposures were then taken of the hair fibres in the wet state, the exposure times varied according to hair type. The exposure times for both the Afro hair types in the dry and wet state were 1.5 seconds and the exposure times for the Chinese, Mullato and European hair types in both the dry and wet states were 0.8 seconds on average.

The raw data collected in this chapter was not collected by myself; it was taken by Dr Ian Tucker of Unilever and gifted to me. The analysis of this dataset was a primary condition in the contract of my PhD which is sponsored by Unilever. It should be noted that an attempt was made to acquire my own data set for a bulk X-ray analysis of single hair fibres at the I22 beamline, Diamond Synchrotron, Oxford, UK. However, the data acquired at this beamtime was of insufficient quality for any analysis to be performed and therefore only the data set shown here could be used.

4.2.1 Experimental X-ray Scattering

All data was collected at the ID02 beamline at the ESRF, Grenoble, France. Full details of the ID02 beamline can be found in Section 3.2.3. The WAXS detector was fixed at a distance of 0.4 m from the sample providing a q range of $5.0 - 60 \text{ nm}^{-1}$ and the SAXS detector was fixed at a distance of 3.0 m from the sample providing a q range of $0.01 - 2.0 \text{ nm}^{-1}$.

4.3 Data Processing

All fibre diagrams were corrected for physical detector distortion and normalisation of pixel efficiency. The WAXS detector was calibrated using *p*-bromobenzoic acid (Urban, Panine et al. 2003) and the SAXS detector was calibrated using silver behenate as the laboratory standard (Huang, Toraya et al. 1993). All fibre diagrams were corrected for air scatter by means of subtracting a scaled background image corrected for transmission.

For the WAXS data, the data was processed using the Fit2d software package (Hammersley, Svensson et al. 1996). Figure 4.1 shows the typical region of the keratin fibre diagram captured by the WAXS detector this corresponds to the meridional centred components of the fibre diagram and contains the 0.515 nm meridional reflections that relate to the axial pitch of the alpha-helices in the Keratin intermediate filaments (KIFs). Fit2d was used to integrate across the entire active detector area to produce a 1-dimensional trace of the scattering intensity (arbitrary units) versus scattering vector ($q \text{ nm}^{-1}$) (see Figure 4.1).

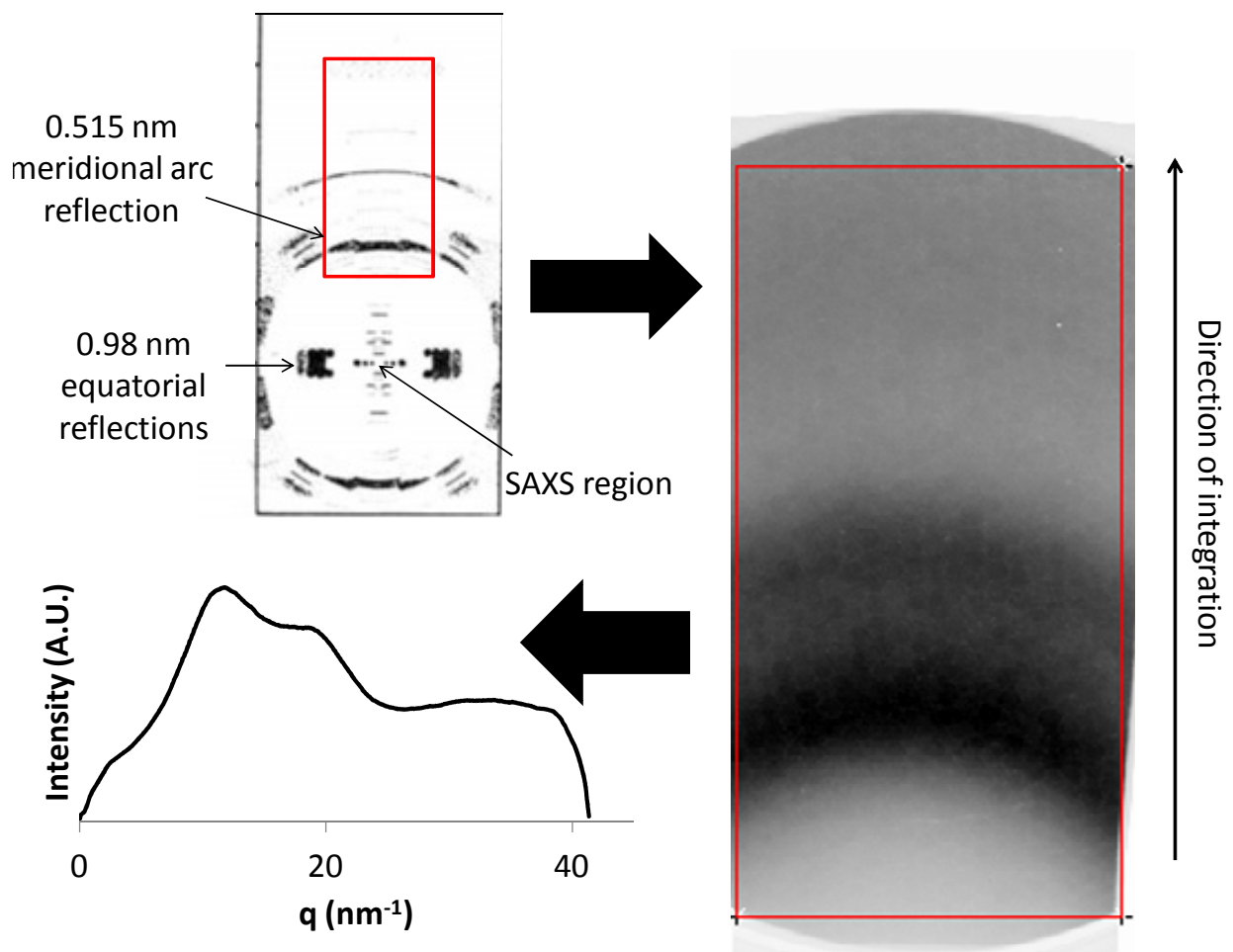


Figure 4.1 - A diagram showing how the 1-dimensional trace was obtained from the WAXS data. Seen in the figure is a wide angle diffraction pattern in the top left hand corner in a q range of $0 - 60 \text{ nm}^{-1}$ in the vertical direction. The red box highlights the meridional arc reflections that were captured by the WAXS detector at the ID02 beamline. The top left image in the figure has been adapted from (Fraser, MacRae et al. 1962). Figure shows the 2-dimensional diffraction pattern for the Chinese hair in the wet state in the WAXS region. The integration was made vertically from the bottom of the image to the top. This integration is used to form a 1-dimensional trace from the 2-dimensional fibre diagram. The 1-dimensional trace has units of intensity in arbitrary units on the y axis, and the x axis is in $q \text{ (nm}^{-1}\text{)}$.

The SAXS fibre diagrams were analysed using in-house software. For these fibre diagrams the integration of intensity versus scattering angle were made over a series of angular and azimuthal

integrations to isolate specific angular features of the equatorial and meridional regions (such as the omission of the lipid diffraction ring or the equatorial interference function of the KIFs). This was performed to allow analysis of isolated regions of scatter such as the low-angle diffuse scatter to examine if hidden correlations between data sets could be observed. Figure 4.2 shows examples of the integration areas made in FibreFix to do this. In each case processes were used to convert the 2-dimensional fibre diagrams into a 1-dimensional trace of intensity (arbitrary units) versus radial scattering angle ($q \text{ nm}^{-1}$). The resulting intensity profiles were then used to undergo PCA using in-house software. Here groups of linear traces from SAXS and WAXS images respectively were normalised and processed to determine base functions and eigenvalue coefficients corresponding to each different hair type. The resulting output was then evaluated for the features observed in the base functions and multi-dimensional plots of eigenvalues were created to inspect for structural similarities between hair types (see Figures 4.11, 4.12 and 4.13).

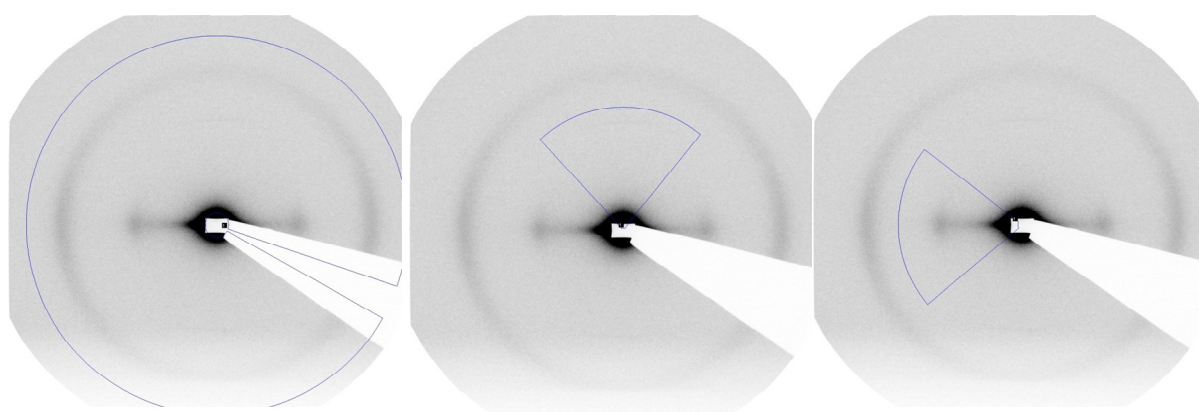


Figure 4.2 - Some of the SAXS scans used in FibreFix to isolate specific areas of the 2-dimensional diffraction patterns to undergo PCA according to where the features lie in both q range and in angular region. The image on the left shows a scan of the entire region containing data. The middle image shows a scan isolating the meridional region capturing the low angle diffuse scatter and the diffuse 6.7 nm arc reflection but omitting the lipid reflection. The image on the right shows a scan isolating the equatorial region capturing the low angle diffuse scatter and the reflection arising from the inter-lateral packing of the KIFs, it omits the lipid ring in this region. All images shown are for the Chinese hair type in the dry state.

4.4 Results

4.4.1 Inter-ethnic observations in the dry and wet states in the WAXS region

Figure 4.3 shows a 2-dimensional fibre diagram for each ethnic hair type in the dry state in the WAXS region. The WAXS images are visually very similar and are dominated by a diffuse scatter in the lower q range. Analysis of the 1-d traces arising from the integration of the diffraction patterns reveal there are negligible differences between the ethnic hair types in the intensity distribution of the diffuse scatter exhibited (not shown here). This indicates that between ethnic hair types the axial pitch of the keratinous fibrous structures remains constant.

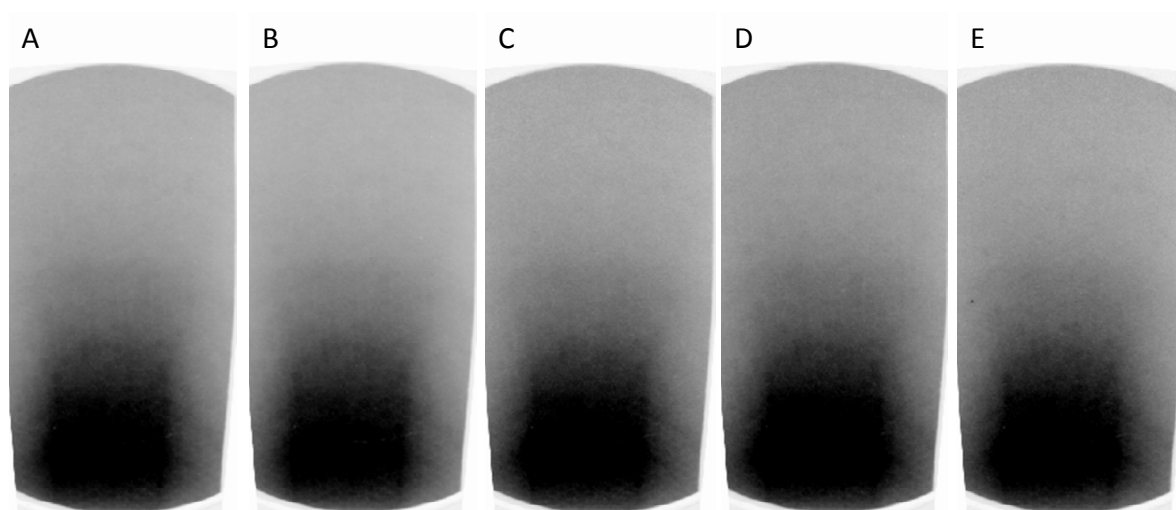


Figure 4.3 –2-d fibre diagrams for each ethnic hair type in the dry state in the WAXS region. A: Afro Rubber, B: Afro Soft, C: Chinese, D: European and E: Mullato. All images are normalised and set to the same intensity scale and the q range of all the images is $5.0 - 60 \text{ nm}^{-1}$.

Figure 4.4 shows a 2-dimensional fibre diagram for each ethnic hair type in the wet state in the WAXS region. The wet state shows the region is rich in at least three spatially overlapping peaks corresponding to the helical diffraction. The intensity distribution of the helical diffraction differs in the wet state between ethnic hair types. The diffuse scatter also appears to exhibit a different intensity distribution between ethnic hair types (not shown here) but these differences are subtle; resolvable differences are discriminated by the subsequent PCA analysis (see Section 4.4.3).

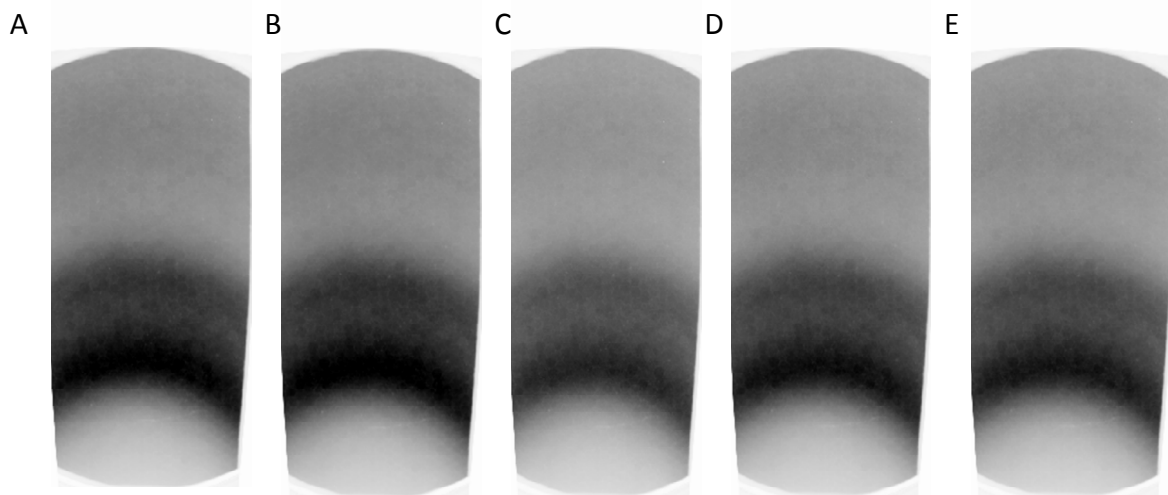


Figure 4.4 –2-d fibre diagrams for each ethnic hair type in the wet state in the WAXS region. A: Afro Rubber, B: Afro Soft, C: Chinese, D: European and E: Mullato. All images are normalised and set to the same intensity scale and the q range of all the images is $5.0 - 60 \text{ nm}^{-1}$.

4.4.2 Inter-ethnic observations in the dry and wet states in the SAXS region

Figure 4.5 shows a 2-d fibre diagram for each ethnic hair type in the dry state in the SAXS region. In contrast to the WAXS region in the dry state, visual differences are seen in the SAXS fibre diagrams. The most obvious difference seen between the fibre diagrams is the presence of the anisotropic lipid ring arising from the crystalline lipid present within the hair fibres.

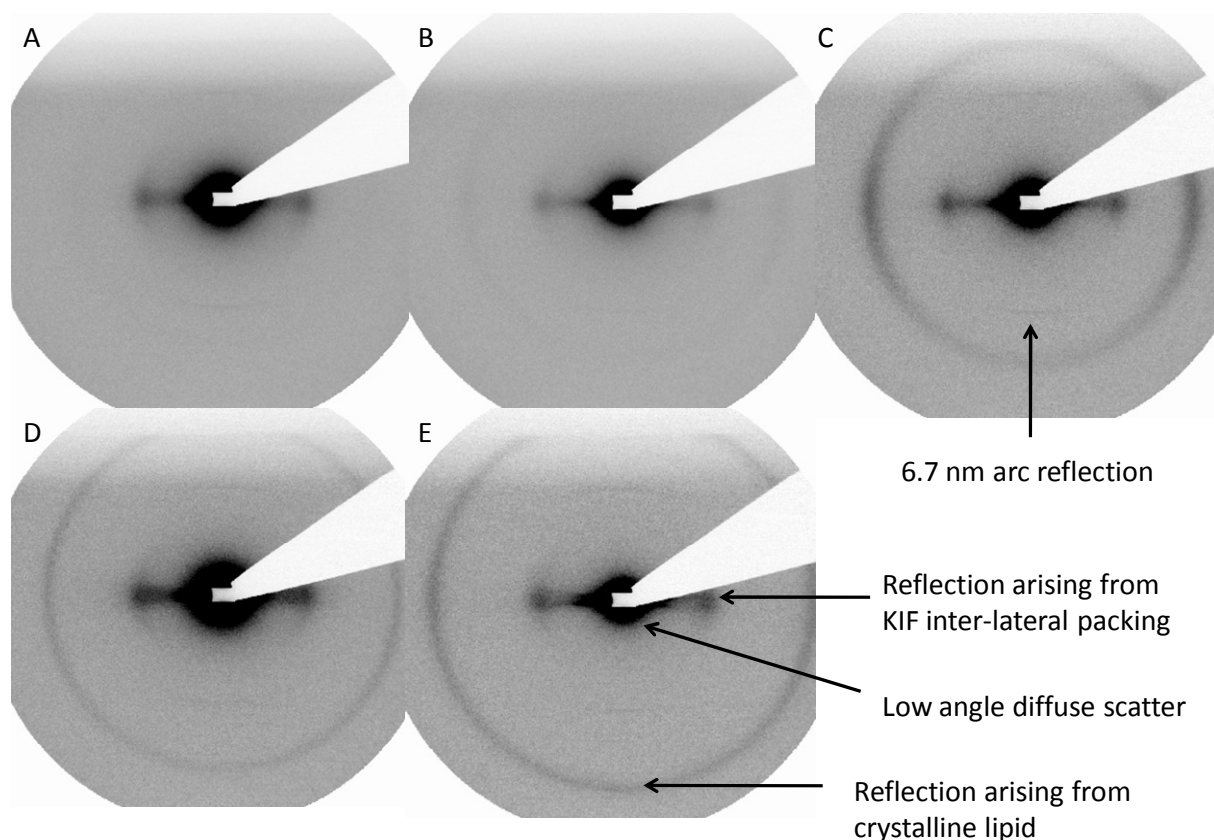


Figure 4.5 –2-d fibre diagrams for each hair type in the dry state in the SAXS region. A: Afro Rubber, B: Afro Soft, C: Chinese, D: European and E: Mullato hair type. All images are normalised and set to the same intensity scale and the q range of all the images is $0.01 - 2.0 \text{ nm}^{-1}$.

The Afro hair types (A and B) exhibit a low intensity lipid diffraction ring in comparison to the other three hair types, and there is a difference in the q spacing of the lipid ring arising in the Mullato hair type in comparison to the other hair types.

The position in q of the equatorial interference function arising from the inter-lateral packing of the KIFs appears to remain constant across all hair types; however differences in intensity above diffuse scatter can be seen between hair types as determined by the 1-dimensional radial traces. There are also differences seen in the azimuthal spread of the KIF interference function between ethnic hair types as determined by azimuthal integrations. The intensity profile and radial distribution of the low angle diffuse scatter is shown to differ between ethnic hair types. The low intensity 6.7 nm meridional reflection can be faintly seen consistently in all the fibre diagrams.

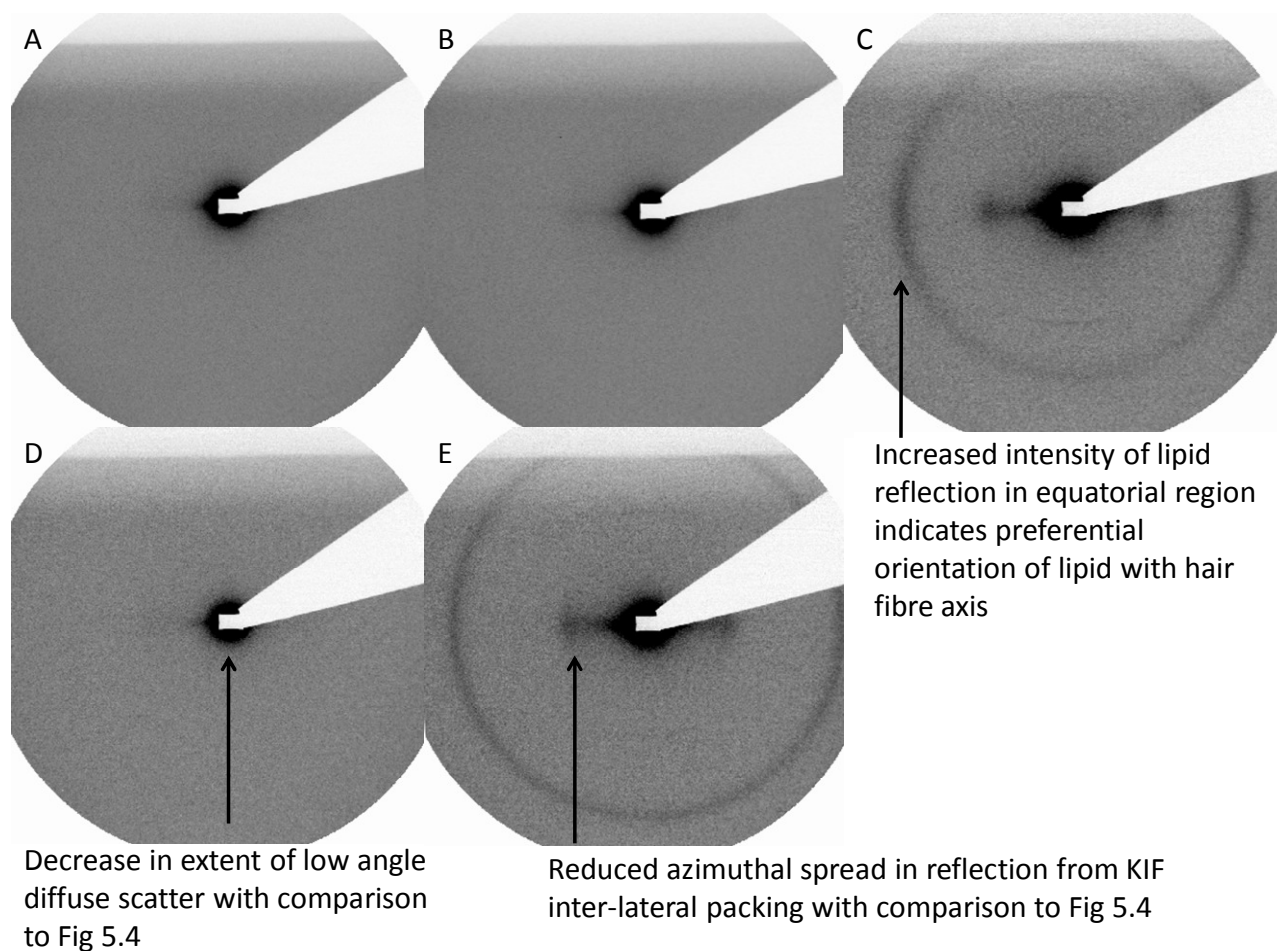


Figure 4.6 –2-d fibre diagrams for each hair type in the wet state in the SAXS region. A: Afro Rubber, B: Afro Soft, C: Chinese, D: European E: Mullato hair type. All images are normalised and set to the same intensity scale and the q range of all the images is $0.01 - 2.0 \text{ nm}^{-1}$.

Figure 4.6 shows a SAXS fibre diagram for each hair type in the wet state. The intensity scale on the wet state fibre diagrams is the same as the dry state. In comparison to the fibre diagrams for the dry hair, visual differences can be seen. Only the Chinese and Mullato fibre diagrams appear to resemble the same pattern as the dry fibre diagrams. Both the Afro hair types and the Euro hair type do not show any distinguishable diffraction features and are dominated by the low angle diffuse scatter which has been reduced in the extent of q range for both the equatorial and meridional regions. However, both hair types continue to produce a WAXS signal. The origins of this effect are most likely due to (1) contrast matching due to change of background from air to water (and corresponding increase in background electron density) and (2) fluidising the hair leading to a partial disruption of order. The Mullato hair type shows similar characteristic changes

to that of the Chinese hair type but also with reduced azimuthal spread in the KIF interference function. These changes are the reduction in the extent of q for the low angle diffuse scatter, the development towards isotropy in the low angle diffuse scatter and the change towards a lower position in q for the KIF interference reflection. Because of the changes in features between hair types and dry/wet for a number of features in the SAXS domain, it is worth examining each feature individually.

4.4.2.1 Observations of the crystalline lipid

One feature seen in the SAXS domain is the contribution from the crystalline lipid contained within the sample. The crystalline spacing of the lipid is approximately 4.5 nm but varies in both position and in peak width between hair types. The increased intensity of the reflection in the equatorial plane arises from the tendency of the lipids to preferentially orientate in planes parallel to the hair fibre axis (Bertrand, Doucet et al. 2003) as seen in Figures 4.5 and 4.6 and indicated in Figure 4.6.

It is seen in Figures 4.5 and 4.6 that the lipid reflection is more intense in the equatorial region of the fibre diagrams. Figure 4.7 shows an azimuthal integration analysis of the KIF inter-lateral packing peak and the crystalline lipid diffraction peak for each hair type over a 360 degree section. The high intensity peaks indicated by the black line relates to the inter-lateral packing arising from the KIFs, the lower intensity broader peaks indicated by the red line in this figure relate to the peaks arising from the diffraction of the crystalline lipid present in the hair. It is seen in Figure 4.7 that all hair types exhibit a co-location of the lipid peak with the KIF inter-lateral packing peak which entails a preferential orientation of the lipids with the hair growth axis. Also seen in Figure 4.7 is the way in which the Chinese, Euro and Mullato hair types exhibit a high intensity co-location of the lipid peak with the peak arising from the KIF inter-lateral packing. A high order and thus high concentration of lipid is seen with direct preferential orientation to the KIFs present in the hair. In contrast to this, there is relatively little intensity and thus little orientation of the lipids in both the Afro hair types and this may be reflected in the bulk hair properties.

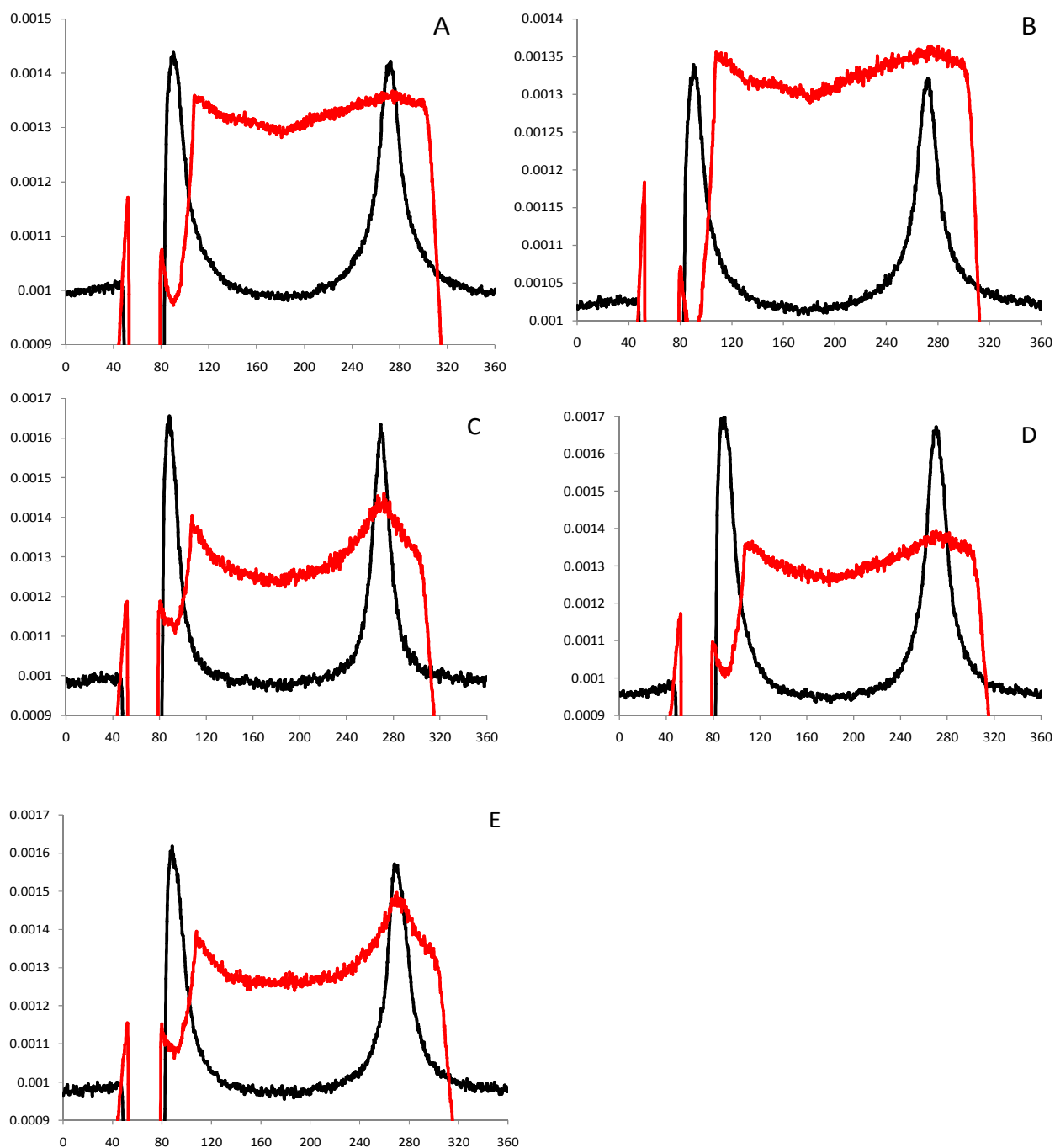


Figure 4.7 – Graphs showing the peaks arising from the inter-lateral packing of the KIFs in each hair type. The black line corresponds to the peak arising from the KIF inter-lateral packing and the red line corresponds to the peak arising from the crystalline lipid present in the hair. The dip in intensity between 40 and 80 degrees is a real effect due to the loss of data associated with the beamstop. The peaks seen here are from a full 360 degree azimuthal integration. The x axis is in degrees and the y axis is intensity in arbitrary units. A: Afro Rubber, B: Afro Soft, C: Chinese, D: Euro, E: Mullato.

Integration of the area underneath the lipid peaks for a full radial scan provides an indication of the total lipid content in each hair fibre. As the position of the lipid peak varied between hair types the integration was made in a q range of $1.0 - 1.8 \text{ nm}^{-1}$ for all hair types. An equal baseline subtraction was then performed for all the 1-d traces leaving only the lipid peak for each hair type and an equal baseline for all hair types thus giving the relative total lipid content. A quantification of the lipid content cannot be made using this technique. Figure 4.8 shows a bar chart displaying the relative total lipid content in each hair type. It is seen in this figure that the Chinese has the highest total lipid content and in decreasing order the pattern seen is; European, Mullato, Afro rubber and Afro Soft.

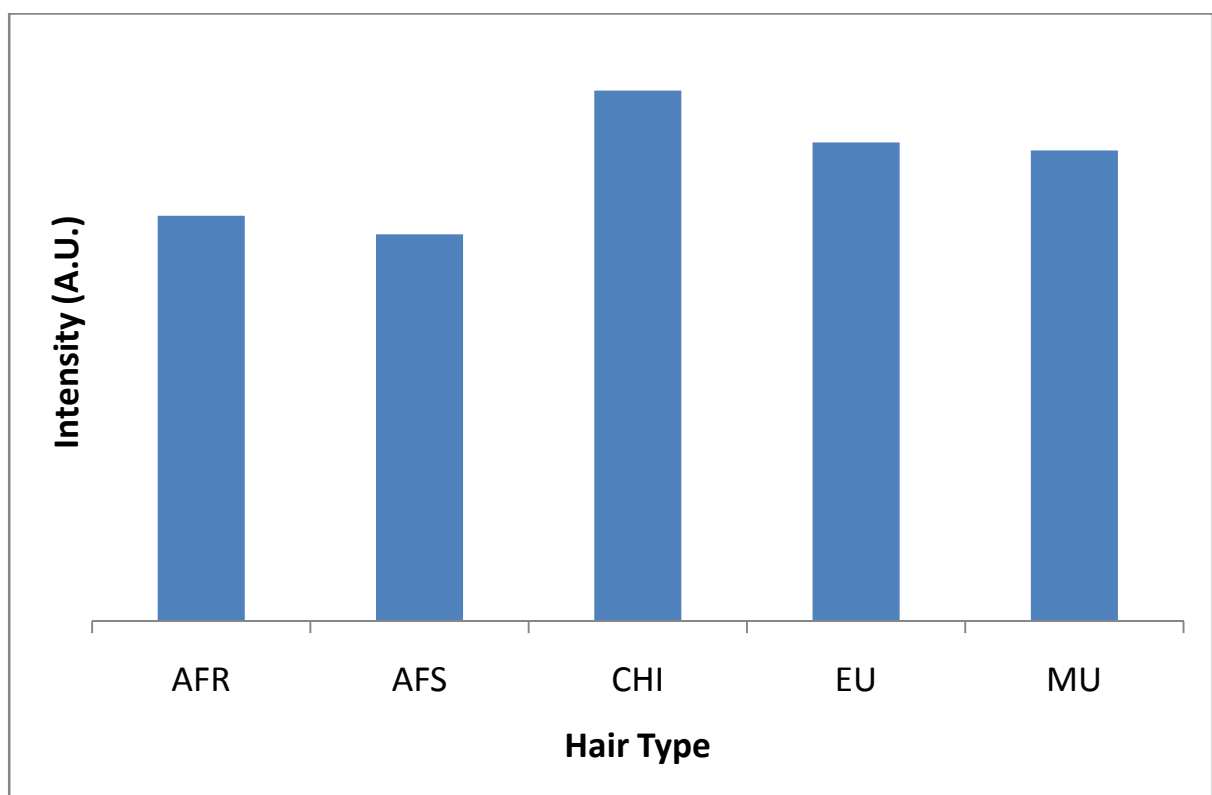


Figure 4.8 - Bar chart displaying the relative total lipid content of each hair fibre as calculated from the integration of the lipid peaks corresponding to the 1-d traces of a full radial scan.

Measurement of the full width half maximum (FWHM) of the peak breadth corresponding to the crystalline lipid reflection from the 1-d radial traces showed the Chinese hair type to have the greatest breadth corresponding to a low degree of crystalline order (measurement not shown

here). In order of decreasing breadth, the pattern seen is; Mullato and Afro Soft (these are equal to each other), Euro, Afro Rubber.

Table 4.1 shows the real space dimensions of the crystalline spacing of the lipids in the dry state calculated from the lipid peaks of the radially integrated 1-d linear traces. From the data it is seen that there are five different crystalline lipid lattice spacings.

Hair Type	Afro Rubber	Afro Soft	Chinese	Euro	Mullato
Lipid spacing (nm) ± 0.1 nm	5.0	4.8	4.7	4.2	4.0

Table 5.1 – Real space dimensions for the crystalline lipid spacing in each hair sample in the dry state.

Figure 4.9 shows a comparison of the radial 1-dimensional traces from the equatorial region of the 2-d fibre diagrams for each hair type in the dry and wet states. The FWHM and position of the peak corresponding to the crystalline lipid present in the sample remains constant between dry and wet states in all hair samples except the Euro and the Afro hair types where the lipid reflection disappears in the wet state.

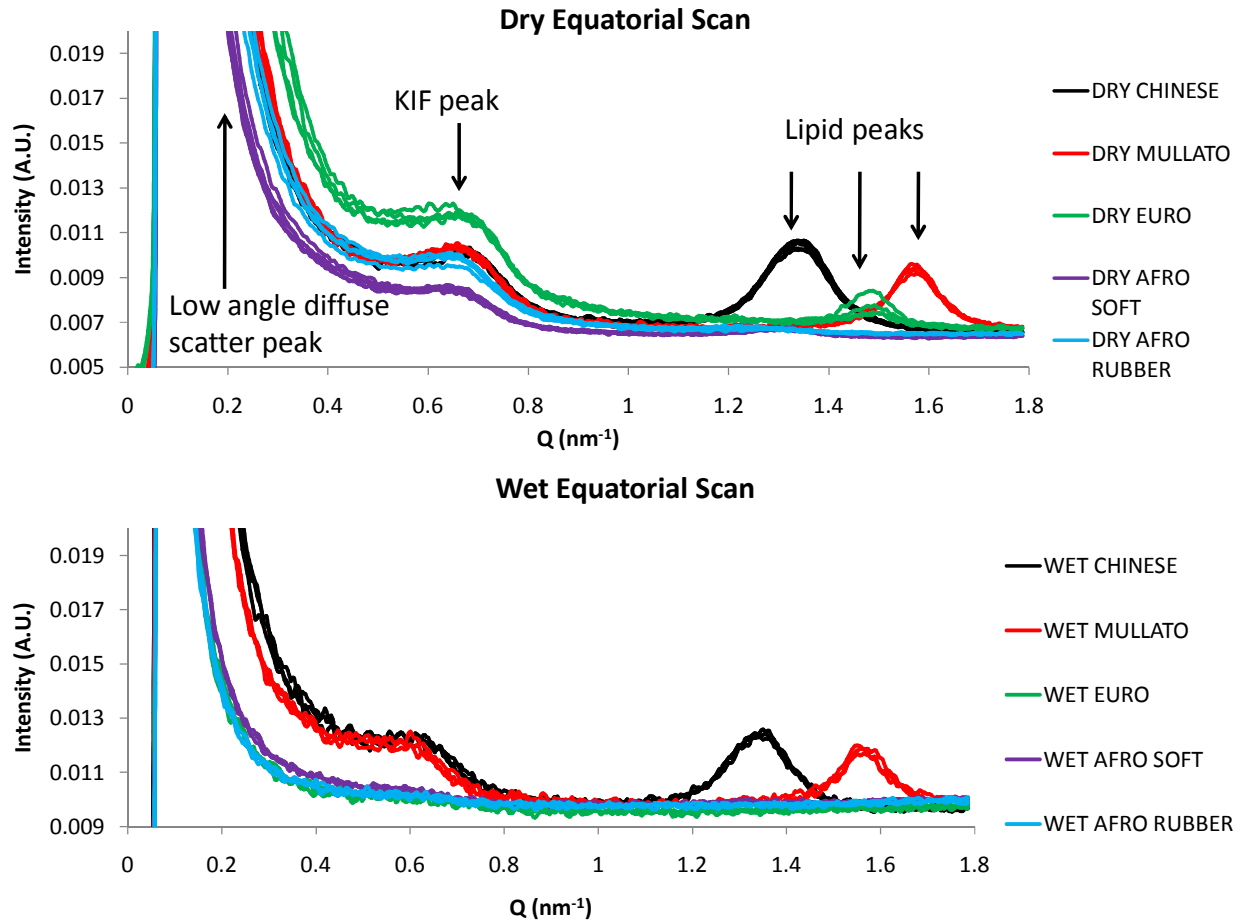


Figure 4.9 – The radial 1-d traces for each hair type in the dry state and the wet state respectively for an equatorial scan in the SAXS region. The arrows indicate what peak corresponds to which feature seen in the 2-d fibre diagram on the 1-d trace. The y axis is intensity measured in arbitrary units and the x axis is q (nm^{-1}). The graph shows $n=3$ for each hair type, thus creating three 1-d traces for each hair type.

4.4.2.2 Inter-ethnic observations of the low angle diffuse scatter

In each hair sample, there is a low angle diffuse scatter component found in a q range of $0.01 - 1 \text{ nm}^{-1}$. Analysis of a $\log I$ versus $\log q$ graph (not shown here) shows that there is a low angle diffuse scattering component with a linear power law decay in a q range of $0.01 - 0.24 \text{ nm}^{-1}$. Due to the anisotropic nature of the fibre diagram we determined the decay constant of diffuse scattering in both the equatorial and meridional directions. For the equator, in the dry state, the power law constant of decay varies from -1.728 in the Euro hair to -1.181 in the Afro Soft hair. In the wet

state, the power law constant of decay varies from -1.851 in the Chinese hair to -1.104 in the Afro Rubber hair. It is observed from the dry to wet state that the power law constant of the decay changes more in the Afro and Euro hair types than in the Chinese and Mullato hair types in the equatorial region.

In the meridional region in the dry state, the power law constant of decay varies from -1.732 in the Mullato hair to -1.187 in the Afro Soft hair. In the wet state in the meridional region, the power law constant of decay varies from -1.195 in the Chinese hair to -0.694 in the Afro Rubber hair. In each case the order of the decay rate constant is retained in the meridional and equatorial regions in both the dry and wet states. However, there is a difference observed in the decay rate between the equatorial and meridional regions in the wet state. Table 4.2 shows the value for the decay rate in each of the hair types in both the dry and wet states in the equatorial and meridional regions.

Hair type	Afro Rubber	Afro Soft	Chinese	Euro	Mullato
Dry equatorial rate (± 0.1)	-1.357	-1.181	-1.411	-1.728	-1.344
Wet equatorial rate (± 0.1)	-1.103	-1.180	-1.851	-1.205	-1.644
Dry meridional rate (± 0.1)	-1.362	-1.187	-1.418	-1.732	-1.354
Wet meridional rate (± 0.1)	-0.694	-0.729	-1.195	-0.767	-0.988

Table 4.2 - Value of the decay rate constant in the equatorial and meridional regions in the dry and wet states for each hair type.

4.4.2.3 Observations of the KIF inter-lateral packing

The interference function corresponding to the inter-lateral packing of the KIFs is seen in the equatorial region of the 2-d fibre diagrams (see Figures 4.4 and 4.5). The approximate q range of the reflection is seen at $0.6 - 0.8 \text{ nm}^{-1}$. The increased azimuthal spread towards the meridional region indicates an increased local disorder in the packing of the KIFs. In the dry state the Afro hair types display a lower intensity of the interference function than the other three hair types, with the Euro showing the largest intensity. The Afro Rubber, Euro and Mullato hair types show an increased azimuthal spread above diffuse scatter for the interference function.

Figure 4.10 shows the equatorial 1-dimensional traces for each hair type in both the dry and wet states highlighting the peak relating to the inter-lateral packing of the KIFs and the peak arising from the crystalline lipid in the samples. It is seen that there is both a peak position shift in q and broadening in the peak for the inter-lateral packing interference function for the Chinese and Mullato hair types in the wet state. In comparison to the dry state both the Afro hair types and the Euro hair type show increased broadening in the KIF interference function peak, towards a state where it is unable to be seen above the diffuse scatter.

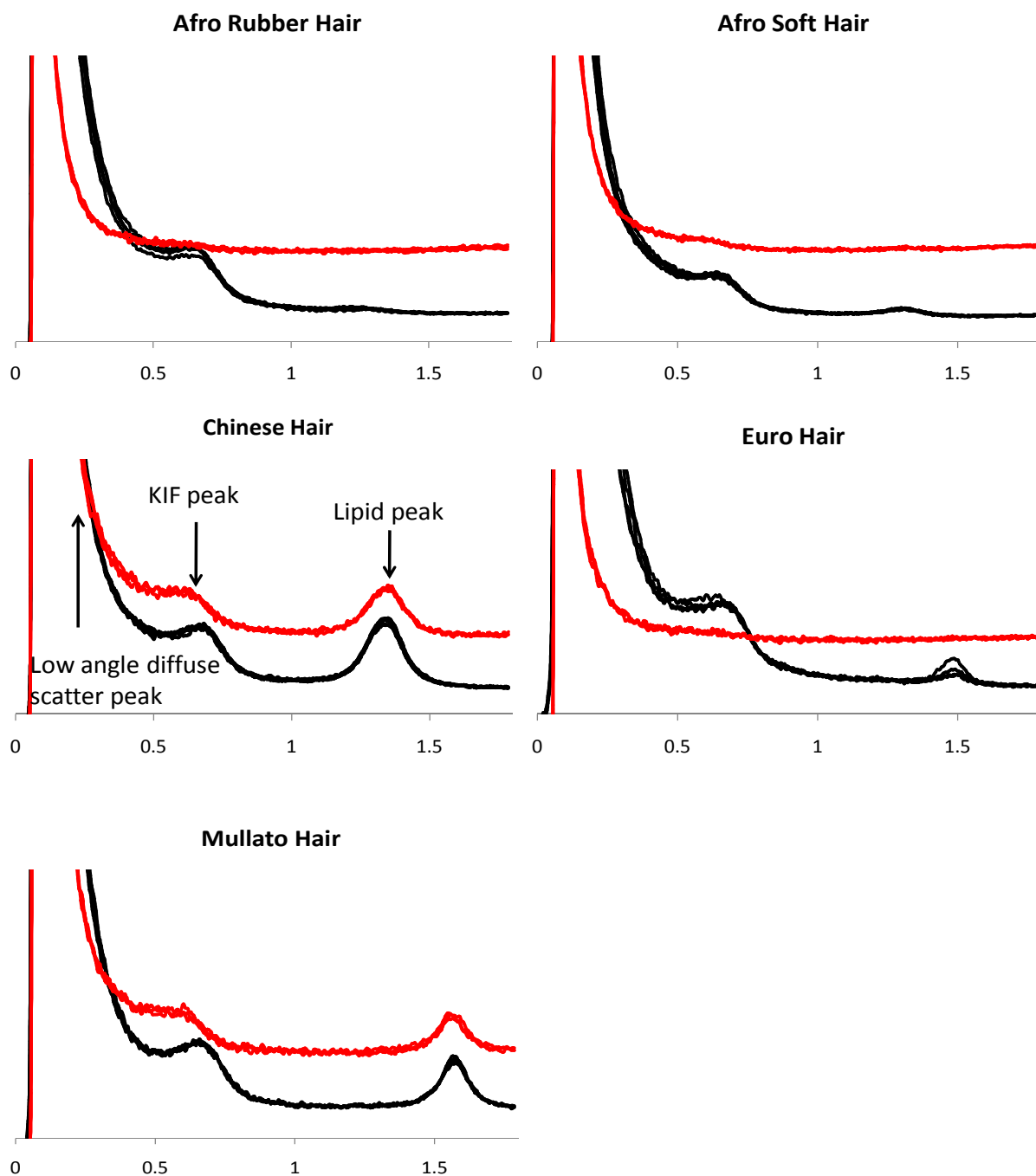


Figure 4.10 –The equatorial radial 1-d traces for each hair type in the SAXS region. The black lines represent the dry hair state and the red lines represent the wet state. The difference in intensity between the dry and wet state 1-d traces is a real effect. The arrows indicate what peak corresponds to which feature seen in the 2-d fibre diagram on the 1-d trace. The horizontal axis is measured in q (nm^{-1}) and the vertical axis is measured in intensity (arbitrary units) for all graphs. The graph shows $n=3$ for each hair type, thus creating three 1-d traces for each hair type.

4.4.2.4 Observations of the 6.7 nm meridional arc reflection

The low intensity sharp meridional peak corresponding to the 6.7 nm axial stagger of the 7th order of the 47 nm longitudinal axial pseudo-period resulting from the packing of keratin coiled coils into a KIF is found at $q = 0.93 \text{ nm}^{-1}$. This reflection is present but weak in all of the dry state fibre diagrams making comparisons difficult and is only seen in the Chinese and Mullato hair types in the wet state. The peak position corresponding to the 6.7 nm meridional arc reflection remains constant between the dry and the wet states for all hair types, however, the intensity for this arc reflection is reduced in all hair types in the wet state along with the prominence in the shape of the peak.

4.4.3 PCA of fibre diagrams

To derive greater certainty and detail in the analysis of the results, PCA was applied to both the SAXS and WAXS data sets. The application of this method has been described previously, (Jolliffe 2002). By producing multi-dimensional plots of the eigenvalue coefficients obtained for each hair sample, presence of clustering by ethnicity (if any) helps to first detect which base functions distinguish between each hair type. The eigenvalue coefficients are automatically calculated and outputted by the PCA software. This is the first step into investigating the discriminating factors between datasets in both the SAXS and WAXS domains.

Secondly, the PCA is used to produce base functions. The base functions are produced from the 1-dimensional traces from selected regions (see Section 4.3) and express a corresponding weighting towards certain features in the fibre diagrams. The features are identified by calibrating the q axis and comparing the intensity peaks of the base functions with the features seen in the fibre diagrams.

Lastly, bar graphs of the average eigenvalues coefficient weightings are produced to identify the weighting in each base function that each hair type possesses, along with the standard error. The significance of this plot is that it shows that in order for the hair types to be significantly different from each other, the bar and associated standard error for each hair type must not overlap if the base function sufficiently describes a distinguishing feature. Using this plot to identify which base

functions discriminate between hair types, referral back to the base function profiles themselves allows for the identification of the scattering feature which distinguishes between the hair types.

The differences between the case of dry and wet hair is sufficiently pronounced and therefore PCA is not used here. The PCA comparisons are restricted to the dry or wet state and seek to uncover discrimination between the ethnic hair types only.

4.4.3.1 PCA of the WAXS region for dry and wet hair

Figure 4.11 shows the average eigenvalues coefficients weightings plot for the dry WAXS patterns. It is seen in this figure that the PCA of the dry WAXS pattern can best resolve between different ethnic hair types in the first three base functions (BF). Base Function 1 distinguishes between the Afro hair types and the other three hair types; within this it also sufficiently distinguishes between the Afro hair types. BF3 shows that the Chinese hair type is different from the remaining hair types on the basis of the scattering features which this base function corresponds to and therefore discriminates this hair type from the rest. The Euro and Mullato hair type are best discriminated from each other in BF4. Figure 4.13 shows the base function profiles for the dry WAXS data. Inspection of the base function profiles shows that BF1 contains elements that will alter the contribution of diffuse scatter / fibre diffraction peaks. The third base function seems to particularly alter the breadth of the major peak observable.

The PCA of the wet WAXS pattern indicates that the second and especially third base function resolve best between the hair types. Figure 4.11 shows the average eigenvalues coefficient weightings plot for the wet WAXS data. It is seen in this figure that BF2 distinguishes the Afro hair types from the remaining hair types and BF3 distinguishes the Chinese, Euro and Mullato hair types from each other. The Afro hair types exhibit the greatest similarity; in fact the Afro hair types cannot be distinguished from each other in any of the base functions. The Chinese hair type shows the greatest difference in the second and fourth base functions. Figure 4.13 shows the base function profiles for the wet WAXS data set. Examination of the base functions for the second, third and fourth base functions indicate that the second base function discriminates on the relative contribution of the fibre diffraction peaks; especially that corresponding to the 0.515nm peak, the third base function makes a contribution that would shift the peak positions of the fibre

diffraction in q and the fourth base function would make a contribution to the relative intensity of the fibre diffraction peak set indicating a subtle change of the molecular arrangement within the structure of the KIF.

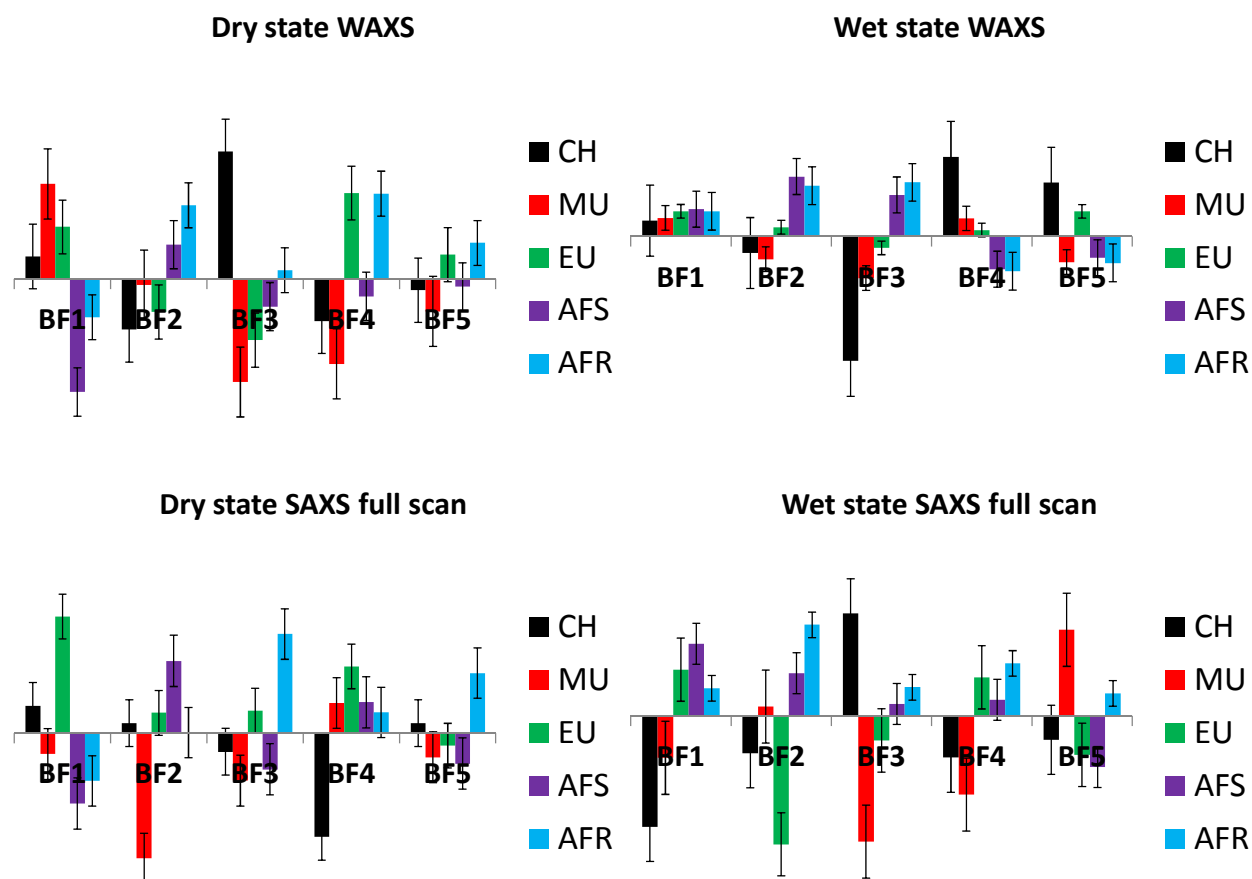


Figure 4.11 –The average eigenvalues coefficient weighting plots for the dry and wet state WAXS data and the dry and wet state SAXS data. The error bars indicate the standard error for the mean eigenvalue coefficient associated with each hair type for the respective base function. The averages are constructed from the corresponding 1-d radial traces of at least 3 different fibre diagrams in all cases. The horizontal axis is the base function number and the vertical axis is measured in intensity (arbitrary units) for all graphs.

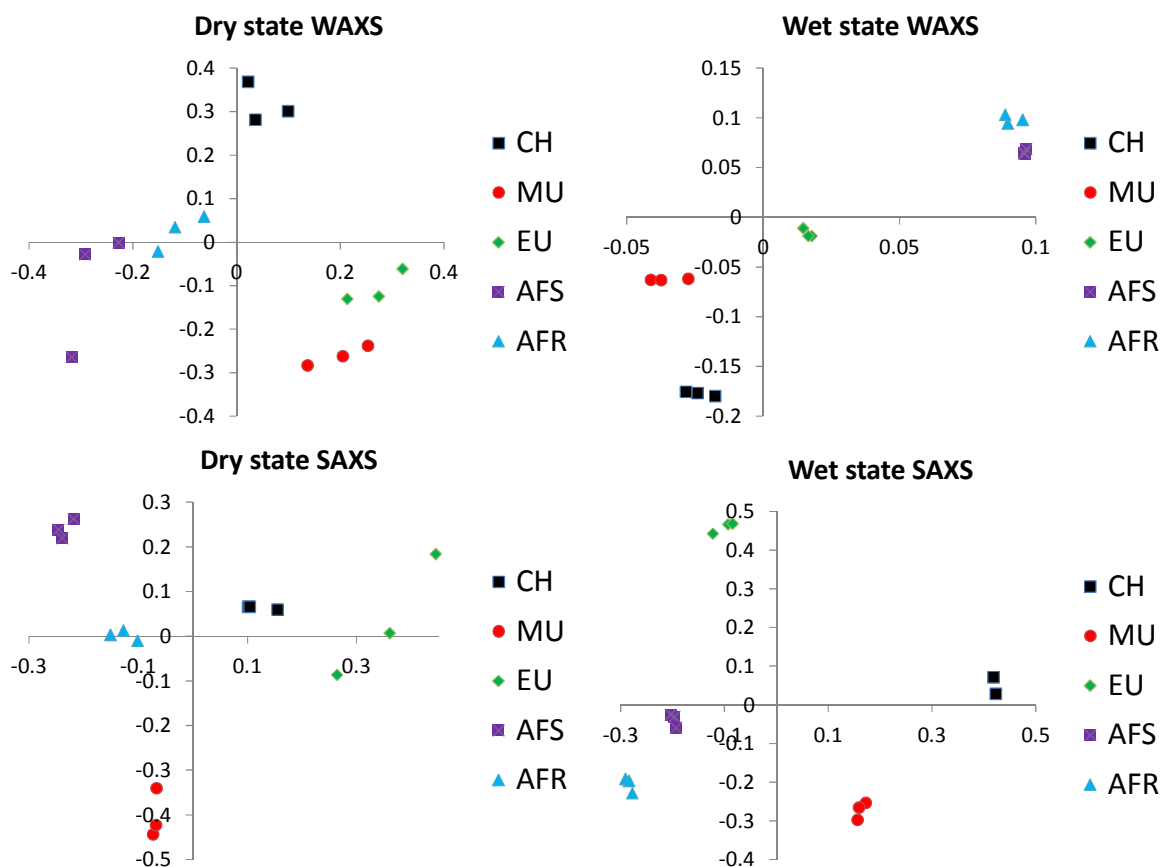


Figure 4.12 –Multi-dimensional plots for the dry and wet state SAXS and WAXS regions. Top left shows a multi-dimensional plot for base function 1 on the x axis and base function 3 on the y axis for the dry state data in the WAXS region. Top right shows a multi-dimensional plot for base function 2 on the x axis and base function 3 for the y axis for the wet state data in the WAXS region. Bottom left shows a multi-dimensional plot for base function 1 on the x axis and base function 2 on the y axis for the full angular scan dry state data in the SAXS region. Bottom right shows a multi-dimensional plot for base function 1 on the x axis and base function 2 on the y axis for the full angular scan wet state data in the SAXS region. Both axes are in arbitrary units for all graphs.

4.4.3.2 PCA of the SAXS region for dry and wet hair

Figure 4.11 shows the average eigenvalues coefficients weightings plot for the dry state full scan of the fibre diagram in the SAXS region. In this figure it is seen that the hair types are best distinguished from each other in the first three base functions. BF1 distinguishes the Afro hair

types from the Chinese and Euro hair type and also the Chinese and the Euro hair type from each other. BF2 shows that the Mullato hair type shows a large negative weighting in this base function which greatly discriminates this hair type from the remaining hair types. BF3 adequately discriminates between the Afro hair types, between the Afro Rubber and Euro hair types and between the Afro Rubber and Euro hair types with respect to the remaining hair types. Thus it is seen from Figure 4.11 that the first three base functions can discriminate between all of the ethnic hair types.

Figure 4.13 shows the base function profiles for the full scan of the SAXS region. Examination of the profiles shows that the base functions that allow discrimination between hair types indicate that they contain contributions from the lowest q parts of the small angle scatter and the region corresponding to the lipid diffraction.

Figure 4.11 shows the average eigenvalues coefficients weightings plot for the wet state full scan of the fibre diagram in the SAXS region. In this figure it is seen that BF1 discriminates the Chinese and Mullato hair types from the remaining hair types and also the two Afro hair types from each other. BF2 best discriminates the Euro hair type from the remaining hair types and also sufficiently discriminates the Afro hair types from each other. BF3 illustrates a large difference seen between the Chinese and the Mullato hair types and also best discriminates the Mullato hair type from the remaining hair types. On this basis, the first three base functions are sufficient to distinguish all the hair types from each other.

Similarly to the dry samples, examination of the base functions indicate that they contain contributions from the diffuse scatter of the lowest q parts of the small angle scatter and the region corresponding to the lipid diffraction (see Figure 4.13). In both the dry and wet samples, by restricting the q scattering range of the data to remove the contribution of the lipid diffraction, the scattering effects at low angle could still discriminate between the different ethnic hair types.

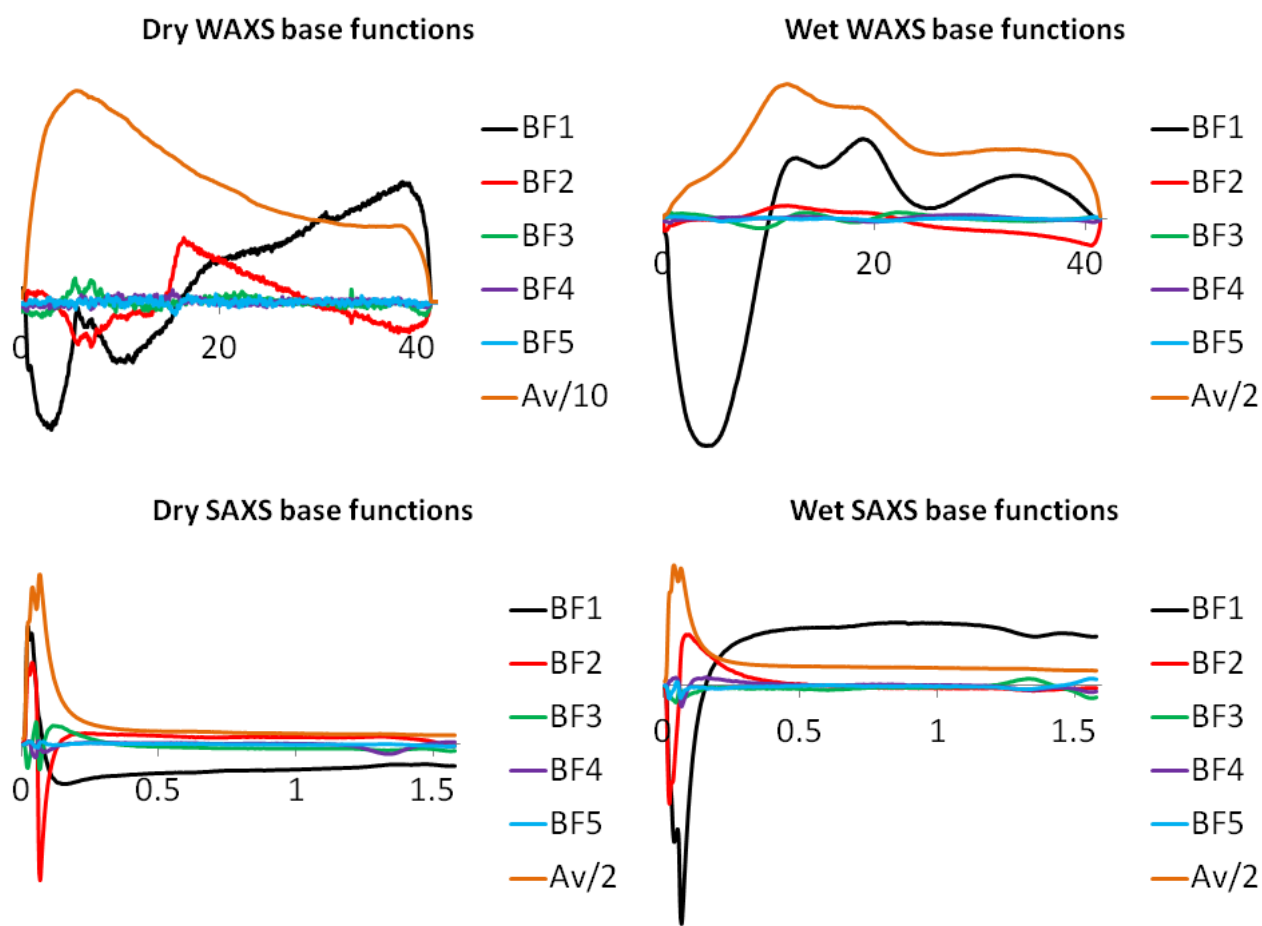


Figure 4.13 –The average base function and the first five base functions outputted by the PCA for the WAXS and SAXS data in both the dry and wet state respectively. All vertical axes are the intensity measured in arbitrary units and all horizontal axes are the respective q ranges measured in nm^{-1} .

4.5 Discussion

The X-ray diffraction data observed in the SAXS and WAXS experiments on different ethnic hair types exhibit a number of features. These correspond to the KIF interference function, the diffraction from endogenous lipid, meridional reflections corresponding to the helical parameters of the KIF / keratin helical structure and diffuse small angle and wide angle scattering. The integration of two dimensional diffraction data in the SAXS and WAXS areas allows quantitative differences between the diffraction of hair types to be evaluated. From this a number of comparisons can be made.

The analysis of data from this study shows that the parameters related to the KIFs does not vary between ethnic hair types. The structure and assembly of KIFs based on the equatorial fibre diagram scattering found in human hair remains an important area of research, as differences in structural modifications are clearly seen in this equatorial reflection under the influence of various chemical treatments but also in simple processes such as water absorption (Feughelman 1959, Feughelman 1994, Briki, Busson et al. 1998, Kreplak, Franbourg et al. 2002, Rafik, Doucet et al. 2004). Evidence in this study showing differences in the equatorial scattering between the dry and wet states confirms previous literature, particularly the mechanical behaviour reported by (Feughelman 1997). However, shown here for the first time are differences seen in the wetting behaviour of human hair by ethnic hair type as evidenced by the differences in scattering between dry and wet states.

Variation seen between ethnic hair types can be with respect to the lipid diffraction. Figure 4.5 shows the fibre diagrams for each hair type in the dry state, 1-dimensional radial integrations and 1-dimensional azimuthal integrations of these images show a difference in the spacing of the crystalline lipids seen between the ethnic hair types (see Figures 4.7 and 4.9) this is most pronounced between the Mullato hair type and the Afro hair types (see Table 4.1). There is a difference in the intensity of the lipid diffraction as a fraction of the total scattering in the SAXS region seen between ethnic hair types; this is most pronounced between the Afro hair types (which show the lowest intensity) and the remaining hair types. This therefore implies that the Afro hair types show less volume of lipid than the other hair types. The azimuthal (angular) distribution of the lipid signal also varies with hair type. The Chinese and particularly the Mullato hair types show high intensity peaks at specific angular locations coinciding with the KIF inter-lateral packing peak suggesting specific structural correlation. Figure 4.7 shows the azimuthal integration for the KIF interference function and the crystalline lipid reflection overlaid for each respective hair type. The Afro hair type demonstrates the least preferential orientation with the keratinous structures within the hair fibre. This indicates that a specific structural correlation of the crystalline lipid with the keratinous structures exists to different extents in hair types.

The cause(s) of the differences seen in the spacing of the lipids leads to three possible points; differences seen in the chain lengths of the lipids themselves, tilting of the lipids in the vertical direction (parallel to fibre axis growth) or a hydration effect. A difference in the chain length of the lipids themselves would cause a difference in the spacing of the lipids due to an overall size

difference of the lipid molecule itself which would alter the way the lipid is packed into crystalline form in the hair fibre. Slight tilting of the lipids so they are offset by an angle ϕ in the vertical direction would cause a difference to be seen in the spacing of the lipid. A hydration effect would alter the spacing of the lipids due to an increased/decreased number of water molecules interacting between the head groups of the lipids causing them to have an increased/decreased spacing. A study (Coderch, Mendez et al.) of internal lipids extracted from hair using SAXS techniques showed that there were two different types of lamellar lipid structures found in hair; one with a capacity to retain water, and one without. The lipid structure without the capacity to retain water was reported to have a spacing of 4.5 nm; here our results have shown that the spacings of lipids varies inter-ethnically, but also that the water retention properties also seems to vary. This result can be inferred from the continuing presence of the lipid peaks in the Chinese and Mullato hair types, but not in the Afro and European hair types. There is no evidence for other larger lipid structures found in our results. An interesting future investigation as a result of a direct consequence of the differences seen inter-ethnically in the crystalline lipids would be to see whether the differences seen have an effect on other macroscopic properties of the hair fibre such as its fibre strength, dimension, porosity and strain resistance.

High intensity low angle diffuse scatter that remains after background subtraction for machine dependent scatter is thought to correspond to the contribution of amorphous/disordered material found in the sample, and the non specific interactions/interfaces between the supramolecular structures. The differences evidenced here may indicate variation at the nanoscopic level between the supramolecular structures or the interfaces between these supramolecular structures. The data presented in Figures 4.5 and 4.6 evidences the difference in low-angle diffuse scatter seen between hair types. In human hair these difference could correspond to signals from smaller, possibly globular Keratin associated proteins (KAPs) which the KIFs are engulfed in that are proposed to bind together forming a matrix (Spei 1975, Feughelman 1994, Feughelman 1997, Briki, Busson et al. 1998) and the interfaces between the supramolecular structures. The structural information available on the KAPs is very limited, and so their contribution to the 2-dimensional fibre diagrams is poorly understood. Very little is known about both the structure of KAPs and the low-angle diffuse scatter may contain valuable information about their size and interaction. Dekio & Jidoi (Dekio and Jidoi 1998) reported that differences

were seen in the ratio of KAPs/KIFs by ethnicity. It may be possible to relate the enhanced levels of diffuse scatter observed here to the increased level of KAPs observed in Afro hair as reported previously.

The data collected from hair samples in the WAXS region correspond to the intra molecular structure of keratins, these exhibit little inter-ethnic variation observed at this distance scale. We were only able to observe the relative intensity of the spatially overlapping peaks corresponding to helical diffraction in the wet state WAXS images and in the relative intensity contribution of the diffuse scatter. Evidence from this experiment also shows that there is little variation of the alpha-helical structure between hair types and in the structure of the KIFs. This further confirms reports from Dekio & Jidoi who did a study on the chemical composition of the KIFs and reported that they did not differ electrophoretically between ethnicities (Dekio and Jidoi 1998).

The data described above indicates that there are differences between ethnic hair types. This was further analysed using PCA of the linear integrations of Intensity versus scattering angle in both SAXS and WAXS regions. The eigenvalues from PCA analysis revealed that the differential ethnic hair types can be distinguished at both the inter-molecular level and the nano and supramolecular levels in both the WAXS and SAXS regions respectively (see Figures 4.11 and 4.12). Although the PCA of the WAXS region shows clustering by ethnicity, particularly more so in the wet state samples, here the Afro hair types are most similar to each other but are sufficiently distinguished from the other hair types. The PCA of the SAXS region reveals that the biggest distinguishing feature between ethnic hair types is the crystalline lipid; specifically the spacing of the lipid present in the hair fibres. The second most distinguishing feature is the low-angle diffuse scatter.

This analysis has shown on the basis of both the lipid and keratinous protein present in the hair and from the low/wide angle diffuse scatter the hair types can be distinguished from each other.

4.6 Summary

The results presented here show that ethnic hair types can be discriminated by a number of different structural features across several levels of scale. Although macroscopically distinct, it

has been shown that there is variation in the nanostructural organisation. Evidence provided here on the basis of the scattering/diffraction from X-ray studies shows differences between hair types which is in contrast with (Franbourg, Hallegot et al. 2003) which reported that no differences were seen between the diffraction patterns from X-ray Diffraction (XRD) by Asian, Caucasian and Afro hair types.

The structural crystalline lipids present differ with ethnicity based on the dimensions of their crystalline spacing, the total and angular intensity of the lipid and the relative angular order. Variation in the properties of low-angle diffuse scatter are visible from the fibre diagrams indicating differences in the size, shape (and probably the interfaces between) supramolecular structures. There are also differences seen between hair types in the dry and wet states that have never been reported before. The fibrous keratinous structures found in hair remains relatively constant between hair types which leads to the hypothesis that the amorphous materials or KAPs may be what causes the largest differences to be seen macroscopically which further supports previous literature (Dekio and Jidoi 1990, Dekio and Jidoi 1998). This evidence points towards further investigation required into the supramolecular structures of ethnic hair types, the contribution of the KAPs as an entity to the bulk properties of hair and also the contribution from the lipids as a molecular component.

While this study has provided vital information on the inter-ethnic variation of hair fibres, it is limited in its scope with regards to the zonal location of the structural variation as the fibre diagrams are the result of the observations averaged over the whole hair fibre. It is therefore necessary to conduct an experiment which probes into the location of the structural variations observed inter-ethnically. A technique such as microfocus X-ray scattering can be used to provide structural information over a small change in sample space. This technique can therefore be used to gain zonal information on the structural variation of lipids, the low angle diffuse scatter and the keratinous structures across the hair fibre.

Chapter 5 – The use of microfocus X-ray diffraction to study differential ethnic hair types

X-ray diffraction is an analytical technique that can be used to investigate the structure of human hair over several levels of scale. Advances in synchrotron science have led to the development of high intensity focussed X-ray beams with a beam size on the micron scale. These can be used to make a detailed textural map of the nanostructural variation of any material on a microscopic length scale. Previous evidence gathered from the SAXS and WAXS experiments on single hair fibres showed that the main variation found was related to the lipid content in the SAXS region and the diffuse scatter in both the SAXS and WAXS regions. This experiment investigated ethnic hair types by examining the ultrastructural architecture and the molecular structures and supramolecular interfaces that comprise it.

Here, this technique has been applied to map out the ultrastructure of hair fibres to identify differences in textural variations seen intra and inter-ethnically; particularly in the lipid diffraction and diffuse scatter contribution to the fibre diagrams. This has been achieved by performing a ‘skin-core’ experiment which has enabled analysis of the way in which the contribution of specific scattering/diffraction components are distributed across the cross section of the hair fibre.

5.1 Sample Preparation

Hair types used in this experiment were; Asian, Afro, Chinese, European (two sources were used labelled type 1 and type 2) and Japanese. All samples used were single hair fibres. Only one hair fibre from each source was used.

5.2 Data Collection

X-ray microfocus diffraction experiments were performed at the ID18F microfocus beamline (Somogyi, Drakopoulos et al. 2001). Full details of the ID18F beamline can be found in Section

3.2.2. The hair was mounted into the X-ray beam using custom built holders; these held each single hair fibre rigidly under a low tension whilst facilitating beam alignment and minimising vibration. The hair fibre axis was held in the horizontal plane and perpendicular to the X-ray beam. The hair fibres were subjected to a “skin-core experiment” (see Figure 5.1) where the X-ray beam was scanned across the hair fibre and an image was taken with a 5 second exposure time every 5 microns across the width of the hair fibre. Diffraction images were collected on a MAR CCD camera (2048 x2048 pixels – 64.45 x 64.45 μm^2 resolution – 16-bit encoding). The q range of the detector was 0 – 20 nm^{-1} . Figure 5.1 shows a schematic of a hair fibre (not used in this study), the arrows drawn across the image detail where the X-ray beam was passed across hair fibres in the experiments.

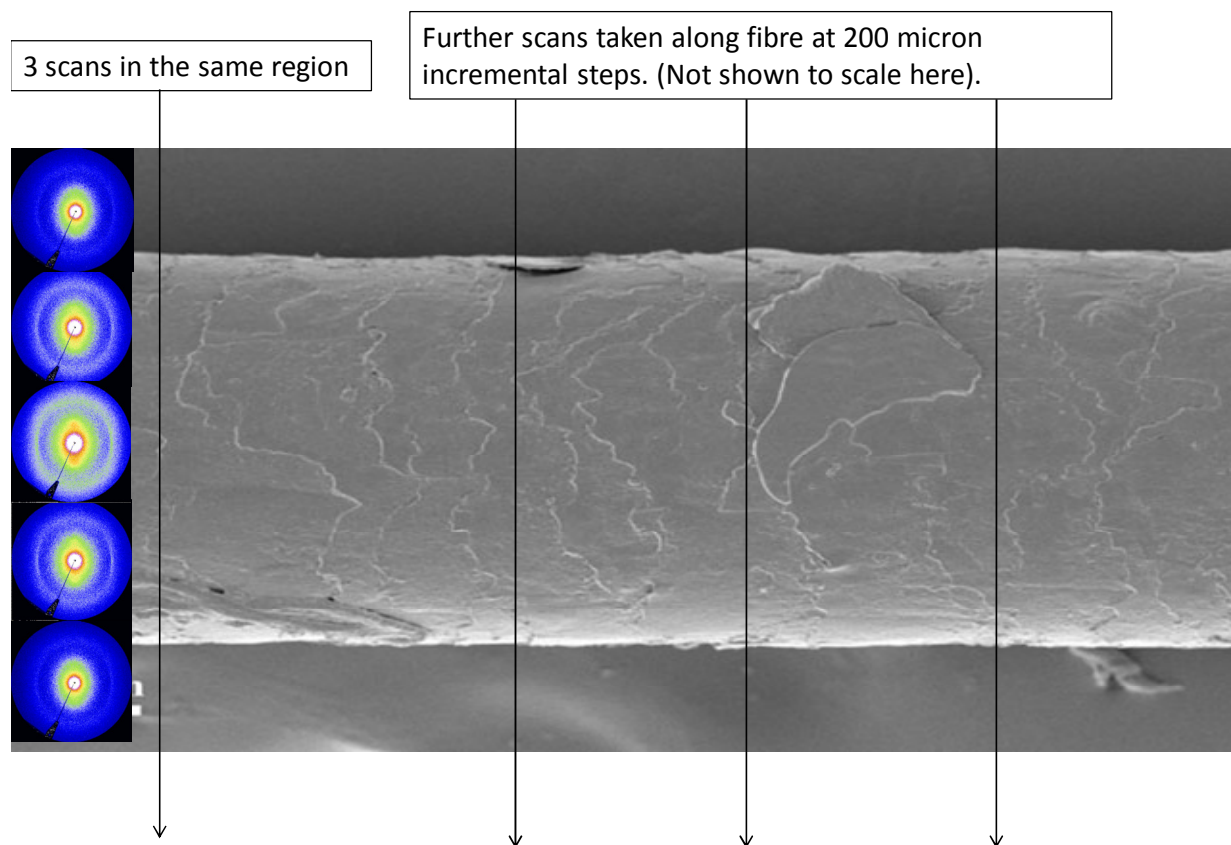


Figure 5.1 – Figure detailing the basis of the skin-core experiments that were used for the data acquisition of the hair types under test at the ID18F beamline at the ESRF. Images taken at 5 micron increments across the hair fibre detail the textural variation of the structure of the hair fibre at different points. A typical scan involved collection of fifty 2-d fibre diagrams. Adapted from (Pierson and Gerts 2008).

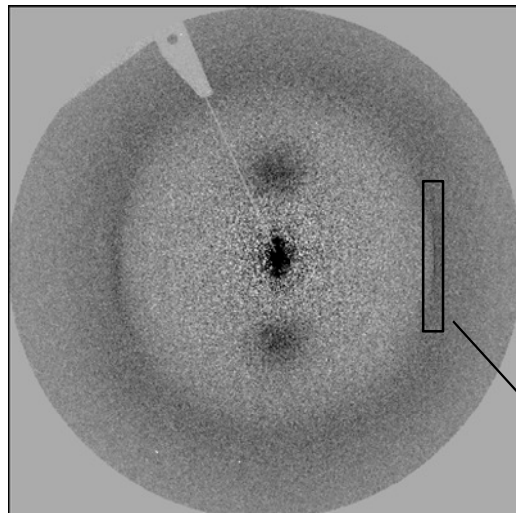
Each experimental measurement involved taking three scans at the same horizontal position across the first section of the hair under test and then subsequent scans across the hair fibre at distances of 200 microns along the hair fibre. This was repeated up to a maximum distance of 1 mm along the hair. Images were taken with the same exposure time in the absence of the hair fibre to provide a background image to subtract from the fibre diagrams.

5.3 Data Processing

The data were processed using a combination of the Fit2d software package (Hammersley, Svensson et al. 1996) and in-house software. This involved the removal of a weighted empty beam background image; a single background image of the scattering in the absence of a sample was recorded for each individual scan to compensate for the scattering arising from the ambient mounting conditions at the time of each scan. The in-house software was developed to perform optimised background subtraction using a Fortran 77 software package to write the code and the Merlin supercomputer from the advanced research computing @ Cardiff facility (ARCCA). The background file and data file for the corresponding hair type are read into the memory. An iterative process attempts to subtract the background file from the data image by a decreasing factor. The end of background subtraction occurs when one of the pixels in the data image becomes less than zero due to the background pixel having a larger intensity than the data pixel (for each individual pixel in the fibre diagram). The data is read back into Fit2d software after it has been processed so that it can display a composite image of the files with optimal background subtraction.

In order to measure changes from specific characteristic parts of the fibre diagram, eight 2-d sectors of the fibre diagram were chosen to monitor the changes in the intensity of the diffraction data between and within samples. Each hair sample therefore yields scans of eight regions of integral intensity at each point of diffraction across the hair. The variation of integrated intensity indicates the variation in contribution of each scattering feature at a specific position within the hair fibre in any one scan. In order to make meaningful comparisons between the different hair types, it was necessary to normalise the intensity of each sector. The eight integral plots enable a systematic analysis of the features of individual fibre diagrams in a scan and provide a robust and efficient way of monitoring the contribution of scattering features across the width of the hair

fibre. Figure 5.2 visually outlines the way in which one of the eight sectors chosen from the fibre diagram is used to produce a 1-d trace of the integrated intensity of a specific scattering feature for an entire scan.



- Pixels within the black box are integrated across the region and outputted as a single figure of intensity.
- This is performed for all eight selected integration sectors of the fibre diagram and for all fibre diagrams in a scan.
- The intensities for each sector are plotted for all the images taken in a scan.
- This produces a 1-d linear trace for the entire scan of the intensities for each of the eight scattering features in a fibre diagram.

The sample was mounted horizontally

- Data analysis is performed by scan and sector.
- Comparisons are made between:
 - Sector integral measurements (scattering features) across the hair
 - Zonal variation along the hair (related to the ultrastructure)
 - Between hair types.

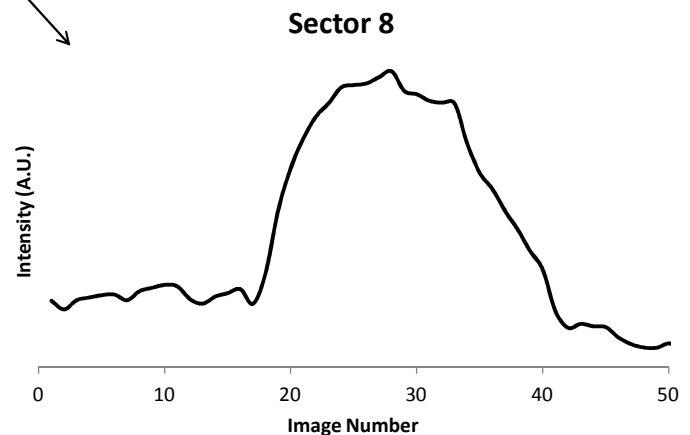


Figure 5.2 – Figure details how one scattering feature in a 2-d fibre diagram is processed to form a 1-d linear trace for all the images taken in a scan across the hair fibre. The sample is horizontal and perpendicular to the X-ray beam.

Figure 5.3 gives a visual description of the sectors that are chosen by the in-house software from the wide angle fibre diagrams.

Sector 1 – total intensity of the fibre diagram (not shown here).

Sector 2 - intensity integral from the lowest angle area of scattering close to the beam stop.

Sector 3 – The area corresponding to lipid diffraction in the small angle region

Sector 4 - 0.98 nm equatorial reflections.

Sector 5 - integral measurement of the diffuse contribution to the scattering pattern at a spatial resolution around 0.35nm

Sector 6 - integral measurement of the diffuse contribution to the scattering pattern at a spatial resolution around 0.55nm

Sector 7 - integral around the backstop at an angle that contains the diffraction from the interference function between KIFs.

Sector 8 – 0.515 nm meridional arc reflections

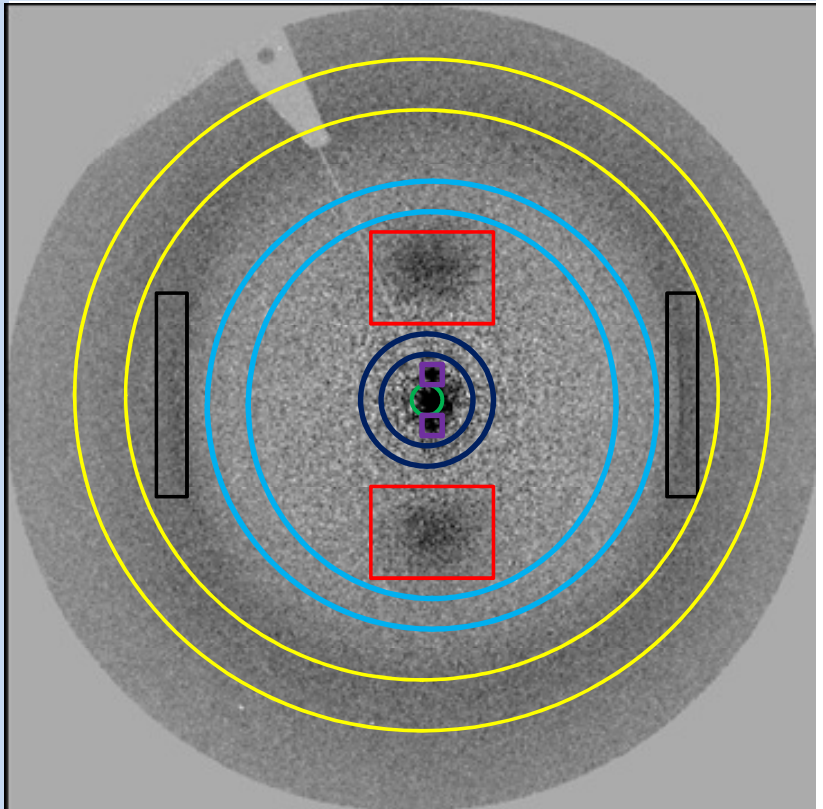


Figure 5.3 – The eight sectors chosen by the in-house software from the 2-d fibre diagrams. Due to the inherent cylindrical symmetry of fibre diagrams, each image allows the opportunity to collect data from at least two equivalent diffraction regions.

The presence of lipid at a specific position along a scan can also be detected; this was identified by looking for the characteristic crystalline diffraction ring via visual inspection of the small angle region using the Fit2d software. This method provides a simple identification of the presence of crystalline lipid in different regions of the hair ultrastructure. Figure 5.4 shows a small angle image from the European type 1 hair sample used in this study containing lipid.

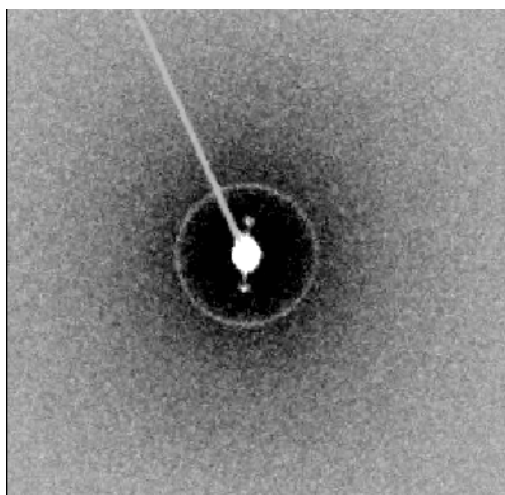


Figure 5.4 – Small angle fibre diagram of the European type 1 hair sample. The ring around the central small angle signal indicates presence of crystalline lipid structure in the sample. The hair sample is horizontal and therefore the equatorial reflections are vertical. The q range in this image extends out to 6 nm^{-1} .

Table 5.1 shows the number of complete scans used in this experiment taken at each position along the hair fibre. Some scans did not complete across the cross section of the hair fibre due to instability of the microfocussed beam at the synchrotron; because of this factor only the complete scans taken across the hair fibres will be presented. Due to severe time limitations and the exploratory nature of the experiment, there were no replicate measurements taken from different hair samples from the same hair source in this data set.

Hair type	No of scans per hair fibre	No of images in scan	Incremental steps (μm) along fibre axis
Afro	2	40	200
Asian	3	60	3 x 200
Chinese	3	50	N/A
Euro type 1	1	50	N/A
Euro type 2	1	44	N/A
Japanese	3	50	3 x 200

Table 5.1 – Hair types used in this experiment and the details of the scans taken for each hair type.

5.4 Results

The following results comprise datasets of the 1-d traces for the integrated intensity of sectors extracted from each fibre diagram at each position in a scan. These allow a comparison between the integral scans made within and between different hair types. The 1-d linear traces are a plot of the normalised integral intensity of the scattering features from the individual fibre diagrams from the scan across the hair fibres plotted against the image number. The image number is a measure of the distance the beam has been moved across the hair fibre width in 5 micron increments. The challenge of the experiment performed here is that a weak diffraction pattern from a single hair has effectively been dissected into 40 to 60 sub images. For ease of interpretation the results have been presented in sections according to the ethnicity of the hair. Only one raster scan for each hair type shall be presented here, the rest of the microfocus scans are in Appendix I.

5.4.1 Afro Hair

Figure 5.5 shows the integrated intensity plots from the skin-core experiment and Figure 5.6 shows a composite image of all the fibre diagrams. By cross referencing information from the two images with each other it is possible to interpret what some of the features in the 1-d traces correspond to in terms of the scattering features seen in the fibre diagrams. From the 1-d trace which represents the total scattering signal for the Afro hair, it is seen that that only 23 of the images correspond to scattering features from the interaction of the X-ray beam with the hair so the fibre can be considered to be approximately 115 μm in width. The most obvious feature about the Afro hair seen in the fibre diagrams is the preferential orientation of the fibre diagram itself; it has an orientation of around 30-45° with reference to the direction of the hair fibre. The sectors taken for the 1-d trace analysis were adjusted to compensate for this orientation effect which is most likely due to the high curl of the hair fibre.

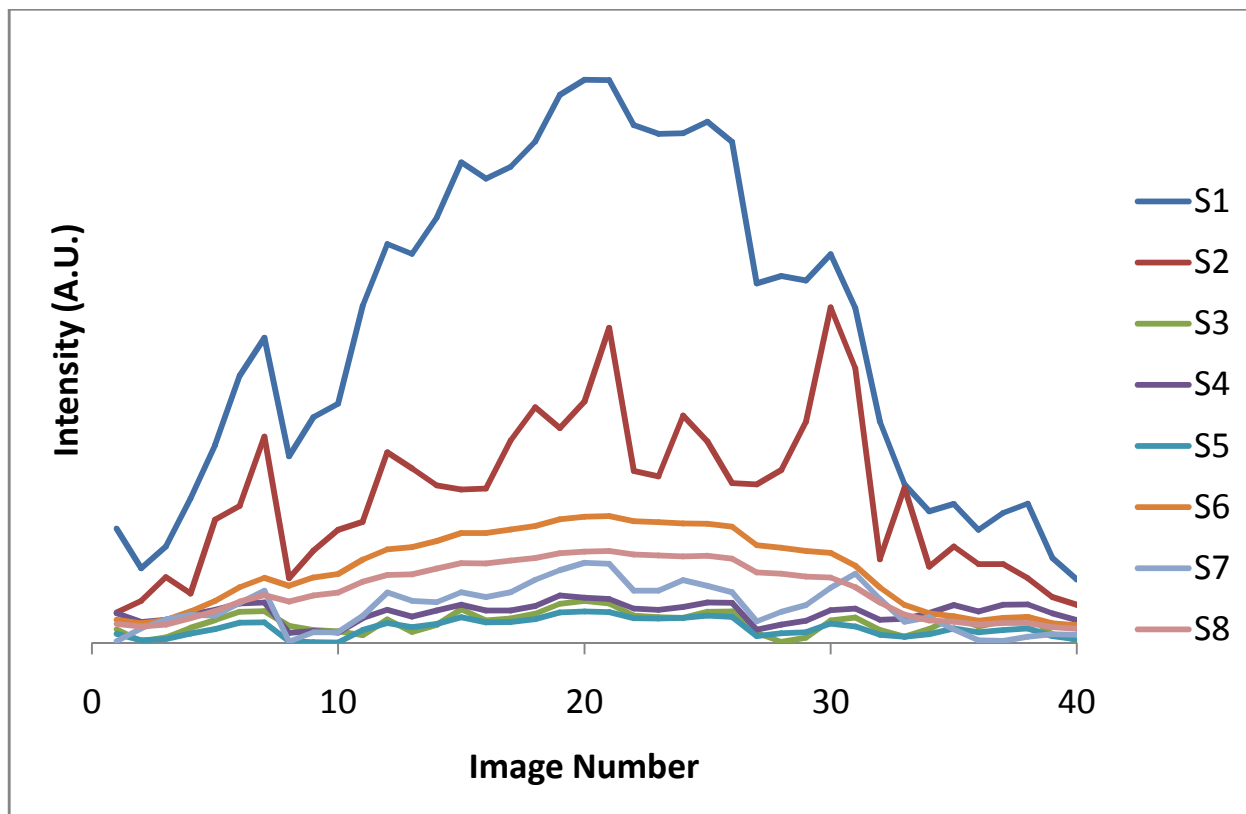


Figure 5.5 - The integrated intensity plots for all of the sectors for the Afro hair type.

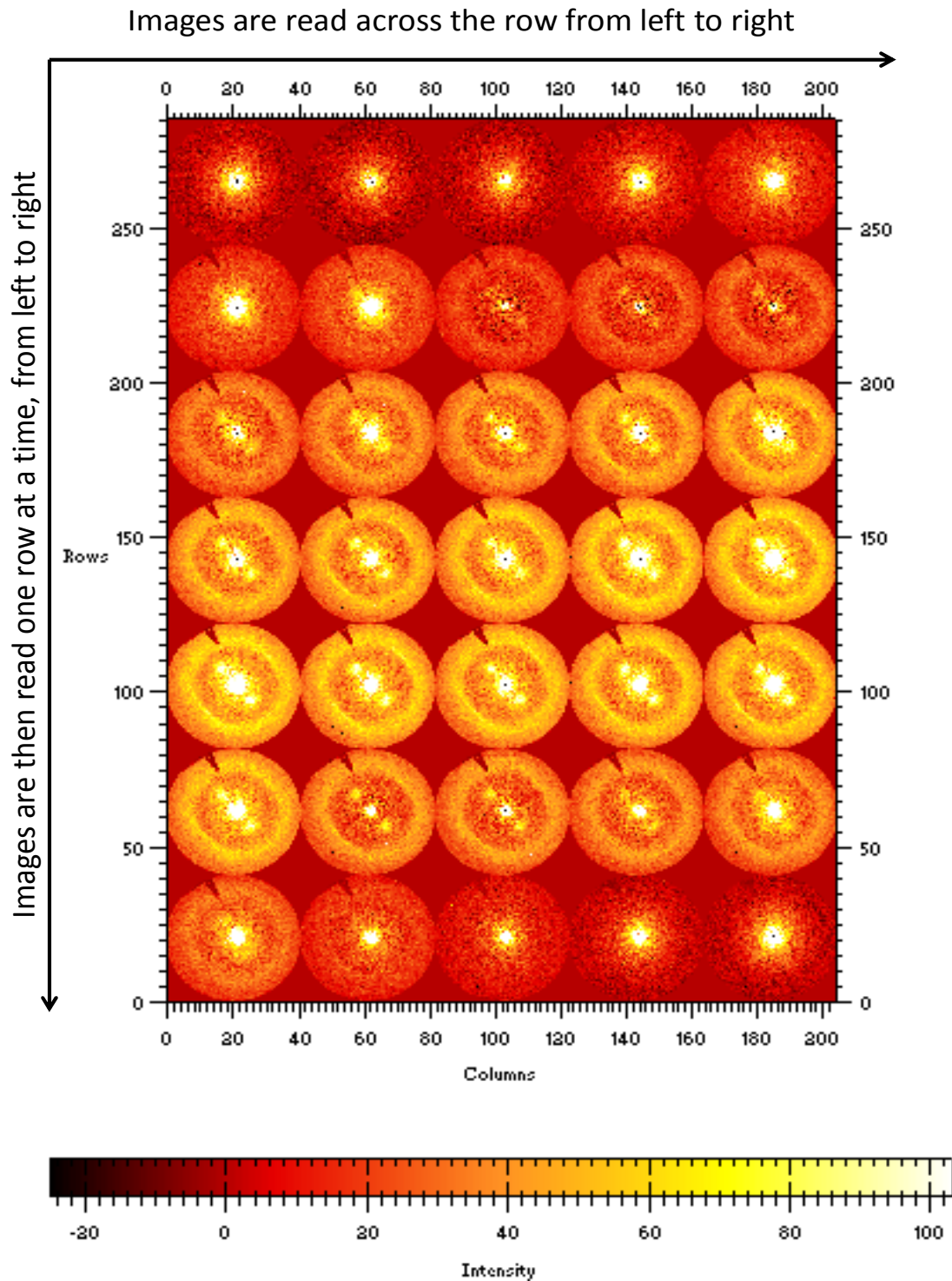


Figure 5.6 - Composite image of the fibre diagrams for the Afro hair type. The scan shows the fibre diagrams arranged in image order from left to right moving downwards in row. Some of the images which do not show scattering from the hair fibre have been omitted from the composite image. Each fibre diagram in the composite image represents an exposure taken in 5 micron incremental steps in the raster scan across the width of the hair fibre. Therefore every row in the above composite image represents 25 microns moved in the scan.

It is seen that there is an increase in intensity for the 1-d traces which correspond to the total scattering, KIF interference function and the small angle signal at image numbers 7 and 30. This is evidence for structures showing a high level of fibrous order which give rise to a high intensity diffraction signal; these may define the edges of the hair fibre and be evidence for scattering from the cuticle structures. There is then a decrease in intensity for these sectors which indicates a lower ordered region seen just inside these edges as seen in Figure 5.6 (see images 8-9 and 28-29). There is also another region of high intensity towards the middle of the hair fibre with two regions of lower intensity either side. This provides evidence for a change in the level of ordering within the central most region of the hair fibre, the relative intensity of the diffraction features as seen in the corresponding fibre diagrams in the composite image also provide evidence for this. From the information presented in this scan, the hair fibre here shows cylindrical symmetry both in its fibre morphology and in the ultra structural features within the fibre; i.e. there is a pseudo mirror symmetry seen in the shape of the 1-d traces.

5.4.2 Asian Hair

The Asian hair had 60 images taken in a scan and like the Afro hair there is an obvious orientation effect to the fibre diagrams, there is a tilt of the scattering and diffraction features of up to 10°; the sectors taken from the in-house software were adjusted to compensate for this. The integrated intensity plots are shown in Figure 5.7 and the composite image is shown in Figure 5.8.

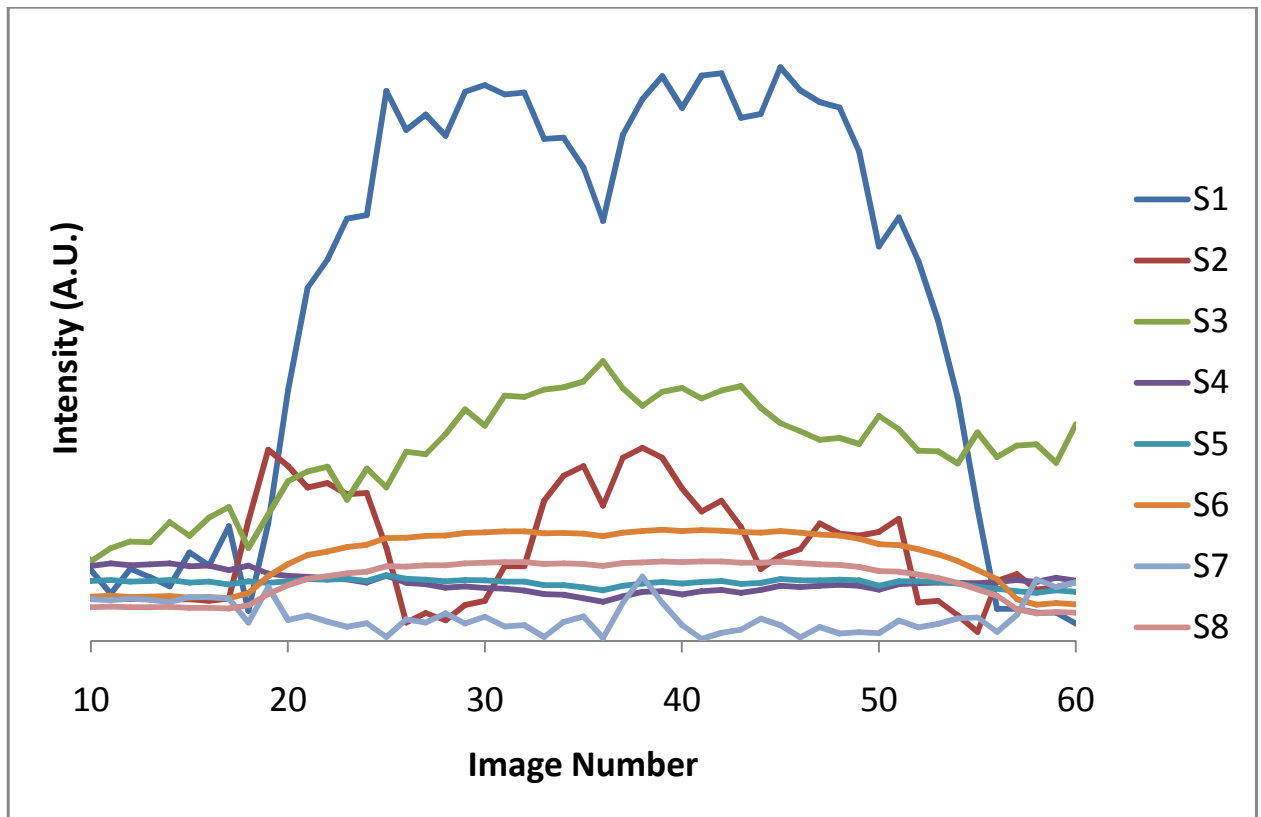


Figure 5.7 - The integrated intensity plots of the sectors for all the fibre diagrams for the Asian hair.

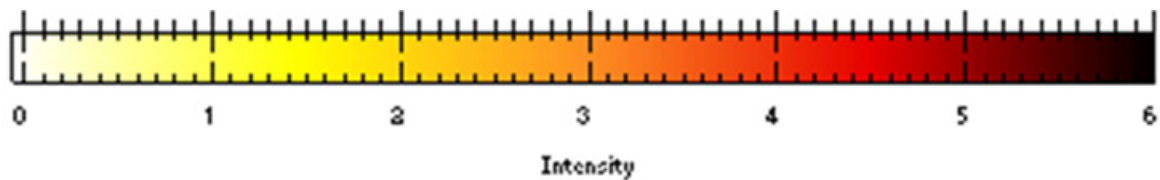
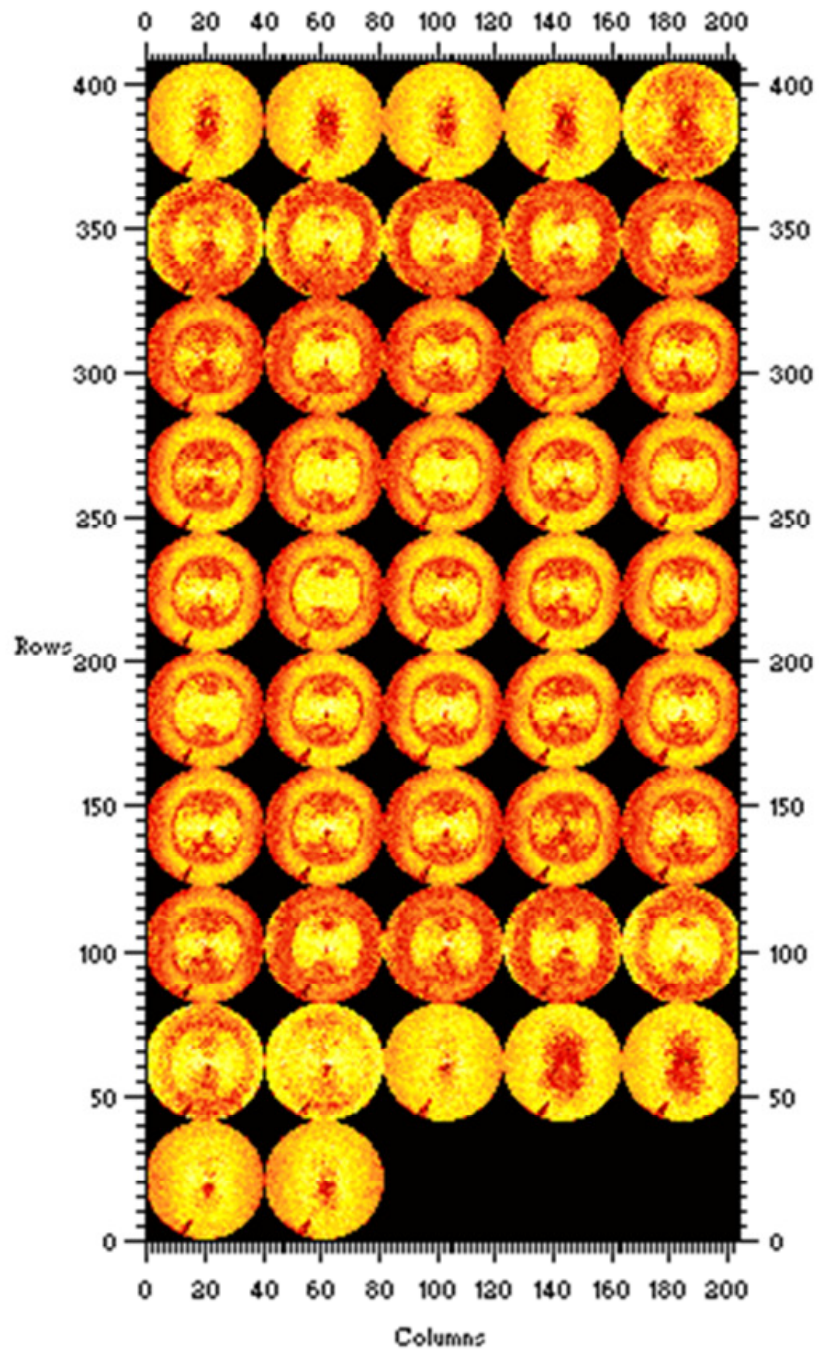


Figure 5.8 - Composite image of the fibre diagrams for the Asian hair type. Some of the images which do not show scattering from the hair fibre have been omitted from the composite image.

The scan displayed in Figure 5.8 shows that there were 40 images corresponding to scattering features from the hair fibre suggesting a fibre width of 200 μm . The shape of the 1-d trace corresponding to the total scattering intensity shows a pseudo symmetry which suggests that this hair fibre shows cylindrical morphology. Towards the middle of the scan at image 37 there is a drop in the total scattering intensity which indicates the presence of a medulla. This drop in signal is correlated with a drop in signal seen in the small angle signal and inversely related to the signal arising from the helical component within the hair. This suggests that in this medulla region there is an increase in the order of diffraction from the helical components which may indicate an increase in the amount of keratin present; this is anti-correlated with a decrease in the signal from the small angle signal which suggests that this is an area of higher keratinous content.

There is a general symmetry seen in the 1-d traces, there is more wide angle diffuse scatter in the mid region of the hair and there is also more small angle intensity in the central most region, with less contribution from this signal towards the edges. The same pattern is seen in the 1-d trace corresponding to the KIF signal.

5.4.3 Chinese Hair

The Chinese hair type had 50 images taken in a scan, cross referencing the 1-d trace corresponding to the total intensity with the composite image shows that the Chinese hair type would be expected to have a fibre width of 195 μm as there were scattering features seen in images 12-51 for the first scan. Figure 5.9 shows the integrated intensity plots of the sectors and Figure 5.10 shows the composite image for the scan.

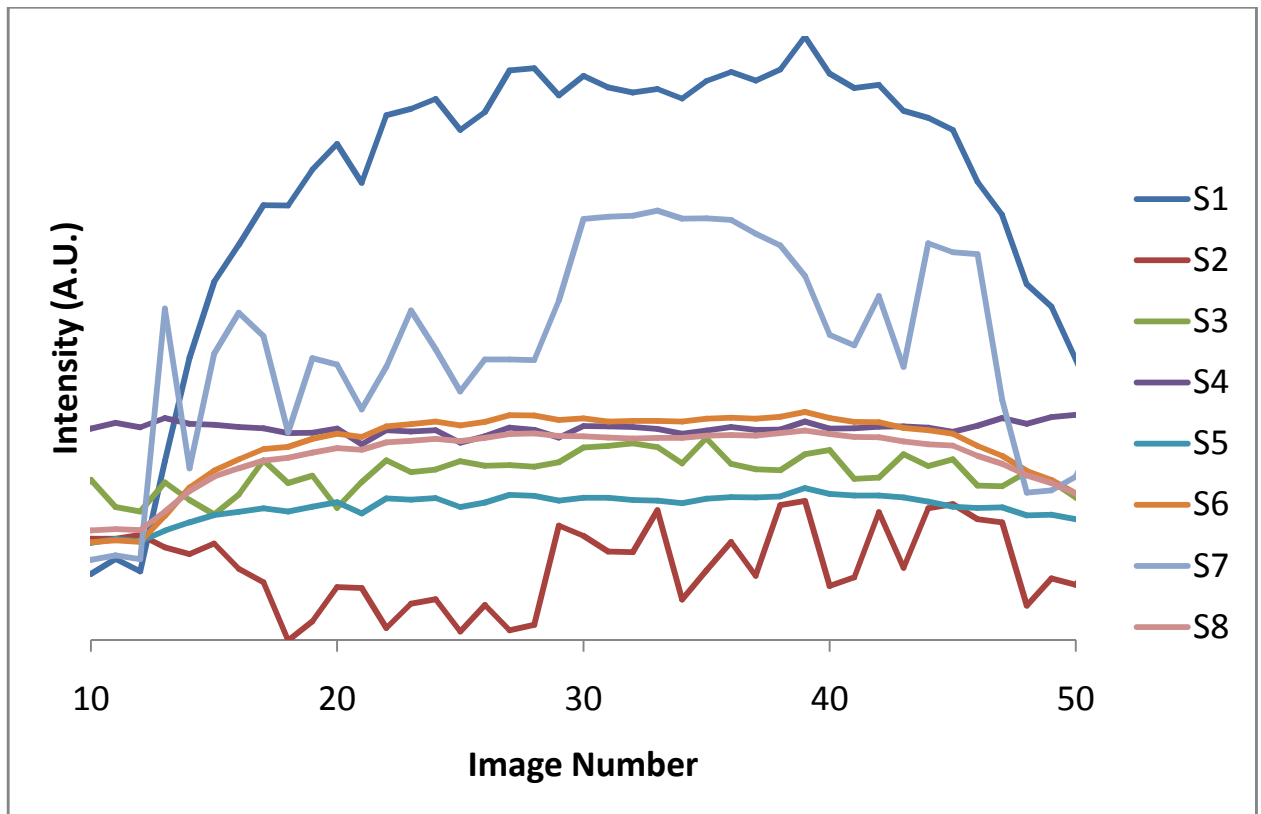


Figure 5.9 - The integrated intensity plots of the sectors outputted for the Chinese hair type.

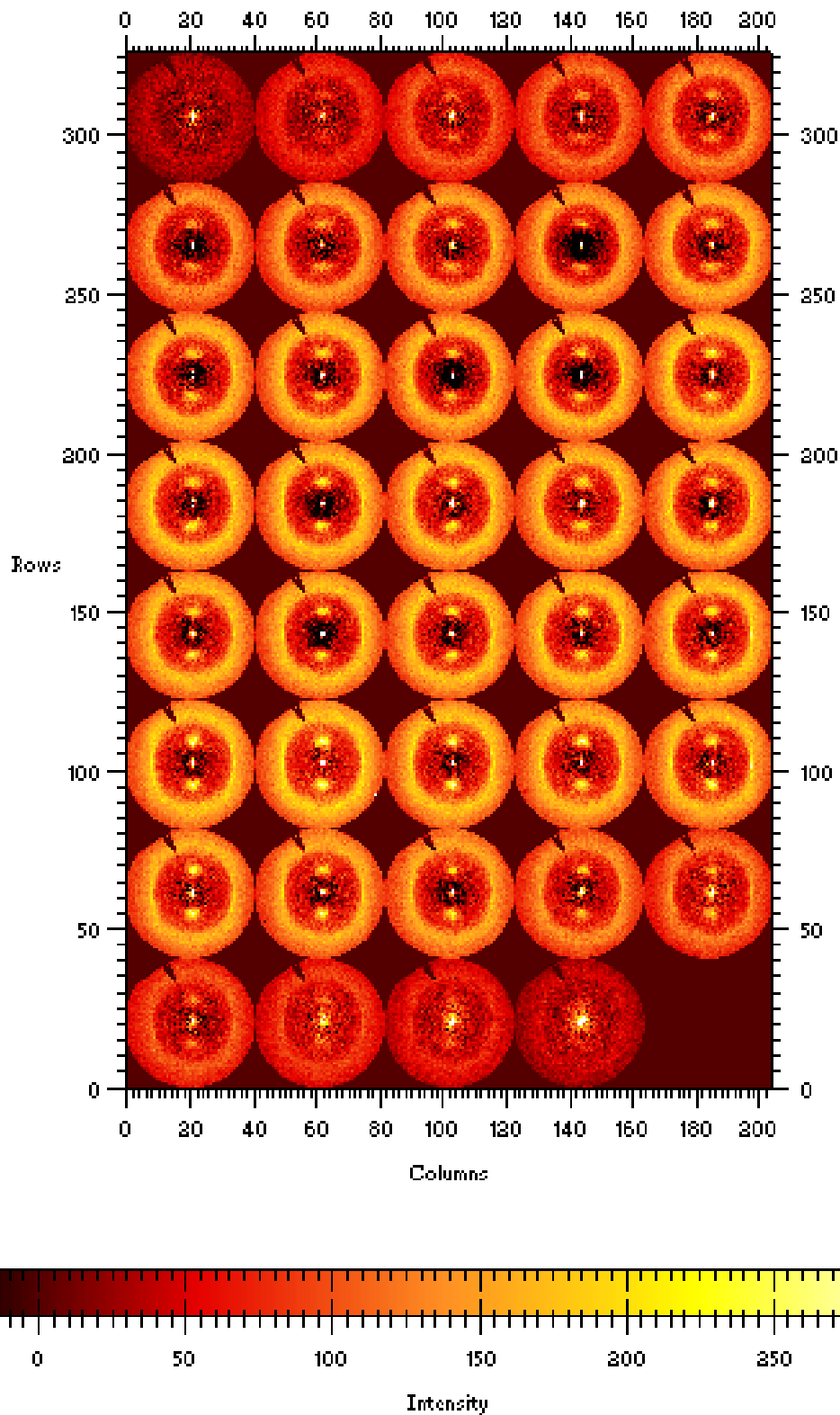


Figure 5.10 - Composite image of all of the fibre diagrams for the Chinese hair type. Some of the images which do not show scattering from the hair fibre have been omitted from the composite image.

As seen in Figure 5.9 there is pseudo symmetry in the plot for the total scattering intensity which implies a cylindrical morphology to the hair fibre. There is high variability in the KIF signal in the initial part of the scan (fibre diagrams 13 - 25), this trend is also seen in the 1-d trace for the small angle signal but with less change in intensity. The image numbers 28-40 show a higher order of the KIF interference function in the central most region of the hair fibre as seen by the higher intensity in the 1-d trace; in the same region there is variability in the small angle signal. The 1-d trace of the KIF signal also shows a high intensity towards the latter side of the scan as seen in images 43-48. This indicates that there is a highly ordered central core section with concentric regions of both lower and higher order towards the outer regions of the fibre. As the total scattering signal does not decrease in the central most region it can be suggested that the rise in signal from the fibrous components is due to a higher ordering, whereas the total scattering signal does decrease towards the edge (images 43-48) so although this shows proof for higher ordering there is probably less fibrous structure found in this region.

5.4.4 European Hair

The European hair had two different sources of hair studied in this experiment; labelled European type 1 and European type 2; therefore this section shall be split into two sections.

5.4.4.1 European type 1 Hair

The European type 1 hair showed the strongest lipid diffraction signal seen in any of the hair types, the signal for this was found in the central-most region of the hair in what is almost certainly a medulla region. Figure 5.11 shows the 1-d traces for this sample, cross referencing the 1-d trace for the total scattering intensity with the composite image shown in Figure 5.12, it can be seen that the scattering features arising from the hair are present in images 16-44 which suggests a hair fibre width of 140 μm .

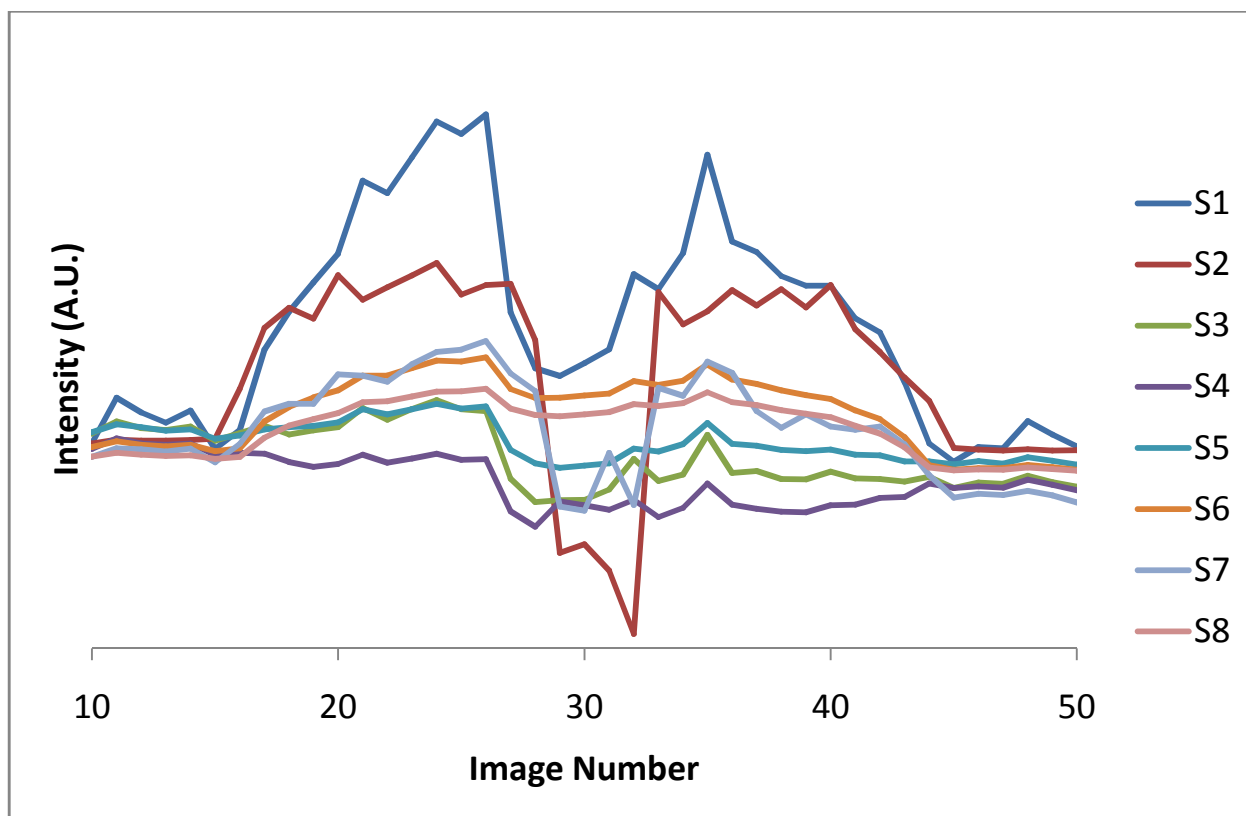


Figure 5.11 - The integral intensity plots for the sectors for the European type 1 hair.

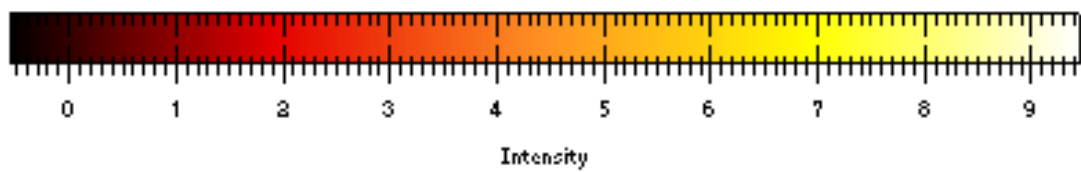
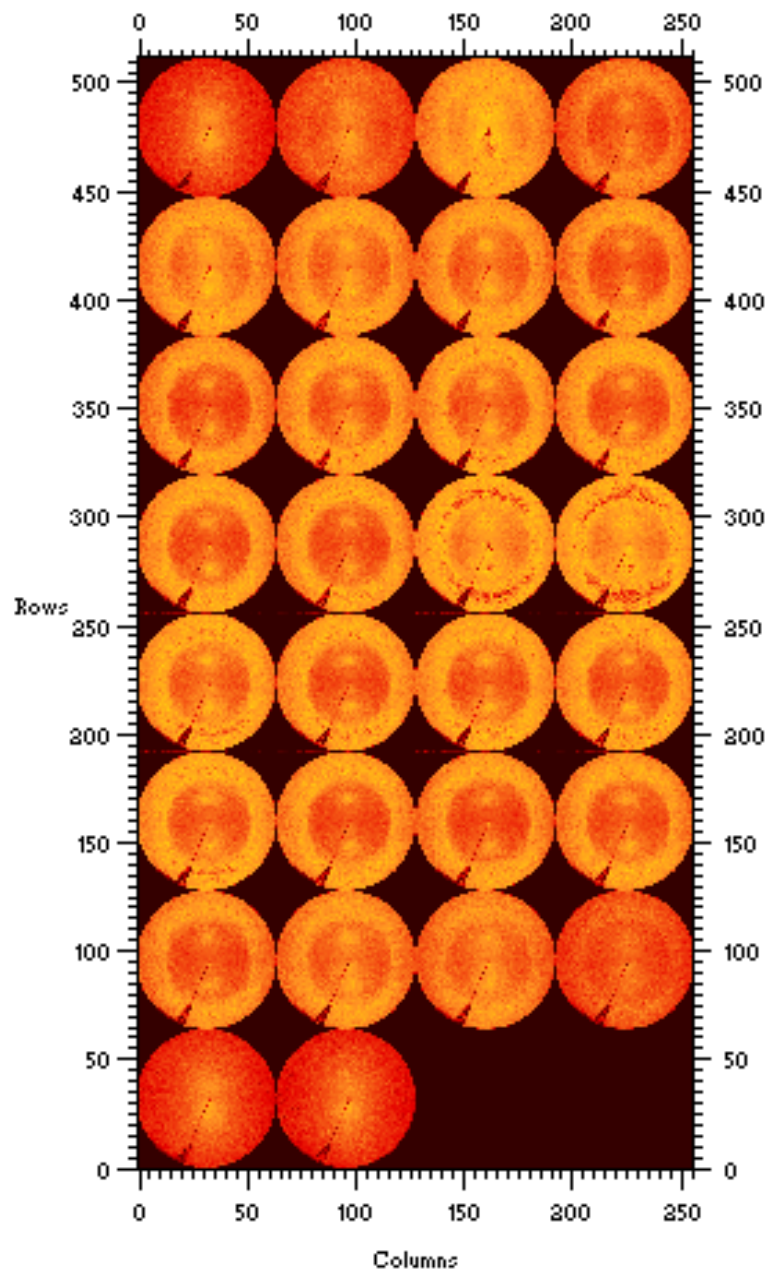


Figure 5.12 - Composite image of all of the fibre diagrams for the European type 1 hair. Some of the images which do not show scattering from the hair fibre have been omitted from the composite image.

The fibre shows a slight asymmetry in the total scattering 1-d trace, with the latter side of the scan showing less contribution to the total scattering intensity. There is large drop in the intensity of both the total scattering and the small angle signal in between images 27 - 33, in fact all the 1-d traces in Figure 5.11 show a drop in the intensity in this region which indicates a region composed of fewer structures which contribute to scattering/diffraction and also less order in the structures. Either side of this central drop in intensity the 1-d traces also show a little variability in the intensity of their features, but generally it is fairly consistent therefore showing no other major structural features. Figure 5.13 shows a series of images in the small angle region which show presence of lipid diffraction.

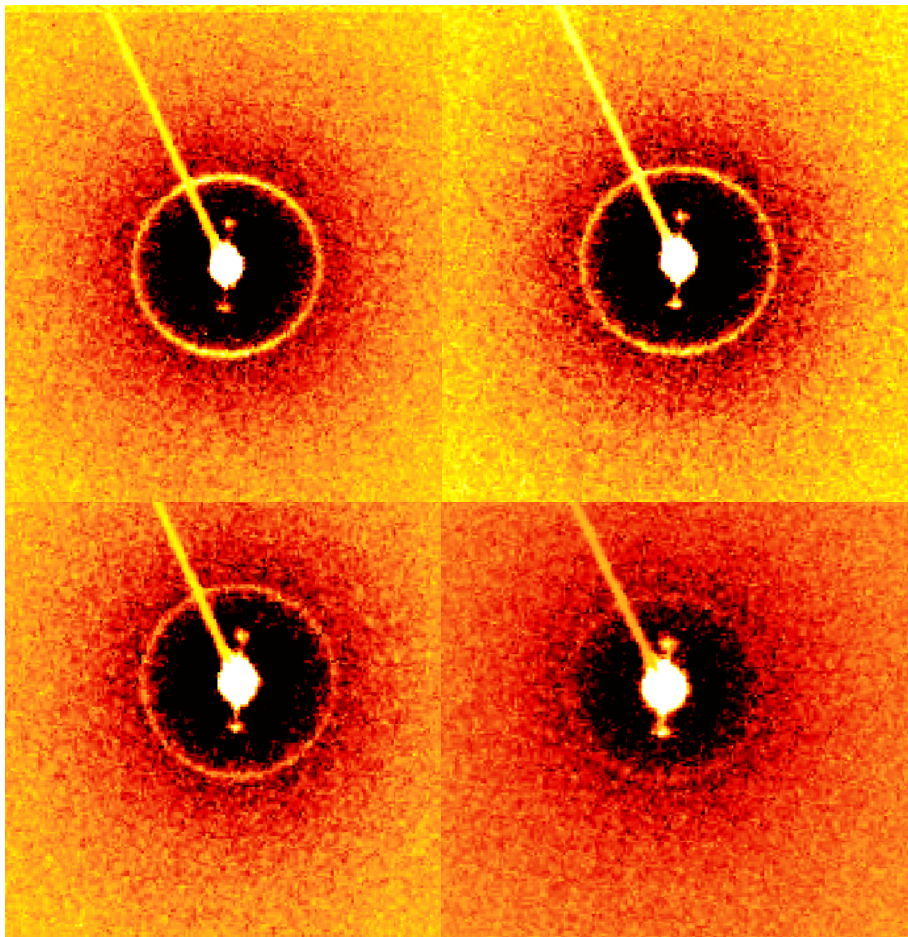


Figure 5.13 - Figure shows a composite image of the lipid diffraction rings found in images 28 - 32 in the European type 1 hair. The intensity and q range of the images is the same in all images.

These images are found in the central most region of the hair; images 28 - 32. This shows that in this hair fibre, there is a strong presence of crystalline lipid located specifically in the medulla region. It is interesting to note that the sector corresponding to the lipid diffraction (sector 3) only showed evidence for there being presence of lipid in image 32 which is why all the fibre diagrams were visually checked. There was no lipid diffraction present in any other part of the hair fibre from analysis of the fibre diagrams.

5.4.4.2 European type 2 Hair

The European type 2 hair had 100 images taken in the scan but as many of them did not contain any signal from the hair fibre, only 44 were used for the analysis presented here. Figure 5.14 shows the integrated intensity plots for the sectors in this hair type and Figure 5.15 shows the composite image of the fibre diagrams. Inspection of the fibre diagrams and the 1-d trace for the total scattering shows that there are scattering features in images 13 - 32 giving an estimation of 95 μm for the width of the hair fibre.

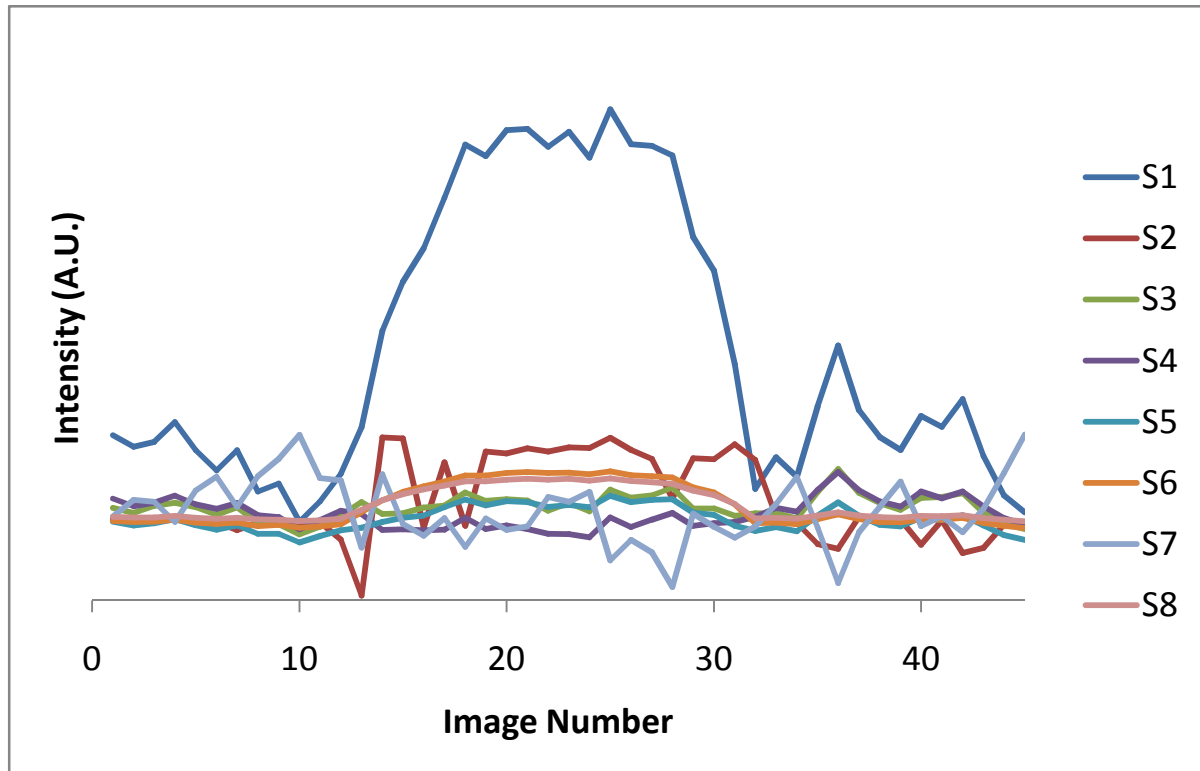


Figure 5.14 - The integrated intensity plots for the sectors for the European type 2 hair.

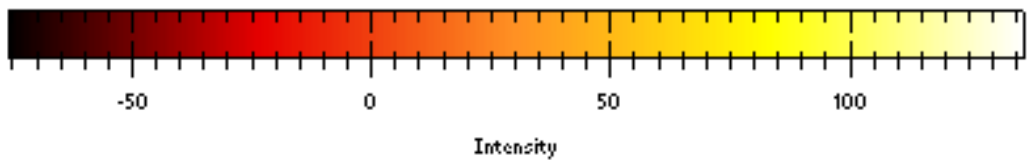
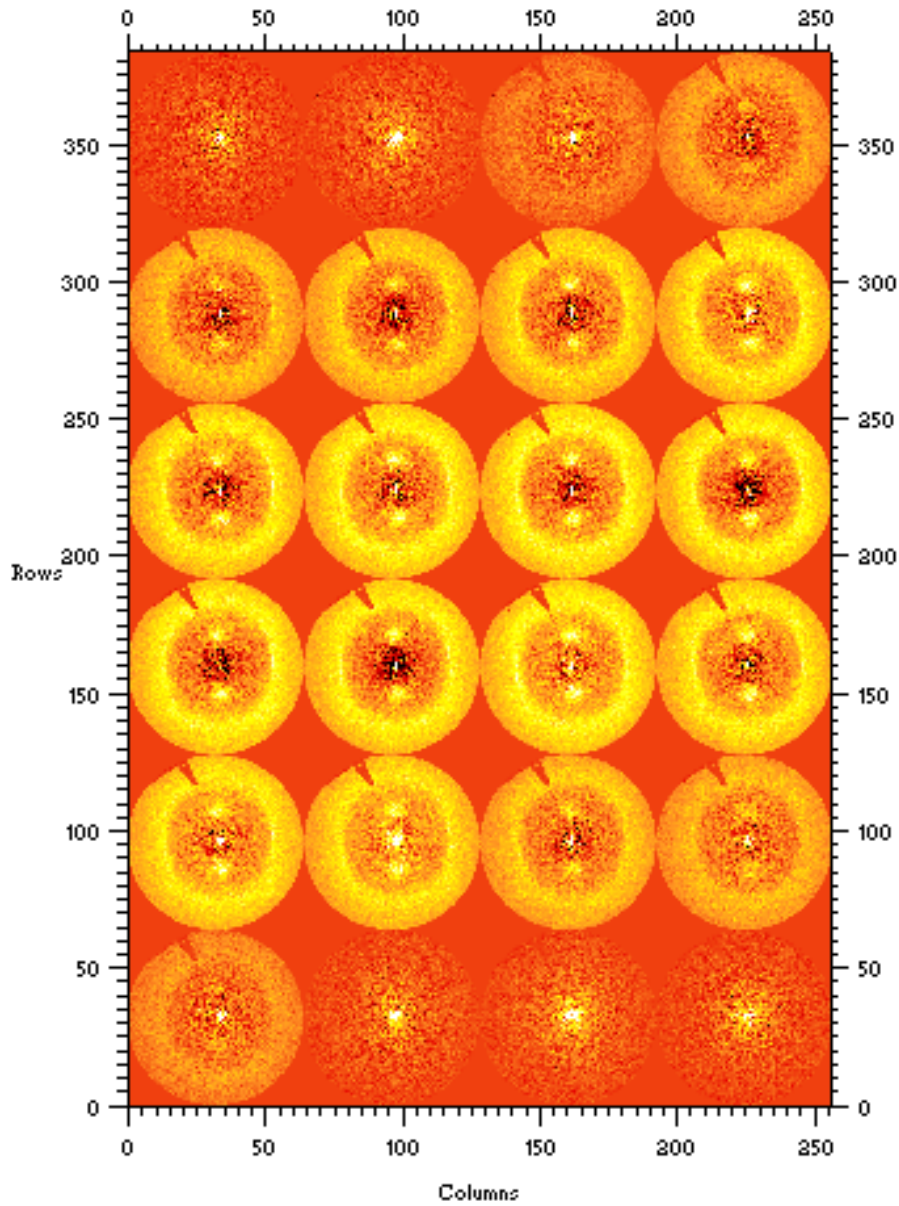


Figure 5.15 - Composite image of all of the fibre diagrams for European type 2 hair. Some of the images which do not show scattering from the hair fibre have been omitted from the composite image.

As seen in Figure 5.14, the 1-d trace for the KIFs is very noisy, but it generally shows two regions of lower intensity for image numbers 15-21 and 25-29 either side of a region with higher intensity in the central region of the hair fibre (images 21-24). This may show that there are two regions with less fibrous order which lie either side of a more ordered central region; this may show that there is a medulla structure in the region defined by images 21-24. No lipid diffraction was observed in any of the fibre diagrams.

5.4.5 Japanese Hair

The Japanese hair had 50 images taken for each scan, and there were 3 complete scans taken across the hair fibre. All scans were taken at 200 μm increments along the hair fibre axis. Figure 5.16 shows the integrated intensity plots for the sectors and Figure 5.17 shows the corresponding composite image of the fibre diagrams. Using a combination of the two images the fibre width was estimated to be 150 μm for the first scan, images 16 - 46 shows features characteristic of hair fibre diffraction.

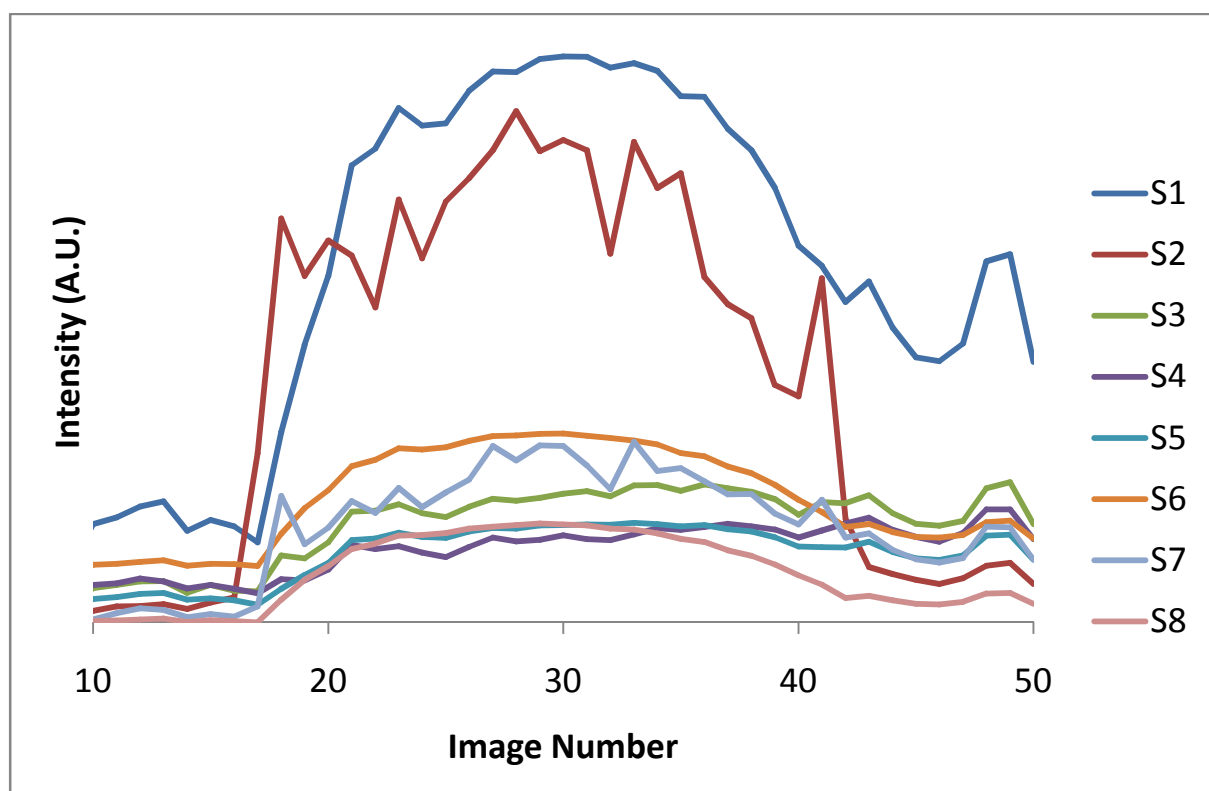


Figure 5.16 - The integrated intensity plots for the sectors for the Japanese hair.

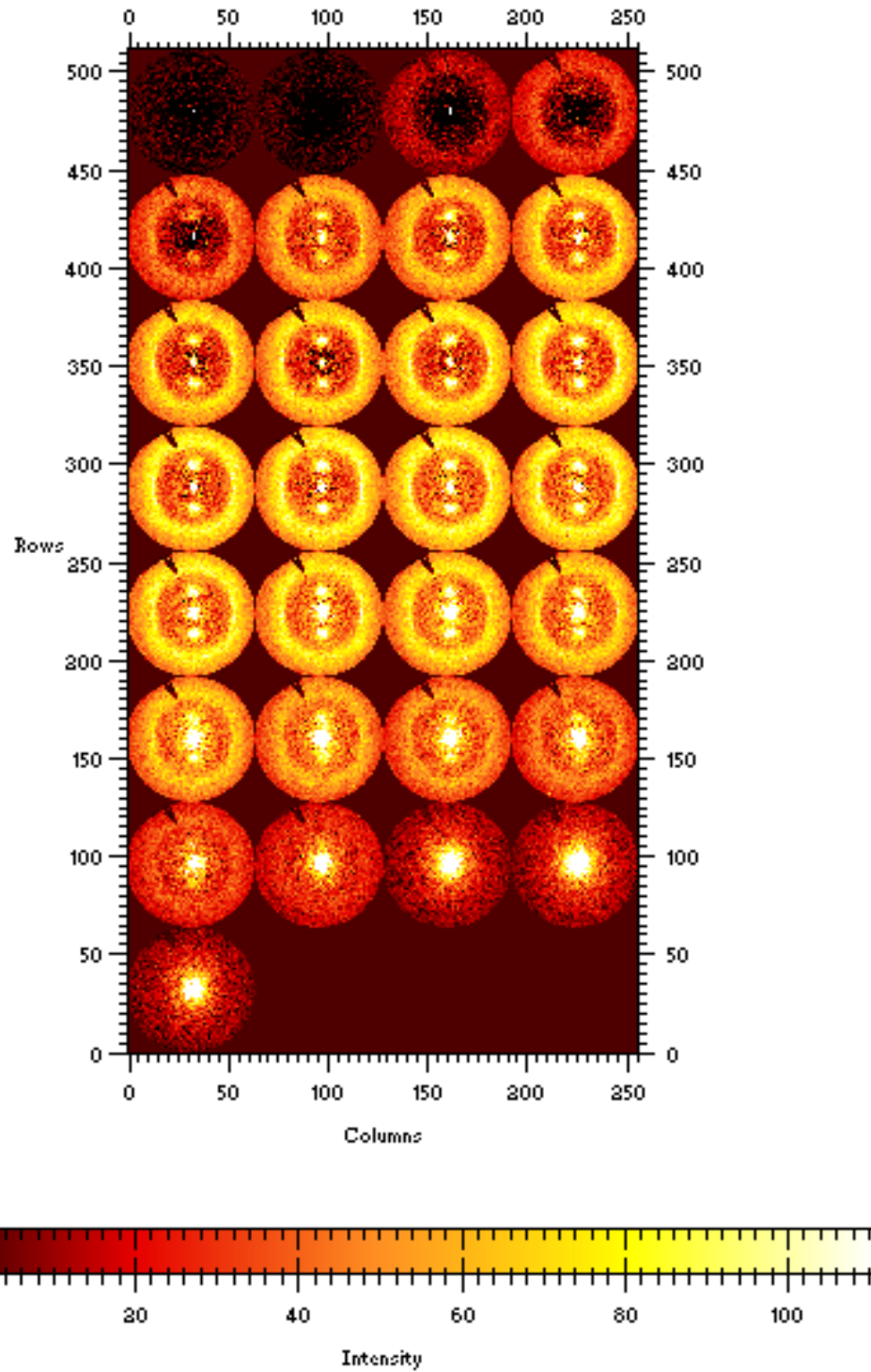


Figure 5.17 - Composite image of all of the fibre diagrams for the Japanese hair. Some of the images which do not show scattering from the hair fibre have been omitted from the composite image.

The total scattering 1-d trace shows that the hair fibre exhibits an overall symmetry suggesting cylindrical morphology. In general, the small angle signal shows less intensity contribution towards the edges and more intensity within the centre region of the hair fibre; this is also correlated with the other 1-d traces for the other sectors suggesting that this shows there is more matter in the centre most region than there is towards the edges.

5.5 Discussion

The results presented in this study are a first in this field of research, never before has a microfocus X-ray diffraction study been performed on differential ethnic hair types in an attempt to investigate and quantify the nanostructural variation. The aim of this investigation was to see if it is possible to use this technique to observe the textural variation of single hair fibres as a function of the ultra structure to see whether differences could be observed between ethnicities. On the basis of the results presented in Section 5.4, there was inter-ethnic variation observed in the hair fibre morphology, the orientation of the nano and supramolecular structures present, the distribution of lipid diffraction and the relative intensities of the various scattering features present in the fibre diagrams. This section will be divided into three sections which discuss the following:

- The interpretation and contextualisation of the differential contribution of specific sectors of the fibre diagrams to the scattering across a hair fibre.
- The variation observed intra and inter ethnically.
- The validity of the data considering experimental conditions.

5.5.1 Interpretation and contextualisation of the specific sectors

The integrated intensity measurements taken from specifically selected parts of the fibre diagram give an indication of the contribution of different structural features at specific points in a hair fibre. In general, it can be observed that across most hair types, the integral sectors of the scattering features follow the same pattern as that of the total scattering intensity which shows an almost parabolic shape to the increase in intensity as the X-ray beam moves across the fibre.

This is the projected density function of a cylinder. The majority of the profiles contain an element of mirror symmetry which is indicative of the cylindrical symmetry that is generally held for hair zonular structures. The deviations from this symmetry are what provide the discussion points for analysis of the variation both intra and inter ethnically; the deviations from symmetry may be due to variations in the relative sizes of specific substructures within hair.

The dissection of the fibre diagrams into sectors shows that for specific features such as the 0.515 nm structure of the alpha-helical keratin (sector 8) and the 0.98 nm interference peak (sector 4) the sectors of integral intensity generally follow the same trend. This indicates that the inherent helical structure of the alpha helix and the way in which it associates and packs inside the KIFs is highly linked. The 1-d trace which corresponds to the KIF interference peak in the small angle region (sector 7) within hair is also correlated to the presence of alpha helix. It should be noted that the inherent large coverage of structural scale over relatively few pixels in the small angle region provides less opportunity to interpret information from this region due to the number of pixels that describe the data. The sectors for the 0.515 nm meridional arc and the 0.98 nm equatorial reflections in the wide angle region produce an envelope that describes the amount of helical keratin present in the hair profile. The variations of this which are shown in the sectors 4, 7 and 8 indicate that the information provided in these scans show that the change in volume/order of the helical keratin is present mostly just inside of the hair fibre itself and located around the centre region of the fibre where a medulla is located (if present within the fibre). There can also be variation seen inter-ethnically on the composition of the medulla and even its presence as indicated by the differences seen in the relative intensity of the sectors corresponding to the helical keratin; some hair types like the European show a definitive drop in the intensity of the helical component, whereas the other hair types such as the Afro and the Chinese hair type show regions of increased intensity in the helical components in the central portion of the hair fibre.

Many of the scans also show variation in the sector relating to the KIF interference function across the cross section of the hair; the larger contributions to the intensity from this sector can be attributed to the cortex region of the hair. This indicates that the differential sub-structures of the hair contain nanoscopic architectures that modulate the scattering contribution of the keratin based components. This may be due in part to the different types of ultra structural regions and the basis for these variations may be due to the augmentation of the KAPs in filling the space between the KIFs. From literature it is known that KAPs possess a disorganised association and so

therefore does not produce an X-ray diffraction signal as they are randomly distributed and orientated, however they will contribute to the scattering signal as all objects produce scatter. The low angle contribution to the intensity around the backstop (sector 2) and the diffuse scatter at a spatial resolution of approximately 0.55 nm (sector 6) could possibly be attributable to the KAPs. As the KAPs are randomly orientated around the KIFs and are thought to show no variation in their distribution along the hair fibre axis (Khumalo, Dawber et al. 2005), the diffuse scatter can possibly be attributed to these structures, at least in part, to the scatter arising from the KAPs in the samples. However, as there are no samples in this experiment where KAPs are not present in the hair fibre, it is difficult to prove this from the dataset.

A direct comparison between the scan profiles of different hair types is primarily confounded by the difference in sample thickness. The recalibration or normalisation of hair profiles to a standard 'hair width' was not carried out here as it does not necessarily follow that the ultra structural sections of the hair scale uniformly in thicker and thinner hairs. As discussed previously though some morphological and geometrical parameters that have been estimated using this technique provide comparisons that can be made with literature. The most significant interpretations that can be made from the scans across all hair types is perhaps the relative contribution of the diffuse scatter in comparison to the signal arising from the helical components in the hair. This is most pronounced in the Asian hair type (see Figure 5.7) and in the second scan of the Afro hair type (see Figure I.4.2 in Appendix I) where there is an inverse relationship between the signal arising from the diffuse scatter contribution to the fibre diagram and the helical components. This indicates that the volume of amorphous structures contributing to the diffuse scatter is inversely related to the amount of helical keratin present. This is perhaps a trivial conclusion as one might expect the level of KAPs to have to increase if the amount of helical keratin decreases given the same volume of space. These regions of anti-correlation may provide evidence of a 'gluing' region such as that between the cortex and the cuticle where more cell membrane complex (CMC) is found to provide adhesion between the structures (Robbins 2009). However, this is not seen across every hair type and generally the two sectors seem to correlate which suggests that any deviations in these sectors is related to the total amount of matter present either increasing/decreasing which is seen by the way in which these sectors mirror the pattern of the total scattering intensity.

5.5.2 Comparisons and variations observed intra and inter ethnically

The most pronounced differences between the hair types arise in the geometrical size and morphology of the fibre as estimated from the total scattering intensity. The other sources of variation were the presence of ordered/disordered regions corresponding to the possible presence of a medulla and other undefined sections, the orientation of the fibre diagrams and thus the material present and the presence of lipid diffraction.

A preliminary feature of this experiment is that skin-core experiments can be used to estimate morphological properties of the hair; specifically the fibre width and its geometrical properties. The Afro hair was estimated to have a fibre width of 115 - 120 μm , the Asian 155- 190 μm , the Chinese 195 μm , the European type 1 140 μm , the European type 2 95 μm , and the Japanese 110-150 μm . All hair types presented in the study here show values for the fibre width that are much higher than expected with comparison to the reports from previous literature (Kreplak, Merigoux et al. 2001, Bertrand, Doucet et al. 2003). However, broadly grouping the ethnicities studied here into Afro, Asian (consisting of the Asian, Chinese and Japanese hair types) and Caucasian (the European hair types), the trend as reported in previous literature that the Asian hair type exhibits the greatest fibre width is also seen in this study. Comparing the results presented here with that of (Franbourg, Hallegot et al. 2003) also shows that for the European type 2 hair type which can be considered as Caucasian, the trend is also followed that this hair type shows a smaller diameter than the Afro. The European type 1 hair shows a larger estimated fibre width than the Afro hair type. Using the 1-d trace corresponding to the total scattering intensity as an estimate of the geometry of the hair fibre it is seen that most of the hair types would be expected to show a cylindrical geometry with slight ellipticity to all of the fibres studied. The European hair type perhaps exhibits the most consistency in the shape as estimated from the total scattering trace, but conclusions for this are difficult to ascertain. The Afro hair fibre shows a 1-d total scattering trace which represents a cylindrical geometry but this is due to it being stretched in the sample holder which therefore does not provide an indication of its native state. Unlike the other hair fibres tested in this study, the Afro hair fibre showed a high degree of curl which implies an elliptical geometry to the fibre. The rest of the hair types used in this study showed little to no

curl. More indication of the geometric and morphological properties of the fibres can be seen in the sectors corresponding to specific scattering features of the fibre diagrams.

The presence of ordered/disordered sections is related to the change in intensity of the 1-d traces corresponding to the diffuse scatter and the helical components (sectors 5, 6 and 4, 8 respectively). The main differences between the hair types are seen in the presence of a highly ordered core section such as in the Afro, Chinese and Japanese hair types and a less ordered core as seen in the Asian and European hair types. This implies that the Afro, Chinese and Japanese hair types have a projected density profile that would be made by a solid cylinder with a core of higher density, where the vast part of the cylinder is represented by the cortex. In contrast to this, the Asian and European hair types would have a cylinder with a hollow core as represented by a medulla. This suggests that on the basis of ethnicity this may not be a genetic effect as the two different structures are seen across the broader definition of the ethnic categories (i.e. Afro, Asian, Caucasian), the cause of the difference in structures may be related to the individual and so hair fibres from different sources and more hair fibres from the same source would need to be studied.

The textural differences that are also mapped by the sectors relating to the diffuse scatter and the helical components of the signal may also signify other sub structural regions. For example, there could be evidence for 'gluing' interfaces/regions just inside the edges of the hair as seen in the Afro hair type, where cross referencing the composite image with the 1-d traces shows that the diffraction features of the fibre diagrams decrease in intensity but the intensity of the diffuse scatter increases; this could be evidence for an amorphous gluing region such as the CMC. However, caution must be used in over-interpretation of this as if this were the CMC one might expect lipid diffraction to arise from the regular lamellar lipid structures that are characteristic of the CMC region. On the other hand as reported in (Robbins 2009) the CMC region between the cortex and the cuticle structures is less ordered than that between cortical cells and cuticle cells and so may possess less lipid order which does not give rise to lipid diffraction; if there are not any multi-layer stacks then a diffraction signal will not be seen.

The orientation of the principal diffraction features of the fibre diagram relative to the axis of the hair fibre is related to the curl of the hair fibre. As seen in the fibre diagrams for the Afro hair type (see Figure 5.5), this hair type shows the most amount of orientation to the fibre diagrams. The Asian hair type also shows a slight orientation to its fibre diagrams. Although, this parameter is not quantifiable by means of analysis using the 1-d traces from the sectors, it should be noted that this has produced an observed variation between the ethnic hair types.

Lipid diffraction was only seen in the European type 1 hair fibre in this study. This indicates that only this hair type had sufficient organisational structure of its lipid content to produce a diffraction signal. However, this does not mean that this was the only hair type to have lipid present, as that would be an unlikely conclusion. It is highly probable that the other hair types possess lipid in their hair fibre, but its random packing within the hair fibre results in the lipid component not showing a signal; it is likely that the diffuse scatter contains contribution from the lipid present in the sample.

The results from Chapter 4 show that all the hair types (Afro, Chinese, Euro and Mullato) showed lipid diffraction in their fibre diagrams; the Afro hair types showed the lowest intensity, the Chinese and Mullato showed the highest intensity particularly in the equatorial region and the Euro hair type showed the median amount. Relating the results presented here to those in Chapter 4 gives both supporting and contradicting evidence. Although there was lipid diffraction found in the European hair type in both studies, on the basis of the data presented in this Chapter, the Afro and Chinese hair types contradict the results in Chapter 4 as they explicitly show no lipid diffraction in any of the fibre diagrams in this study. The Mullato hair type was not used in this study so a comparison cannot be made for this hair type. As mentioned previously, it is highly unlikely that these hair types possess no lipid content, however, it can be suggested that perhaps on the basis of the study presented here that the lipid content, at least in the hair fibres used in this study, do not show a high enough regularity of their lipid content to produce a diffraction signal. There are also two other possibilities to account for the lack of lipid diffraction seen in this study. Firstly, the regions of the hair fibre that were scanned with the X-ray beam, may not have contained organised lipid, but that does not necessarily mean that there is no organised lipid seen at different positions along the hair fibre axis. As some of the scans were taken in the same

position, or only traversed up to a maximum of 1 mm along the hair fibre axis, this distance may not be representative of the properties seen along the hair fibre. For example, one might expect the hair to contain more lipid closer to the root of the fibre as this is closer to the sebaceous glands which are known to excrete sebum which contains lipids. The second possibility is that the lipid diffraction seen in Chapter 4 was a contribution of the signal from the entire content of organised lipid across the hair fibre at one point. It is possible that in some of the hair types, lipid diffraction is only produced when the X-ray beam completely bathes the fibre so that the diffraction is only produced when all of the lipid content is cumulatively added. This may be the case if the lipid was exclusively present in the cuticle; if the microfocus beam does not optimally interact with the cuticle then a lipid diffraction pattern will not be seen, however, if the X-ray beam bathes the whole fibre, then all of the lipid present in the cuticle will contribute to a diffraction signal. This argument can also be extended; if the microfocus beam does not interact with a position in the cortex which contains organised lipid such as the lamellar structures of the CMC then lipid diffraction will not be seen. However, one might expect this might not be such a plausible argument as the probability of the interaction of an X-ray beam with dimensions of $2.0 \mu\text{m} \times 12 \mu\text{m}$ in 5 micron incremental steps with the lipids present in the CMC with lamellar layer dimensions of 2.0 - 4.0 nm (Ohta, Oka et al. 2005) would be quite high.

It is interesting to note that the European type 1 hair type shows the lipid diffraction signal within its medulla, this shows that highly ordered lipid is exclusively present in the central most region of the hair in its hollow core. This would have implications for the hair care industry as it would ensue that this lipid would be relatively inaccessible to hair products.

5.5.3 Consideration of experimental conditions

The 1-d traces of specific integration sectors of the fibre diagrams were used in an attempt to interpret the contribution of specific scattering features to the many components that are present in hair. All components present in hair will make a contribution to the scattering as all components scatter (such as the fibrous keratin components, KAPs and lipids). However, some keratinous structures and lipids have sufficient structural organisation to produce diffraction

signal which is more exclusively associated with their organisation. The KAPs are not thought to contribute to diffraction components as they are sufficiently disordered, therefore it is possible that they make a significant contribution to the diffuse scatter that is present in both the small and wide angle regions. Therefore it is not possible to make definitive conclusions based on the scattering features that are present in the fibre diagrams considering that all components within the hair will make a contribution to this. However, the conclusions that are drawn from the diffraction components of the fibre diagrams can be considered to be more valid as they definitively provide information about their organisational structure that has been well documented.

The resolution of the fibre diagrams, particularly in the small angle region, makes interpretation and conclusions from the data in this region difficult. Due to the nature of the diverging beam from the focussing optics, only a certain camera length and thus q -range can be used before the beam quickly diverges and the information is lost. The challenge in an experiment such as this is that the conditions to map both the WAXS and SAXS regions in sufficient resolution to be able to make interpretations from both regions of data are difficult to obtain. The WAXS region is needed in order to ultra structurally map the position of the X-ray beam in relation to the distance that it has moved across the hair fibre; the information from the 0.515 nm meridional arc and the 0.98 nm equatorial reflections corresponding to the fibrous keratin structure provides the information to do this. The SAXS signal also provides information on the fibrous keratin structure from the ~ 9 nm KIF interference function. Additionally it provides data on the low angle diffuse scatter and the crystalline lipid diffraction should this be present. However, increasing the resolution for the SAXS region would come at a cost of decreasing the resolution of the WAXS region, therefore eliminating the ability to effectively map the position of the X-ray beam. Consequently, it is necessary to obtain sufficient resolutions in both the WAXS and SAXS regions to effectively map the position of the X-ray beam and in the experiment presented here the WAXS region was considered to produce valuable data, and this has therefore presented some complications in the interpretation of some of the results arising from the poor resolution in the SAXS region.

There is also a considerable systematic error associated with mounting the samples in ambient air conditions; the need for an optimal background subtraction is critical in these conditions, and as seen in some of the composite images, this was not achieved, making optimal background subtraction from each individual fibre diagram a considerable problem. This unoptimised

background subtraction only contributed to loss of data in the small angle region which further makes interpretation from the data in this region difficult.

The presence of the cryostream jet also presented some challenges with the acquisition of data. The jet was present in order to reduce the radiation damage arising from a highly focussed X-ray beam of high flux. The problem encountered by the cryostream was the movement of the single hair fibres in the air produced by the cryostream jet. The problem was countered by moving the jet further away from the hair fibres in an attempt to reduce the movement, however it still had an effect which gave rise to problems in the optimal alignment of the beam either side of the hair fibre to begin a scan, but also, more importantly, the movement of the hair fibre while the X-ray beam was being scanned across the fibre. This produced a number of hair fibres which produced incomplete scans which could not be used for analysis as there were no background images either side of the scans to calibrate the position of the X-ray beam. A more important consequence of the movement of the hair fibres in the cryostream was the possibility of duplicate measurements during a scan. As seen in the results presented, some of the hair fibres gave estimated fibre widths of almost 200 μm which seems higher than would be expected for any ethnicity of human hair. Assuming that the hair fibres were not this thick, this therefore means that duplicate exposures were taken, or extra exposures were taken that were a smear of two positions. Nevertheless, even if duplicate measurements are taken which may affect the interpretation of the morphology and zonal location of ultra structural sections of each hair type, conclusions made about the relative intensities of the scattering and diffraction components, presence of lipid and orientation are still valid as they are unaffected by this effect.

Caution has also been made with respect to over-interpreting the results presented here as the data obtained is from a single hair fibre from one source of each ethnicity. The extreme time pressure at a world class synchrotron does not afford the luxury of running several replicate measurements. To counter this, beamtime at the I22 beamline at the Diamond Light Source Synchrotron, Didcot, UK was applied for and obtained. The experiment at I22 was designed to increase the n number of single hair fibres used for microfocus X-ray diffraction analysis so that some statistical analysis could be performed on the results presented here and the validity of the conclusions drawn from the results could be checked. However, we were unable to obtain any meaningful results from this beamtime due to various complications in experimental design and setup at the beamline.

5.6 Conclusions

In conclusion the experiment performed in this chapter has provided information on a method which can be used to characterise the textural differences found across the cross section of various ethnic hair types. Using microfocus X-ray diffraction combined with a skin-core experimental method, there have been differences quantified between hair fibres in terms of their morphology, lipid content and the keratinous content of their ultra -structure. The results presented here show that there is a high degree of variability in the molecular architecture that build the ultra -structure of hair, and there are specific sections within some hair fibres that are not present in others. This provides evidence that based on some of the observations seen in this experiment, the macroscopic variation of ethnicities may also be a function of differential interfaces within hair fibres, but also that these interfaces may themselves be different in terms of varying levels of keratinous protein, KAPs and the lipid content. There have also been clearer morphological differences quantified intra and inter-ethnically as well as along the axis of fibre growth.

A comprehensive consideration of the experimental difficulties encountered during this experiment has also been presented. Although the results show that there has been some quantifiable variation observed it should be noted that the experiment has much room for improvement with regards to the quality of the data obtained, particularly the resolution of the small angle scattering features distinguishable in the fibre diagrams and the optimal level of background subtraction. The low number of samples used also provides challenges in validating the applicability of assigning definitive conclusions to each ethnic hair type from the results. However, an attempt was made to rectify this problem by performing the experiment again at the Diamond Synchrotron to increase the n number of the sample set but unfortunately no meaningful results could be obtained from this beamtime.

The results and conclusions shown in Chapters 4 and 5 have shown that the non-keratinous components of hair show the most variation inter-ethnically, and are spatially dependent within the hair fibre. Having performed bulk and microfocus X-ray diffraction analyses mainly focussing on the content of the cortex it is logical to try to isolate and characterise other parts of the hair fibre. The cuticle plays an important role in the chemical and mechanical behaviour of the hair

fibre at the surface and so a study on its structure may provide complementary data to that already gathered. By using a different technique such as infrared spectroscopy, the information that this provides on the chemical structure can be used in combination with the X-ray data already gathered to gain an interdisciplinary approach to analysing hair fibres.

Chapter 6 – Investigation of the surface structure of ethnic hair types using ATR-FTIR

The cuticle layer is the interface between the hair fibre and the surrounding environment. The chemical properties of the cuticle contribute to a large proportion of the bulk mechanical properties of a hair fibre in terms of the shearing and bending properties. Perhaps one of the most important properties it is solely responsible for is the hydration of the hair fibre via the diffusion pathways which are still not fully understood. The cuticle is comprised of four different structures (see Section 1.3.1) which contribute to its properties, two of which have properties that are critical to the diffusion of substances into the hair fibre; the epicuticle which is hydrophobic and the endocuticle which is porous. Between these two structures the hydration of a hair fibre is determined. Here we hypothesise that a variation in the chemical conformation of the cuticle layer could in turn lead to a difference in the macroscopic properties of the hair fibre, particularly in the hydration properties. The aim of this experiment is to see if any differences in chemical composition of the cuticle structure can be observed amongst ethnic hair types.

Attenuated total reflection fourier transform infrared spectroscopy (ATR-FTIR) is a technique that can be used to investigate the surface structure of materials. This chapter provides an investigation into the chemical conformation of the surface structure of ethnic hair types using ATR-FTIR. This technique has been combined with PCA and a second derivative de-convolution analysis of the spectra, to distinguish between ethnic hair types and discriminate inter-ethnic structural chemical differences.

6.1 Sample preparation

Hair types used in this experiment are; Afro (n=5), Chinese (n=3), Euro (n=4), Mullato (n=5), Spanish (n=5) and Thai (n=4). Single hair fibres were used from each of the sources and three measurements were taken from each hair fibre. Three hair fibres were used from each source. The n number here denotes how many different sources from the same ethnicity were used in this experiment.

6.2 Data Collection

Each hair fibre was placed onto a diamond ATR crystal and clamped down using the ATR pressure tower attachment to a set force of 70N on the scale as determined by the Perkin Elmer software. The spectra generated from each hair fibre were an average of 32 scans. This was repeated using 3 incremental steps of 0.2 mm at the root end of each hair fibre; 3 different hair fibres from each source were used and 3 different sources were used for each ethnic hair type. There were a total of at least 27 measurements taken for each hair type. The sample stage was cleaned between every measurement using lint-free tissue and industrial methylated spirit (IMS).

Spectral images were taken using a Perkin-Elmer Spectrum One Spectrometer system with the Universal ATR sampling accessory fitted. The ATR accessory uses a diamond crystal which provides a useful sample contact area of approximately 500 microns in diameter. Each measurement was taken and averaged by the Perkin-Elmer software. The software used was Perkin Elmer Spectrum version 5.01.

This work was performed with in collaboration with Pangiota Manti who loaned me the use of her spectrometer system and provided technical assistance.

6.3 Data Analysis

The spectra were analysed using PCA from in-house software and the second derivative de-convolution analysis function in the Peakfit software program. This allows for the averaged spectra to be de-convoluted into the original spectra that contributed to it. This method highlights any differences seen between ethnic hair types in the spectra arising from the various vibrational modes.

6.4 Results

The results obtained from the experiment have been divided up into their own sections based on the analysis technique that was used; PCA or second derivative analysis.

6.4.1 Analysis of the spectra arising from keratin across differential ethnic hair types

Figures 6.1A and 6.1B show typical spectra from the Chinese hair type in the wavenumber regions $\approx 800\text{-}1750\text{ cm}^{-1}$ and $\approx 2750\text{ - }3550\text{ cm}^{-1}$ respectively. Figure 6.1A is dominated by the Amide I and II bands which correspond to the peptide backbone of the keratinous structure; the Amide III band also provides information on the conformation of the peptide backbone but contributes less intensity. The position in wavenumber of the amide bands reveals information on the secondary structure of the keratin present; although human hair is primarily composed of alpha-helical keratin, other conformations of keratin can be present and these can affect the wavenumber of the amide bands (Ambrose and Elliott 1951, Baddiel 1968, Akhtar, Edwards et al. 1997). In human hair the peptide bonding in the keratinous alpha-helical structure gives rise to a series of characteristic absorptions. These arise from the Amide I envelope found between ≈ 1600 and $\approx 1690\text{ cm}^{-1}$. This bonding is predominantly a peptide carbonyl stretching vibration of the CO-NH unit together with an out of phase C-N stretching component and a small contribution from the C-N-N deformation. The Amide II envelope which is found between ≈ 1480 and $\approx 1575\text{ cm}^{-1}$ arises from a combination of the C-N stretching mode, an in-plane N-H bend, the C-O in plane bend and an N-C stretch. The Amide III envelope is found between ≈ 1210 and $\approx 1320\text{ cm}^{-1}$ and arises from a combination of in-plane bending of the N-H bonding and C-N stretching, the C-C stretch and C-O in-plane bends (Adams 1995).

Further absorptions are found between ≈ 1460 and $\approx 1471\text{ cm}^{-1}$ due to C-H deformation; between ≈ 1443 and $\approx 1453\text{ cm}^{-1}$ due to the CH_2 vibrational mode resulting from the bonding along the backbone of the peptide chains and between ≈ 1399 and $\approx 1411\text{ cm}^{-1}$ due to the CH_3 vibrational mode from the deformation of the amino acid side chain groups.

Also seen in Figure 6.1A is the signal arising from the various oxidation products of the cysteine containing amino acids in keratin. The variation in the oxidation product arises from the oxidation of different cysteine containing amino acids (Joy and Lewis 1991). These products may be caused by chemical treatment to the hair, bleaching or photo-oxidative damage from UV light (Joy and Lewis 1991, Signori and Lewis 1997), here these oxidation products are suggested to be a cause of UV damage as they have not been subjected to chemical treatment. Absorption bandings are also found from the asymmetric and symmetric cysteic acid stretches at ≈ 1171 and ≈ 1040 cm^{-1} respectively, a symmetric cysteine dioxide stretch at ≈ 1121 cm^{-1} and a cysteine monoxide stretch at ≈ 1071 cm^{-1} (Adams 1995).

The lipids present in the CMC of hair produce a signal in the wavenumber region $\approx 1735 - 1740$ cm^{-1} for the C=O ester groups, primarily from lipids and fatty acids. The signal arising from the CH series of bonding in the wavenumber region $\approx 2700 - 3100$ cm^{-1} , is also representative of the lipid alkyl chains present in hair (Akhtar, Edwards et al. 1997). However, this region overlaps with the signal seen from the CH bonding within the keratin. These stretches are seen in Figure 6.1B. The anti-symmetric and symmetric stretches for the CH_3 are seen at ≈ 2958 cm^{-1} and ≈ 2927 cm^{-1} respectively. The anti-symmetric and symmetric stretches for the CH_2 can be found at ≈ 2872 and ≈ 2855 cm^{-1} respectively.

Higher modes and overtones of the Amide envelopes have absorptions in the region of $\approx 3060 - 3300$ cm^{-1} . The Amide A and B bands arise almost exclusively from the overtone of the N-H stretch. The Amide A band is found at ≈ 3295 and the Amide B at ≈ 3062 (Adams 1995). Table 6.1 shows all of the vibrational modes and their corresponding assignments for human hair for the wavenumber range of $1000-4000$ cm^{-1} .

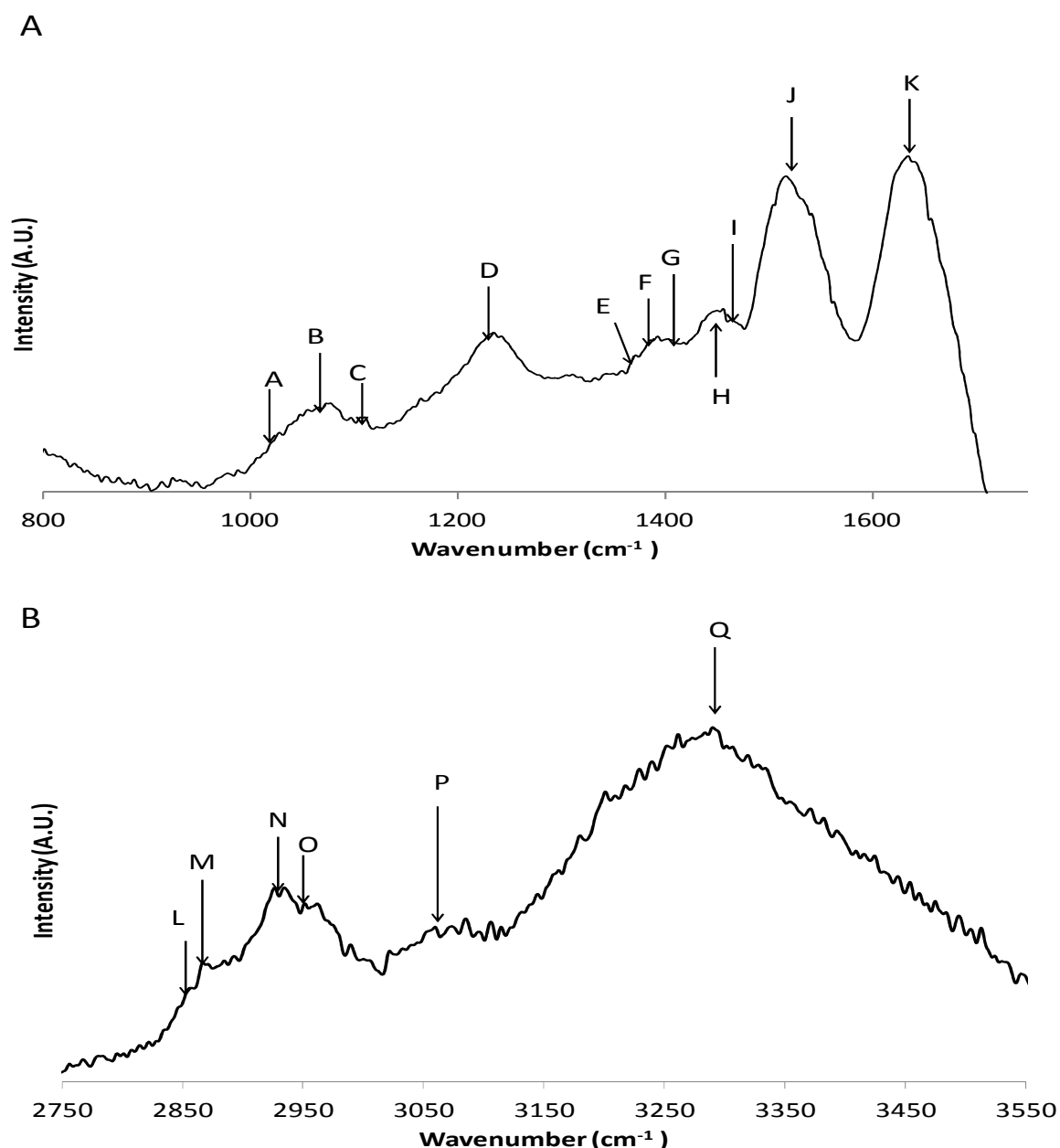


Figure 6.1 – A typical spectra from a Chinese hair sample. Figure 7.1A shows all of the vibrational modes arising in the wavenumber region of 800 – 1750 cm^{-1} . A: cysteic acid stretch, B: cysteine monoxide stretch, C: cysteine dioxide stretch, D: Amide III band, E: CH_3 symmetric deformation, F: anti-symmetric CH_3 deformation mode, G: CH_3 bending mode, H: CH_2 bending mode, I: CH deformation, J: Amide II band, K: Amide I band. Figure 7.1B shows all of the vibrational modes arising in the wavenumber range of 2750 – 3550 cm^{-1} . L: CH_2 symmetric mode, M: CH_2 anti-symmetric mode, N: symmetric CH_3 mode, O: CH_3 anti-symmetric mode, P: Amide B band, Q: Amide A band. The vertical axis on both of the graphs is intensity measured in arbitrary units.

Assignment	Wavenumbers (cm ⁻¹)
Amide A	3295
Amide B	3062
CH ₂ anti-symmetric stretch	2958
CH ₃ anti-symmetric stretching	2927
Symmetric CH ₂ stretch	2872
Symmetric CH ₃ stretching	2855
C=O carbonyl stretch	1735
Amide I band	1690, 1657-1650, 1646, 1637, 1605-1588
C=O carboxylate stretch	1576, 1570-1563
Amide II band	1545, 1532, 1518, 1505
C-H deformation	1471-1460
CH ₂ bending mode	1453-1443
CH ₃ bending mode	1411-1399
CH ₃ symmetric deformation	1387, 1371-1365
Amide III band	1310-1278, 1260-1255, 1241-1231, 1225
SO ₂	1121
SO	1071
S=O	1038-1040

Table 6.1 – Wavenumbers for all vibrational modes seen in human hair in the range 1000 - 4000 cm⁻¹. The Amide envelopes have a number of modes arising from several independent vibrations.

6.4.2 Principal Component Analysis (PCA) of the FTIR spectra

From the PCA it is possible to generate multi-dimensional plots of the eigenvalue coefficients obtained from the FTIR spectra of each hair sample. Using the multi-dimensional plots, we can determine if clustering of eigenvalues occurs which informs us that the samples have the same base function weightings by ethnicity. This can be used to determine which spectral features in the data are similar/different and help us characterise how the chemical vibrations can be related

to structural alterations between samples. Figure 6.2A shows a typical multi-dimensional plot created from the output of the eigenvalues coefficients from the PCA. The eigenvalues from BF2 are plotted against BF4; the circles highlight clustering by ethnic hair type.

Further representation of the data using bar graphs of the average eigenvalue coefficient weightings help to identify the size of the weighting for each BF from each hair type. The main use of this plot is to show which BFs characterise differences between the hair types. In order for the hair types to be significantly different from each other, the bar and associated standard deviation for each hair type must not overlap if the BF sufficiently describes a distinguishing feature. Using this plot to identify which BFs discriminate between hair types, further referral to the BF profiles themselves allows for the identification of the vibrational modes which contribute to distinguishing between the hair types. Figure 6.2B shows the average BF eigenvalue coefficient weightings plot for the data set. Here it is observed that BF1 can be used to discriminate the Chinese and Mullato hair types from the Thai and Afro hair types. The Mullato hair can also be distinguished from the remaining hair types for this BF. BF2 distinguishes the Mullato and Spanish hair types from the others; BF3 distinguishes the European hair type from the Chinese, Thai, Afro and Spanish and also the Afro and Spanish hair types from the remaining hair types. BF4 discriminates the Chinese and Spanish hair types from the Thai, Afro and Mullato and the European from the Thai and BF5 differentiates the Afro and Mullato hair types from the remaining.

The BF profiles generated from the PCA can be used to characterise which spectral features change between samples. The spectral features are identified by calibrating the intensity peaks seen in the BF profiles with the corresponding wavenumbers of the vibrational modes reported in Table 6.1.

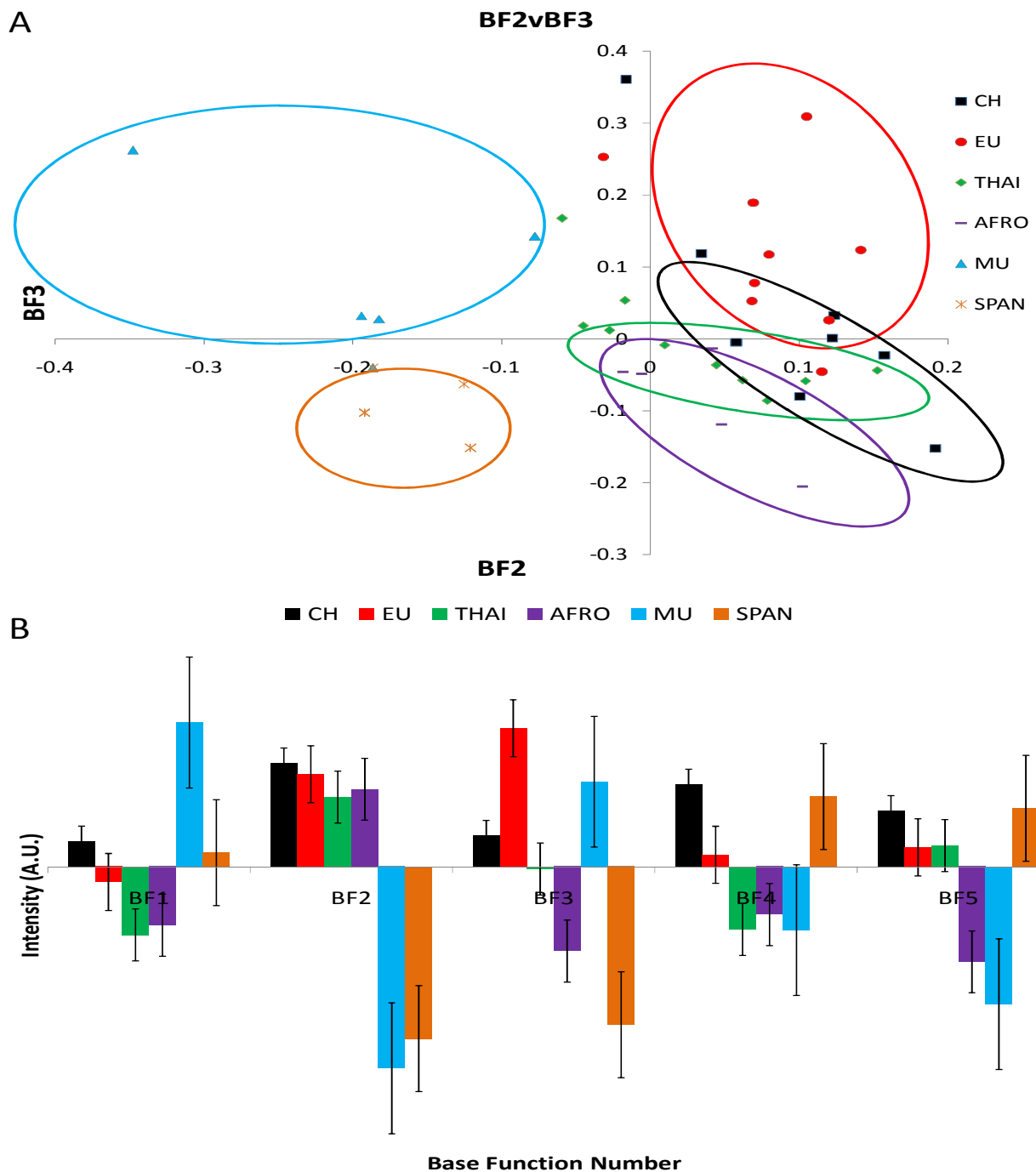


Figure 6.2 – Figure 6.2A: A multi-dimensional plot of the eigenvalues coefficients. The horizontal axis is BF 2 and the vertical axis is BF 3. Both axes represent the intensity measured in arbitrary units. The ellipses highlight the clustering seen by ethnic hair type. Figure 6.2B: The average base function eigenvalues coefficient weightings for each hair type in each base for the full spectral range. The hair types are arranged in the same order as indicated by the legend. The horizontal axis denotes the base function number and the vertical axis is the intensity measured in arbitrary units.

Figures 6.3 - 6.5 show an annotation of the average base function profile, and BFs 1-5 highlighting the vibrational modes that change within the data set. BF1 corresponds to the largest spectral changes within the data set, BF2 the second largest and so on. Figure 6.3A shows BF1; here we observe an intensity increase in the Amide I and Amide II envelopes, the C-H and CH₃ deformation modes and broadening in the Amide III envelope and cysteine banding. Figure 6.3B shows BF2, where a decrease of intensity of the Amide I, II and III envelopes, the CH₃ stretch and the S=O stretch is observed. In the wavenumber region 2500 – 3750 cm⁻¹, BF2 is noisy and so validation of any vibrational modes in this region is hard to determine, although there is an indication that an increase in intensity of the Amide B band occurs. BF3 is shown in Figure 6.4A. The largest spectral features to change are a shift in the wavenumber position of the Amide I and Amide II envelopes. We also observe an increase for the S=O and SO stretches at $\approx 1009 - 1093 \text{ cm}^{-1}$, a decrease in intensity for the SO₂ stretch at $\approx 1117 - 1129 \text{ cm}^{-1}$, the CH₃ asymmetric and symmetric stretches at $\approx 2850 \text{ cm}^{-1}$ and $\approx 2920 \text{ cm}^{-1}$, and an anti-correlation of the Amide A and B bandings, where the Amide B is seen to increase while the Amide A decreases. Figure 6.4B shows BF4; here a correlation between an increase in intensity of the Amide I, II and III envelopes and a decrease in the intensity of the CH₃ asymmetric and symmetric stretches is seen. Figure 6.5A shows BF5, a correlation between an increase in intensity of the Amide II, shifting of the absorption wavenumber of the Amide I and a decrease in intensity of the Amide A and B bandings can be observed. Figure 6.5B shows the average BF outputted by the PCA. Further analysis of the vibrational modes can be sought from the second derivative analysis. Second derivative analysis provides information on the spectra that originally contributed to the averaged spectra which provides an insight of the peaks that have been averaged out by the software. This analysis can give further detail of the variation in wavenumber of the vibrational modes between hair types.

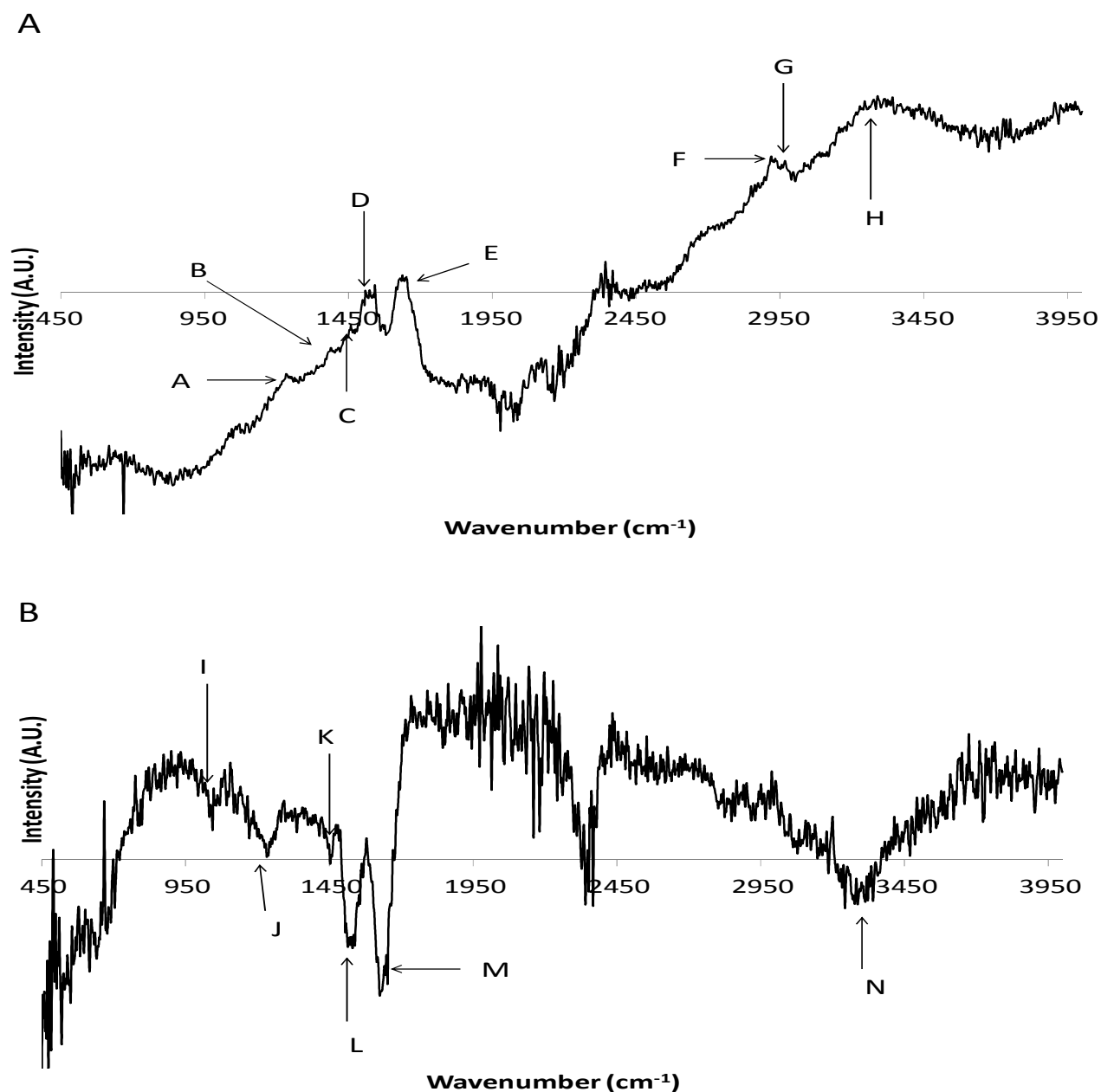


Figure 6.3 – Figure 6.3A: BF1 outputted by the PCA for the full spectral range for all hair types. Highlighted in the figure are all the vibrational modes seen in this base function across the entire spectral range. A: Amide III band, B: symmetric CH₃ deformation, C: CH deformation, D: Amide II band, E: Amide I band, F: symmetric CH₂ stretch, G: anti-symmetric CH₃ stretch, H: Amide B band. Figure 6.3B: BF2 outputted by the PCA for the full spectral range for all hair types. Highlighted in the figure are all the vibrational modes seen in this base function across the entire spectral range. I: cysteic acid stretch, J: Amide III band, K: CH₃ bending mode, L: Amide II band, M: Amide I band, N: Amide B band. The vertical axis is the intensity measured in arbitrary units on both graphs.

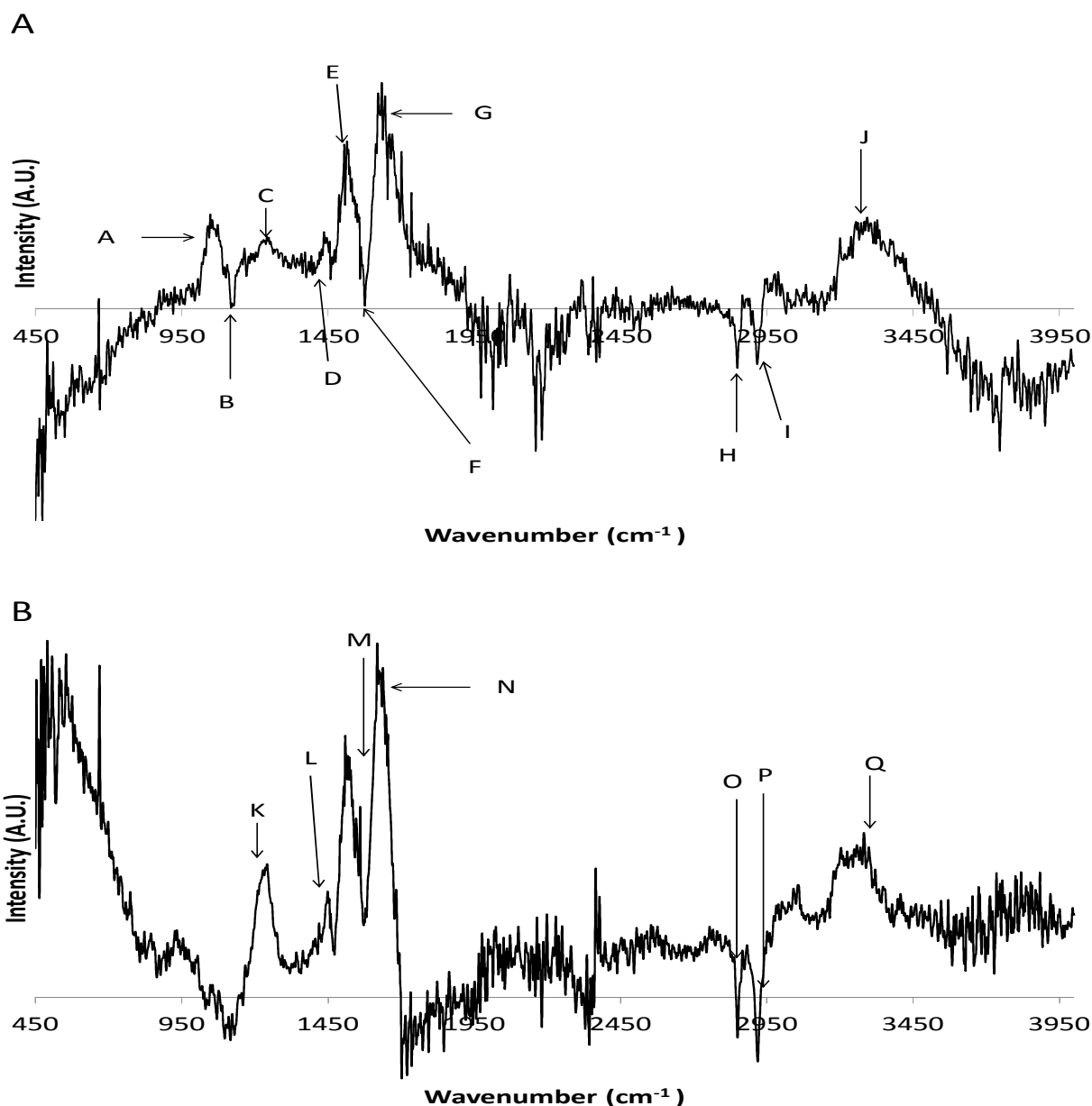


Figure 6.4 – Figure 6.4A: BF3 outputted by the PCA for the full spectral range for all hair types. Highlighted in the figure are all the vibrational modes seen in this base function across the entire spectral range. A: cysteic acid and cysteine monoxide stretches, B: cysteine dioxide stretch, C: Amide III band, D: CH₂ bending mode, E: Amide II band, F: carboxylate stretch, G: Amide I band, H: symmetric CH₂ stretching mode, I: anti-symmetric CH₂ stretching mode, J: Amide B band. Figure 6.4B: BF4 outputted by the PCA for the full spectral range for all hair types. Highlighted in the figure are all the vibrational modes seen in this base function across the entire spectral range. K: Amide III band, L: CH₃ bending mode, M: Amide II band, N: Amide I band, O: symmetric CH₂ stretch, P: anti-symmetric CH₂ stretching mode, Q: Amide B band. The vertical axis is the intensity measured in arbitrary units on both graphs.

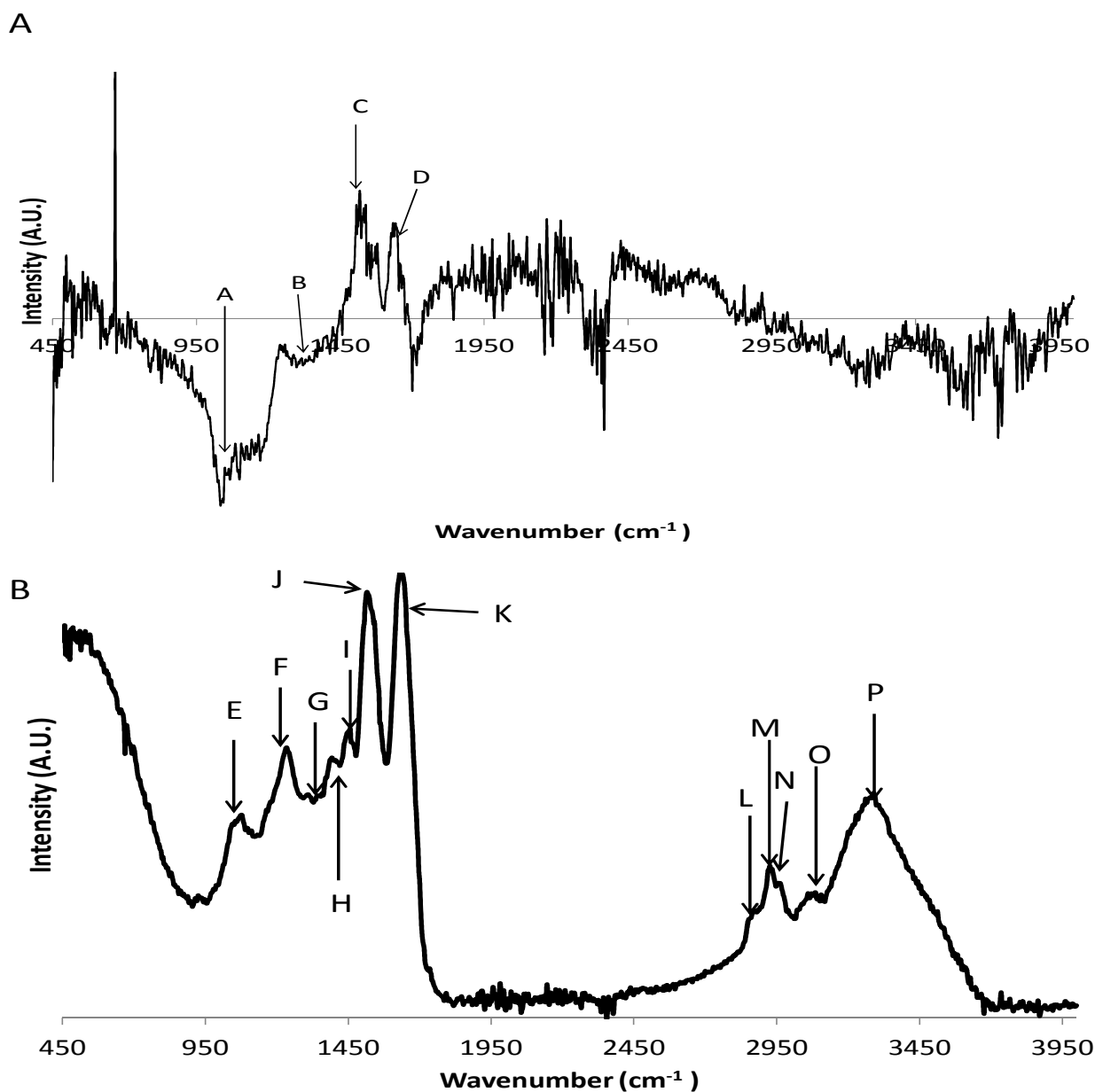


Figure 6.5 – Figure 6.5A: BF5 outputted by the PCA for the full spectral range for all hair types. Highlighted in the figure are all the vibrational modes seen in this base function across the entire spectral range. A: cysteic acid stretch, B: Amide III band, C: Amide II band, D: Amide I band. Figure 6.5B: the average base function outputted by the PCA for the full spectral range. Highlighted in the figure are all the vibrational modes seen in this base function across the entire spectral range. E: cysteine monoxide stretch, F: Amide III band, G: CH₃ deformation, H: CH₂ bending mode, I: CH deformation, J: Amide II band, K: Amide I band, L: CH₂ symmetric mode, M: CH₂ anti-symmetric mode, N: symmetric CH₃ mode, O: Amide B band, P: Amide A band. The vertical axis on both of the graphs is intensity measured in arbitrary units.

6.4.3 Second Derivative Analysis of the Amide bands in all hair types

The results of the second derivative analysis for the Amide bandings are shown in Table 6.2.

Hair type	Amide I band (cm ⁻¹) (± 3)	Amide II band (cm ⁻¹) (± 3)	Amide III band (cm ⁻¹) (± 3)
Afro	1635, 1668	1513, 1536, 1570	1234
Chinese	1635, 1668	1520, 1567	1236
Euro	1634, 1668	1516, 1568	1233
Mullato	1639	1526	1230
Spanish	1637, 1677	1524, 1566	1229
Thai	1634, 1682	1519, 1570	1234

Table 6.2 – Average wavenumber value for each vibrational mode population in each respective Amide bandings across all hair types.

From the results we observe that the Amide I envelope has two contributing vibrational modes; a band at $\approx 1634 - 1640 \text{ cm}^{-1}$ and a shouldering band at $\approx 1666 - 1677 \text{ cm}^{-1}$, the one exception is the Mullato hair type which only has one contributing vibrational mode. The Mullato and Spanish hair types both exhibit absorption maxima at higher wavenumbers for the $1634 - 1640 \text{ cm}^{-1}$ band in comparison to all the other hair types. The Spanish and Thai hair both show absorption maxima at higher wavenumbers for the shouldering band in comparison to the Afro, Euro and Chinese hair types.

All hair types exhibit two modes for the Amide II envelope except the Afro type which exhibits three. The first mode is a band at $\approx 1512 - 1528 \text{ cm}^{-1}$; the second mode is a shouldering band at $\approx 1564 - 1570 \text{ cm}^{-1}$. The Afro, Euro and Thai hair type all show lower wavenumbers for the first mode in comparison to the Chinese, Mullato and Thai hair types. The Afro and Thai hair types both show the highest wavenumbers for the second/third modes in comparison to the other hair types.

All hair types show one population for the Amide III envelope which is a low intensity band located at $\approx 1230 - 1237 \text{ cm}^{-1}$. The Spanish and Mullato hair type show the lowest wavenumbers for the Amide III band, with the Chinese showing the highest. The Afro and Thai exhibit similar wavenumbers and the Euro hair type slightly lower than the Afro and Thai.

6.4.4 Second Derivative Analysis of the polypeptide chain vibrational modes

The results of the second derivative analysis for the cysteine stretches are shown in Table 6.3.

Hair type	Average SO ₂ cysteine dioxide vibrational mode (cm ⁻¹) (± 3)	Average SO cysteine monoxide vibrational mode (cm ⁻¹) (± 3)	Average S=O cysteic acid vibrational mode (cm ⁻¹) (± 3)
Afro	1113	1080	1043
Chinese	-	1076	1044
Euro	-	1080	1043
Mullato	-	-	-
Spanish	-	-	-
Thai	1110	1070	-

Table 6.3 –Average wavenumber value for the corresponding polypeptide vibrational modes in each hair type.

The Mullato and the Spanish hair types do not show absorption peaks for any of the SO₂ vibrational modes from second derivative analysis. Only the Afro and Thai hair types showed a peak corresponding to this cysteine dioxide vibrational mode. The cysteine monoxide mode (SO) was seen in the Afro, Chinese, Euro and Thai hair types in a range of $\approx 1068 - 1080 \text{ cm}^{-1}$; the Thai showed the lowest wavenumbers and the Afro showed the highest. The Afro, Chinese and the Euro all showed a narrow range of wavenumbers for the cysteic acid band (S=O) ($1041 - 1044 \text{ cm}^{-1}$) which is a little higher than reported in literature (See Table 6.1).

6.4.5 Second Derivative Analysis of the Amino Acid side chain groups

The results of the second derivative analysis for the cysteine deformations are shown in Table 6.4.

Hair type	Average CH band (cm^{-1}) (± 3)	Average CH_2 band (cm^{-1}) (± 3)	Average CH_3 band (cm^{-1}) (± 3)
Afro	-	1450	1392
Chinese	-	1450	1392
Euro	-	1454	1390
Mullato	-	1447	1403
Spanish	-	1451	1400
Thai	-	1452	1394

Table 6.4 – Average wavenumber value for the corresponding amino acid vibrational modes in each hair type.

None of the hair types showed a peak from second derivative analysis for the C-H band. The CH_2 band was seen in all of the hair types in a range of $\approx 1445 - 1461 \text{ cm}^{-1}$. The CH_3 band was also observed in all hair types in the range $\approx 1385 - 1402 \text{ cm}^{-1}$. It is seen in Table 6.4 that the biggest difference in the CH_2 and CH_3 band is between the Euro and Mullato hair type. Additionally, the CH_3 band of the Spanish hair type shows a similarity to the Mullato hair type. The other hair types are consistent for both vibrational modes in second derivative analysis.

6.4.6 Second Derivative Analysis of the Higher Harmonics

Table 6.5 shows the wavenumbers for the corresponding vibrational modes for the Amide bands and the amino acids found between $2750 - 4000 \text{ cm}^{-1}$.

Hair Type	Amide A (cm ⁻¹) (±3)	Amide B (cm ⁻¹) (±3)	Anti-symmetric CH ₂ (cm ⁻¹) (±3)	Anti-symmetric CH ₃ (cm ⁻¹) (±3)	Symmetric CH ₂ (cm ⁻¹) (±3)
Afro	3292	3076	2958	2927	2873
Chinese	3290	3076	2958	2929	2870
Euro	3302	3080	2958	2928	2878
Mullato	3285	3071	2966	2929	2869
Spanish	3280	3074	2964	2926	2880
Thai	3290	3072	2959	2928	2872

Table 6.5 – Wavenumbers seen in second derivative analysis for all types of bonding in the wavenumber region 2850 – 3300 cm⁻¹ for all ethnic hair types.

The largest difference of wavenumber value for the Amide A peak is seen between the Euro and the Spanish hair type; all the other hair types have a similar absorption wavenumber apart from the Mullato which shows a slightly lower value. The biggest difference in the Amide B band is observed between the Euro and the Mullato hair types. The Spanish and Mullato hair types show a larger wavenumber value for the anti-symmetric CH₂ stretch, in comparison to the remaining hair types which remain consistent in wavenumber value. The anti-symmetric CH₃ is consistent in wavenumber across all hair types. The largest difference in wavenumber seen for the symmetric CH₂ stretch is seen between the Euro and Spanish hair types with respect to the Chinese and Mullato.

6.5 Discussion

From the PCA it is possible to distinguish differences between the FTIR spectra of samples and therefore discriminate between ethnic hair types. This is observed by the clustering of hair types in Figure 6.2A. BFs 2, 3 and 4 show spectral differences of the wavenumbers and intensity of

vibrational modes between ethnic hair types; this is proposed to be due to variation in the structural composition of the cuticle layer between hair types.

BF2 discriminates the Spanish and Mullato hair types from the other hair types by the intensity of the Amide I, II and III bandings. The basis of the increased intensity could be a greater thickness of the cuticle layer which permits absorption from more vibrators in thicker samples. Other contributors could be a higher concentration of α -helical conformations at the surface of these hair fibres, additional vibrations arising from the cortex, or an increased water content within the surface structure (Baddiel 1968). It is possible that the surface structure is more hydrophilic in these two hair types in comparison to the others, leading to increased intensity of the vibrational mode at $\approx 1633 \text{ cm}^{-1}$ which is related to the hydrogen bonding in water molecules (Barton 2011).

Further evidence that the cuticle has differing quantities of α -helical structures in ethnic hair types can be observed in BF3. Here, there is an observed shift in the Amide I and II absorption maxima, which suggests that the contribution from individual vibrators has changed. Using BF3 it is possible to discriminate the Euro, Chinese and Mullato from the Afro and Spanish hair types. The larger Amide I and II envelope wavenumbers exhibited by the Euro, Chinese and Mullato samples signifies a greater intensity of the absorption band at $\approx 1668 \text{ cm}^{-1}$ and $\approx 1568 \text{ cm}^{-1}$ respectively, and indicates more α -helical structures are present in respect of the α -helical and β -pleated sheet ratio within the cuticle. There was also an observed intensity increase of the S=O stretch at $\approx 1038 \text{ cm}^{-1}$ suggesting that the Spanish and Mullato hair types have been subject to excessive exposure of UV light, since this vibrational mode corresponds to the oxidation of cysteine to cysteic acid (Joy and Lewis 1991). This may be a direct factor of the geographical location of the source of the hair fibres.

We were unable to detect any signal arising from the lipids using this technique, although it is likely that there are lipids present in some or even all of the hair fibres under test, neither the PCA nor the second derivative analysis showed any peak relating to the carbonyl stretch at $\approx 1735 - 1740 \text{ cm}^{-1}$. As the CH series of stretches in the wavenumber region $\approx 2700 - 3100 \text{ cm}^{-1}$ also relate to the CH bonding present in the keratin, signal arising in this region cannot be justifiably assigned to the CH bonds in the lipid alkyl chains.

The second derivative analysis shows that within the Amide I envelope, the Spanish and Mullato hair types show a higher wavenumber for the vibrational mode at $\approx 1633 \text{ cm}^{-1}$ which relates to the

H-O-H bend adsorption of water. This is most likely to be responsible for the discrimination between the Spanish and Mullato hair types from the others in the PCA. The vibrational mode at $\approx 1667 \text{ cm}^{-1}$ shows that the Afro, Euro and Chinese hair types exhibit a signal from the β -pleated sheet conformation. The Amide II envelope also shows that the Afro hair type has two vibrational modes whereas the remaining hair types exhibit one mode. The mode seen in the range of $\approx 1613 - 1626 \text{ cm}^{-1}$ among the hair types relates to the C-N stretch and in-plane N-H bend of the β -pleated sheet conformation of keratin. Here the presence of the α -helical structures increases the wavenumber of the vibrational mode. This implies that the Spanish and Mullato hair types show either increased signal from the α -helical structures in the cortex due to greater weathering, or possess more α -helical structures on the cuticle surface. It also suggests that the Afro, Chinese, Euro and Thai hair types would have increased β -pleated sheet structures, with the Afro showing the most.

In the wavenumber region $2750 - 4000 \text{ cm}^{-1}$, the most significant difference seen between hair types from second derivative analysis is the presence of a peak corresponding to the H-O-H stretch at $\approx 3430 \text{ cm}^{-1}$, observed in the Spanish and Mullato hair types only. This supports evidence gathered from PCA which discriminates between the Spanish and Mullato hair types with respect to the remaining hair types on the basis of the water content and thus hydrophilic properties of the cuticle surface structures.

6.6 Conclusions

Using both PCA and second derivative analysis, it has been proven that differential ethnic hair types can be distinguished from each other on the basis of the signal arising from the α -helical, β -pleated sheet and random/amorphous conformations of the keratin structures, the weathering of the hair fibres (due to evidence gathered from the cysteine vibrational modes) and the water content and hydrophilic nature of the surface of the hair fibres. The results presented in this chapter therefore conclude that on the basis of structural differences present in the cuticle layer of hair fibres as discussed above, it is possible to inter-ethnically discriminate hair fibres using ATR-FTIR. This has important consequences for both forensic science and hair care product development; for the former as it allows a quick, non-destructive technique to distinguish

between the race of individuals, and the latter for targeting of products to specific ethnic requirements.

Chapter 4, 5 and 6 have used both X-ray analysis and infrared spectroscopy techniques to analyse the structure of both the keratin and non-keratinous components within the cortex and at the cuticle surface. Across all these studies it has been observed that there are quantifiable differences that must all contribute in part to the macroscopic variation observed between ethnicities and also in various mechanical properties. As structural studies on the two most important parts of the hair fibre have been performed (the cortex and cuticle) it is now logical to try and isolate and study the non-keratinous components that are expected to play a significant contributing role in producing ethnic disparity. The lipids are possibly the most important non-proteinaceous molecular structure found in hair and are thought to play a vital role in the hydration properties of hair; therefore a study revealing any information on this will be valuable in this field of research.

Chapter 7 – A biochemical analysis of lipids extracted from differential ethnic hair types

Lipids comprise the largest class of non-proteinaceous matter found in human hair fibres. Lipids found in hair originate from two different sources: the sebum excreted from the sebaceous glands at the hair follicle, or cell membrane remains found internally. This gives two different groups of lipids: exogenous and endogenous lipids. Evidence from the SAXS and WAXS experiments (see Chapter 4) reports for the first time that there is inter-ethnic variation observed in the spacing of the structural crystalline lipids found within the cortex. These are likely to be free fatty acids in crystalline form or may arise from the crystallisation of other components present in cells such as the mitochondria after keratinisation (Fraser, MacRae et al. 1963, Bertrand, Doucet et al. 2003). We propose that the inter-ethnic variation in spacing of the crystalline lipid is directly correlated to a difference in the individual classes as well as to a difference in the fatty acid (FA) patterns of lipids found internally in the hair fibres. The variation in spacing could also be a result of a tilting effect of the lipids in the vertical plane (i.e. the plane parallel to the axis of fibre growth) or a hydration effect (both of which will not be investigated here). Therefore the aim of this experiment is to elucidate whether there are differences seen in the chemical composition of the lipids extracted from differential ethnic hair types.

This study has used a biochemical approach to differentially extract and analyse both the surface lipids found at the cuticle of the hair fibre as excreted by the sebaceous glands and the endogenous lipids. A combination of thin layer chromatography (TLC), gas chromatography coupled with fire ionization detection (GC/FID) and ultra performance liquid spray mass spectroscopy (UPLC/MS) has been used to analyse the lipids extracted.

7.1 Sample Preparation

Hair types used in this experiment are; Afro (n=5), Chinese (n=3), European (n=4), Mullato (n=5), Thai (n=4) and Spanish (n=5). 250 mg of each source was used to take the measurements for each hair type. The n number here denotes the number of different sources used for each ethnicity.

7.2 Data collection

In this study, two different methods were employed to analyse the lipids that were extracted from hair. One method used a lipid extraction as outlined in Section 3.4 combined with UPLC/MS in order to analyse the lipids. The conditions for the UPLC/MS analysis can also be found in Section 4.8.1. This method of lipid extraction was performed in collaboration with Valerie O' Donnell, Victoria Hammond and Madhav Monde. The extraction of the lipids from the hair was completely performed by myself with technical advice/assistance from Madhav. The UPLC/MS analysis and subsequent PCA was performed by Madhav, the interpretation of the results was done by myself. The other method used a different lipid extraction procedure discussed in Section 3.5, the lipids extracted from this method were combined with TLC and GC/FID for analysis. The run conditions for the TLC and GC/FID analysis can be found in Sections 3.5.4 - 3.5.6. This work was performed in collaboration with Irina Guschina and John Harwood. The extraction procedures were performed by myself with technical assistance from Irina. The GC/FID runs, GC/MS and analysis of chromatograms was provided by Irina; technical discussions and interpretations of the results with Irina, John, Tim and myself occurred to fully establish the information gathered from the data set.

7.3 Data Processing

The data collected by the UPLC/MS methods were analysed with PCA using a software package. Full details can be found in Section 3.4. The data collected via the TLC and GC/FID methods was analysed using the Perkin Elmer Total Chrom software and outputted into Excel.

7.4 Results

The results from the initial lipid analysis using the UPLC-MS method combined with PCA show that the lipids extracted from the hair types show some loose clustering by ethnicity. Figure 7.1 shows a multi-dimensional PCA plot displaying the clustering by hair type. As the hair fibres were ground into a fine powder with the assistance of liquid nitrogen, it is valid to assume that the results are from a bulk analysis of the entire lipid content present in the hair fibre. Therefore the results cannot be inferred to lipids from a specific spatial location in the hair fibre. The purpose of this initial study was to investigate the ethnic based variation of the lipid content in order to see if it is a valid area of study.

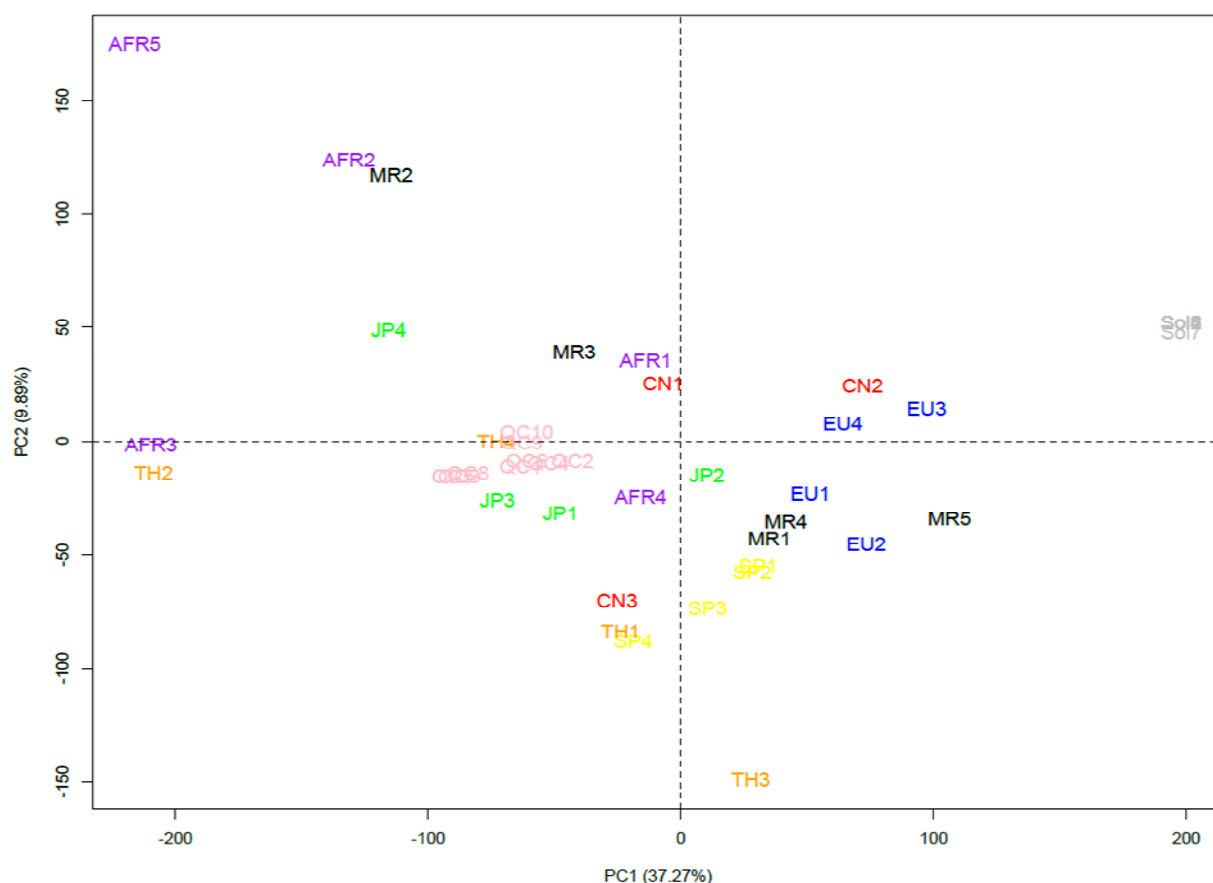


Figure 7.1 –Multi-dimensional plot of the lipids from the UPLC-MS analysis. The horizontal axis is the first principal component describing 37.27% of the variance in the data and the vertical axis is the second principal component which describes 9.89% of the variance in the data set. The codes on the diagram describe each sample that was used in the experiment and are labelled by ethnicity and sample number, for example EU1 is the first sample of the European hair type. The

codes for ethnicities are; AFR=Afro, CN=Chinese, EU=European, JP=Japanese, MR=Mullato, SP=Spanish, TH=Thai, QC=Pooled sample and Sol=solvent. A pooled sample (QC) was created by combing an aliquot of all the samples used in the study and was run at the beginning following two runs of blank solvent (Sol) for column conditioning and quality control analysis.

As seen in Figure 7.1, the tightest clustering seen by hair type is in the European and Spanish hair types. The Afro and Thai hair types show the least clustered formation suggesting that these hair types show the most variance in the lipids extracted between individuals. The Mullato hair type also shows a large spread, although two of the hair types are very similar. The inter-ethnic differences seen in Figure 7.1 in the spatial position and stringency of the clustering on the multi-dimensional plot merit further investigation into the lipid content of ethnic hair types. The results presented here suggest that on the basis of the clustering of the eigenvalues there are differences by hair type highlighted by PCA and it may be expected that there is variation in the lipid content of the hair types.

The results of the multi-dimensional plot therefore suggest the need for a systematic analysis of the lipids that can be extracted from the hair fibres to investigate the quantity and variation in composition. This was performed by using several complementary lipid extraction methods in order to optimally extract lipids that are present/bound to the hair fibres in different spatial locations.

7.4.1 Results from TLC and GC/FID analysis

The results from the TLC and GC/FID analysis presented a systematic way in which lipids were preferentially extracted from different spatial positions of the hair fibres using three different extraction procedures. The hair fibres were first subjected to a hexane:diethyl ether wash to remove the surface lipids, they were subsequently extracted using solvent solutions (chloroform:methanol) to extract lipids that were ionically bound to the hair fibres and lastly the hair fibres were subjected to a hydrolysis step which removes lipids that are either present within proteinaceous structures in the hair fibre, or covalently bound to the hair fibre (as in the case of 18-MEA at the cuticle surface). The lipids extracted were first separated and identified into their

individual lipid classes using TLC. The lipids were then methylated to convert their fatty acid residues to Fatty Acid Methyl Esters (FAMES) in order to analyse them by GC/FID. The lipids extracted in each procedure were quantified based on their fatty acid contents. The results are divided up into the following sections:

- The total lipid content in each ethnicity and the contribution to the total lipid content from each extraction procedure.
- The lipid composition grouped by class found in each extraction process (i.e. content of triacylglycerols, polar lipids, free fatty acids and wax esters).
- A description of the FAs from the extraction groups and individual lipid profiling.
- A summary of the results.

7.4.1.1 Total lipid content and contribution of different extraction groups.

The results show the Mullato hair type, on average, has the largest total lipid content amongst all hair types, and in decreasing order the pattern observed is; Afro, Thai, Spanish, Japanese, Chinese, European. The Mullato hair type also shows the largest variation in the total lipid content, in decreasing order the pattern seen is; Thai, Japanese, Chinese, Afro, Spanish, European (Figure 7.2 and Table 7.1).

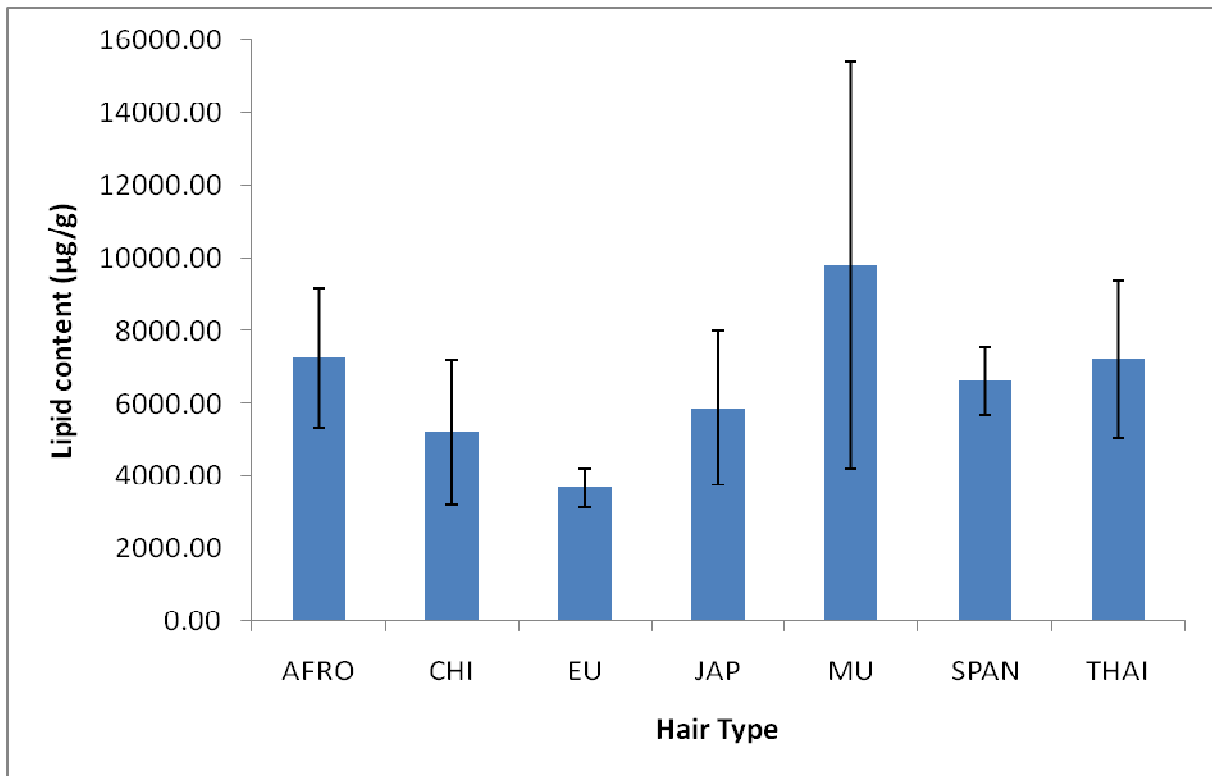


Figure 7.2 - Total lipid content (μg of fatty acids/g biomass) for each hair type. Data as means \pm SD (n=3-5).

Hair type	Afro	Chinese	European	Japanese	Mullato	Spanish	Thai
Total lipid content ($\mu\text{g/g}$ hair biomass)	7254.41 \pm 1939.45	5198.66 \pm 1984.73	3686.06 \pm 534.98	5884.02 \pm 2118.52	9818.26 \pm 5589.90	6616.49 \pm 928.66	7208.09 \pm 2169.82
Lipid:biomass (%)	3.14 \pm 0.84	2.29 \pm 0.88	1.47 \pm 0.21	2.83 \pm 1.02	3.91 \pm 2.23	2.74 \pm 0.39	2.88 \pm 0.87

Table 7.1 - Total amount of lipids ($\mu\text{g/g}$ hair biomass) in different ethnic hair types and the relative (% of biomass) lipid content in hair; this provides an indication of how much of the hair fibre is lipid in each hair type.

Table 7.2 and Figure 7.3 shows the contribution of the total lipid content extracted in each hair type by the different procedures expressed as a percentage. It is seen that the solvent extraction using chloroform:methanol extracted the most amount of lipid from the hair, followed by the fraction that was hydrolysed, and the hexane wash extracted relatively low amounts of lipids.

Hair Type	Afro	Chinese	European	Japanese	Mullato	Spanish	Thai
Hexane Wash (%)	8.66 ± 6.94	1.3 ± 0.7	1.65 ± 0.93	0.40 ± 0.24	0.84 ± 0.91	0.48 ± 0.16	1.25 ± 0.70
Solvent Extraction (%)	67.04 ± 11.59	55.0 ± 18.9	63.70 ± 5.44	64.28 ± 9.49	57.60 ± 13.69	73.90 ± 7.01	61.90 ± 1.97
Hydrolysed Fraction (%)	24.32 ± 8.86	43.7 ± 18.8	34.65 ± 5.62	35.33 ± 9.48	41.56 ± 13.77	25.62 ± 6.93	36.85 ± 2.33

Table 7.2 - Relative percentage of the total lipid content extracted from each extraction process.

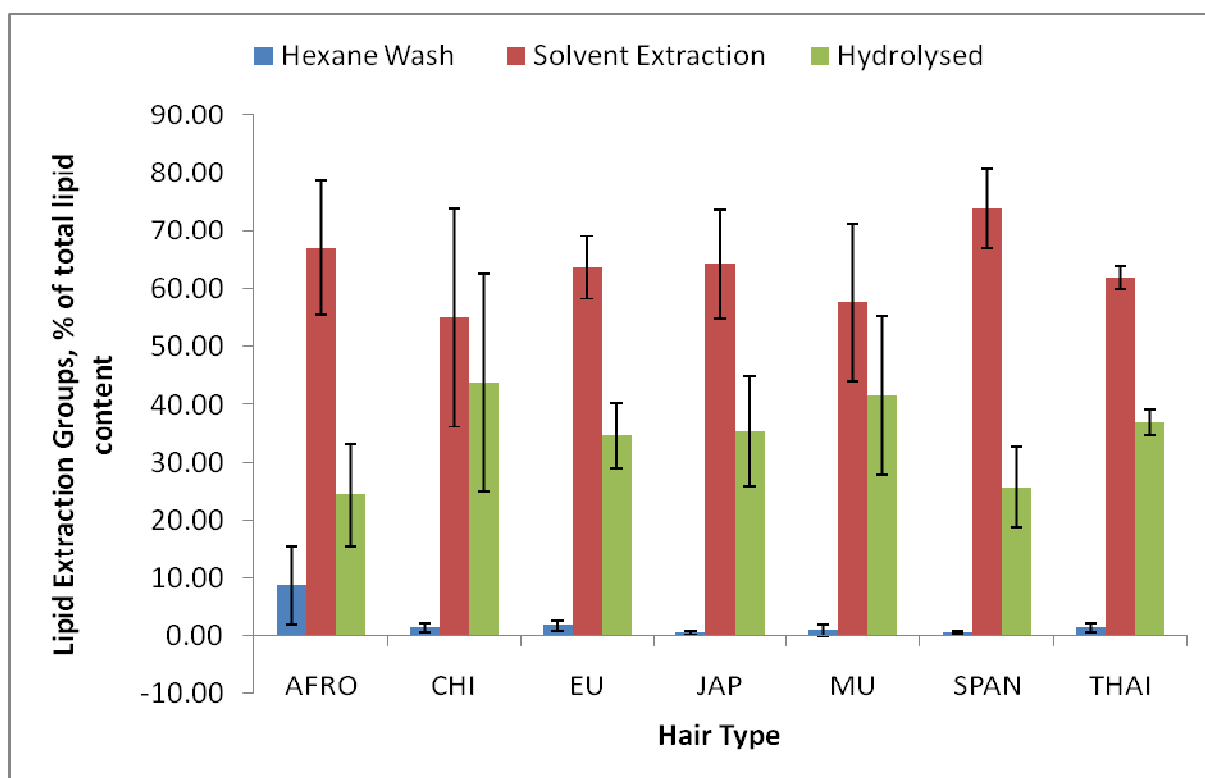


Figure 7.3 - Relative lipid content (% of total lipids) extracted by each extraction procedure. Data as mean \pm SD (n=3-5).

As seen in Figure 7.3, the solvent (chloroform: methanol) extracts the most lipid by percentage weight; all of the hair types showed at least 55% of the total lipid content extracted via this method, the Spanish hair type showed the most and the Chinese hair type the least. The hexane wash extracted the least; all hair types showed less than 10% of their total lipid content extracted via this method, the Afro hair type showed the most, the Japanese the least. The hydrolysed fraction extracted at least ~25% of the total lipid content amongst all hair types, the Chinese hair type showed the most and the Afro the least.

7.4.1.2 Composition and content of individual lipid classes in different extraction groups

The total content of lipids from the hexane wash and the solvent-extractable fractions were separated into their individual components using TLC (for the details of TLC separation, see Section 3.5.4). The major individual fractions in both groups were free fatty acids (FFA), wax esters (WE), triacylglycerols (TAG) and hydrocarbons (HC). In the solvent-extractable group, the total polar lipid fraction was also present and analysed. Ceramides have been shown to be the principal

compounds found in this fraction (Coderch, Mendez et al. 2008). It should be noted that a small amount of cholesterol was also present (data not shown).

7.4.1.2.1 Results from the Hexane Wash

The hexane:diethyl ether wash extracted very small amounts of lipids (1-8% of the total lipids found in hair) and this fraction consisted of WE, FFA and TAG. WE and FFA were the dominant lipids eluted by the hexane wash, TAG were found mainly in the Mullato hair type (in four of the five samples analysed). In the Spanish, European, Thai and Chinese hair types, TAG were identified only in 1-2 samples from 3-5 of those analysed. It is interesting to note that no TAG were found in the hexane wash from the Japanese and Afro hair types. The total lipid content of these individual lipids in the hexane wash fraction is shown in Table 7.3 and Figure 7.4.

Hair type	Afro	Chinese	European	Japanese	Mullato	Spanish	Thai
WE ($\mu\text{g/g}$)	414.07 \pm 270.89	29.78 \pm 16.73	13.07 \pm 14.26	7.67 \pm 3.43	33.80 \pm 39.44	6.27 \pm 2.35	30.12 \pm 24.37
FFA ($\mu\text{g/g}$)	157.54 \pm 164.04	28.00 \pm 12.09	40.63 \pm 27.71	11.66 \pm 9.46	21.43 \pm 15.12	22.52 \pm 9.16	62.97 \pm 44.09
TAG ($\mu\text{g/g}$)	n.d.	3.19 \pm 4.51	5.76 \pm 11.53	n.d.	24.45 \pm 24.39	2.39 \pm 3.53	1.65 \pm 3.31
TOTAL ($\mu\text{g/g}$)	571.62 \pm 434.14	60.97 \pm 33.34	59.47 \pm 53.51	19.34 \pm 12.90	79.69 \pm 78.96	31.19 \pm 15.05	94.75 \pm 71.78

Table 7.3 – Content of each lipid class extracted and the total lipid content extracted from the hexane wash. n.d. denotes that the lipid was not detected. Data as mean \pm SD (n=3-5).

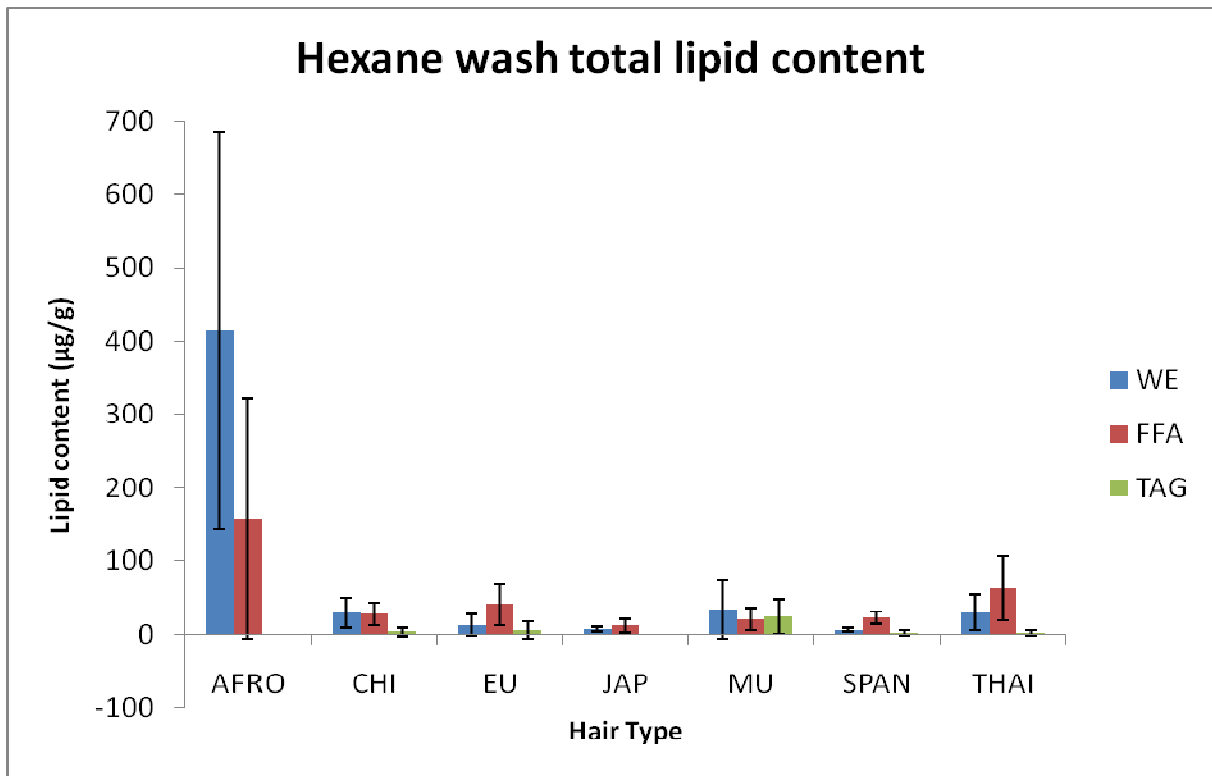


Figure 7.4 - Bar graph displaying the content of wax esters (WE), free fatty acids (FFA) and triacylglycerols (TAG) in the hexane wash ($\mu\text{g/g}$ biomass). Data as mean \pm SD (n=3-5).

Table 7.4 and Figure 7.5 show the relative percentage of each lipid class as a proportion of the total lipid content extracted in the hexane wash.

Hair type	Afro	Chinese	European	Japanese	Mullato	Spanish	Thai
WE (%)	72.44 ±	48.84 ±	21.98 ±	39.68 ±	42.42 ±	20.11 ±	31.79 ±
	47.25	27.44	23.98	17.78	49.50	7.56	25.73
FFA (%)	27.56 ±	45.92 ±	68.32 ±	60.32 ±	26.90 ±	72.20 ±	66.46 ±
	28.70	19.84	46.61	48.93	18.98	29.36	46.54
TAG (%)		5.24 ±	9.70 ±		30.68 ±	7.69 ±	1.75 ±
	0.00	7.41	19.40	0.00	30.60	11.34	3.50
TOTAL (%)	100 ±	100 ±	100 ±	100 ±	100 ±	100 ±	100 ±
	79.95	54.69	89.99	66.71	99.08	48.26	75.77

Table 7.4 - Relative content (% of total in the hexane wash) of each individual lipid class in the hexane wash. Data as mean ± SD (n=3-5).

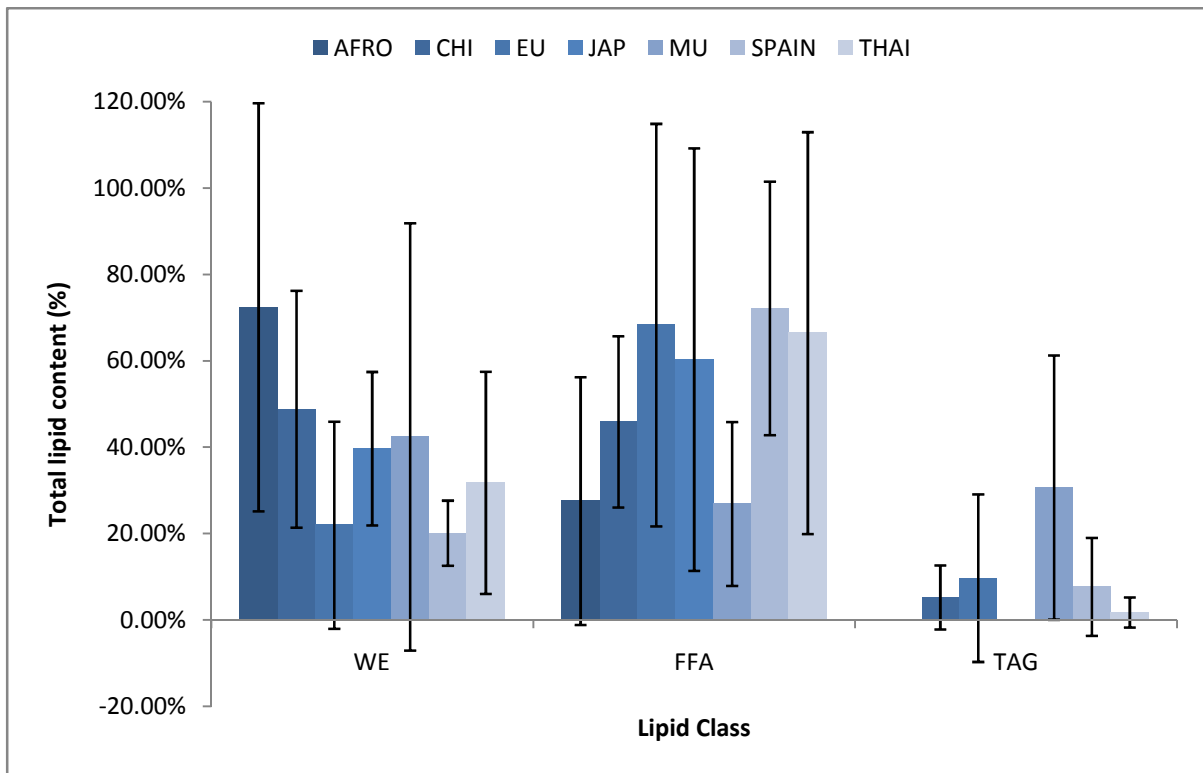


Figure 7.5 - Bar graph displaying the relative content (% of total) of wax esters (WE), free fatty acids (FFA) and triacylglycerols (TAG) in the hexane wash. Data as mean ± SD (n=3-5).

Table 7.5 shows each lipid class extracted in the hexane wash presented as a percentage of the total hair biomass along with the associated standard deviation.

Hair type	Afro	Chinese	European	Japanese	Mullato	Spanish	Thai
WE (%)	0.18 ±	0.01 ±	0.01 ±		0.01 ±		0.01 ±
	0.12	0.01	0.01	0.00	0.02	0.00	0.01
FFA (%)	0.07 ±	0.01 ±	0.02 ±	0.01 ±	0.01 ±	0.01 ±	0.03 ±
	0.07	0.01	0.01	0.00	0.01	0.00	0.02
TAG (%)					0.01 ±		
	0.00	0.00	0.00	0.00	0.01	0.00	0.00
TOTAL (%)	0.25 ±	0.03 ±	0.02 ±		0.03 ±		0.04 ±
	0.19	0.01	0.02	0.01	0.03	0.01	0.03

Table 7.5 - Total lipid content extracted by lipid class expressed as a percentage of the total hair biomass used for extraction.

7.4.1.2.2 Results from the solvent extraction

The solvent extraction eluted the most lipids (up to 70% from the total lipids, Figure 7.3) and this fraction consists of WE, FFA, TAG and polar lipids, PL (ceramides). The total lipid content of each lipid class is shown in Table and Figure 7.6.

Hair type	Afro	Chinese	European	Japanese	Mullato	Spanish	Thai
PL ($\mu\text{g/g}$)	240.71 \pm 79.33	399.86 \pm 169.12	259.97 \pm 114.08	366.51 \pm 27.57	648.77 \pm 447.37	317.80 \pm 99.13	277.39 \pm 47.67
FFA ($\mu\text{g/g}$)	3617.63 \pm 1125.27	1910.96 \pm 704.28	1595.99 \pm 277.70	3199.45 \pm 1648.81	3817.12 \pm 2472.94	4073.12 \pm 753.17	3629.23 \pm 1007.59
TAG ($\mu\text{g/g}$)	53.52 \pm 14.52	115.86 \pm 148.43	246.17 \pm 251.77	72.78 \pm 52.43	783.22 \pm 696.42	403.83 \pm 116.10	82.52 \pm 87.80
WE ($\mu\text{g/g}$)	894.91 \pm 431.10	287.67 \pm 168.94	241.94 \pm 176.19	178.43 \pm 113.41	665.43 \pm 952.62	102.53 \pm 16.00	469.17 \pm 433.35
TOTAL ($\mu\text{g/g}$)	4806.78 \pm 1650.23	2714.35 \pm 1190.77	2344.08 \pm 819.75	3817.18 \pm 1842.24	6067.29 \pm 4898.95	4897.29 \pm 984.42	4458.33 \pm 1576.41

Table 7.6 - Content of polar lipids (PL), wax esters (WE), triacylglycerols (TAG) and free fatty acids (FFA) in the solvent- extractable fraction (μg of fatty acids/g biomass). Data as mean \pm SD (n=3-5).

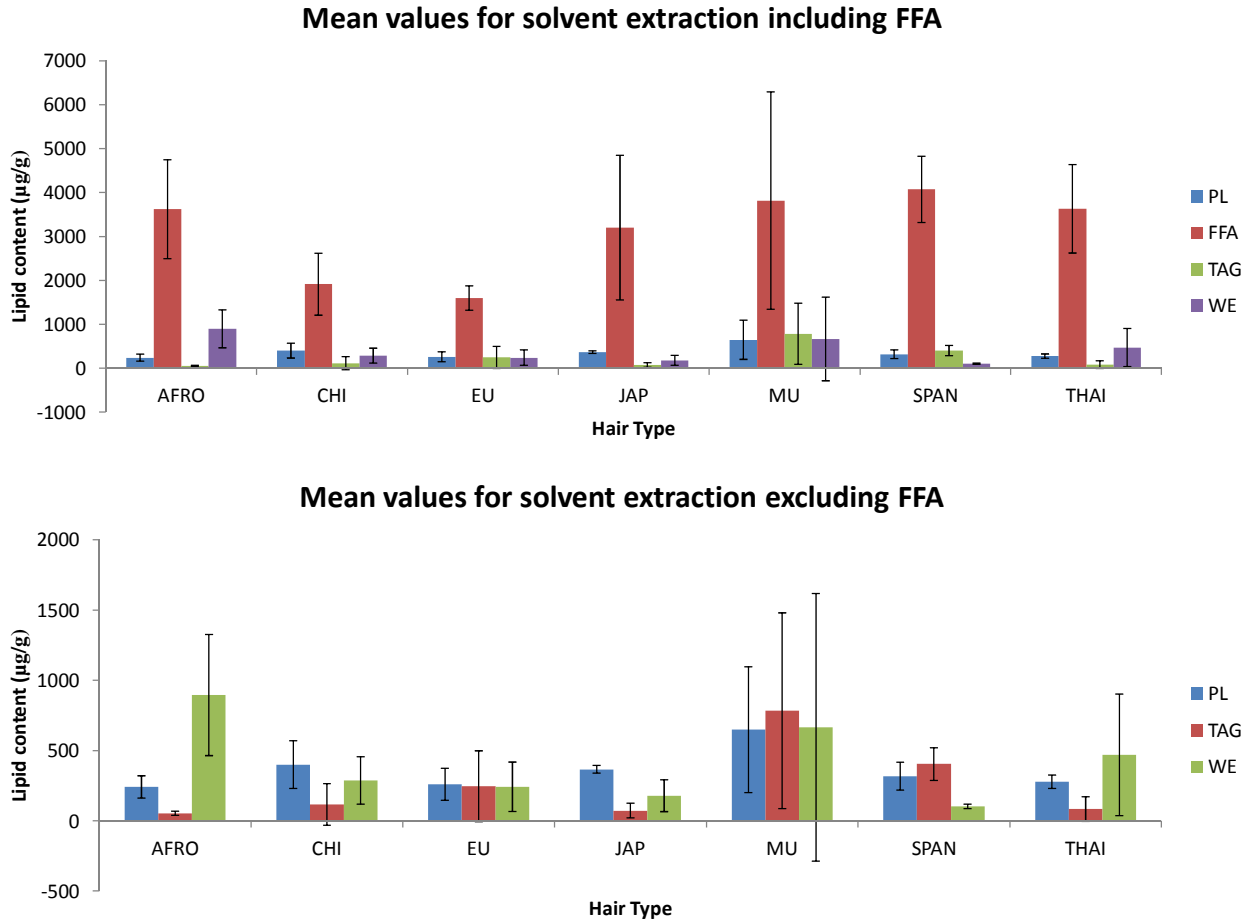


Figure 7.6 - Bar graphs of the individual lipid content of each class of lipid extracted from the hair using the chloroform:methanol procedure ($\mu\text{g/g}$ biomass). The bar graph at the top includes the values of FF and the graph at the bottom excludes the FFA. Data as mean \pm SD ($n=3-5$).

Table 7.7 shows the relative percentage of each lipid class in the solvent extraction. Figure 7.7 shows a bar graph displaying the relative percentage of each lipid class.

Hair type	Afro	Chinese	European	Japanese	Mullato	Spanish	Thai
PL (%)	5.01 ±	14.73 ±	11.09 ±	9.60 ±	10.97 ±	6.49 ±	6.22 ±
	1.65	6.23	4.87	0.72	7.56	2.02	1.07
FFA (%)	75.26 ±	70.40 ±	68.09 ±	83.82 ±	64.54 ±	83.17 ±	81.40 ±
	23.41	25.95	11.85	43.19	41.81	15.38	22.60
TAG (%)	1.11 ±	4.27 ±	10.50 ±	1.91 ±	13.24 ±	8.25 ±	1.85 ±
	0.30	5.47	10.74	1.37	11.77	2.37	1.97
WE (%)	18.62 ±	10.60 ±	10.32 ±	4.67 ±	11.25 ±	2.09 ±	10.52 ±
	8.97	6.22	7.52	2.97	16.11	0.33	9.72
TOTAL (%)	100.00 ±	100.00 ±	100.00 ±	100.00 ±	100.00 ±	100.00 ±	100.00 ±
	34.33	43.87	34.97	48.26	77.26	20.10	35.36

Table 7.7 - Lipid content of each lipid class expressed as a percentage of the total lipid extracted in the solvent extraction.

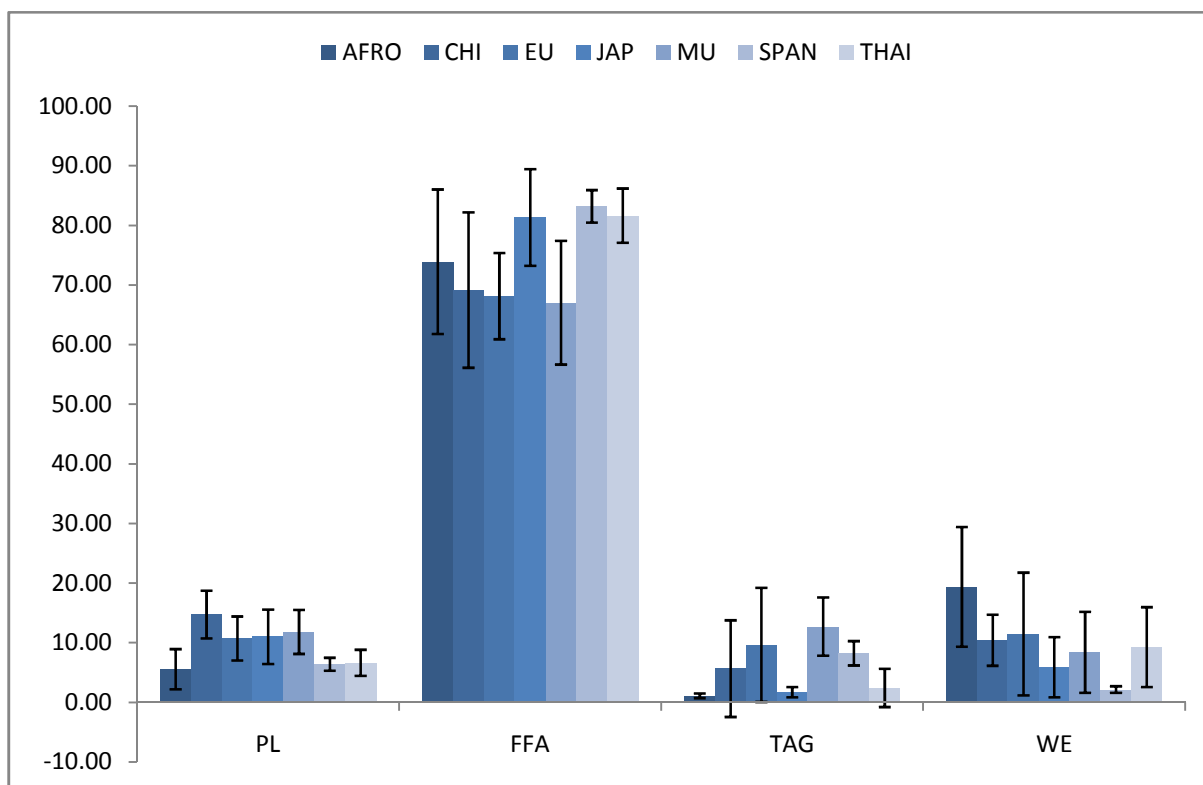


Figure 7.7 - Bar graph displaying the relative content (% of total) of polar lipids (PL), wax esters (WE), triacylglycerols (TAG) and free fatty acids (FFA) in the solvent- extractable fraction. Data as mean \pm SD (n=3-5).

Table 7.8 shows the lipid content extracted in the chloroform:methanol extraction expressed as a percentage of the total biomass content of the hair by lipid class.

Hair type	Afro	Chinese	European	Japanese	Mullato	Spanish	Thai
	0.10 ±	0.18 ±	0.10 ±	0.18 ±	0.26 ±	0.13 ±	0.11 ±
PL (%)	0.03	0.07	0.05	0.01	0.18	0.04	0.02
	1.57 ±	0.84 ±	0.64 ±	1.54 ±	1.52 ±	1.69 ±	1.45 ±
FFA (%)	0.49	0.31	0.11	0.79	0.98	0.31	0.40
	0.02 ±	0.05 ±	0.10 ±	0.04 ±	0.31 ±	0.17 ±	0.03 ±
TAG (%)	0.01	0.07	0.10	0.03	0.28	0.05	0.04
	0.39 ±	0.13 ±	0.10 ±	0.09 ±	0.27 ±	0.04 ±	0.19 ±
WE (%)	0.19	0.07	0.07	0.05	0.38	0.01	0.17
	2.08 ±	1.20 ±	0.94 ±	1.84 ±	2.36 ±	2.03 ±	1.78 ±
TOTAL (%)	0.71	0.53	0.33	0.89	1.82	0.41	0.63

Table 7.8 - Lipid classes expressed as a percentage of the total biomass of the hair used for the solvent extraction. Data as mean ± SD (n=3-5).

As seen in the figures and tables presented above, the total content of FFA extracted from the hair fibres is much higher than the other lipid classes. The Spanish hair type shows the most amount of FFA extracted from it, in decreasing order the pattern seen is; Mullato, Thai, Afro, Japanese, Chinese, European. The Mullato hair type shows the highest variability in its FFA content, in decreasing order of variability, the pattern seen is; Japanese, Afro, Thai, Spanish, Chinese, European. The Mullato hair type shows the highest amount of PL extracted using this procedure, in decreasing order the pattern seen is; Chinese, Japanese, Spanish, Thai, European, Afro. The variability does not follow the same pattern, the pattern seen starting from the highest hair type variability in decreasing order is; Mullato, Chinese, European, Spanish, Afro, Thai, Japanese. For the TAG lipid class, the highest content detected by hair type was Mullato and in decreasing order the pattern seen is; Spanish, European, Chinese, Thai, Japanese, Afro. The variability pattern in the lipid content for TAG starting with the highest is; Mullato, European, Chinese, Spanish, Thai, Japanese, Afro. The Afro hair type, shows the highest amount of WE extracted using this procedure, in decreasing order, the pattern seen is; Mullato, Thai, Chinese, European, Japanese, Spanish. The variability in the content of WE found shows that the Mullato hair type shows the highest variability and in decreasing order; Thai, Afro, Chinese, European, Japanese, Spanish.

7.4.1.2.3 Results from the Hydrolysed Fraction

Table 7.9 shows the concentrations of these hydrolysed fractions in different hair types. Figure 7.8 shows a bar graph of the lipid content in the hydrolysed fraction.

Hair Type	Afro	Chinese	European	Japanese	Mullato	Spanish	Thai
Lipid content (µg/g)	1876 ± 1269.22	2423.33 ± 1853.03	1282.5 ± 288.25	2047.5 ± 891.04	3824 ± 1534.38	1688 ± 457.78	2655 ± 843.66

Table 7.9 – Total lipid content in µg/g of the lipids extracted from the hydrolysed fraction.

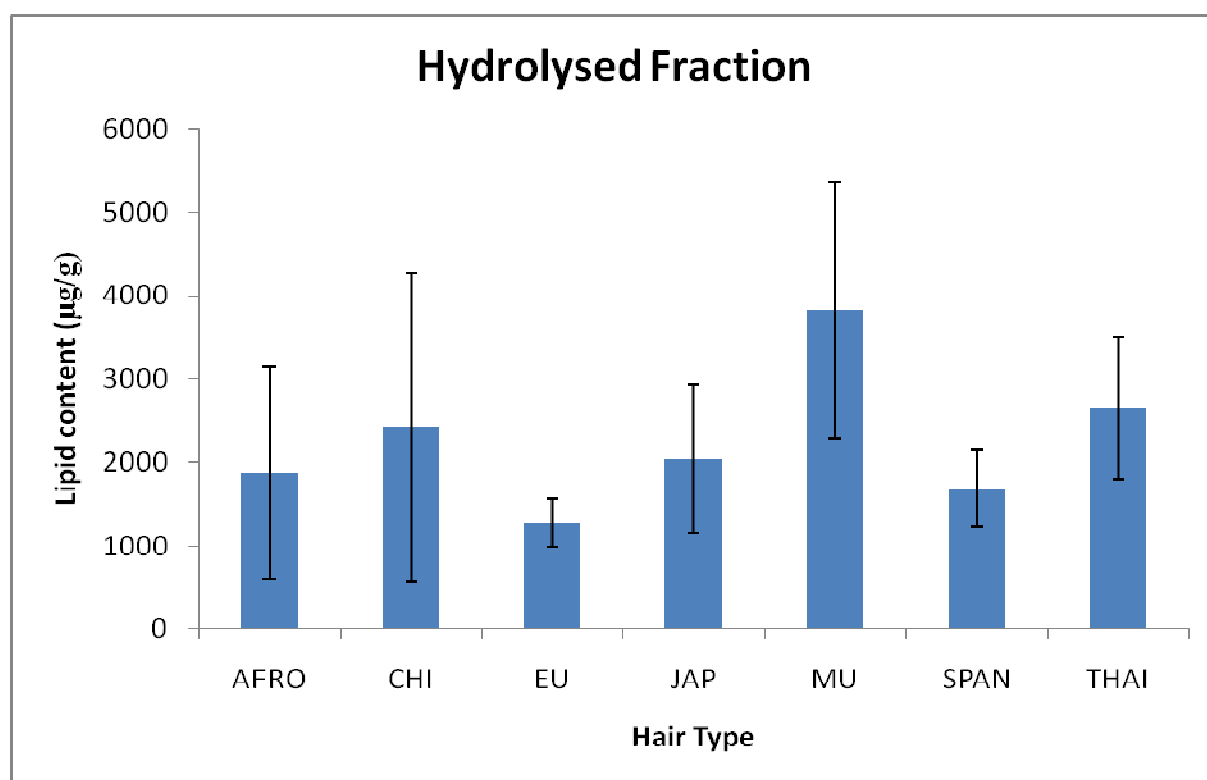


Figure 7.8 - The concentrations of the hydrolysed fraction (in µg of fatty acids/g) for all hair types. Data as mean ± SD (n=3-5).

As seen from this figure, the Mullato hair type exhibits the highest amount of this fraction, in decreasing order the pattern seen is; Thai, Chinese, Japanese, Afro, Spanish, European. The variability in these values does not follow the same pattern, starting from the hair type which

shows the highest variability and decreasing, the pattern seen is; Chinese, Mullato, Afro, Japanese, Thai, Spanish, European.

Table 7.10 shows the hydrolysed fraction expressed as a percentage of the biomass of the hair

Hair Type	Afro	Chinese	European	Japanese	Mullato	Spanish	Thai
Lipid content (%)	0.81 ± 0.55	1.07 ± 0.82	0.51 ± 0.11	0.99 ± 0.43	1.52 ± 0.61	0.70 ± 0.19	1.06 ± 0.34

Table 7.10 - Content of the hydrolysed fraction expressed as a percentage of the total hair biomass. Data as mean ± SD (n=3-5).

Although HCs were detected in both the hexane wash and the chloroform:methanol extraction in all hair types, they were detected in very low amounts (less than 10 µg per sample) and were therefore not included in the results. However, the Afro hair type contained more types of HC and in larger quantities than the other hair types and GC/MS was used to analyse their composition. The Afro 4 sample showed a relatively large level of HC when analysed by GC/FID and is shown in Figure 7.11. Figures 7.9 and 7.10 show spectra of docosane and tetracosane respectively which were used to identify the hydrocarbons present in the samples.

Abundance

Docosane

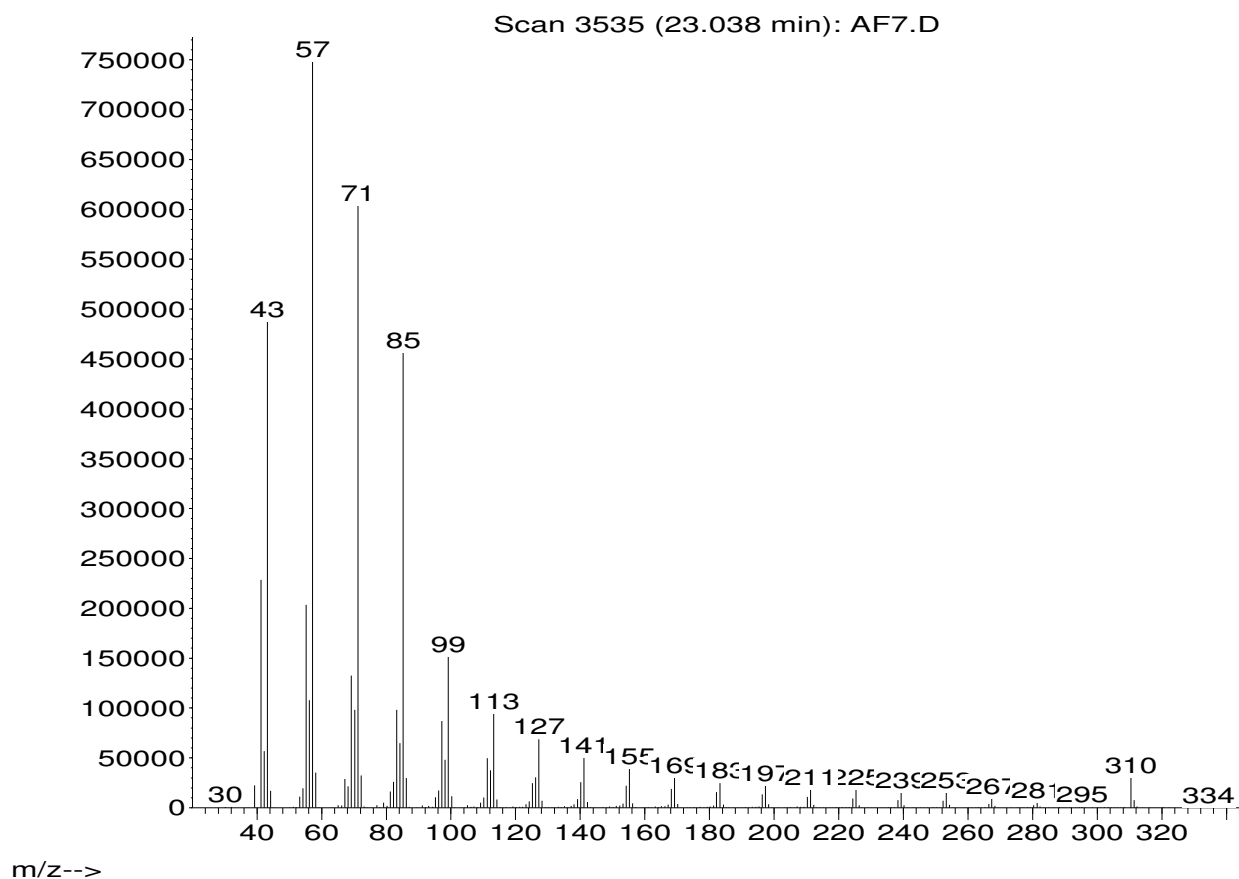


Figure 7.9 - Spectra of Docosane ($C_{22}H_{46}$) run on the GC/MS. The x axis is the charge to mass ratio (m/z) and the y axis is abundance measured in arbitrary units.

Abundance

Tetracosane

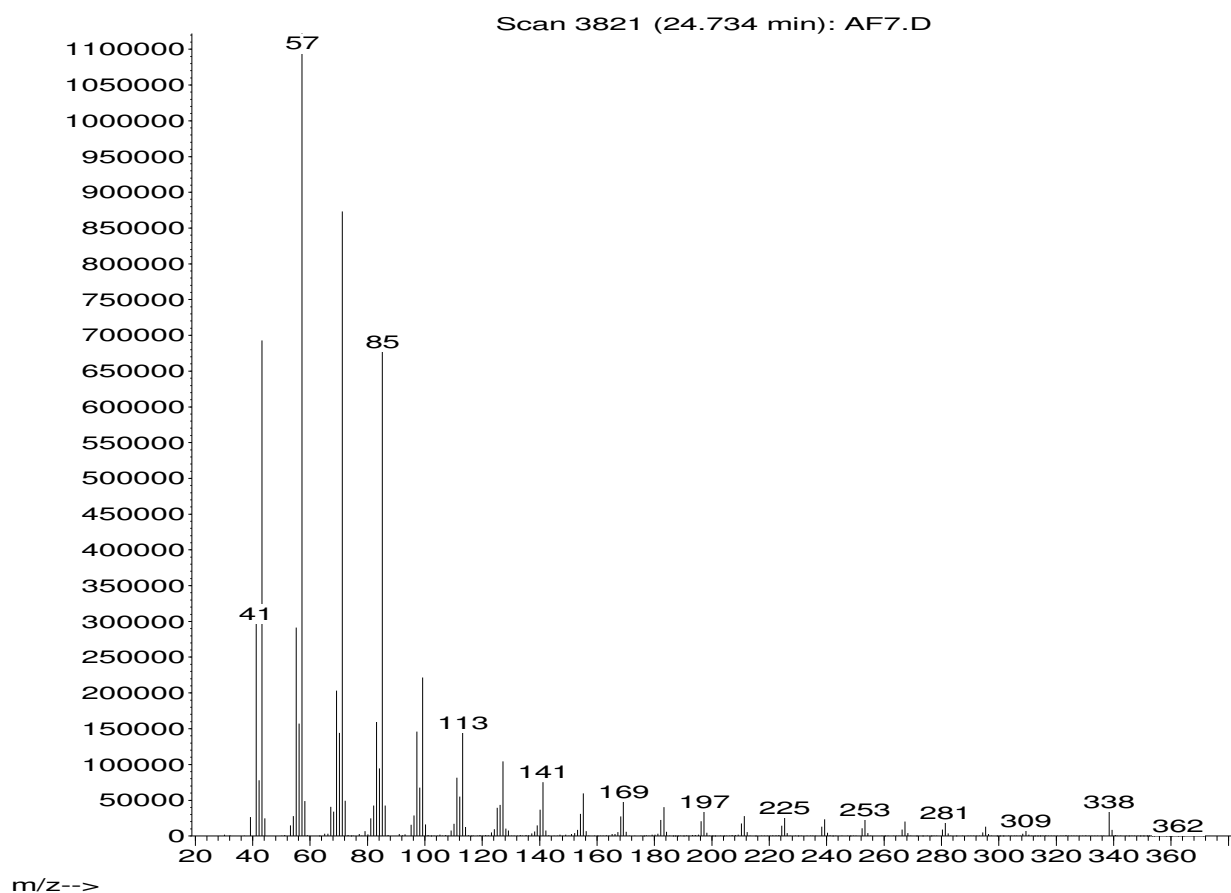


Figure 7.10 - Spectra of tetracosane($C_{24}H_{50}$) run on the GC/MS. The x axis is the charge to mass ratio (m/z) and the y axis is abundance measured in arbitrary units.

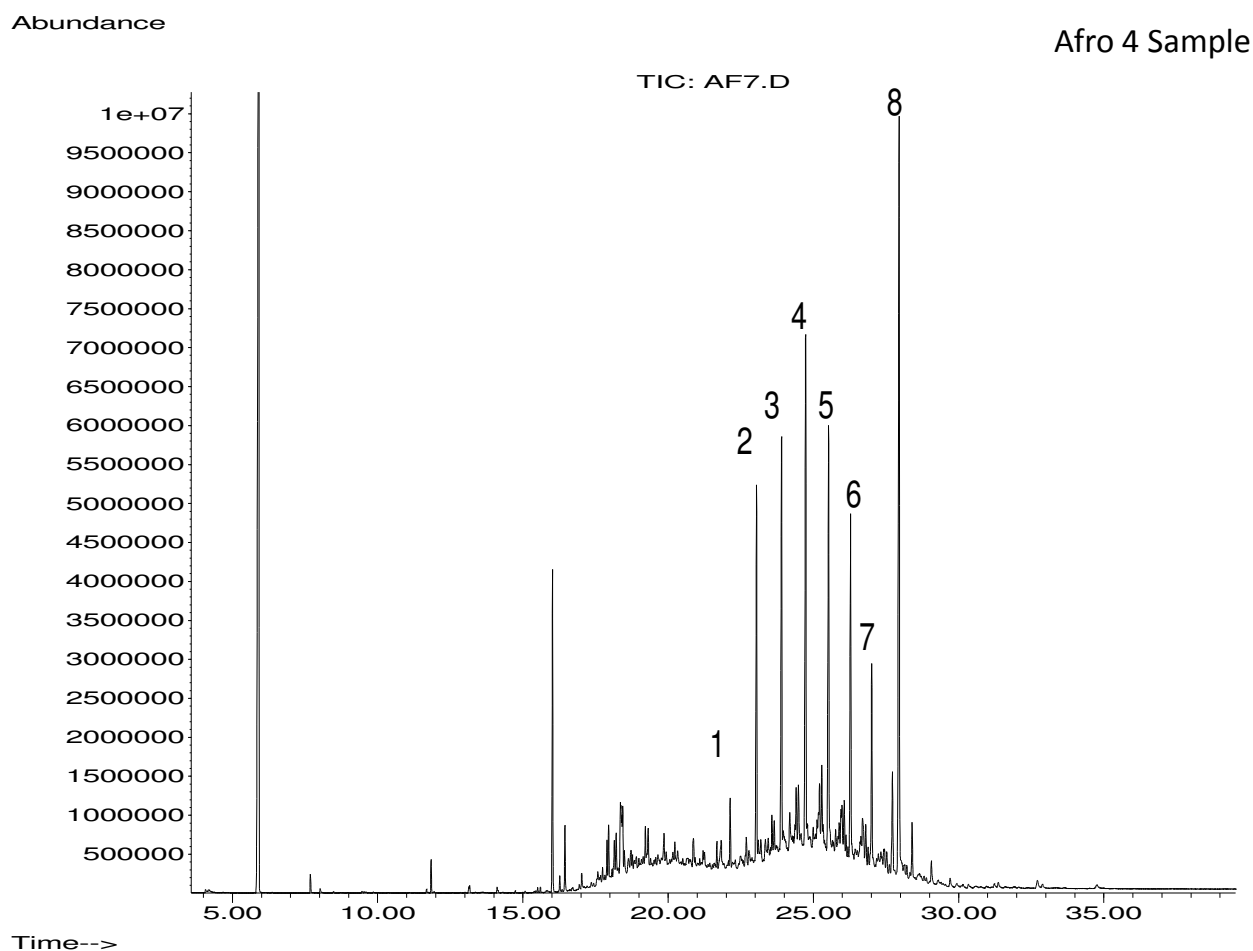


Figure 7.11 - GC/MS chromatogram of hydrocarbons from the AFRO4 hair sample. 1 – heneicosane $C_{20}H_{42}$, 2 – docosane $C_{22}H_{46}$, 3 – tricosane $C_{23}H_{48}$, 4 – tetracosane $C_{24}H_{50}$, 5 – heptacosane $C_{27}H_{56}$, 6- octacosane $C_{28}H_{58}$, 7 – nonacosane $C_{29}H_{60}$, 8 – Internal Standard (squalene).

7.4.1.3 GC/FID analysis of fatty acid patterns in individual lipid classes extracted by different procedures from the hair types

The results from the GC/FID analysis are organised into three sections based on how the lipids were extracted from the hair fibres. The hair fibres were first subjected to a hexane wash to remove the surface lipids, they were subsequently extracted using chloroform:methanol solutions to extract lipids that were ionically bound to the hair fibres and lastly the hair fibres were

subjected to a hydrolysis step which removes FAs from the lipids that are either present within proteinaceous structures in the hair fibre, or covalently bound to the hair fibre (as in the case of 18-MEA at the cuticle surface). Therefore each analysis has been presented separately, for further information on the extraction process see Sections 3.5.1 – 3.5.3.

Figures 7.12 and 7.13 show examples of some of the chromatograms from the resulting GC/FID analysis of the FA profiles of lipids extracted using this procedure.

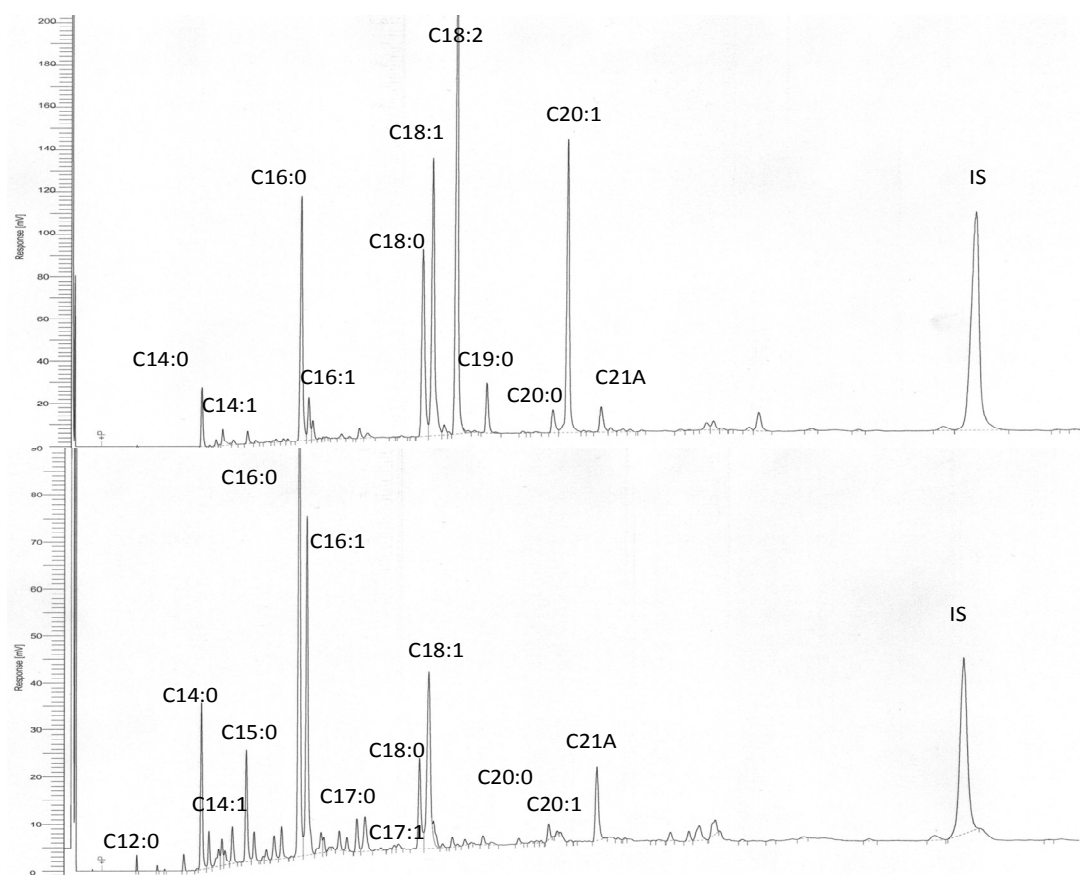


Figure 7.12 – Chromatogram showing the fatty acid profile for the hydrolysed fraction for the Spanish 2 sample at the top and the Afro 2 sample at the bottom. The x axis on both graphs is time (mins) and the y axis is intensity (arbitrary units). The C21A stands for the 18-MEA fatty acid and IS denotes the internal standard (C24:1).

Examples of GC/MS spectra of some unusual fatty acids, C21A, C14:0, C14:1 and C15:0 can be found in Appendix II.

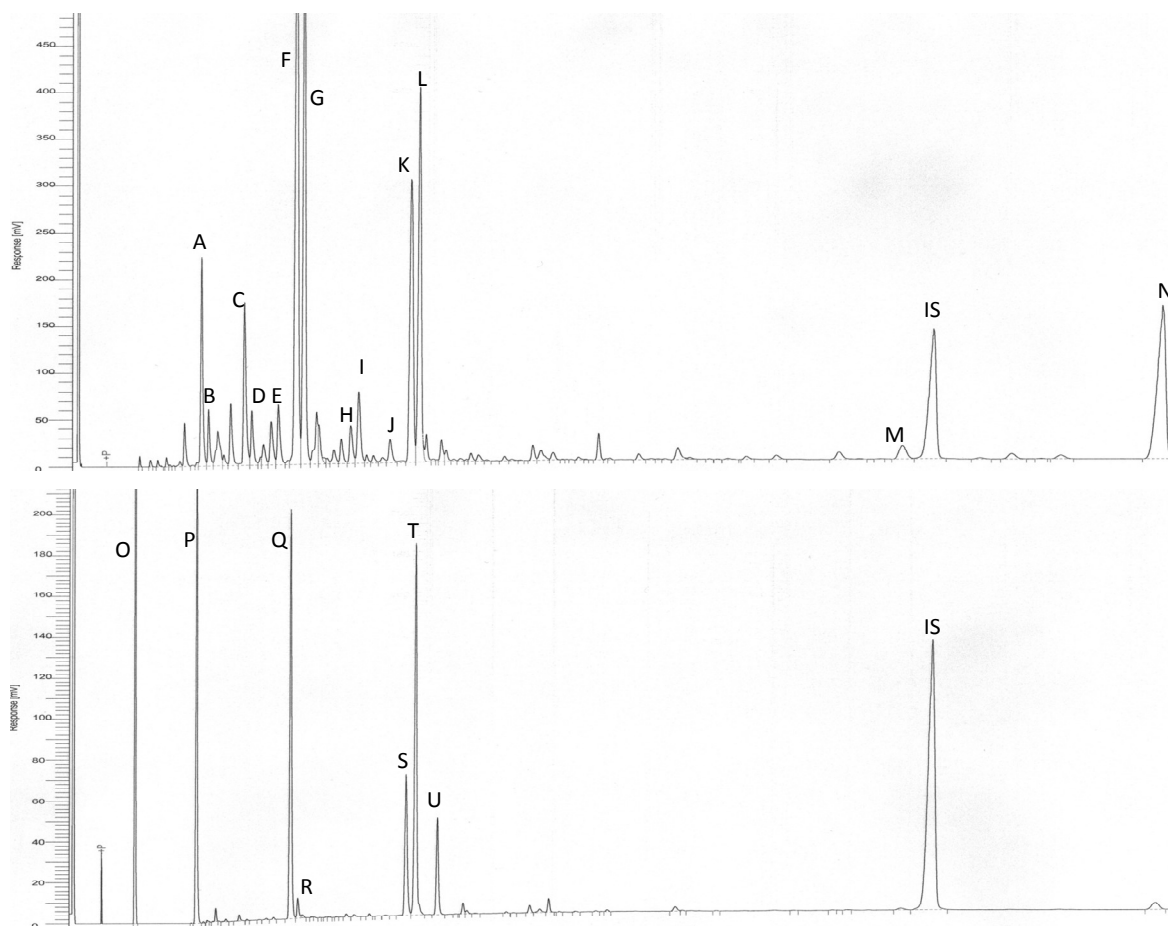


Figure 7.13 –Chromatogram showing the fatty acid profile of the TAG lipid species from the solvent extraction (chloroform:methanol). The x axis on both graphs is time (mins) and the y axis is intensity (arbitrary units). The top chromatogram is the Mullato 3 sample. A denotes the C14:0 isomer, B - C14:1i, C - C15:0, D - C15:1, E - C15:1i, E - C16:0, F - C16:1, G - C16:1i, H - C17:0, I - C17:1, J - C17:1i, K - C18:0, L - C18:1, M - C24:0, N - C26:0. The bottom chromatogram shows the Spanish 2 sample. O shows the C12:0 isomer, P - C14:0, Q - C16:0, R - C16:1, S - C18:0, T - C18:1, U - C18:2. IS represents the internal standard on both chromatograms. The Mullato hair type shows a high proportion of C14 and C15 fatty acid isomers and C26:0 acid, the Spanish hair type shows large contents of C12:0 and C14:0 fatty acids. The internal standard is C24:1.

GC/MS used to identify the structures of unusual fatty acids and examples of some of the spectra are shown in Appendix II.

As seen from the data, together with the common fatty acids found in human tissues, e.g. C16:0, C16:1, C18:0, C18:1, C18:2, C20:0, C20:1, C24:0 and C26:0, large amounts of short-chain fatty acids

were found, namely C12:0, C14:0 and their monounsaturated isomers. In addition, a large range of odd-chain FA was also identified in the analysed samples, C15:0, C17:0 and C19:0 along with their monounsaturated isomers. It is interesting to note that together with C21A (18-MEA) reported for hair fibres previously, some other anteiso branch-chain fatty acids were also identified, e.g. anteiso C15 and C17. Anteiso represents isomers of fatty acids that are unidentified; i.e. C15:1i, C17:1i. The GC/MS spectra of these can be found in Appendix II. The distribution of fatty acids in individual lipid classes in different hair types will be described in the next section.

7.4.1.3.1 Fatty acid profiles of the individual lipid classes from the hexane wash

Tables containing the quantified content of the FA profiles for each hair type in each extraction process can be found in Appendix III. Figure 7.14 shows the fatty acid composition of the WEs extracted in the hexane wash.

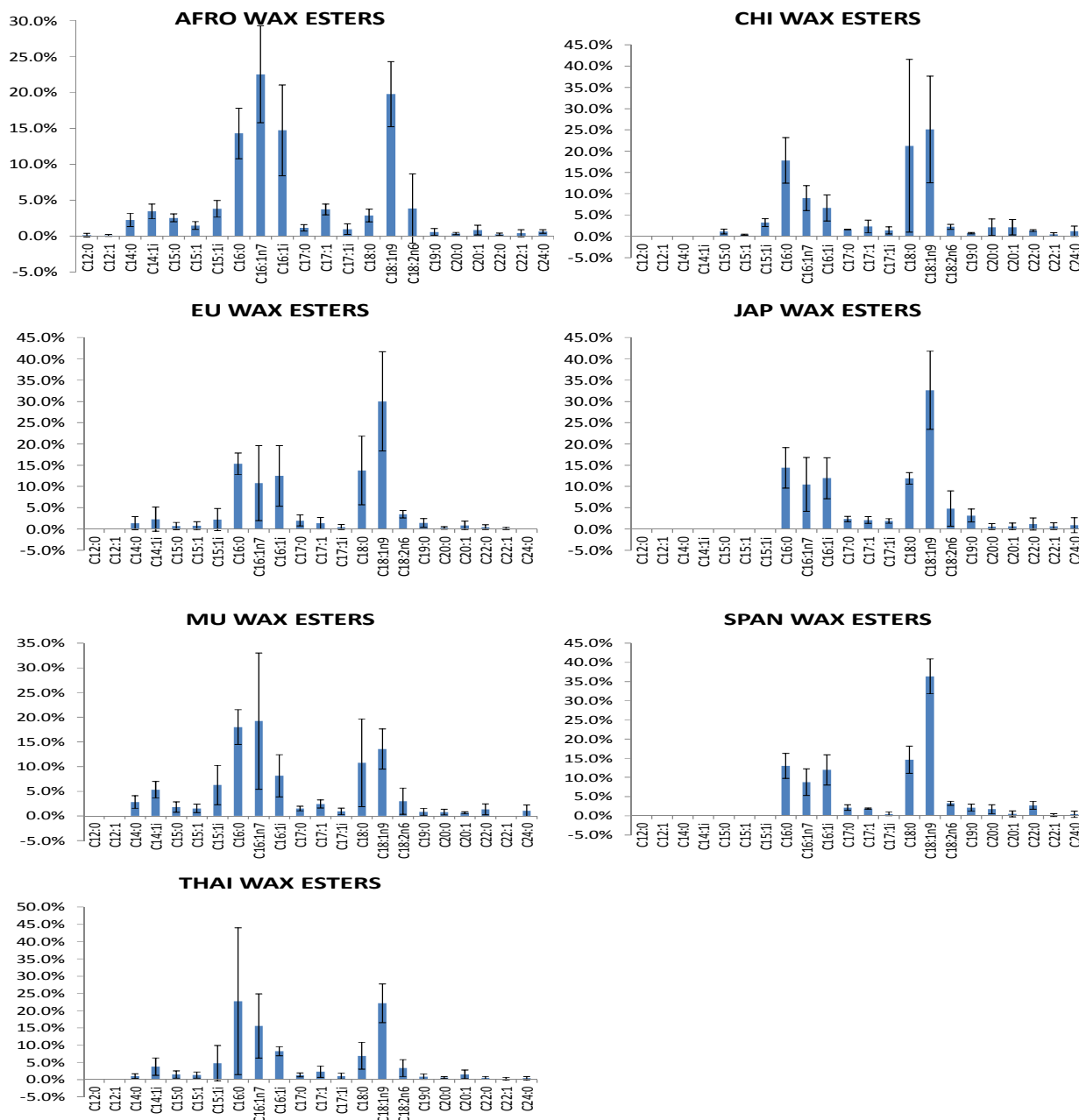


Figure 7.14- Bar graphs showing the FA content of the WEs extracted from the hexane wash for all the hair types. Data as mean \pm SD (n=3-5).

Figure 7.15 shows the distribution of FA in the FFA fraction extracted in the hexane wash.

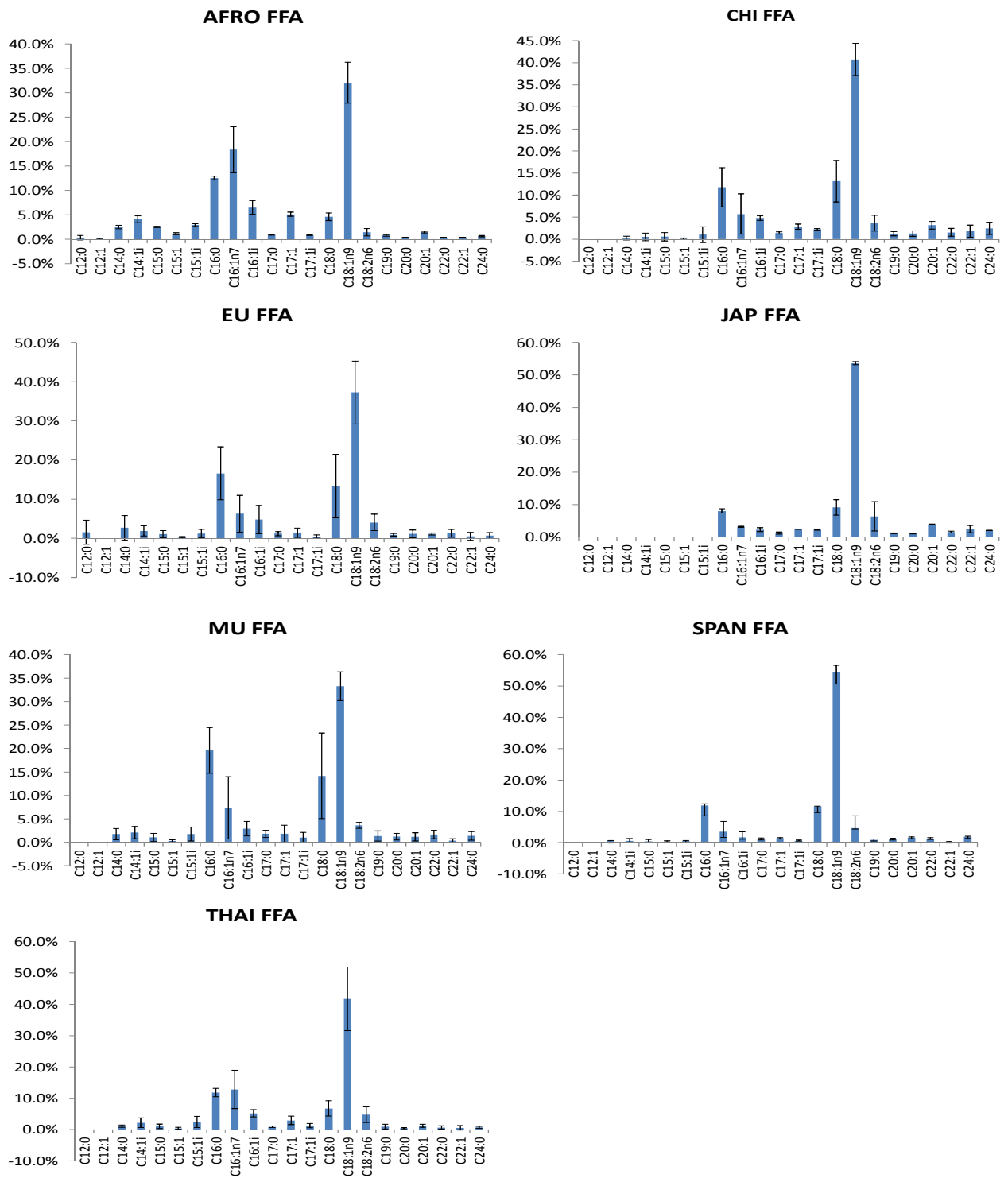


Figure 7.15 – Bar graphs showing the relative fatty acid content (% of total FFAs) of the FFAs extracted from the hexane wash for all hair types. Data as mean \pm SD (n=3-5).

The TAG content in the hexane wash was variably present among the hair types and samples; most hair samples did not contain any TAGs in the hexane wash. In detail, only one of the European samples showed TAGs, four Mullato, two Spanish, one Thai and one Chinese hair type. The Afro and Japanese hair types showed no detectable TAGs. Figure 7.16 provides the data for the fatty acid composition of TAGs extracted with the hexane wash, the values for the Mullato and the Spanish hair types are mean values. The values shown for the Chinese, European and Thai are the ones that were able to be detected.

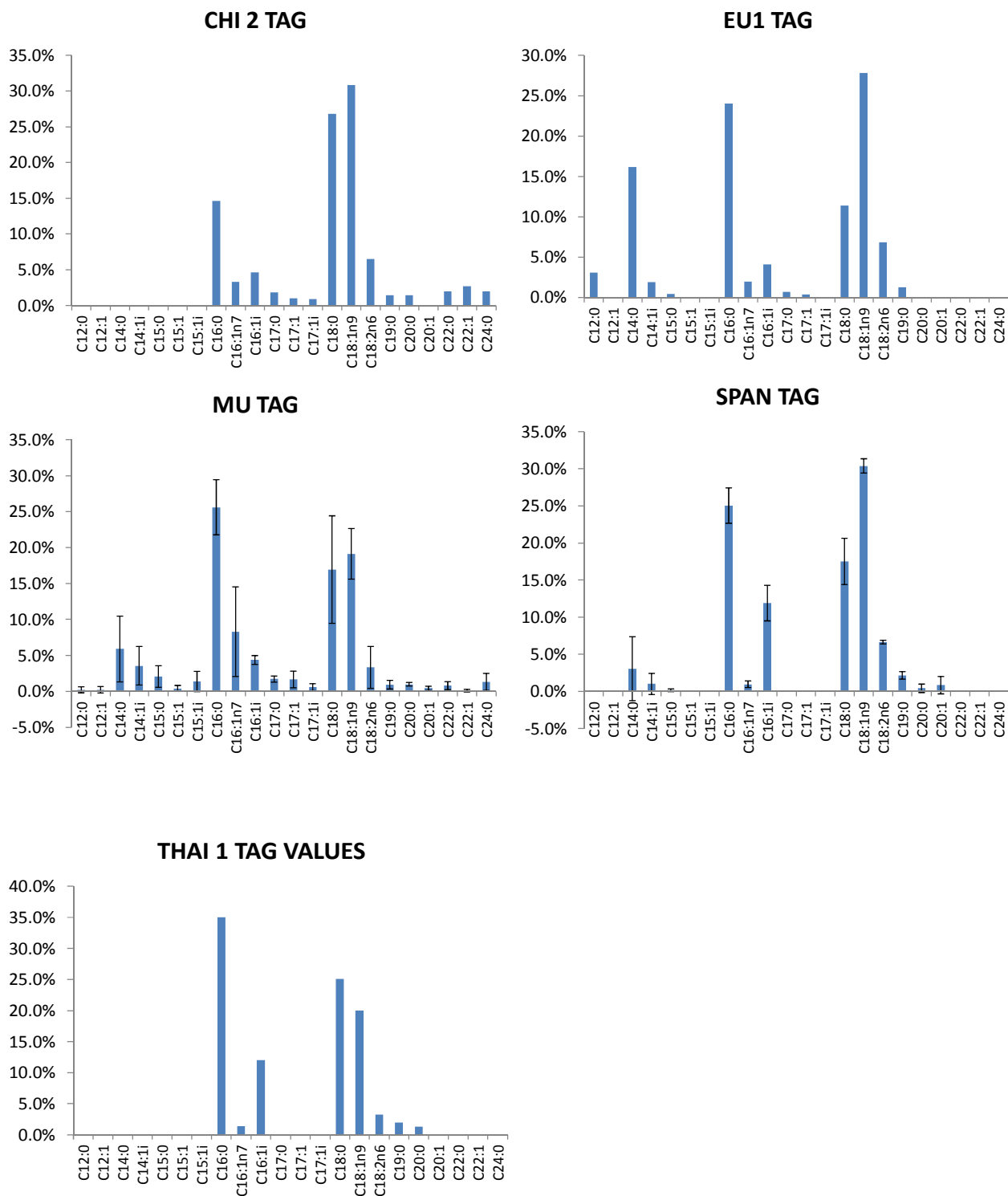


Figure 7.16 – Bar graphs showing the fatty acid composition of the TAGs extracted from the hexane wash for the Chinese, European, Mullato, Spanish and Thai hair types.

7.4.1.3.2 Fatty acid profiles of the individual lipid from the solvent extraction

Figure 7.17 shows the bar charts for the FA content for the PLs extracted with chloroform: methanol.

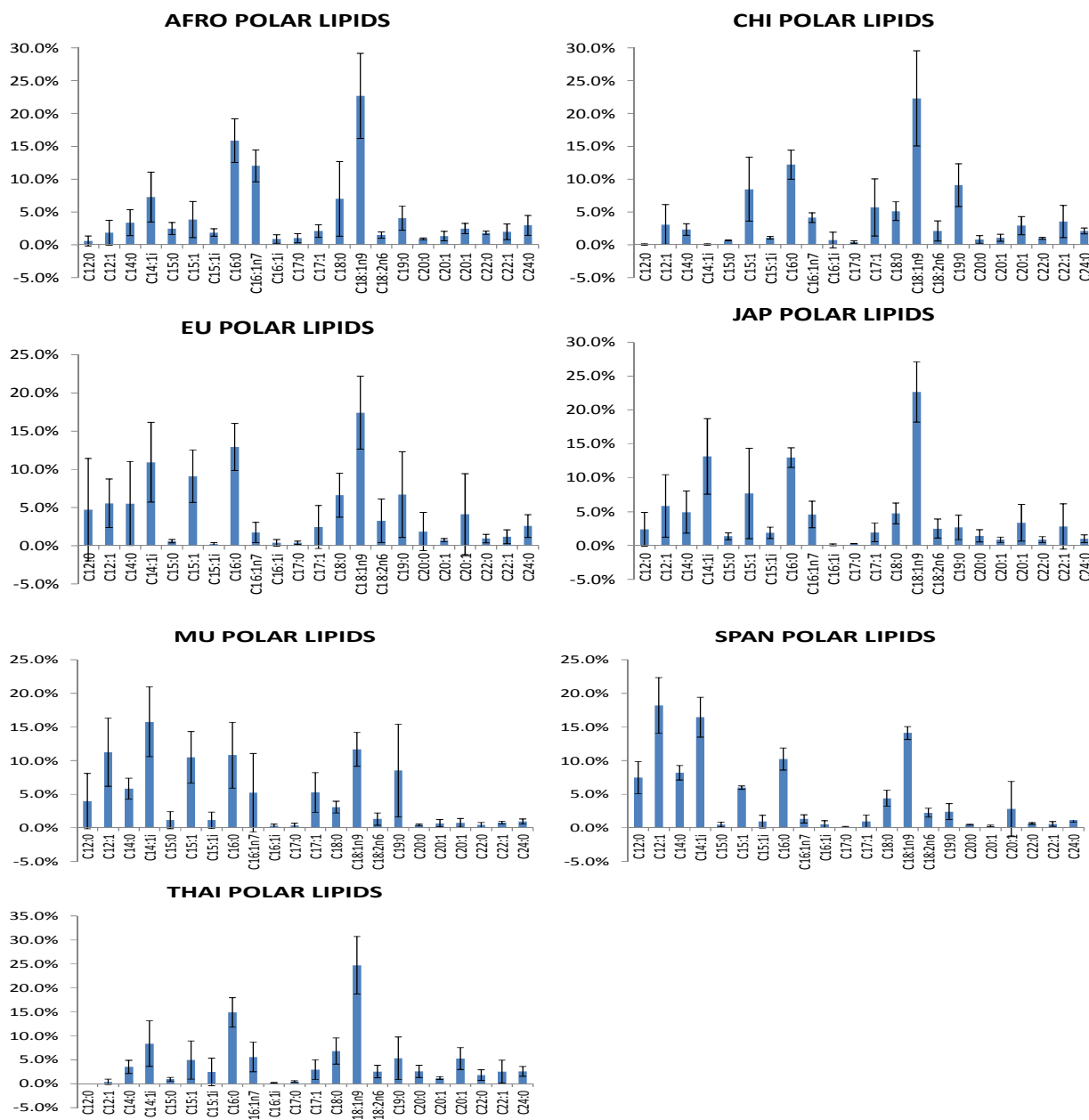


Figure 7.17 – Bar graphs showing the fatty acid content (% of total FAs) of the PLs extracted for all hair types. Data as mean \pm SD (n=3-5).

Figure 7.18 shows bar charts of the fatty acid profiles of the FFA fraction extracted with chloroform:methanol.

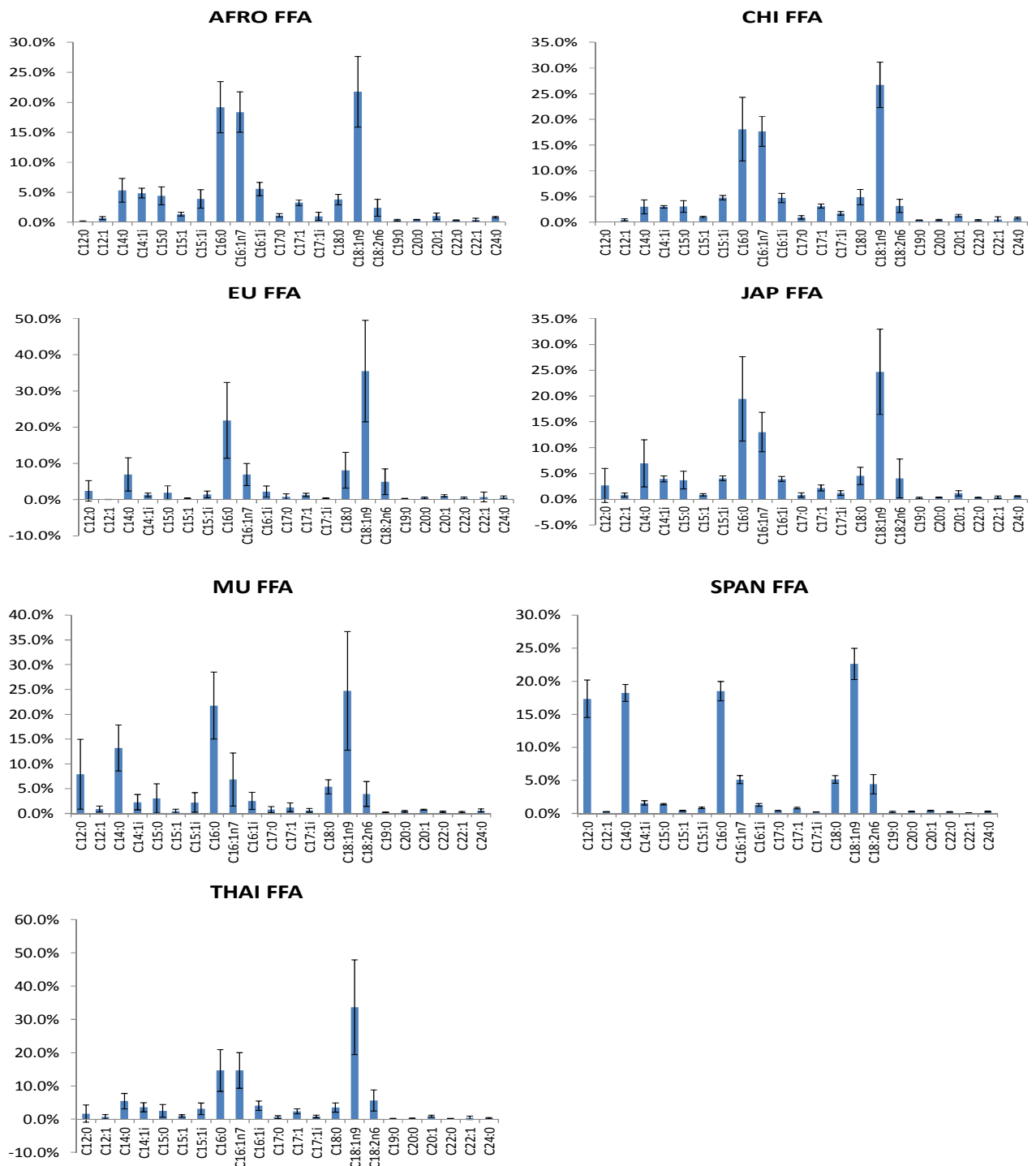


Figure 7.18 – Bar graphs showing the relative content of fatty acids (% of total FAs) of the FFA fraction extracted with chloroform:methanol for all hair types. Data as mean \pm SD (n=3-5).

Figure 7.19 shows bar charts of the FA content of the TAGs extracted with chloroform:methanol.

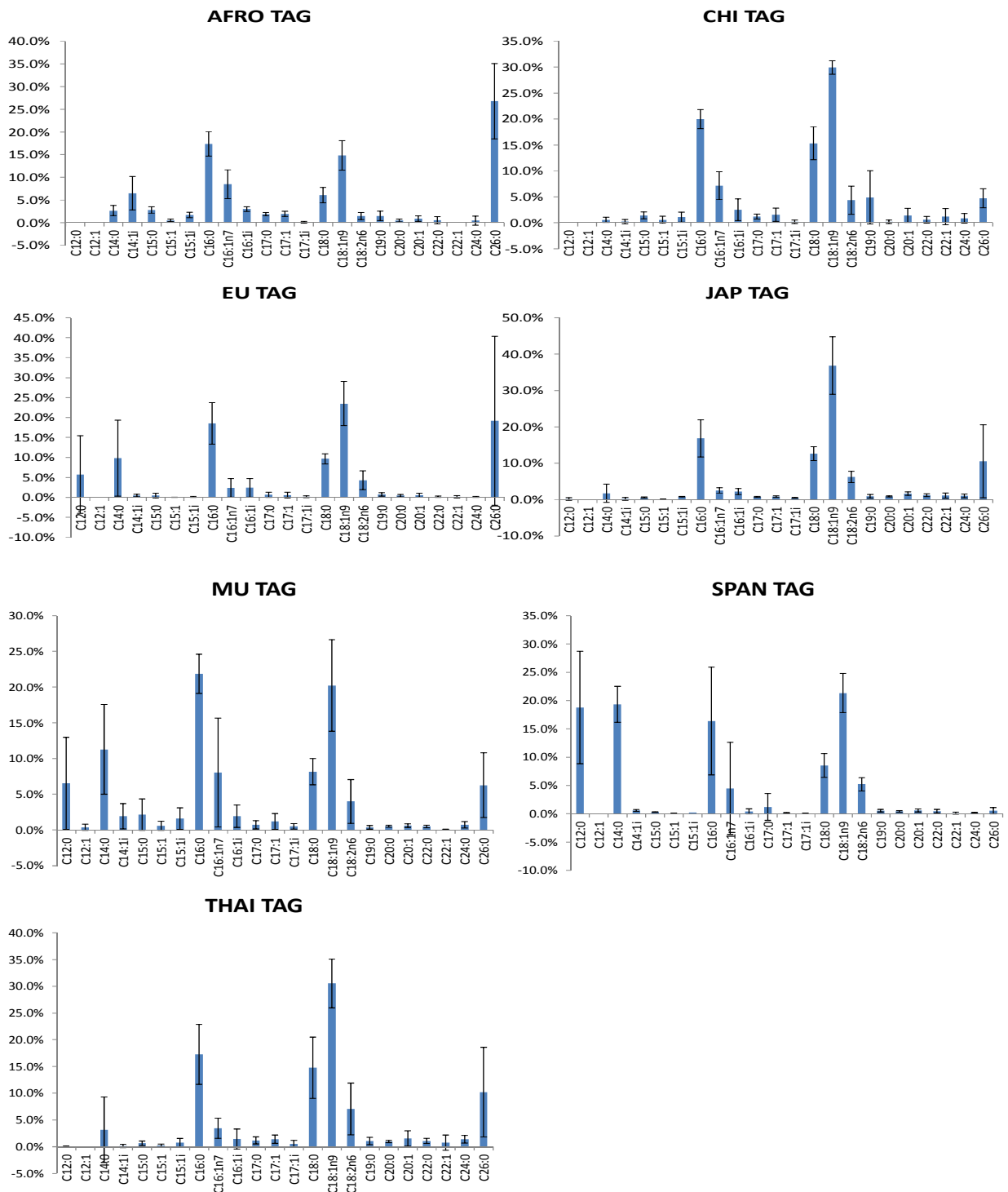


Figure 7.19 - Bar charts showing the FA content of the TAGs extracted with chloroform:methanol for all hair types. Data as mean \pm SD (n=3-5).

Figure 7.20 shows bar charts of the FA content of the WEs extracted with chloroform:methanol.

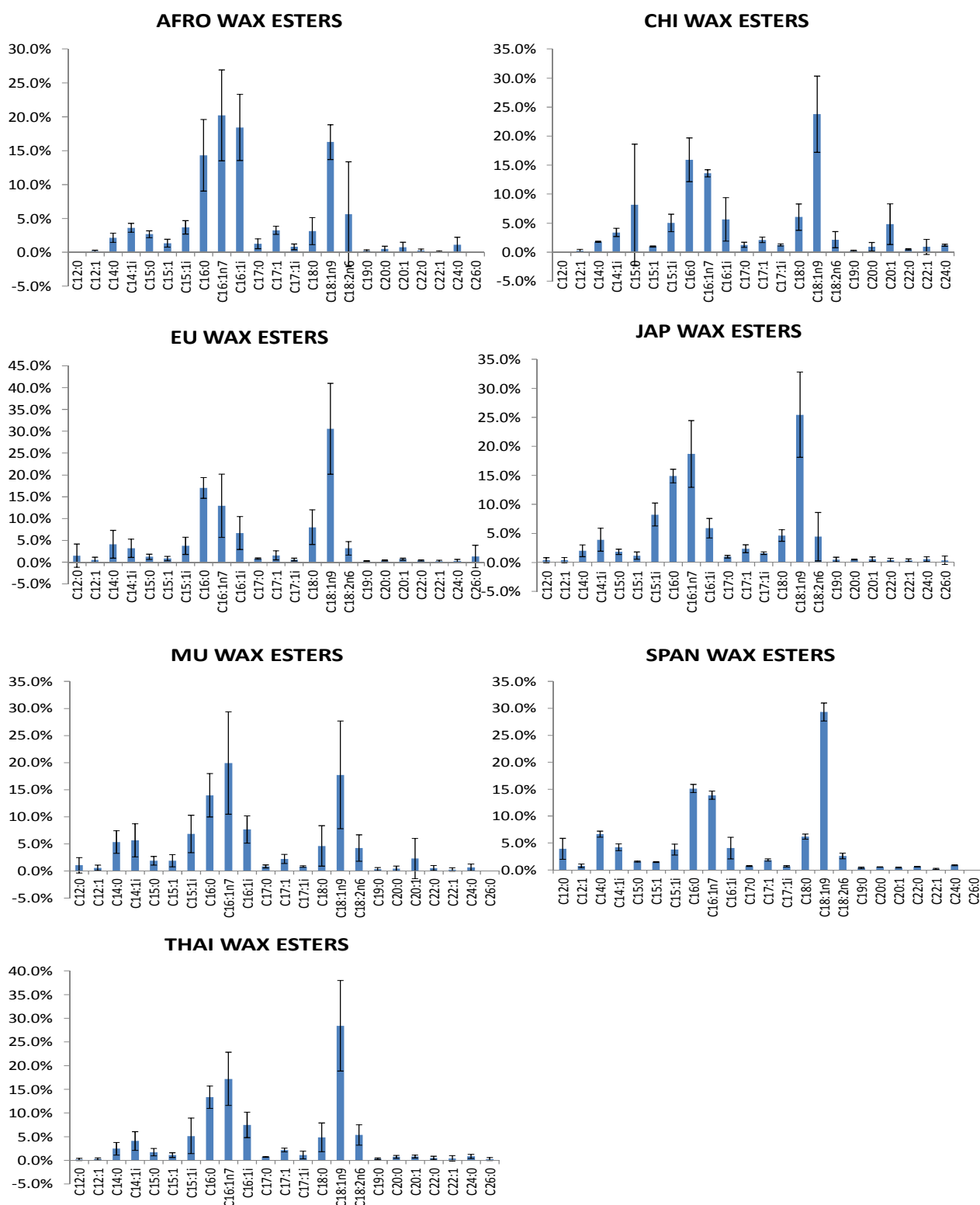


Figure 7.20 - Bar charts showing the FA content of the WEs extracted with the chloroform:methanol solvents from the Mullato, Spanish and Thai hair types. Data as mean \pm SD (n=3-5).

7.4.1.3.3 Fatty acid profiles of the hydrolysed fraction

The following results are from the hydrolysed fraction. This was the last step in lipid extraction procedure, and was used to analyse fatty acids from any remaining lipids that were covalently bound (or otherwise) to the hair fibre. This extraction step exclusively removes 18-MEA that is found covalently bound to the cuticle surface; this fatty acid is denoted by C21A in the resulting table of contents. Figure 7.21 shows bar charts for the FA content of the lipids extracted using this procedure.

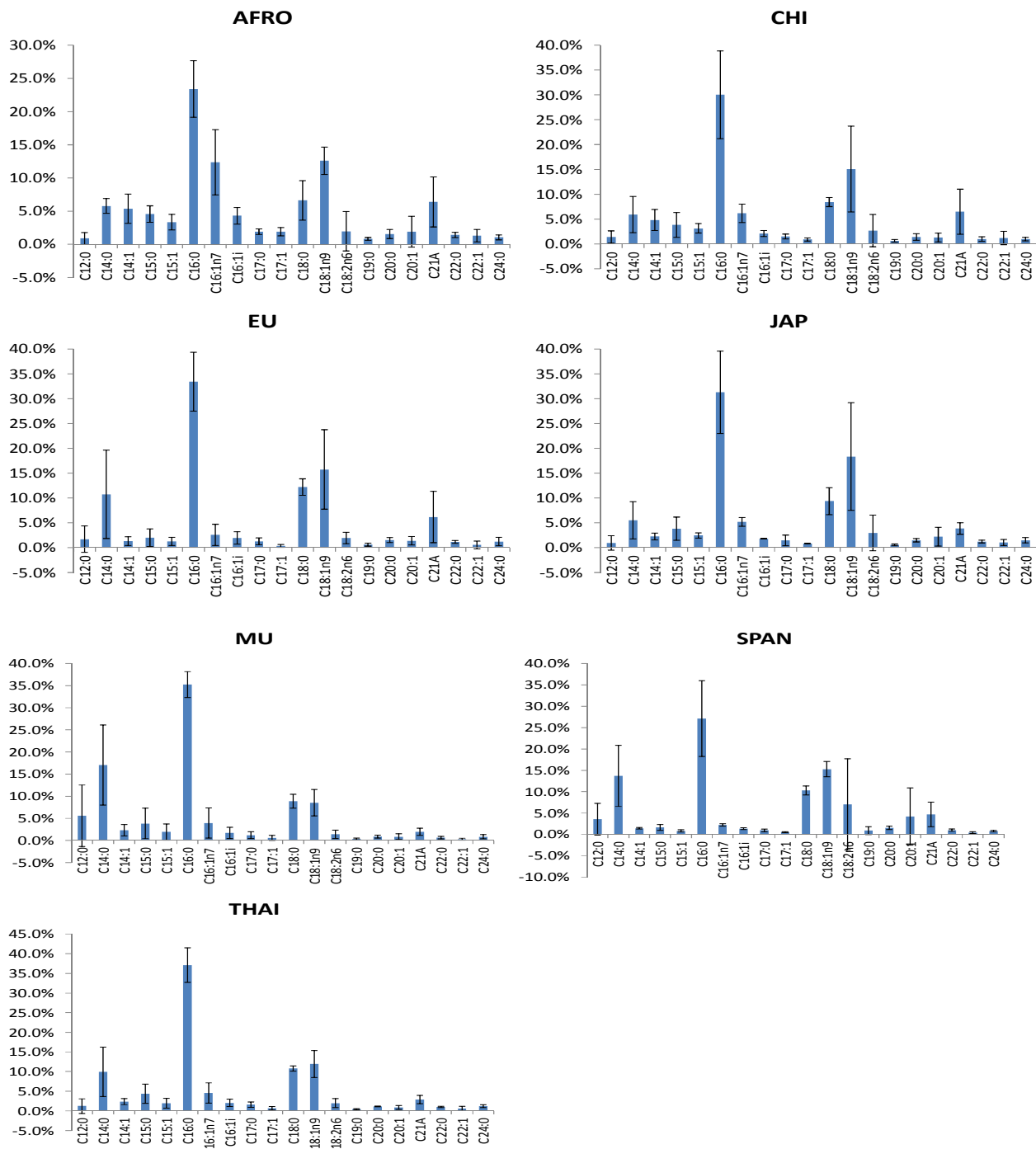


Figure 7.21 - Bar charts showing the fatty acid composition of the hydrolysed fraction for the Mullato, Spanish and Thai hair types. Data as mean \pm SD (n=3-5).

7.4.2 Summary of the results from the TLC and GC/FID analysis

The results from the TLC and GC/FID analysis of the lipids and FAs from the three extraction processes generated a vast amount of data on the lipid content and fatty acid patterns in each hair type. The Mullato hair type showed the most amount of lipid in any hair type and also showed the largest variability in the amount of lipids extracted and the largest percentage of lipids as a function of the biomass. In contrast to this, the European hair type showed the lowest amount of lipids extracted, the highest consistency in the amount of lipids extracted (consistently the lowest amounts by hair type) and the lowest percentage of lipids as a function of biomass. In fact, both the Mullato and the Afro hair type show over twice as much lipids as a function of biomass than the European hair type on average.

The hexane wash extracted less than 10% of all lipids in all hair types, the solvent extraction more than 55% in all hair types and the hydrolyses step extracted more than ~25% in all hair types, and in the Chinese hair type it almost extracted 45% of the total lipid content. PL accounted for less than 10% of the total lipid content in all hair types, FFA accounted for more than 75% in all hair types, TAG less than 10% in all hair types and WE accounted for less than 10% in all hair types except the Afro hair type which showed almost 20% of its total lipid content as WE.

In addition to this it should be noted that relatively large percentages of all fatty acids identified across all the hair types are quite unusual in that they are odd chain FAs. Most FAs found in humans are all even chain FAs with C16, C18 and their associated isomers being the most common; the presence of C15, C17 and C19 is unusual in human tissue, the presence of C21A (18-MEA) is also exclusively found in hair fibres.

The following is a summary of the main points of conclusion from the data presented by each extraction step.

7.4.2.1 Summary of the results from the hexane wash

The Afro hair type showed a much larger amount of both WE and FFA extracted using this method than any of the other hair types, however, like the Japanese it did not show any TAG extracted. The Afro hair type also showed a very high variability in the amount of lipid extracted. The Mullato

hair type showed the highest variability in lipid content among the rest of the hair types excluding the Afro.

7.4.2.1.1 Summary of the results of the fatty acid profiles from the WEs extracted

- All hair types show C18:1n9 as the highest fatty acid present; the Mullato showed the lowest, the Spanish the highest.
- C16:0, C16:1n7, C16:1i, C18:0, C18:1n9 accounted for most of the fatty acid content across all hair types
- Afro was the only hair type that showed presence of C12:0 and C12:1
- The Thai hair type shows a large variability in the content of C16:0 (>20%)
- C14:0 and C14:1i not detected in the Chinese, Japanese or Spanish hair types, but all other hair types.
- C15:0, C15:1, C15:1i not detected in Japanese and Spanish, but was found in all others.
- C22:1 not detected in Mullato hair type, but found in all others.
- C24:0 not detected in European hair type, but found in all others.

7.4.2.1.2 Summary of the results of the fatty acid profiles from the FFAs extracted

- All hair types show a high percentage of C18:1n9 (>30%). The Japanese hair type shows a very low standard deviation for this lipid type (0.48%) and the Thai shows the highest (10.16%).
- C16:0, C16:1n7, C16:1i, C18:0, C18:1n9 account most of the fatty acids present with C18:1n9 being the most dominant by weight. The rest of the fatty acids account for less than 10% each.
- C12:0 only detected in Afro and European hair types
- C12:1 only detected in the Afro hair type.
- Japanese hair type was the only hair type not to show C14:0, C14:1i, C15:0, C15:1, and C15:1i

7.4.2.1.3 Summary of the results of the fatty acid profiles for the TAGs extracted

- Only one Chinese, one European, one Thai, four Mullato and two Spanish hair types showed any presence of TAG in this extraction method; no TAG was found in any of the Afro or Japanese samples in the hexane wash.
- C16:0, C18:0, C18:1n9 accounted for most of the fatty acids by weight.
- C16:0, C16:1n7, C16:1i, C18:0, C18:1n9, C18:2n6 and C19:0 were the only FA types present across all hair types; all the other FAs were variably present.
- High variability in the presence of FA types found across all hair types.
- The Chinese sample showed >15% of C14:0.

7.4.2.2 Summary of the results from the solvent extraction

In the chloroform:methanol extraction there was a much higher amount of FFA extracted than any other lipid class using this method, the other lipid classes extracted were PLs, TAGs and WEs. The Mullato hair type showed a very large variation in the FFA content, and also in the variation of the TAG and WE lipid classes. The Afro hair type, much like the hexane wash, showed a large amount of WEs extracted. The TAGs accounted for the least amount of lipid present apart from in the Mullato and Spanish hair types.

7.4.2.2.1 Summary of the results of the fatty acid profiles from the PLs extracted

C18:1n9 was the dominant fatty acid in all hair types except the Mullato and Spanish (>10%)

- Thai was the only hair type not to show C12:0
- C16:0 also accounted for a considerable percentage in all hair types (>10%)
- Spanish hair type showed a high amount of C12:1 (>15%)
- Mullato hair type showed a high amount of C15:1 (>10%)
- Afro hair type showed a high amount of C16:1n (>10%)

7.4.2.2 Summary of the results of the fatty acid profiles from the FFAs extracted

- C18:2n6, C16:0 and C16:1n7 account for the most amount of FAs across all hair types.
- Chinese was the only hair type not to show C12:0
- The Spanish hair type shows a high relative amount of C12:0 and C14:0 (>15%)
- The Mullato hair type shows a high relative amount of C14:0 (>10%)

7.4.2.3 Summary of the results of the fatty acid profiles from the TAGs extracted

- C16:0 and C18:1n9 account for most of the FA content by weight across all hair types (>15%)
- The Afro and Chinese hair types do not show C12:0; all other hair types do
- Only the Mullato hair type showed presence of C12:1
- Only the Afro hair type did not show any presence of C22:1
- Afro shows a high amount of C26:0 (>25%)
- The European shows a high amount of C26:0 (~20%) with a large standard deviation.
- Spanish hair type shows a high amount of C12:0 and C14:0 (>15%)
- Mullato hair type shows a high amount of C12:0 (>5%) and C14:0 (>15%)
- The Spanish hair type shows the least content of C26:0 (<1%)

7.4.2.4 Summary of the results of the fatty acid profiles from the WEs extracted

- C18:1n9 accounted for most of the FA across all hair types (>15%), C16:0 and C16:1n7 also account for most of the FAs across all hair types (>10%)
- C12:0 not present in Afro and Chinese hair types
- C26:0 only present in the European, Japanese and Thai hair types.
- There is a large variability in the content of C15:0 in the Chinese hair type.
- The Afro shows a large content of C16:1i (>15%)
- The Afro hair type shows a large variability in the content of C18:2n6.

7.4.2.3 Summary of the results for the fatty acid composition of the hydrolysed fraction

The hydrolysed fraction was the only fraction of the lipid extraction to contain the 18-MEA fatty acid (denoted here as C21A) bound to the cuticle surface. The Mullato hair type showed the highest amount of lipid extracted from the hydrolysed fraction and in decreasing order the pattern seen is; Thai, Chinese, Japanese, Afro, Spanish, European. The highest content of C21A was found in the Chinese hair type and in decreasing order the pattern seen is; Afro, European, Spanish, Japanese, Thai, Mullato. Other highlights in the results are:

- C16:0 accounted for the most FA present across all hair types (>20%)
- High variability seen in the Spanish hair type for C18:2n6 and C20:1
- Afro shows a high amount and high variability in the amount of C16:1n7
- Mullato hair type shows a high variability in the amount of C12:0

7.5 Discussion

The results presented in this chapter have shown that there are differences in the quantity, lipid class and the type of lipid species present in hair fibres inter-ethnically. The presence of clustering in the multi-dimensional PCA plot (see Figure 7.1) as constructed from UPLC-MS analysis gave the first indication that there was variation in the lipid content across the hair types which merited further investigation. The TLC and GC/FID analysis was then performed to give a comprehensive profiling of the lipids extracted from all the hair types in a systematic way. This comprehensive study of both the lipid content and profiling of the fatty acids in various ethnic hair types has never been performed before and for the first time reveals a detailed analysis on the variation of lipid inter-ethnically.

The three extraction steps provided a systematic way for the lipids to be optimally extracted from different spatial locations of the hair. The hexane:diethyl ether wash would be expected to preferentially extract all lipids from the hair surface, and lipids that are not bound to the hair fibre due to the fact that both solvents are non-polar and so therefore do not interact with any salt linkages or ionic bonding present between the lipids and the hair fibre. As seen in Table 7.2 and Figure 7.3, less than 10% on average of all lipids were extracted using this method which shows

that most lipids present in the hair fibre are bound in some way. The chloroform:methanol solutions contain polar solvents which can interact with the lipids that are present in the fibre which are bound via salt linkages or polar bonds (Robbins 2009). On average at least 55% of the total lipid content was extracted using this method which implies that at least half of the lipid content found within all hair types is bound via salt linkages or polar bonds. The hydrolysis step further removes lipids that are bound covalently, such as the 18-MEA bound to the cuticle surface, or other fatty acids and lipids otherwise covalently bound to the hair fibre. The hydrolysis step can also be expected to cleave the fatty acids from the lipids that are present as part of other structures in the hair fibre such as proteolipid membranes. Therefore the lipid content here contains only fatty acids, the lipid classes were not analysed in this fraction.

The Mullato hair type shows the highest content of lipid extracted as well as the highest variability in the lipid extracted. This shows that perhaps on the basis of the ethnic mix of the source (which is unknown), a high variability in the lipid content is observed (it is highly likely that other structures and components are affected as well). This provides further supporting evidence that the ethnicity of the source has considerable effect on the structural properties of the hair fibres. However, without knowing the source of the hair fibre, it is not possible to draw definitive conclusions on this basis. The Afro hair as expected from the findings of previous literature also shows a high volume of lipid content extracted from the hair fibres. While all the other hair types in this study showed a relatively constant low amount of lipid extracted in the hexane:diethyl ether wash, the Afro hair type was observed to have a much higher (almost 10% on average) amount of the total lipid content extracted from this hair type using this extraction procedure. This result leads to the possibility of a couple of different factors responsible for this observation. Firstly, assuming that the lipid extracted with the hexane:diethyl ether wash arises from the exogenous source, i.e. the sebum from the sebaceous glands, it indicates that the Afro hair type contains more exogenous lipids than the remaining hair types. The cause of this may be a genetic function for Afro ethnicities to produce more sebum in general. Secondly, the higher lipid content extracted via this method may indicate that the lipids present in the Afro hair type may be less bound to the hair fibre; as the hexane:diethyl ether wash removes all unbound lipids, it may be inferred that Afro hair type has less lipids bound to its structure. Considering that the Afro hair type also shows the lowest amount of lipids extracted from the hydrolysis step and the second highest amount of lipids extracted from the solvent extraction, the concept that the Afro hair type

contains less bound lipids is plausible based on this supporting evidence. On the converse end of the scale, the European hair type shows the least amount of total lipids extracted, and also shows the lowest variability which implies that the European hair type consistently contains the least amount of lipids across all hair types studied here. As a function of the biomass, the European hair type shows less than half the lipid content than both the Afro and Mullato hair types; just 1.47% on average of the total biomass of the European hair type is represented by lipids. This observation could be the result of the following factors. At least two types of the European hair were noted to be very thin in morphology; this could be a factor in the lower lipid content as the hair fibre itself is smaller in comparison to the other hair fibres which means that it contains less mass and therefore structural components than other hair types. The lower lipid content could also be a genetic effect of the European ethnicity to not only produce less sebum to contribute to the exogenous lipids, but also produce less endogenous lipids that are found in the CMC of the hair.

The analysis of individual lipid classes showed that the fraction of FFAs accounts for most of the lipid present in all hair types, with PL and TAG accounting for less than 10% of the rest of the lipid classes (see Tables 7.6 and 7.7 and Figures 7.6 and 7.7). WEs were also found to account for less than 10% of the total lipid content extracted in all hair types except the Afro hair type, which showed that nearly 20% on average of the total lipids was WE fraction. This is an important result as it is significantly different from the rest of the hair types and may be the cause of some of the differences seen in the properties of the Afro hair type, particularly those relating to hydration. It has been suggested in previous literature that the increased lipid content of the Afro hair type is likely to be a direct cause in the lower hydration properties seen in this hair type (Coderch, Mendez et al. 2008). The Afro hair type is also the only hair type that showed a detectable amount of hydrocarbons present in the sample, all the other hair types contained less than 10 μg of hydrocarbons in the sample and also showed fewer peaks in the GC/FID analysis. This shows that the Afro hair type also shows presence of a completely different lipid class, albeit in a small amount, to the rest of the hair types which may contribute to some of the differences in its properties.

The large amount of results in this chapter present the opportunity for many comparisons and inferences to be made amongst the hair types presented in this thesis and with previous literature. Therefore, the discussion will be split up to follow the same structure which the results

were presented in, making comparisons with previous literature where necessary. The first section will therefore be the discussion of the lipids analysed from the hexane:diethyl ether wash.

In the study presented here, assuming that the hexane:diethyl ether wash exclusively extracts the lipids at the surface of the hair fibre which can be assumed to be the exogenous lipids arising from the sebum source, the composition of this lipid source is not only different inter-ethnically, but is also different to that reported in literature (Bertrand, Doucet et al. 2003, Gunstone, Harwood et al. 2007, Coderch, Mendez et al. 2008). As discussed, all hair types except the Afro show a very low content of lipids extracted using this method which implies that there was a low amount of lipids present from the sebum source (exogenous lipids).

The composition of the lipid extracted from the initial hexane:diethyl ether wash also provides surprising results with reference to the composition of lipids previously reported to be excreted from the sebaceous glands. In previous literature the exogenous lipids were reported to have a composition of 41% TAG, 25% WE, 16% FFA, 12 % squalene and other lipids making up the rest of the remaining 6% of the lipids found from this source (Downing, Strauss et al. 1969, Bertrand, Doucet et al. 2003). A later study then reported the lipids from the sebaceous source to have a different composition to that as previously reported. In this study they reported a composition comprising of; 27.78% cholesterol esters, 6.64% TAG, 38.89% FFA, 12.50% fatty alcohols, 6.94% cholesterol, 2.78% ceramides, 2.78% glycosyl ceramides and 1.39% cholesterol sulphates, the total yield as a proportion of the biomass of hair was reported to be 0.72% (Coderch, Mendez et al. 2008). The hair types used in this study were not disclosed, neither was the amount of hair used for the lipid extraction. The extraction method used in the study was a Soxhlet extraction, first with t-butanol and then with n-hexane for 4 hours.

Tables 7.4 and 7.5 in Section 7.4.1.2 show the total lipid content extracted by lipid class in the hexane wash expressed as a percentage of the total lipid content extracted in the hexane wash and as a percentage of the total biomass used for extraction respectively. It can be seen in Table 7.5 that the yield from the hexane:diethyl ether wash as used in this experiment provides a much lower lipid content as a proportion of the hair biomass as compared to (Coderch, Mendez et al. 2008). As the extraction techniques are different in each study, it makes comparisons difficult, as the difference in results may be a result of different extraction techniques used. However, using Table 7.11 which shows the lipid content by class expressed as a percentage of the total lipid content extracted in the hexane wash, a rough comparison can be made of the relative content of

the lipid classes. Table 7.11 shows the results presented in this study along with the same figures previously reported in literature for comparison.

Hair type	Afro	Chi	Eu	Jap	Mu	Span	Thai	Ref (Downing, Strauss et al. 1969)	Ref (Coderch, Mendez et al. 2008)
WE (%)	72.44 ± 47.25	48.84 ± 27.44	21.98 ± 23.98	39.68 ± 17.78	42.42 ± 49.50	20.11 ± 7.56	31.79 ± 25.73	25.0	-
FFA (%)	27.56 ± 28.70	45.92 ± 19.84	68.32 ± 46.61	60.32 ± 48.93	26.90 ± 18.98	72.20 ± 29.36	66.46 ± 46.54	16.4	38.89
TAG (%)	0.00	5.24 ± 7.41	9.70 ± 19.40	0.00	30.68 ± 30.60	7.69 ± 11.34	1.75 ± 3.50	41.0	6.64

Table 7.11 - Relative contribution of each individual lipid class extracted in the hexane:diethyl ether wash expressed as a percentage of the total lipid extracted. Also given are the corresponding values as quoted in previous literature for the lipid classes from the sebaceous source.

As seen in Table 7.11, the biggest contrast in values is for the TAG lipid class, the biggest differences in values are seen between the two references provided, but also in the Mullato, Afro and Japanese hair types with respect to the remaining hair types in this thesis and the references provided. All hair types in this study which show presence of TAG in the hexane wash lie within the range of (Coderch, Mendez et al. 2008), but only the Mullato hair type lies within the range of (Downing, Strauss et al. 1969), which reported a much higher percentage of TAG. All the hair types

in this study, except the Mullato and possibly the European show a much lower percentage of TAG in comparison to (Downing, Strauss et al. 1969).

The Afro hair type also shows the highest percentage by far for the WE lipid class extracted using this method; it shows almost 3 times the amount on average as reported in (Downing, Strauss et al. 1969). The Chinese also shows a much higher amount on average; almost twice the amount as reported in (Downing, Strauss et al. 1969) and the Japanese and Mullato hair types also show a high amount of WE as a proportion of the total lipid extracted using this method. Comparing the results from this study with those provided in the literature is difficult as the ethnic source of the hair types used in literature are undisclosed, but it can be seen that the differences are pronounced and this could be an effect of either the ethnic variation of the hair, or the procedure used. Due to the difference in procedure used a definitive comparison cannot be made, but it is interesting to note the difference in results.

This study provides the results on analysis of the fatty acid patterns of individual lipids that have never been reported before. It is known, that C16:0 and C18:0 are the most abundant saturated fatty acids in nature; typically, C16:0 comprises 20-30% of all fatty acids with C18:0 making up a slightly smaller percentage of the total fatty acid types present in the majority of biological samples (Gunstone, Harwood et al. 2007). Two short-chain fatty acids, C12:0 and C14:0 are normally found at levels of about 1-2% in animals. C14:0 has been found specifically in proteolipids where it is linked via an amide bond to an N-terminal glycine residue and is essential to the function of the protein components (Gunstone, Harwood et al. 2007). The C15:0, C17:0 and C19:0 are usually determined as parts of bacterial membranes, and these fatty acids are very uncommon for the human tissues (Coates and Reffner). In this connection, the identification of C14:0, C15:0, C17:0 and C19:0 acids in relatively large amounts, as well as some anteiso methyl-branched FA in this study is an interesting result. Although the presence of odd-chain and branched-chain FA has been reported for the mammalian hair fibres (Gunstone, Harwood et al. 2007) their distribution within the individual lipid classes has not been reported before. As to methyl-branched fatty acids, only the role of 18-MEA in the structure of hair fibres has been reported.

The lipid classes present in the hexane wash and their FA spectra provide interesting results. By dividing the FA analysis up by lipid class (i.e. describing the FA profiles seen in WE, FFA and TAG) a brief summary of some of the results were presented in Sections 7.4.2.1.1 - 7.4.2.1.3. Both the

Mullato and the Afro hair types show more contribution to the WE lipid class in some of the more unusual fatty acid chains; C14:0, C14:1i, C15:0, C15:1, and C15:1i, the Mullato was the hair type that showed more of a variation in these types of FA. Considering that both the Japanese and the Spanish hair types did not show any presence at all of any of the above named FA, it may be considered that this is initial evidence in this lipid class at least, that based on the ethnicity of the hair source, definite differences are seen in the WE fatty acid patterns present in the sebum source of lipids.

Looking at the FFA composition across the hair types in the hexane:diethyl ether wash does not produce any unusual results as most of the lipid in this class is described by the C16 and C18 isomers which is not unusual, however looking at the TAG content does produce unusual results. The TAG class was not present in any of the Afro or Japanese hair types which shows a definitive ethnic difference on the basis of this lipid class. Analysing the lipid species of the hair types that did show TAG in the European, Chinese, Thai, Spanish and Mullato hair types shows that the European sample shows a much higher content of C14:0 (>15%) which is not present in the Chinese and Thai hair types; the Mullato and Spanish hair types also show a high variability in the presence of this FA. In fact for the C12:0, C12:1, C14:0, C14:1i, C15:0, C15:1 and C15:1i isomers, there is a high amount of variability in both the content and the presence of these FA amongst these hair types which again implies an ethnic factor.

The chloroform:methanol solution extracted on average at least 55% of the total lipid content extracted in all the hair types. This shows that most of the lipids are bound in some way to the hair fibre. By looking at the composition of the lipid classes extracted from this method as seen in Table and Figure 7.7 it is again seen that the fraction of FFA accounts for most of the lipid extracted, with the PL, TAG and WE accounting for ~10% or less on average across all hair types. The exceptions to this are the Chinese hair type which shows that ~15% of the lipids extracted using the solvent method were PL, and the Afro hair type which shows ~20% of the extracted lipids as WE. Comparisons between the composition of the lipids extracted in the study presented here and previous literature can be made. The results from (Coderch, Mendez et al. 2008) and (Cruz, Fernandes et al. 2013) are given in Table 7.12, the PL have been calculated by adding together the results from the ceramides and glucosyl ceramides in the hair which can be classed

as PL. The ethnicity of the hair in (Coderch, Mendez et al.) was not disclosed and will therefore be denoted as unknown, TAG were not reported in (Cruz, Fernandes et al. 2013).

Lipid Class	Unknown hair (Coderch, Mendez et al. 2008)	Asian (Cruz, Fernandes et al. 2013)	Afro (Cruz, Fernandes et al. 2013)	Caucasian (Cruz, Fernandes et al. 2013)
FFA (%)	0.77	0.66	0.92	0.85
TAG (%)	0.03	-	-	-
PL (%)	0.19	0.19	0.19	0.18

Table 7.12 - Values reported in previous literature for the percentage of each lipid class as proportion of the hair biomass.

Comparing the results to those reported in this study seen in Table 7.8 it is seen that the Afro, European, Spanish and Thai hair types show a lower value for the PL, the European, Mullato and Spanish hair types show a much higher value for the TAG and the FFA in all the hair types is generally a lot higher than that reported in literature (Coderch, Mendez et al. 2008, Cruz, Fernandes et al. 2013), the exception to this is the Chinese and European hair types which show a similar percentage.

Table 7.13 shows the contribution of individual lipid classes expressed as a percentage of the total percentage of the lipid extracted as quoted in literature. The results for the PL were calculated by adding the values for the ceramides and glucosyl ceramides together.

Lipid Class	Unknown hair (Coderch, Mendez et al. 2008)	Asian (Cruz, Fernandes et al. 2013)	Afro (Cruz, Fernandes et al. 2013)	Caucasian (Cruz, Fernandes et al. 2013)
FFA (%)	50.33	54.10	54.76	57.82
TAG (%)	1.96	-	-	-
PL (%)	12.42	15.57	11.31	12.25

Table 7.13 - Values quoted in literature for the lipid content expressed as a percentage of the total lipids.

Comparing the results to those reported in this study as seen in Table 7.8 it is seen that the Afro, Spanish, Thai and Japanese hair types all show less PL than would be expected from literature (Afro, Spanish and Thai almost 50% less than the figures reported in literature). For all hair types the FFA values were on average at least 10% higher in this study than previously reported (the Japanese hair type showed almost 33% higher on average than (Coderch, Mendez et al. 2008)) and the TAG content that was reported in (Coderch, Mendez et al. 2008) was far lower on average than the Euro, Mullato and Spanish hair types reported in this study.

The PL extracted in all hair types in this study show a wide range of fatty acid chains from the GC/FID analysis. Although C16:0 and C18:1n9 were the most abundant fatty acid chains seen in all hair types, all of the hair types also showed quite high levels of the unusual C12:0, C12:1, C14:0, C14:1i, C15:1, C17:0 and C19:0 (~5% or more), they also showed a large variation in the relative amounts of these FA.

The results presented in this chapter show that the highest level of 18-MEA was found in the Chinese hair type and in decreasing order the pattern observed is Afro, European, Spanish, Japanese, Thai and Mullato. 18-MEA is exclusively found covalently bound to the cuticle surface via thioester linkages in a monolayer form and is responsible for producing both the hydrophobic properties of the outer layer of the cuticle and a lubricant effect giving hair a sleek property. This implies that on the basis of the level of 18-MEA present in the hair types studied here, the

Chinese, Afro and European hair types (the levels of 18-MEA were very similar amongst these hair types) would have higher hydrophobic properties in comparison to the other hair types, particularly the Mullato hair type which consistently showed the lowest amount of this lipid type. This supports (Coderch, Mendez et al. 2008) which proposed that the Afro hair type showed the least radial swelling percentage as seen in (Franbourg, Hallegot et al. 2003) due to the higher levels of lipids with hydrophobic properties. However, this contradicts some of the results that were presented in Chapter 4, particularly related to that of the Mullato hair type. The Mullato hair type in Chapter 4 was seen to retain a high level of order in its internal structure in the wet state as indicated by the retention of the diffraction features. This implies that this hair type lets less water diffuse into the cortex of the fibre which would create disorder leading to a decrease in the diffraction signal. However, the results presented here show that this hair type consistently contained the least amount of 18-MEA at its hair surface which suggests that it would also contain the least hydrophobic properties of all the hair types and would be more susceptible to water diffusion across the cuticle layer. However, this hair type was also found to contain the highest volume of lipid content amongst any hair type and so it may be considered that due to the high level of lipids present in this hair type, it still manages to retain a high level of structural order under increased hydration conditions despite the low level of 18-MEA at the hair surface.

The results from Chapter 4 show that the Chinese, Mullato and Euro hair types show the most amount of lipid in the hair fibres and the highest co-location of lipid with the KIF inter-lateral packing reflection which shows preferential orientation to the fibre growth axis. The Afro hair types also showed an anisotropic lipid ring present in the dry state, but on hydration of the hair fibres, these lipid rings disappeared leading to a loss in diffraction signal, the lipid diffraction ring in the Euro hair type also disappeared under hydration conditions. This was proposed to be due to the increase in local order caused by the hydration of the hair fibre. It was also reported that there were differences seen in the crystalline lipid spacing of the lipids between ethnicities and that these could be due to the three possible causes; variation in the lipid classes and especially their fatty acid patterns (chain lengths of the fatty acid residues and number of double bonds in unsaturated fatty acids), a hydration effect or tilting of the lipids in the vertical direction (parallel to fibre axis growth). The results presented in this chapter show that in contradiction to the results present in Chapter 4 where the Afro hair types were reported to have the least amount of lipid as deduced from their scattering signal, the Afro hair types used in this biochemical analysis

have been shown to have a high amount of lipid content. The Mullato hair type has been shown to have a high lipid content which agrees with the results presented from Chapter 4 and the Chinese hair type shows a relatively high amount of lipids which would confirm the results reported in Chapter 4. As shown in this study, the Euro hair consistently shows the least amount of lipids when compared to other hair types analysed, and so with reference to the results from Chapter 4, this may be a slightly contradictory point. The integration of the lipid peak area in the X-ray data gives an indication of the total amount of lipids present in the hair types; since the Afro hair type in the study presented in this chapter shows a high variability in the total amount of lipids extracted, it is plausible to suggest that the source used in Chapter 4 for the bulk X-ray scattering analysis may well have been the Afro hair types which showed a lower amount of lipids. A quantitative volume of the amount of lipids present in the hair fibre cannot be deduced from the integration of the lipid peak in the X-ray diffraction data. However, the lipid content relative to each hair type shows that if the Afro hair types used in the X-ray diffraction study were the types displaying lower lipid content (as seen in this chapter), then the patterns of the lipid content observed deduced by the X-ray scattering analysis agree with the results reported in this chapter.

The difference observed in the crystalline lipid spacing of the bulk X-ray analysis can also be considered using the results presented in this chapter; the difference in chain lengths of fatty acids will be considered first. The solvent extraction procedure was shown to be the most effective method for extracting the lipids present in hair, as discussed earlier it is inferred that the hexane:diethyl ether wash only extracts non-bound and exogenous lipids and the hydrolysis step extracts covalently bound lipids and all other lipids present within the hair fibre such as proteolipid membranes. It can therefore be concluded that the lipids extracted from the solvent wash are most likely to be the ones responsible for the diffraction signal seen in the SAXS fibre diagrams of Chapter 4, and because the FFA are the most abundant class of lipids found in the hair and in this extraction it can be suggested that the diffraction signal comes from FFA. The C18:2n6, C16:0 and C16:1n7 are the dominant fatty acids found in all hair types in the fraction of FFA after the solvent extraction so it is likely that the diffraction signal is a result of highly ordered lamellar structures in the hair constructed from these lipid classes. However, the Mullato hair type was shown to have the smallest crystalline lipid spacing in comparison to the other hair types and the results presented in this chapter show that the Mullato hair type, on average, shows a much higher percentage of C14:0 in its FFA fraction in the solvent extraction (>10%), it also shows a

higher percentage of C12:0 than the other hair types used in the X-ray scattering study. While these FA cannot be directly ensued to be responsible for the difference in the crystalline lipid spacing observed in the X-ray diffraction data, it is likely that the higher levels of these FA in the Mullato hair type make a contribution to the difference in the diffraction signal observed. It is also interesting to note that the FA profile of the Euro hair type is very similar in percentage contribution of the short-chain fatty acids to that of the Mullato hair type (but in smaller relative amounts) and that this hair type showed a crystalline lipid spacing only slightly higher than that of the Mullato hair type, which made it the second smallest crystalline lipid spacing observed amongst the hair types. There are also differences observed in the types of fatty acids identified in the Chinese hair type (this was the only hair type not to contain C12:0) and the Spanish, although not studied in the X-ray scattering experiment, showed larger amounts of C12:0 and C14:0. This shows that there are inter-ethnic differences in the fatty acid patterns, and this could be a factor determining the differences seen in the X-ray diffraction signal.

The FWHM of the crystalline lipid peak in the X-ray scattering data also reveals details on the lipids present in the hair fibre; it is an indicator of the size and organisation of the crystallites present. The Chinese hair type was shown to have the greatest breadth and in decreasing breadth order the pattern seen was; Mullato and Afro Soft (these were equal), Euro, Afro Rubber. The FWHM of the X-ray scattering data gives an indication of the different chain lengths that contribute to the crystalline lipids that are formed within the hair fibre. A broader peak implies that there is more variability in the type of lipids and fatty acids present than a narrower peak. The data from the X-ray scattering therefore suggests that the Chinese hair type has the most amount of variation in the lipids that it contains. Cross referencing the results of the inter-ethnic differences seen in the breadth of the lipid peak in the X-ray data with the FFA profiles of the FFA fraction in the solvent extraction enables some comparisons to be made. It is seen that although the Chinese hair type in the X-ray data shows the highest breadth, from the analysis of the FFA profiles presented in this chapter, this hair type shows less variation in the content of its FFA lipid species with respect to the Afro and Mullato hair types which were also used in the X-ray study. This shows that from the results presented in this chapter, the Afro and Mullato hair types agree with the results in Chapter 4 which indicate that these hair types would show a wider variation in their FA profile corresponding to a greater breadth in the lipid peak observed, however, the Chinese hair sample

would be expected to have less breadth than the aforementioned hair types which contradicts the results in Chapter 4.

7.6 Conclusions

This study used a three step extraction process to comprehensively remove all the lipids present at different spatial locations of the hair fibre. The hexane:diethyl ether wash removed exogenous lipids at the surface of the fibre, the solvent extraction removed lipids that are bound ionically or via salt linkages and the hydrolysis step removed lipids that are covalently bound to the fibre, such as 18-MEA to the cuticle surface, or present within proteinaceous components within the hair fibre. This three step technique allowed for a broad profiling of all the lipid classes contained throughout the hair fibre structure and also enabled for a complete description of the FA profiles to be made for each class of lipid extracted.

The results presented in this chapter have shown that there are inter-ethnic differences seen in the content of the lipid, the class of lipid and the FA profiles within each class of lipid. The differences that have been quantified have attempted to be related to some of the properties of ethnic hair fibres and in addition to this, have been proposed to contribute to other properties. The largest difference seen in the lipid content between the hair types is seen between the Afro hair type with respect to the remaining hair types. This hair type showed a large amount of lipid content, a large variation in the content of the lipid, a larger content and profile of HC, a much larger amount of lipid extracted in the hexane wash indicating a larger amount of exogenous lipids and a larger variation in the classes of lipids present amongst extraction processes used. These results indicate that this hair type may exhibit properties that are different to the remaining hair types on the basis of its lipid content and requires further investigation, and the results presented here confirm previous reports which suggested that the poor hydration of the Afro hair type was related to its lipid content (Coderch, Mendez et al. 2008). An investigation relating the larger content of the HC and WE seen in the Afro hair type could reveal properties that are important in the field of cosmetic science.

There are differences in the FA profiles amongst all hair types which show ethnic variation that could be genetically dependant but also could be related to the variation in signal seen in the X-ray diffraction study presented in Chapter 4. The results in this chapter have shown that the FA

profiles of the FFA content in the Mollato and Euro hair types show a larger content of shorter chain fatty acids; these hair types were shown to have the lowest crystalline lipid spacing in the X-ray study in Chapter 4.

Comparisons have been made to previous studies and there are differences shown in both the content and composition of the lipid extracted in the hair types used in this study.

Chapter 8 – Conclusions & Future Work

In this thesis a combination of complementary techniques have been used in order to investigate the fundamental structure of keratins and differences in the structure of ethnic hair types. There have been several findings from the work presented that have not been reported in literature that contribute to the field in this area of research. There are always opportunities for improvements that can be made by further research, these are considered here.

8.1 Findings & Conclusions

The work presented here has furthered research on the origins of structural differences between ethnic hair types over several levels of scale. This has been carried out using a variety of interdisciplinary techniques to investigate structural changes within ethnic variations of human hair. The following is a summary of the new findings made not reported before in literature.

Chapter 4 presented a bulk X-ray scattering experiment on ethnic hair fibres which produced the following results. There are inter-ethnic differences seen in the:

- Spacing of the crystalline lipids present in hair.
- Total intensity and thus volume of lipids present and also in the preferential structural orientation of the lipid arrangement.
- Low-angle diffuse scatter component of the SAXS fibre diagrams. The differences seen are in the power law region of the component, the extent of the diffuse scatter in q range, the angular behaviour of the low angle diffuse scatter and the behaviour of the low angle diffuse scatter under hydration conditions. This may be due, in part, to the KAPs present in the hair fibres.
- Azimuthal spread of the reflection arising from the inter-lateral packing of the KIFs in hair fibres in the SAXS fibre diagrams. This is due to variations in the packing of the KIFs.

Chapter 5 presented a microfocus X-ray scattering experiment to investigate inter-ethnic zonal structural variations. The following results were produced:

- There are zonal variations in the keratinous and non-keratinous structures present in hair fibres.
- There are both intra and inter-ethnic zonal structural variations observed in the hair fibres under test. The differences seen are in the size and location of specific hierarchical keratinous assembly structures, but also in the ultrastructure of the hair fibre as a whole.

Chapter 6 reported the results from an ATR-FTIR experiment on the chemical composition of the surface structure of hair fibres. The following results were produced:

- There are inter-ethnic structural variations in the water content of hair fibres which are proposed to give rise to differences in the hydrophobicity of the epicuticle layer on the surface of the cuticle. This in turn will lead to differences seen in the hydro-mechanical behaviour.
- There are variations in the products of the cysteine containing structures due to weathering between ethnic hair types. This may be due to differences in the amount of UV radiation the subjects have been exposed to due to their geographical location.
- Differences in wavenumbers of the Amide I and II envelopes could be due to inter-ethnic variation of the thickness of the cuticle structure as an ultrastructural object leading to signal arising from the cortex in certain ethnic hair types.

Chapter 7 showed a study from the preferential extraction of lipids in different spatial locations of the hair fibre using a three step protocol for several ethnic hair types. From this study the following conclusions were made:

- There is variation seen in the total lipid content extracted from each hair type. The largest difference is seen between the Mullato (which showed the highest) and the European hair type (which showed the lowest).
- There is variation in both the lipid classes present and the fatty acid profiles of each lipid class across ethnicities. The largest differences seen here were between the Afro hair types with respect to the remaining hair types used in the study.

- The variation in the fatty acid profiles between hair types can possibly be related to the difference in signal seen in the X-ray diffraction study.
- The variation in the total lipid content, composition and fatty acid profile is highly likely to contribute, at least in part, to the hydro-mechanical behaviour of hair fibres and possibly to macroscopic appearance.

The results in Chapter 4 showed that the most consistent component between hair types was the fibrous keratin present within the KIFs and the largest source of variation was in the lipid content and the low angle diffuse scatter which is thought to be related, at least in part, to the KAPs present in the hair fibre. Chapter 5 reported differences on the basis of the ultra structure of the hair and also in the lipid content. It was seen that the hair morphology and sub-structural sections were variable both intra and inter-ethnically. Chapter 6 showed that ATR-FTIR was an effective technique that can be used to study the chemical compositional structure exclusively in the cuticle and that combining this technique with PCA, differences were reported in the hydrophilic properties of the cuticle and most likely in the keratinous structure of the cuticle between ethnicities. Chapter 7 provided a comprehensive description of the lipid content across several ethnicities and how this varied according to the total content extracted from different spatial locations within the hair fibre, the types of lipid present and the fatty acid profiles of each lipid class.

With reference to Section 1.7 which detailed the hypothesis for this thesis, the following conclusions can be made. It has been proven from the results in Chapter 4 that the most consistent structural component within hair fibres of all ethnicities used in this thesis is the keratinous matter present within the KIFs. The variation was suggested to be due, at least in part, to the KAPs and the lipids present within the hair, but also maybe due to the interfaces between components within hair. Chapter 7 showed how the lipid content differed between hair types and this shows that the lipid content must play a role in contributing to the macroscopic differences in both the appearance of the hair but also in some of its properties such as hydro-mechanical behaviour and the lubrication properties on the cuticle surface which gives hair its sleekness. Chapter 5 showed how there are differences in the textural variation of the components that build

the ultra structural sections of the hair fibre and how this may be due to the presence of different sizes of interface sections in different spatial locations of the hair fibres. The data shown in this chapter confirms the heterogeneity of hair fibres and provides vital information into showing how this may contribute not only to the macroscopic variation but also in the use of this technique to study hair. The ATR-FTIR study showed how variation in the hydrophilic properties of the hair fibre may contribute to differential properties between hair types, although this may be related to the lipid content of the hair fibres, this was unable to be proven using this study. However, this technique also highlighted variation in the keratinous structures present at the cuticle surface and suggested that between hair types there is likely to be different cuticle thicknesses in relation to this structure as an ultra structural component of the hair (i.e. as a bulk object, not an individual cuticle cell). This is also thought to play a role in the macroscopic variation observed between ethnicities. The difficulty in ascribing a signal from the KAPs to a specific feature in the X-ray data remains a problem in validating any data relating to these structures and so it continues to be a problem to acquire any information on KAPs.

To summarise, the hypothesis that the most consistent structures within hair are the keratinous structures has been proven by the results in Chapter 4. The results in Chapter 5, Chapter 6 and most importantly Chapter 7 all give evidence that the lipid content of the hair fibre makes an important contribution to the inter-ethnic macroscopic variation and it is also highly likely that the KAPs also play an important role. However, without being able to attain validity on the involvement of KAPs in the X-ray signal seen in the small angle region, it cannot be fully justified. However, the low angle diffuse scatter in the small angle signal is a significant distinguishing feature and is likely to arise from KAPs and other amorphous interfaces within hair and so with some supporting evidence from the microfocus study it should be considered that this also plays a crucial role in creating macroscopic variance between ethnicities.

8.2 Evaluation of the current work

While the work in this thesis has been successful in reporting several original findings, there are always areas in which there is room for improvement. An evaluation of the work shall therefore be presented in the following.

Chapter 4 presented a bulk analysis of single hair fibres from five different ethnic hair types. In an ideal situation there would be an increased amount of time to study more hair fibres at a world class synchrotron which would provide the means to carry out statistical analysis on the results. However, it is generally accepted within the synchrotron community that due to severe time constraints and the quality of the data that is produced from using such instruments that the data taken from one source is representative of a whole data set. This notion also carries onto the microfocus study that was presented in Chapter 5. Although, it should be noted that additional beamtime was granted to improve the statistical number of the hair fibres used in the microfocus study, multiple complications with the experimental setup and experimental design unfortunately resulted in no additional measurements. The results in Chapter 6 were the product of a much higher statistical number of hair fibres, sources and measurements made in this experiment with comparison to the results in Chapters 4 and 5. In total the spectra presented were the results of 27 different measurements taken and so this is not an area that would need improvement. The results from Chapter 7 are also the product of a high number of hair fibres used from at least 3 different sources for each ethnicity and the statistical analysis made therein is sound.

Many of the complications associated with the microfocus experiment were addressed in the discussion and conclusions section of Chapter 5 (see Sections 5.5.2 and 5.5.3). Due to the nature of the experiment it was inherently very challenging to perform. The largest problems encountered were the optimal background subtraction of the images, the preferential alignment of the X-ray beam with the hair fibre and the spatial resolution obtainable using the equipment available. From the results obtained and presented in Chapter 5, a future microfocus experiment could be improved by increasing the resolution of the small angle signal to provide more information on the scattering features in this region as they give more detail on the components of the hair fibre that are not consistent; i.e. the lipid, interfaces and the low angle diffuse scatter. This may be the result of adjusting the camera length so that it is further away from the sample

thus providing better resolution in this region or this could be the result of an improvement in the equipment available at synchrotrons. Improving the background subtraction is also an issue that needs to be addressed. The analysis software or code that is written to optimally subtract the background from data files needs to be improved so a greater signal-to-noise ratio in the images can be obtained. The thickness of the hair fibre as the X-ray beam is traversed across the cross section causes a difference in the level of background subtraction that needs to be applied to each image; there is inevitably an increase in the thickness of a cylindrical object towards the middle and this causes a difference in the level of background subtraction.

8.3 Future Work

There are many further areas of work in this area of research that could be performed leading on from the experiments presented here that would further the knowledge of the origins of the macroscopic variation in ethnic hair types. One main area of research would be to try and further characterise the KAPs and the role and functionality that they have within hair, both individually, and as a bulk entity forming the matrix within macrofibrils. Possible ways in which this could be done would be by performing a further structural investigation on other KAPs using X-ray solution scattering; this would provide details on the atomic envelope and tertiary structure. Circular dichroism experiments would reveal more details on the tertiary structure, fold of the protein and whether or not it contains helical or beta sheeted structures (which is unlikely as they are thought to show an amorphous or globular structure) and dynamic light scattering which would provide information on the size of the proteins. This research could be used on different types of KAPs to try and build up a database of information on the various structural properties of KAPs where there is currently very little information available.

Having sourced this information, it could then be used to build models of the assemblies seen in the cortex of the hair fibre to reconstruct KAP/KIF architecture. A greater knowledge of the way in which KAPs are folded and arranged with respect to each other and the KIFs would give rise to the opportunity of a greater understanding of the interactions between KAPs and also between KAPs and KIFs at the nanoscopic level. Considering the mechanics of the KAPs as a mass hydrophobic structure has given some success in interpreting and understanding the properties of the hair fibre as a whole object under conditions of increased hydration but this assumption may not be

suitable at the nanoscopic level. Further understanding of the structures of the KAPs may help to elucidate their mechanical behaviour on a smaller scale.

Investigation into the level of expression (as a volume) of which each KAP is expressed in specific ethnicities may also give further clues into the ethnic macroscopic or morphological variation. There may be specific ethnicities that produce specific KAPs or families of KAPs in different volumes and this may have an effect on the mechanical properties and the macroscopic appearance of the hair fibre. Further investigation on the structure of KAPs may also lead to further insight into their structural function and may reveal details on the need for differential KAP expression and the differences and roles of the KAP subfamilies. Possible sub-routes of research from this could be if KAPs do not have specific structural functions related to each one, is there a reason why there is not just one KAP expressed? If they do, what are their individual structural functions?

One way in which this could possibly be answered is using a Biacore experiment to test the interactivity and binding properties of each of the KAP proteins. A Biacore experiment uses Surface Plasmon Resonance (SPR) to give information on the binding kinetics of proteins in real time, this in turn should give evidence on the way in which individual KAPs may interact with each other, other types of KAPs and with KIFs. However, a Biacore experiment will only give useful information on the KAPs if they are in their native state; a study needs to be done on the effects of expressing the KAPs and the extraction and purification of the KAPs to compare the two to identify differences in the structure and reveal information on which technique gives the most accurate description of a KAP in its native state.

KAPs are just one type of binding medium found in the cortex of the hair fibre. It is unclear whether or not the matrix which binds the macrofibrils together in the cortical cells is made from the same structures, or type of structures as found in the intermicrofibrillar matrix. This is a whole untouched area of research that needs to be performed. Possible research areas here could be the preferential extraction of this medium so that it can be studied in its native state (if this is possible), characterising its chemical structure and mechanical behaviour and whether this is different to the inter-microfibrillar matrix, and whether or not the intermacrofibrillar matrix is responsible in some way for ethnic variation. This role that KAPs play and understanding their

functionality is analagous to that of proteoglycans in collagen based tissues where recent advances in characterisation have revealed details about specificities of interactions.

Investigating the role that lipids play within hair fibres also provides opportunities for further research in this field. The evidence presented in Chapter 7 shows that the Afro hair type has a far higher content of wax esters than the other hair types, this may be a the cause of a specific functionality of this lipid class; there is opportunity to try to relate the functionality of each lipid class and how this contributes to the properties of the hair, and how different ratios of these lipid classes may or may not result in bespoke properties. The way in which lipids are distributed along the hair fibre axis and their orientation with respect to this distribution may also be an area of research worth merit. Chapters 4 and 5 have shown evidence for different orientations and spatial locations of lipids across ethnicities but this has not been fully characterised. It is also not clear whether or not the lipids interact with other structures within hair fibres and if different concentrations, classes of lipids or volume content affects these structures in some way which may contribute to differential mechanical properties and possibly the macroscopic appearance.

The techniques, methods and core competencies used and developed in the production of this thesis have also been applied to other areas of science where they have contributed to manuscripts. Knowledge of X-ray diffraction and its subsequent analysis was used in order to study the role that hair fibres play within lime plaster and its deformation. A contribution has also been made towards studying the effect of degradation of collagen within parchment using FTIR techniques. These manuscripts have been added to the back of this thesis following the appendices to show how the competencies developed in this field of science have been applied to other areas of research.

References

- Ackermann, K. R., J. Koster and S. Schlucker (2008). "Polarized Raman microspectroscopy on intact human hair." Journal of Biophotonics 1(5): 419-424.
- Adams, M. J. (1995). Chemometrics in Analytical Spectroscopy. Cambridge, Royal Society of Chemistry.
- Akhtar, W., H. G. M. Edwards, D. W. Farwell and M. Nutbrown (1997). "Fourier-Transform Raman Spectroscopic Study of Human Hair." Spectrochimica Acta Part A 53: 1021-1031.
- Allen, A. K., J. Ellis and D. E. Rivett (1991). "The presence of glycoproteins in the cell membrane complex of a variety of keratin fibres." Biochimica et Biophysica Acta 1074(2): 331-333.
- Ambrose, E. J. and A. Elliott (1951). "Infra-red spectra and structure of fibrous proteins." Proceedings of the Royal Society A: Mathematical, Physical & Engineering Sciences 206(1085): 206-219.
- Astbury, W. T. (1933). "Some Problems in the X-ray Analysis of the Structure of Animal Hairs and Other Protein Fibres." Transactions of the Faraday Society 29: 193-211.
- Astbury, W. T. and W. A. Sisson (1935). "X-Ray Studies of the structure of hair, wool and related fibres. III The Configuration of the keratin molecule and its orientation in the biological cell." Proceedings of the Royal Society of London A 150: 533-551.
- Astbury, W. T. and A. Street (1932). "X-Ray Studies of the Structure of Hair, Wool, and Related Fibres. I. General." Philosophical Transactions of the Royal Society of London. Series A, Containing Papers of a Mathematical or Physical Character 230: 75-101.
- Astbury, W. T. and H. J. Woods (1934). "X-Ray Studies of the Structure of Hair, Wool, and Related Fibres. II - The Molecular Structure and Elastic Properties of Hair Keratin." Philosophical Transactions of the Royal Society of London. Series A, Containing Papers of a Mathematical or Physical Character 232: 333-394.
- Baddiel, C. B. (1968). "Structure and Reactions of Human Hair Keratin: an Analysis by Infrared Spectroscopy." Journal of Molecular Biology 38: 181-199.
- Bandli, B. Human Hair. Scanning Electron Microscopy Laboratory, University of Minnesota.
- Barton, P. M. J. (2011). A forensic investigation of single human hair fibres using FTIR-ATR spectroscopy and chemometrics. PhD, Queensland University of Technology.
- Berg, J. M., J. L. Tymoczko and L. Stryer, Eds. (2002). Biochemistry. New York, Freeman.
- Bertrand, L., J. Doucet, A. Simionovici, G. Tsoucaris and P. Walter (2003). "Lead-revealed lipid organisation in human hair." Biochimica et Biophysica Acta 1620: 218-224.
- Bhushan, B. (2008). "Nanoscale characterization of human hair and hair conditioners." Progress in Materials Science 53: 585-710.
- Birbeck, M. S. C. and E. H. Mercer (1956). "The electron microscopy of the human hair follicle: Part 1. Introduction and the hair cortex." The Journal of Biophysical and Biochemical Cytology 3(2): 203-221.
- Bogaty, H. J. (1969). "Differences between adult and children's hair." Journal of the Society of Cosmetic Chemistry 20: 159-171.
- Bouillon, C. and J. D. Wilkinson (2005). The Science of Hair Care. Boca Raton, Florida, CRC Press, Taylor & Francis Group.
- Bradbury, J. H. and J. D. Leeder (1969). "Keratin Fibres IV. Structure of Cuticle." Australian Journal of Biological Sciences 23: 843-854.
- Briki, F., B. Busson and J. Doucet (1998). "Organization of microfibrils in keratin fibers studied by X-ray scattering: modelling using the paracrystal concept." Biochimica et Biophysica Acta 1429: 57-68.
- Bryson, W. G., D. P. Harland, J. P. Caldwell, J. A. Vernon, R. J. Walls, J. L. Woods, S. Nagase, T. Itou and K. Koike (2009). "Cortical cell types and intermediate filament arrangements correlate with fiber curvature in Japanese human hair." Journal of Structural Biology 166: 46-58.

Caldwell, J. P., D. N. Mastrorarde, J. L. Woods and W. G. Bryson (2005). "The three-dimensional arrangement of intermediate filaments in Romney wool cortical cells." Journal of Structural Biology 151: 298-305.

Chandrashekhara, M. N. and C. Ranganathaiah (2009). "Diffusion of permanent liquid dye molecules in human hair investigated by positron lifetime spectroscopy." Colloids and Surfaces B: Biointerfaces 69: 129-134.

Coates, J. and J. Reffner (1999). "Visualization of Micro-ATR Infrared Spectroscopy." Spectroscopy 14(4): 34-45.

Coderch, L., S. Mendez, C. Barba, R. Pons, M. Marti and J. L. Parra (2008). "Lamellar rearrangement of internal lipids from human hair." Chemistry and Physics of Lipids 155: 1-6.

Conway, J. F. and D. A. D. Parry (1988). "Intermediate filament structure: 3. Analysis of sequence homologies." International Journal of Biological Macromolecules 10: 79-98.

Crewther, W. G. and D. A. Parry (1977). "Structure of alpha-keratin: structural implications of the amino acid sequences of the type I and type II chain segments." Journal of Molecular Biology 113(2): 449-454.

Cruz, C. F., M. M. Fernandes, A. C. Gomes, L. Coderch, M. Marti, S. Mendez, L. Gales, N. G. Azoia, U. Shimanovich and A. Cavaco-Paulo (2013). "Keratins and lipids in ethnic hair." International Journal of Cosmetic Science: 1-6.

Davidson, M. W. (2004). "Intermediate Filaments." Retrieved 25/01/13, 2013, from <http://micro.magnet.fsu.edu/cells/intermediatefilaments/intermediatefilaments.html>.

Dekio, S. and J. Jidoi (1990). "Amounts of Fibrous Proteins and Matrix Substances in Hairs of Different Races." The Journal of Dermatology 17: 62-64.

Dekio, S. and J. Jidoi (1998). "Hair low-sulphur protein composition does not differ electrophoretically among different races." The Journal of Dermatology 15: 393-396.

Delta, D. (2010). "Bragg's Law." Retrieved 23/06/2010, 2010, from <http://www.diracdelta.co.uk/science/source/b/r/braggs%20law/image002.gif>.

Dowling, L., D. A. D. Parry and L. G. Sparrow (1983). "Structural homology between hard alpha-keratin and the intermediate filament proteins desmin and vimentin." Bioscience Reports 3: 73-78.

Downing, D., J. Strauss and P. Pochi (1969). "Variability in the Chemical Composition of Human Skin Surface Lipids." The Journal of Investigative Dermatology 53: 322-327.

Elliot, D. (2009). "Haircare packs: A family affair." Retrieved 12/01/2012, 2012, from <http://www.packagingnews.co.uk/news/haircare-packs-a-family-affair/>.

Ferraro, J. R. and K. Krishnan (1990). Practical Fourier Transform Infrared Spectroscopy: industrial and laboratory chemical analysis. Michigan, Academic Press.

Feughelman, M. (1959). "A Two-Phase Structure for Keratin Fibers." Textile Research Journal: 223-228.

Feughelman, M. (1994). "A Model for the Mechanical Properties of the alpha-keratin Cortex." Textile Research Journal 64(4): 236-239.

Feughelman, M. (1997). Mechanical Properties and structure of alpha-keratin fibres: wool, human hair and related fibres. Sydney, University of New South Wales Press.

Formanek, F., Y. D. Wilde, G. S. Luengo and B. Querleux (2006). "Investigation of dyed human hair fibres using apertureless near-field scanning optical microscopy." Journal of Microscopy 224(2): 197-202.

Franbourg, A., P. Hallegot, F. Baltenneck, C. Toutain and F. Leroy (2003). "Current Research on Ethnic Hair." Journal of American Academy of Dermatology 48(6): 115-119.

Fraser, R. D. B. and T. P. MacRae (1958). "Structural Implications of the Equatorial X-Ray Diffraction Pattern of Alpha-Keratin." Biochimica et Biophysica Acta 29: 229-240.

Fraser, R. D. B. and T. P. MacRae (1983). "The structure of the alpha-keratin microfibril." Bioscience Reports 3: 517-525.

Fraser, R. D. B., T. P. MacRae and A. Miller (1964). "The coiled coil model of alpha-keratin structure." Journal of Molecular Biology 10(1): 147-156.

Fraser, R. D. B., T. P. MacRae and G. E. Rogers (1959). "Structure of Alpha-Keratin." Nature 183: 592-594.

Fraser, R. D. B., T. P. MacRae and G. E. Rogers (1962). "Molecular organization in alpha-keratin." Nature 193: 1052-1055.

Fraser, R. D. B., T. P. MacRae and G. E. Rogers (1963). "Lipids in keratinized tissues." Journal of Molecular Biology 7: 90-91.

Fraser, R. D. B., T. P. MacRae and G. E. Rogers, Eds. (1972). Keratins; Their Composition, Structure and Biosynthesis, Springfield.

Fujikawa, H., A. Fujimoto, M. Farooq, M. Ito and Y. Shimomura (2012). "Characterization of the Human Hair Keratin-Associated Protein 2 (KRTAP2) Gene Family." Journal of Investigative Dermatology 132: 1806-1813.

Garbus, J., H. F. Deluca, M. E. Loomans and F. M. Strong (1963). "Rapid incorporation of phosphate into mitochondrial lipids." Journal of Biological Chemistry 238: 59-63.

Geisler, N., U. Plessman and K. Weber (1982). "Related amino acid sequences in neurofilaments and non-neural intermediate filaments." Nature 296: 448-450.

Gillespie, J. M. (1964). "The isolation and properties of some soluble proteins from wool, part IX: The proteins in wools of increased sulphur content." Australian Journal of Biological Sciences 17: 548-560.

Glatter, O. and O. Kratky, Eds. (1982). Small Angle X-ray Scattering. London, Academic Press.

Gong, H., H. Zhou, G. W. McKenzie, Z. Yu, S. Clerens, J. M. Dyer, J. E. Plowman, M. W. Wright, R. Arora, C. S. Bawden, Y. Chen, J. Li and J. G. H. Hickford (2012). "An Updated Nomenclature for Keratin Associated Proteins (KAPs)." International Journal of Biological Sciences 8(2): 258-264.

Grooming, P. G. B. (2007). "Hair Structure." Retrieved 20/07/2010, 2010, from <http://www.pgbeautygroomingscience.com/assets/images/twoh/Chapter%201/Hair%20Structure%206.jpg>.

Gummer, C. L. (2001). "Elucidating penetration pathways into the hair fiber using novel microscopy techniques." Journal of Cosmetic Science 52: 265-280.

Gunstone, F. D., J. L. Harwood and F. B. Padley, Eds. (2007). The Lipid Handbook, Taylor & Francis Group.

Hammersley, A. P., S. O. Svensson, M. Hanfland, A. N. Fitch and D. Hausermann (1996). "Two-dimensional detector software: From real detector to idealised image or two-theta scan." High Pressure Research 14(4): 235-248.

Hoppe, W., W. Lohmann, H. Markl and H. Ziegler, Eds. (1983). Biophysics. Berlin, Springer-Verlag Berlin Heidelberg.

Huang, T. C., H. Toraya, T. N. Blanton and Y. Wu (1993). "X-Ray Powder Diffraction Analysis of Silver Behenate, A Possible Low-Angle Diffraction Standard." Journal of Applied Crystallography 26: 180-184.

Inoue, T., Y. Iwamoto, N. Ohta, K. Inoue and N. Yagi (2007). "Structural analysis of the cell membrane complex in the human hair cuticle using microbeam x-ray diffraction: Relationship with the effects of hair dyeing." Journal of Cosmetic Science 58: 11-17.

Jolles, P., H. Zahn and H. Hocker, Eds. (1997). Formation and Structure of Human Hair. Berlin, Deutsche Bibliothek Cataloging-in-Publication Data.

Jolliffe, I. T., Ed. (2002). Principal Component Analysis, Second Edition. Springer Series in Statistics. New York, Springer-Verlag.

Jones, L. N. and D. E. Rivett (1997). "The role of 18-Methyleicosanoic acid in the structure and formation of mammalian hair fibres." Micron 28(6): 469-485.

Joy, M. and D. M. Lewis (1991). "The use of Fourier Transform infra-red spectroscopy in the study of the surface chemistry of hair fibres." International Journal of Cosmetic Science 13: 249-261.

Kajiura, Y., S. Watanabe, T. Itou, A. Iida, Y. Shinohara and Y. Amemiya (2005). "Structural analysis of single wool fibre by scanning microbeam SAXS." Journal of Applied Crystallography 38: 420-425.

Kajiura, Y., S. Watanabe, T. Itou, K. Nakamura, A. Iida, K. Inoue, N. Yagi, Y. Shinohara and Y. Amemiya (2006). "Structural analysis of human hair single fibres by scanning microbeam SAXS." Journal of Structural Biology 155: 438-444.

Kamath, Y. K., S. B. Hornby and H. D. Weigmann (1984). "Mechanical and fractographic behavior of Negroid hair." Journal of the Society of Cosmetical Chemists 35: 21-43.

Kaplin, I. J. and K. J. Whiteley (1978). "An Electron Microscope Study of Fibril: Matrix Arrangements in High- and Low-crimp Wool Fibres." Australian Journal of Biological Sciences 31: 231-240.

Kariya, N., Y. Shimomura and M. Ito (2005). "Size Polymorphisms in the Human Ultrahigh Sulfur Hair Keratin-Associated Protein 4, KAP4, Gene Family." The Journal of Investigative Dermatology 124: 1111-1118.

Kassenbeck, P., C. Orfanos, W. Montagna and G. Stuttgen, Eds. (1981). Morphology and fine structure of hair. Berlin, Springer-Verlag.

Kelch, A., S. Wessel, T. Will, U. Hintze, R. Wepf and R. Wiesendanger (2000). "Penetration pathways of fluorescent dyes in human hair fibres investigated by scanning near-field optical microscopy." Journal of Microscopy 200(3): 179-186.

Khumalo, N. P., R. P. R. Dawber and D. J. P. Ferguson (2005). "Apparent Fragility of African Hair is Unrelated to the Cysteine-Rich Protein Distribution: A Cytochemical Electron Microscopic Study." Journal of Experimental Dermatology 14: 311-314.

Kidd, F. (1965). Cell structures in coarse kertinous fibres. 3rd International Wool & Textile Research Conference, Paris.

King, N. L. R. and J. H. Bradbury (1967). "The Chemical Composition of Wool." Australian Journal of Biological Sciences 21: 375-384.

Korner, A., S. Petrovic and H. Hocker (1995). "Cell membrane lipids of wool and human form liposomes." Textile Research Journal 65: 56-58.

Kreplak, L., F. Briki, Y. Duvault, J. Doucet, C. Merigoux, F. Leroy, J. L. Leveque, L. Miller, G. L. Carr, G. P. Williams and P. Dumas (2001). "Profiling lipids across Caucasian and Afro-American hair transverse cuts, using synchrotron infrared microspectroscopy." International Journal of Cosmetic Science 23: 369-374.

Kreplak, L., A. Franbourg, F. Briki, F. Leroy, D. Dalle and J. Doucet (2002). "A New Deformation Model of Hard Alpha-Keratin Fibers at the Nanometer Scale: Implications for Hard Alpha-Keratin Intermediate Filament Mechanical Properties." Biophysical Journal 82(4): 2265-2274.

Kreplak, L., C. Merigoux, F. Briki, D. Flot and J. Doucet (2001). "Investigation of human hair cuticle structure by microdiffraction: direct observation of cell membrane complex swelling." Biochimica et Biophysica Acta 1547: 268-274.

Krotoszynski, B. K., L. L. Gershbein and S. B. Needleman (1955). "Properties of hair fat from adult males according to race and hair condition." Journal of Investigative Dermatology 26: 311-316.

L, L., R. MA, W. H, P. S and S. J (2001). "The catalog of human hair keratins. II. Expression of the six type II members in the hair follicle and the combined catalog of human type I and II keratins." Journal of Biological Chemistry 276: 35123-35132.

Langbein, L., M. A. Rogers, H. Winter, S. Praetzel, U. Beckhaus, H.-R. Rackwitz and J. Schweizer (1999). "The Catalog of Human Hair Keratins: I. Expression of the nine type I members in the hair follicle " The American Society for Biochemistry and Molecular Biology, Inc 274(28): 19874-19884.

Leeder, J. D. (1986). "The cell membrane complex and its influence on the properties of the wool fibre." Wool Science Reviews 63: 3-35.

Leeder, J. D., J. A. Rippon and F. E. Rethery (1985). "Use of the transmission electron microscope to study dyeing and diffusion processes." Proceedings of the 7th International Wool & Textile Research Conference 5(Tokyo): 99-108.

Luell, E. and V. E. Archer (1992). "Hair medulla variation with age in human males." American Journal of Physical Anthropology 22: 107-110.

Masukawa, Y., H. Shimogaki, K. Manago and G. Imokawa (2005). "A novel method for visualizing hair lipids at the cell membrane complex: Argon sputter etching/scanning electron microscopy." Journal of Cosmetic Science 56: 297-309.

Masukawa, Y., H. Tsujimura and G. Imokawa (2005). "A systematic method for the sensitive and specific determination of hair lipids in combination with chromatography." Journal of Chromatography B 823: 131-142.

Menkart, J., L. J. Wolfram and I. Mao (1966). "Caucasian Hair, Negro Hair, and Wool: Similarities and Differences." Journal of the Society of Cosmetical Chemists 17: 769-787.

Mitchell, G. P., J. Mifsud, D. E. Rivett and A. K. Allen (1992). "Characterisation of formic acid-derived cell membrane complex proteins from wool." Biochemical Society Transactions 20(2): 90S.

Nagase, S., M. Tsuchiya, T. Matsui, S. Shibuichi, H. Tsujimura, Y. Masukawa, N. Satoh, T. Itou, K. Koike and K. Tsujii (2008). "Characterization of curved hair of Japanese women with reference to internal structures and amino acid composition." Journal of Cosmetic Science 59: 317-332.

Nappe, C. and M. Kermici (1989). "Electrophoretic analysis of alkylated proteins of human hair from various ethnic groups." Journal of the Society of Cosmetical Chemistry 40: 91-99.

Nicolaidis, N. and S. Rothman (1952). "Studies on the chemical composition of human hair fat I. The squalene-cholesterol relationship in children and adults." Journal of Investigative Dermatology 19: 389-391.

Nicolaidis, N. and S. Rothman (1953). "Studies on the chemical composition of human hair fat II. The overall composition with regard to age, sex and race." Journal of Investigative Dermatology 21: 9-14.

O'Connor, S. D., K. D. Komisarek and J. D. Baldeschwieler (1995). "Atomic force microscopy of human hair cuticles: a microscopic study of environmental effects on hair morphology." Journal of Investigative Dermatology 105: 96-99.

Ohta, N., T. Oka, K. Inoue, N. Yagi, S. Kato and I. Hatta (2005). "Structural analysis of cell membrane complex of a hair fibre by micro-beam X-ray diffraction." Journal of Applied Crystallography 38: 274-279.

Orfanos, C. E., W. Montagna, G. Stuttgen and J. A. Swift, Eds. (1981). Hair Research. Berlin, Springer-Verlag.

Orwin, D. F. G., J. L. Woods and S. L. Ranford (1984). "Cortical cell types and their distribution in wool fibres." Australian Journal of Biological Sciences 37: 237-255.

Parry, D. A. (1996). "Hard alpha-keratin intermediate filaments: an alternative interpretation of the low-angle equatorial x-ray diffraction pattern, and the axial disposition of putative disulphide bonds in the intra- and inter-protofilamentous networks." International Journal of Biological Macromolecules 19: 45-50.

Parry, D. A. D., R. D. B. Fraser and T. P. MacRae (1979). "Repeating patterns of amino acid residues in the sequences of some high sulphur proteins from alpha-keratin." International Journal of Biological Macromolecules 1: 17-22.

Parry, D. A. D. and A. C. T. North (1998). "Hard alpha-keratin intermediate filament chains: Substructure of the N- and C- terminal domains and the predicted structure and function of the C-terminal domains of Type I and Type II chains." Journal of Structural Biology 122: 67-75.

Parry, D. A. D. and P. M. Steinert (1995). Intermediate Filament Structure. Georgetown, Texas, USA, R.G. Landes.

Parry, D. A. D., S. V. Strelkov, P. Burkhard, U. Aebi and H. Herrmann (2007). "Towards a molecular description of intermediate filament structure and assembly." Experimental Cell Research 313: 2204-2216.

Pauling, L., R. B. Corey and H. R. Branson (1951). "The Structure of Proteins: Two Hydrogen-Bonded Helical Configurations of the Polypeptide Chain." Proceedings of the National Academy of Science in Washington 37: 205-211.

Pierson, E. and H. Gerts. (2008). "Electron Microscope (FESEM) applications: Hair." Retrieved 30/07/2010, 2010, from http://www.vcbio.science.ru.nl/images/fesem_hair001.jpg.

Plowman, J. E., W. G. Bryson and T. W. Jordan (2000). "Application of proteomics for determining markers for wool quality traits." Electrophoresis 21: 1899-1906.

Plowman, J. E., S. Deb-Choudhury, W. G. Bryson, S. Clerens and J. M. Dyer (2009). "Protein Expression in Orthocortical and Paracortical cells of Merino Wool Fibres." Journal of Agricultural and Food Chemistry 57: 2174-2180.

Plowman, J. E., L. N. Paton and W. G. Bryson (2007). "The differential expression of proteins in the cortical cells of wool and hair fibres." Journal of Experimental Dermatology 16: 707-714.

Potsch, L. and M. R. Moeller (1996). "On pathways of smaller molecules into and out of human hair fibers." Journal of Forensic Science 41(1): 121-125.

Rafik, M. E., J. Doucet and F. Briki (2004). "The Intermediate Filament Architecture as Determined by X-Ray Diffraction Modeling of Hard Alpha-Keratin." Biophysical Journal 86(6): 3893-3904.

Robbins, C. (2009). "The cell membrane complex: Three related but different cellular cohesion components of mammalian hair fibers." Journal of Cosmetic Science 60: 437-465.

Robbins, C., H.-D. Weigmann, S. Ruetsch and Y. Kamath (2004). "Failure of intercellular adhesion in hair fibers with regard to hair condition and strain condition." Journal of Cosmetic Science 55: 351-371.

Rogers, G. E. (1959a). "Electron microscope studies of hair and wool." Annals of the New York Academy of Sciences 83: 378-399.

Rogers, G. E. (1959b). "Electron microscopy of wool." Journal of Ultrastructure Research 2: 309-330.

Rogers, G. E., Ed. (1964). The Epidermis. Lake Arrolhead, Academic Press.

Rogers, M. A., L. L. H. Winter, B. I. S. Praetzel and J. Schweizer (2004). "Characterization of a second high sulfur KAP gene domain on human chromosome 21q22.1." Journal of Investigative Dermatology 122: 147-158.

Rogers, M. A., L. Langbein, S. Praetzel-Wunder, H. Winter and J. Schweizer (2006). "Human Hair Keratin-Associated Proteins (KAPs)." International Review of Cytology 251: 209-263.

Rogers, M. A., L. Langbein, H. Winter, C. Ehmann, S. Praetzel, B. Korn and J. Schweizer (2001). "Characterisation of a cluster of human high/ultrahigh sulphur keratin associated protein genes embedded in the Type I keratin gene domain on chromosome 17q12-21." The Journal of Biological Chemistry 276(22): 19440-19451.

Rogers, M. A., L. Langbein, H. Winter, C. Ehmann, S. Praetzel and J. Schweizer (2002). "Characterisation of a first domain of human high glycine-tyrosine and high sulphur keratin associated protein (KAP) genes on chromosome 21q22.1." The Journal of Biological Chemistry 277(50): 48993-49002.

Rogers, M. A. and J. Schweizer (2005). "Human KAP Genes, Only the Half of it? Extensive Size Polymorphisms in Hair Keratin-Associated Protein Genes." Journal of Investigative Dermatology 124: 7-9.

Shimomura, Y., N. Aoki, J. Schweizer, L. Langbein, M. A. Rogers, H. Winter and M. Ito (2002). "Polymorphisms in the Human High Sulphur Hair Keratin-associated Protein 1, KAP1, Gene Family." The Journal of Biological Chemistry 277(47): 45493-45501.

Shimomura, Y. and M. Ito (2005). "Human Hair Keratin-Associated Proteins." The Society for Investigative Dermatology 10: 230-233.

Signori, V. and D. M. Lewis (1997). "FTIR investigation of the damage produced on human hair by weathering and bleaching processes: implementation of different sampling techniques and data processing." International Journal of Cosmetic Science 19: 1-13.

Snigirev, A., V. Kohn, I. Snigireva and B. Lengeler (1996). "A compound refractive lens for focusing high-energy X-rays." Nature 384: 49-51.

Somogyi, A., M. Drakopoulos, L. Vincze, B. Vekemans, C. Camerani, K. Janssens, A. Snigirev and F. Adams (2001). "ID18F: a new x-ray fluorescence end-station at the European Synchrotron Radiation Facility (ESRF): preliminary results." X-ray Spectrometry 30: 242-252.

Spei, M. (1975). The ordered matrix: fact or artefact. 5th Wool and Textile Research Conference, Aachen.

Stilson, J. (2009). Good Hair. U.S.A., Roadside Attractions.

Swift, J. A. (1999). "Human hair cuticle: biologically conspired to the owner's advantage." Journal of Cosmetic Science 50: 23-47.

Swift, J. A. and A. W. Holmes (1965). "Degradation of human hair by papain. Part II. Some electron microscope observations." Textile Research Journal 35: 1014-1019.

Synchrotron, S. (2005). "Synchrotron Radiation." Retrieved 23/06/2010, 2010, from http://en.wikipedia.org/wiki/File:Sch%C3%A9ma_de_principe_du_synchrotron.jpg.

Takizawa, T., T. Takizawa, S. Arai, M. Osumi and T. Saito (1998). "Ultrastructure of Human Scalp Hair Shafts as Revealed by Freeze-Substitution Fixation." The Anatomical Record 251: 406-413.

Urban, V., P. Panine, C. Ponchut, P. Boesecke and T. Narayanan (2003). "Two-dimensional camera for millisecond range time-resolved small-and wide-angle X-ray scattering." Journal of Applied Crystallography 36: 809-811.

Wagner, R. D. C. C., P. K. Kiyohara, M. Silveira and I. Joekes (2007). "Electron microscopic observations of human hair medulla." Journal of Microscopy 226(1): 54-63.

Wei, G., B. Bhushan and P. M. Torgerson (2005). "Nanomechanical characterization of human hair using nanoindentation and SEM." Ultramicroscopy 105: 248-266.

Wertz, P. and D. Downing (1989). "Integral lipids of mammalian hair." Comparative Biochemistry and Physiology Part B: Comparative Biochemistry 92(4): 759-761.

Wertz, P. W., W. Abraham, L. Landmann and D. T. Downing (1986). "Preparation of liposomes from stratum corneum lipids." Journal of Investigative Dermatology 87(5): 582-584.

Young, H. D., R. A. Freedman and L. Ford, Eds. (2007). University Physics with Modern Physics, Addison-Wesley.

Appendix I – Microfocus X-ray diffraction scans

This appendix shows the integrated intensity plots and the composite images for the scans which were not shown in Chapter 6. The integrated intensity plots of the eight sectors and the composite images will be shown for each hair type in turn along with a commentary on the data as in Chapter 6.

I.1 – Afro Hair

Figure I.1 shows that in this scan of the Afro hair type there is less cylindrical symmetry and the images showing scattering features lie in the range of image 5 - 29 which suggests a fibre width of 120 μm . There are two large dips in the intensity of the small angle signal which are anti-correlated with the signal arising from the KIF interference function at images 4, 25 and 26. Cross referencing the 1-d trace with the composite image for this scan shows that the feature seen at image 4 is not an effect of the scattering from the hair as there are no scattering or diffraction features seen at all in the fibre diagram which means it must be an anomalous effect of the detector or otherwise. However, the features seen at images 25 and 26 are real effects of the scattering arising from the hair. Cross referencing the 1-d trace with the fibre diagrams in the composite image shows that the dip region in the 1-d trace may be evidence of a region towards the edge of the hair fibre which shows a more highly ordered fibrous diffraction signal from the KIFs and less scatter from the amorphous objects such as the KAPs and other structures; this shows evidence of a region with more fibrous structure.

There is a slight asymmetry in the 1-d trace of the small angle signal showing a region with higher intensity towards the latter side of the scan which is correlated with a drop in the total scattering intensity. This may be evidence for a medullary structure with more amorphous structures present to give a larger SAXS signal in these images. There was no evidence seen for lipid diffraction.

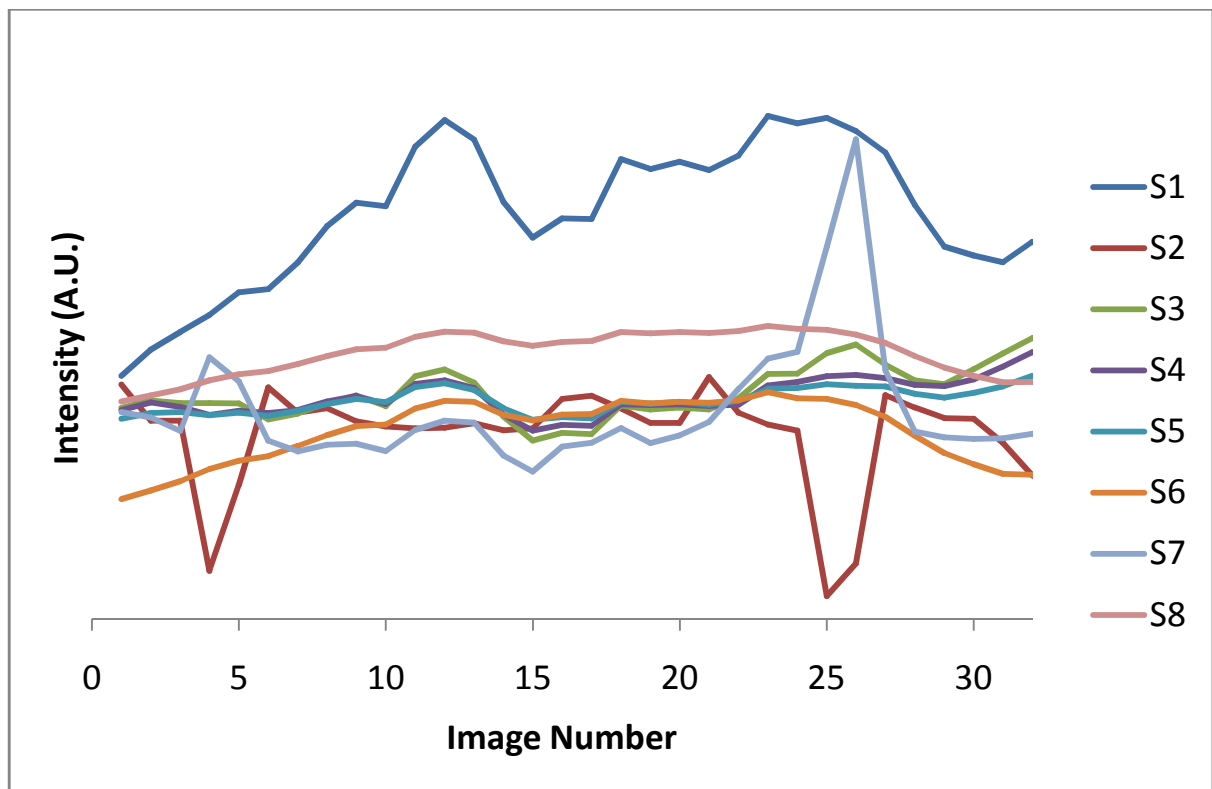


Figure I.1 – The integrated intensity plots for the Afro hair.

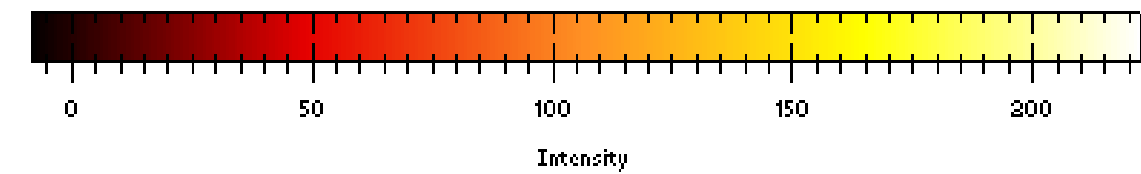
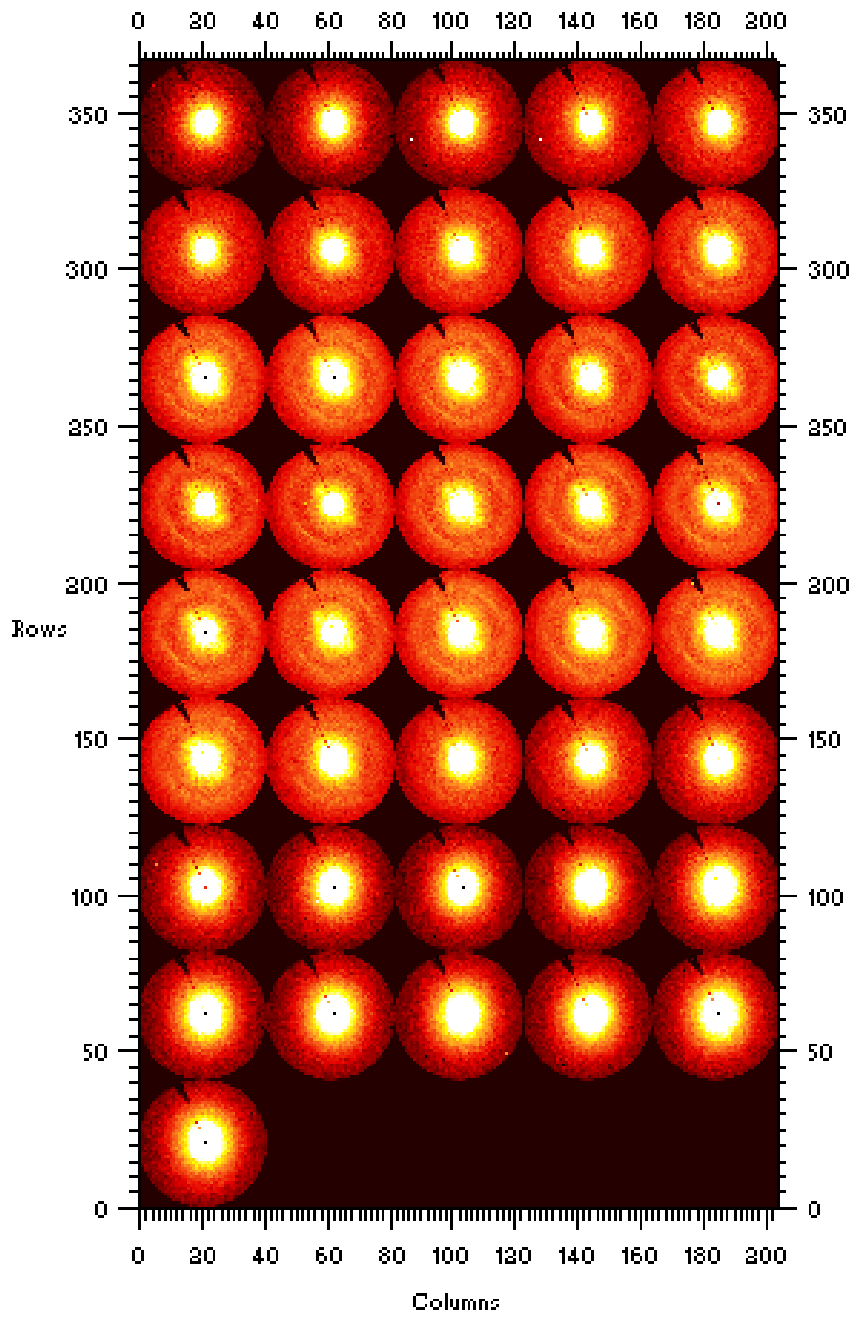


Figure I.2 – Composite image for one of the scans of the Afro hair type.

I.2 – Asian Hair

The Asian hair had 3 complete scans taken in total, the two not shown in Chapter 6 will be presented here.

The scan shown in Figure I.3 had 60 images taken, it can be seen from the 1-d trace corresponding to the total scattering intensity of the fibre diagrams and the composite image that the fibre diagrams that show scattering and diffraction features from the hair lie between images 9-40 which implies a fibre width of 155 μm . The shape of the total scattering 1-d trace shows symmetry with a little less intensity on the latter side of the scan, this implies the hair fibre shows a cylindrical morphology. The data from this 1-d trace also shows regions of higher and lower ordered structures seen from the changes in intensity at image numbers 17-22 and 30-35, these lay either side of what might possibly be a medulla region in the images 24 - 29 (images 26 and 27 mostly). Evidence for this comes from the drop in intensity in both the KIF signal and the total scattering signal. The effect of the large anti-correlation between the small angle signal and the total scattering signal is an effect of the background subtraction. There are large drops in the intensity of the signal arising from the KIFs in the sample at images, 13, 16 and 34 respectively; this implies the presence of sections showing less fibrous order/less fibrous structures. The drop in intensity at image 16 is anti-correlated with a rise in intensity of the small angle signal; this could show less fibrous structures in this region and more amorphous structures such as KAPs.

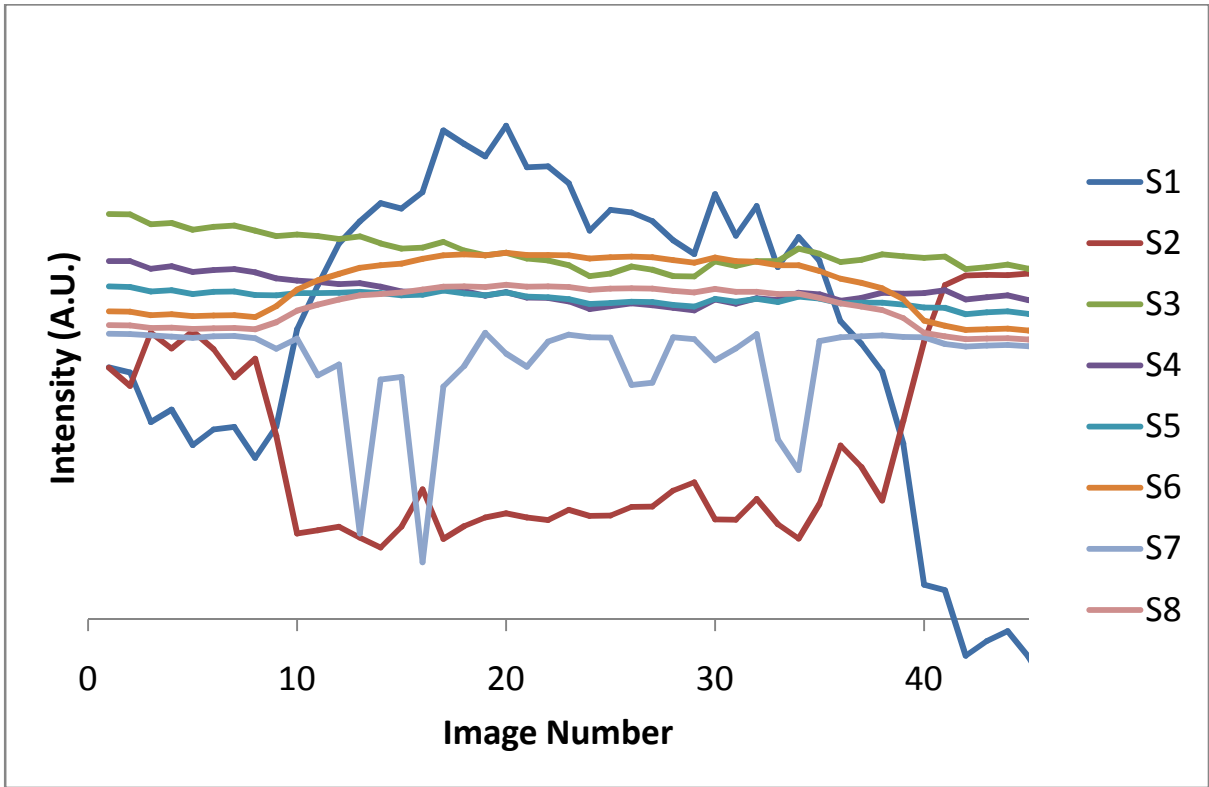


Figure I.3 – The integrated intensity plots for one of the scans of the Asian hair.

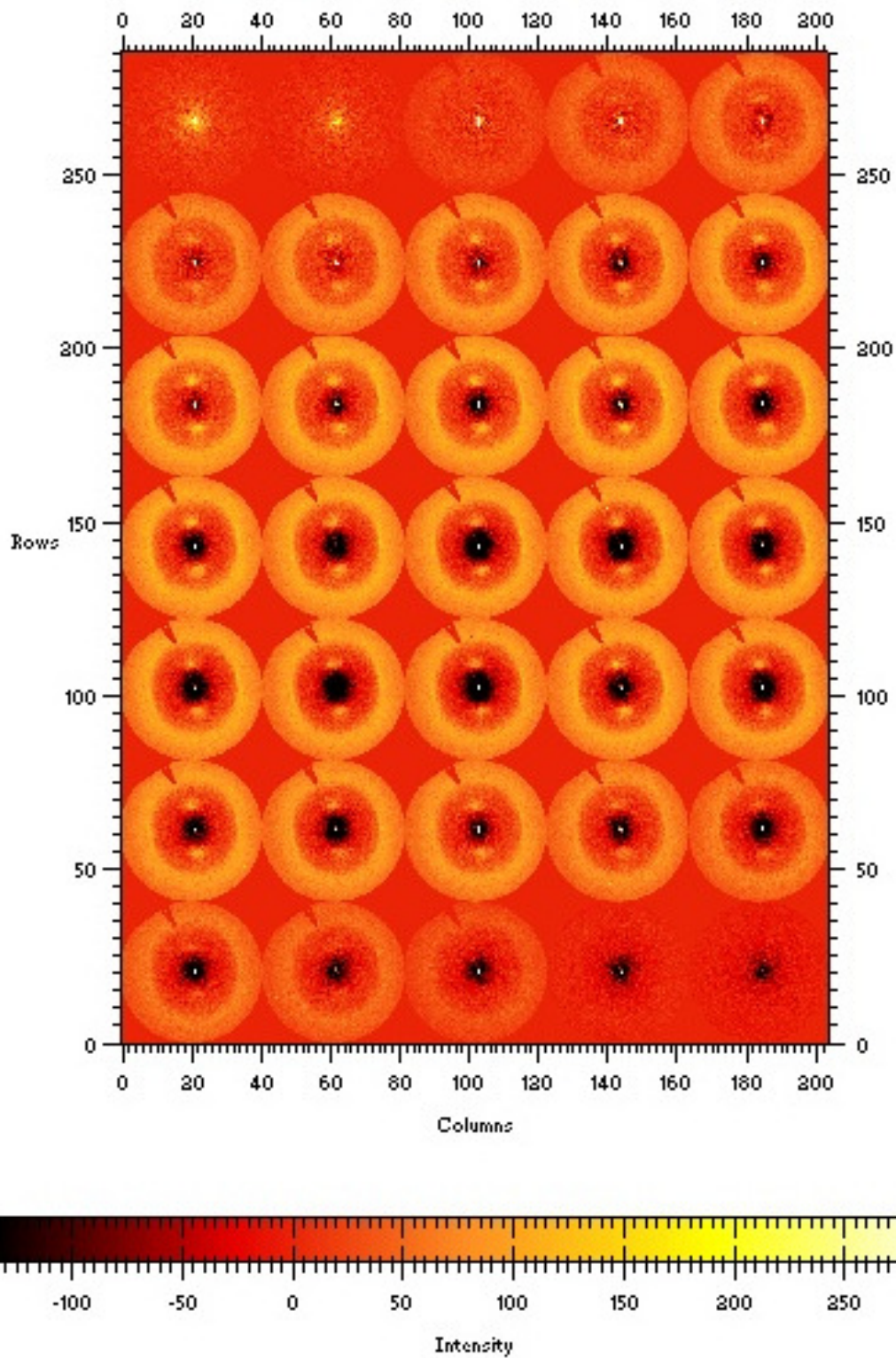


Figure I.4 – Composite image corresponding to the scan for the integrated intensity plots as shown in Figure I.3. The fibre diagrams that did not show any characteristic scattering features from hair were omitted in the composite image shown above.

Figure I.5 shows the integrated intensity plots for one of the scans of the Asian hair. As seen in this figure, the sectors reveal little information as the background subtraction was so poor. There is also evidence for an overall decrease in the flux of the x-ray beam as seen in the way the total scattering intensity falls off towards the latter side of the scan.

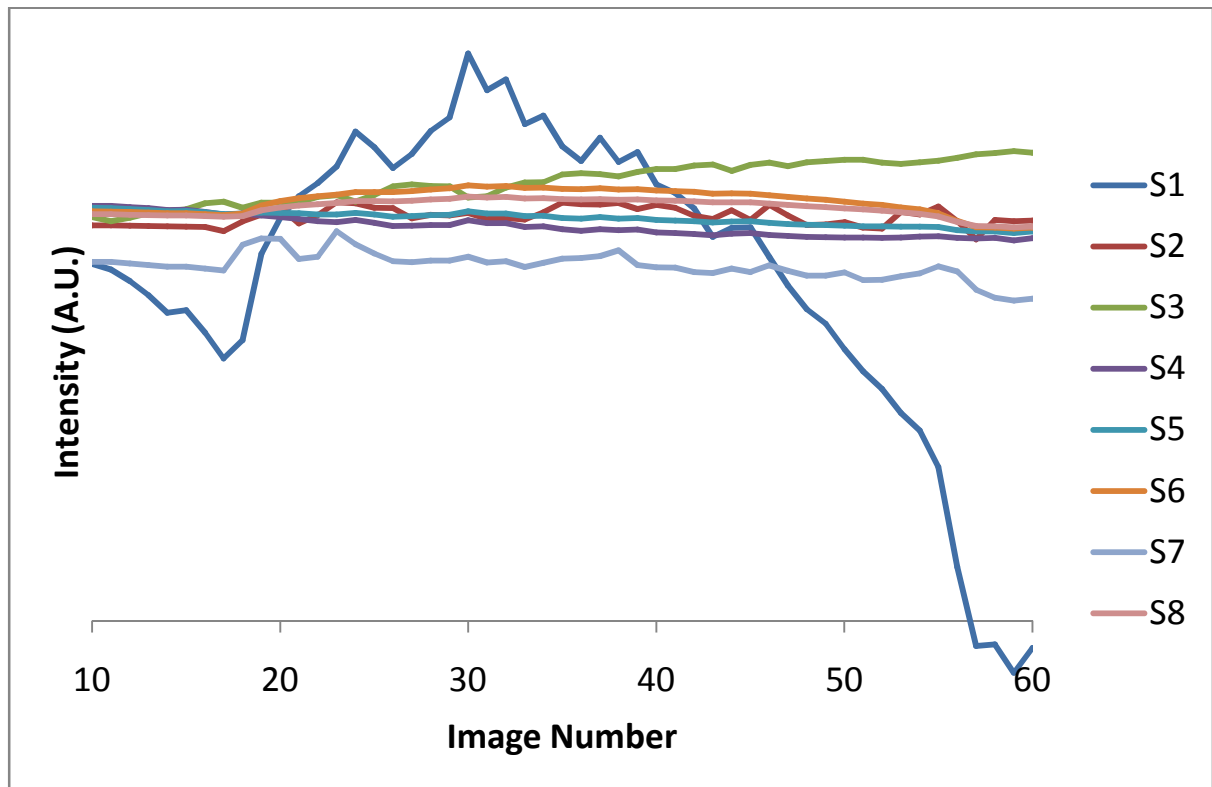


Figure I.5 – The integrated intensity plots for one of the scans for the Asian hair type.

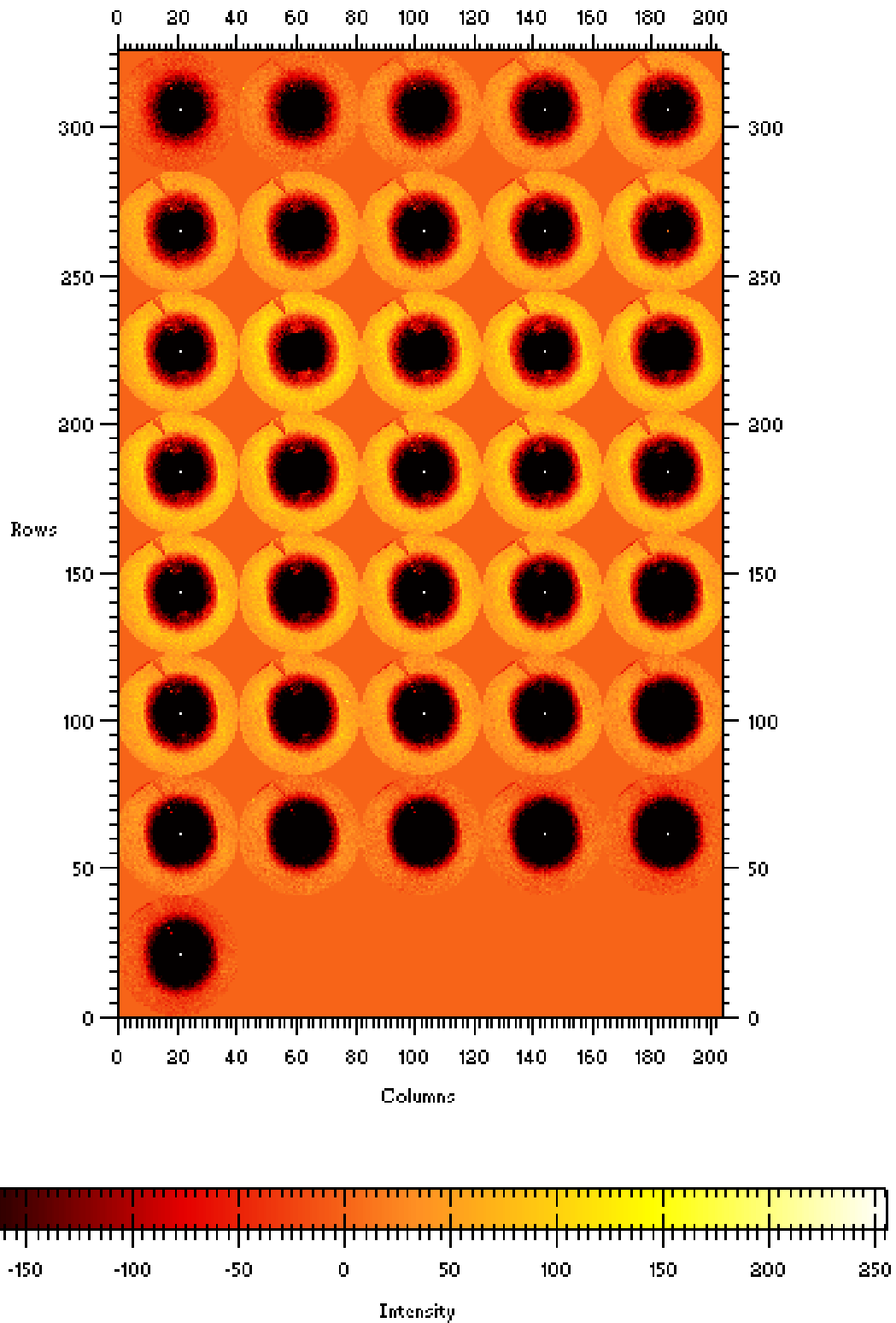


Figure I.6 – Composite image corresponding to the scan for the integrated intensity plots as shown in Figure I.5. The fibre diagrams that did not show any characteristic scattering features from hair were omitted in the composite image shown above.

I.3 – Chinese Hair

The Chinese hair had another two scans taken in the same position as the scan shown in Chapter 6. As can be seen in the scans shown in this appendix, there is a high consistency in the patterns of the integrated intensity plots for all sectors which is evidence of the consistency of the textural variation of the hair fibre at the point of the scan. Figures I.7 and I.8 show the integrated intensity plots for the Chinese hair type. The main differences seen in the 1-d traces between the scans arise from the 1-d traces for the small angle signal and the wide angle diffuse scatter; the traces of these in the scans shown in this appendix shows a lot more variability in the intensity contribution. There is no evidence for lipid diffraction in any of the scans and the 1-d trace of the total scattering intensity implies high consistency in the estimation of the fibre width. The effect of a lower total scattering intensity that is seen between the first scan and the subsequent scans is a direct effect of the flux of the beam; the storage ring of the synchrotron was re-filled shortly after these measurements were taken.

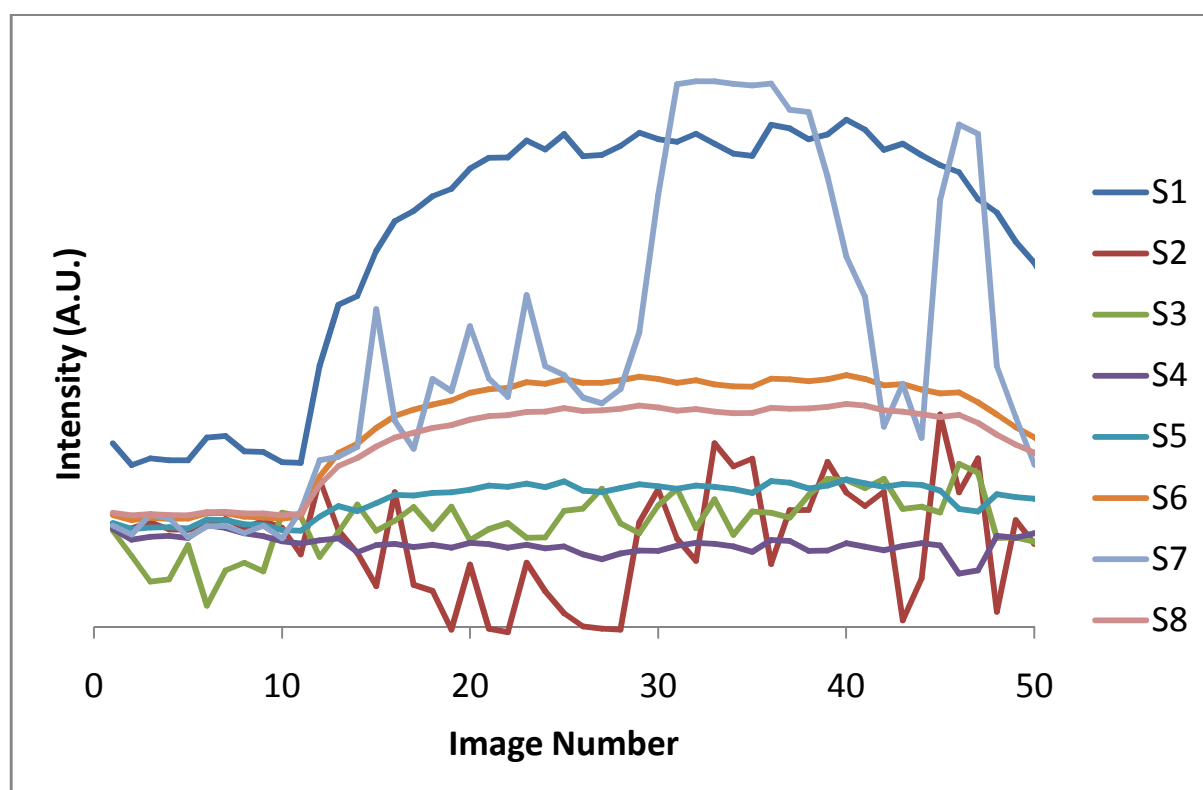


Figure I.7 – The integrated intensity plots for one of the scans of the Chinese hair type.

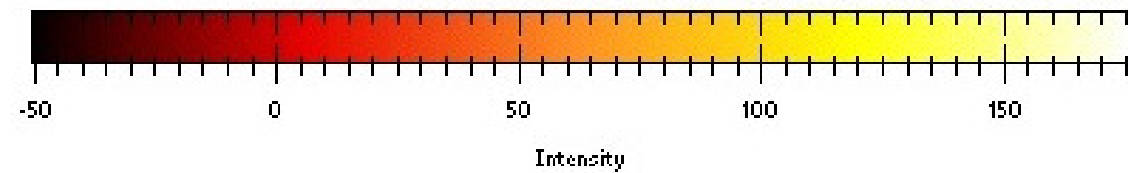
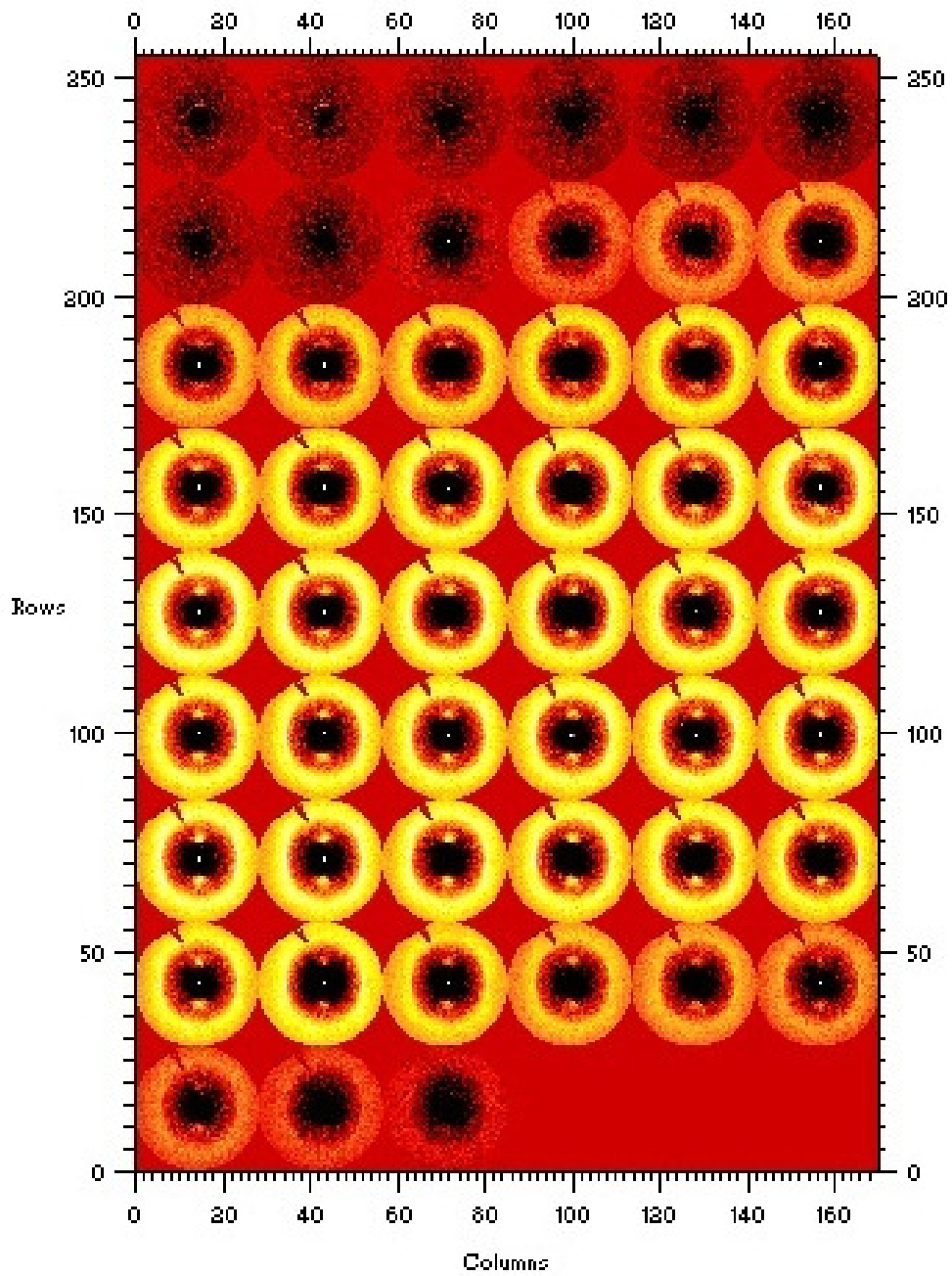


Figure I.8 – Composite image for one of the scans for the Chinese hair type. The composite image shown here is for the scan that is shown in Figure I.7.

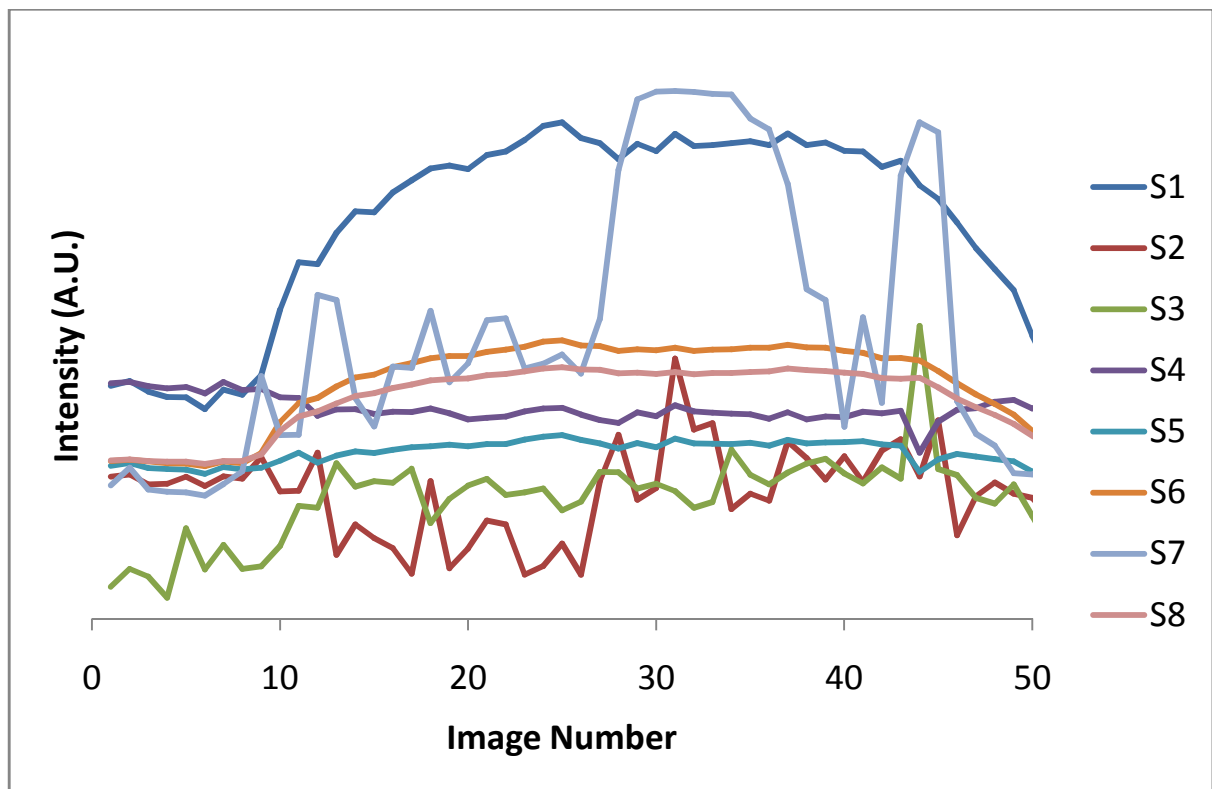


Figure I.9 – The integrated intensity plots for one of the scans of the Chinese hair type.

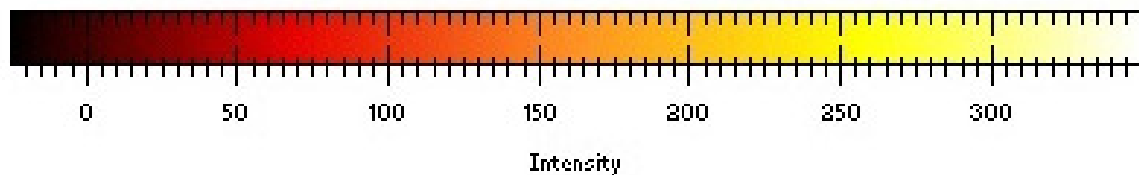
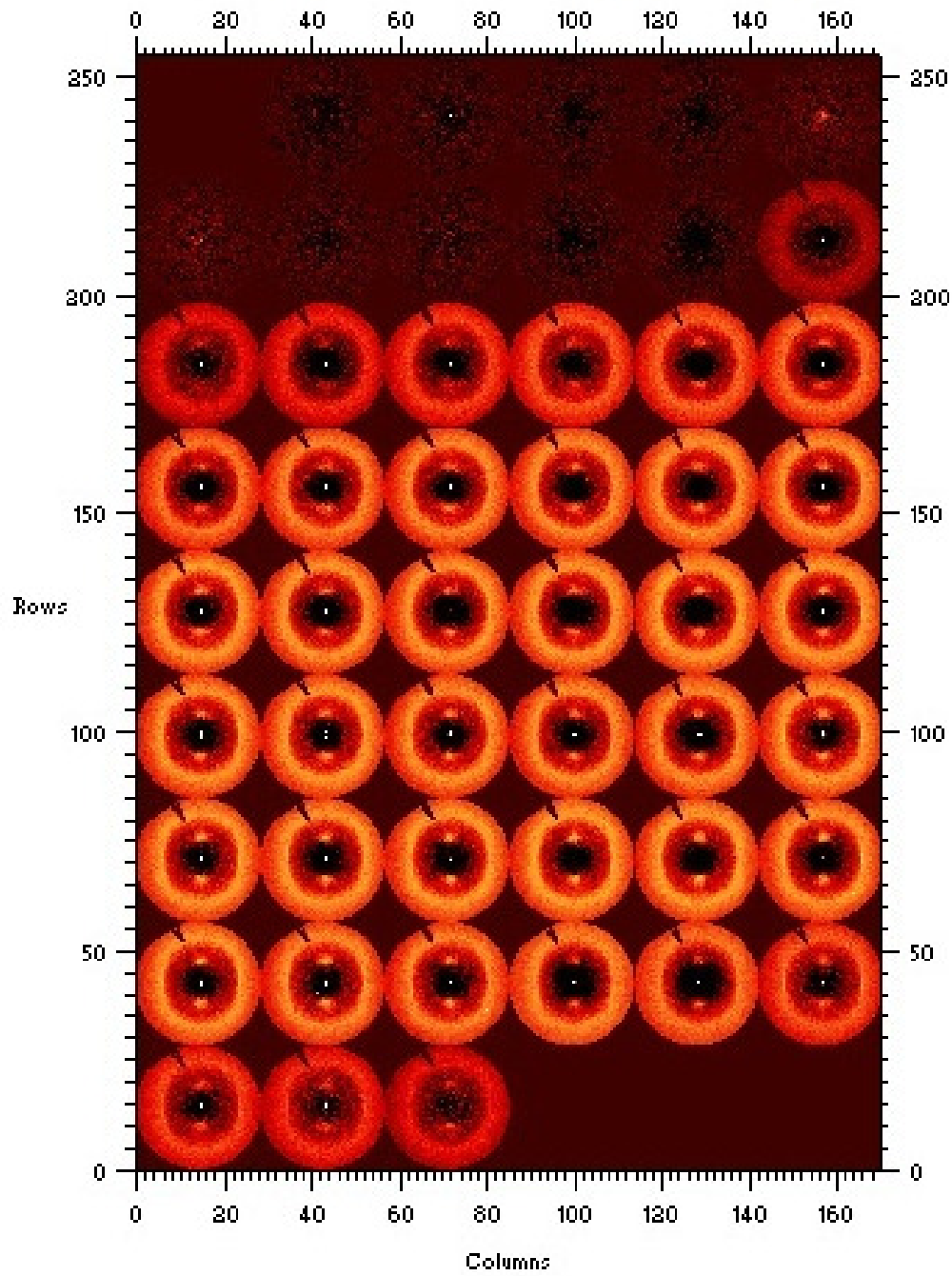


Figure I.10 – Composite image for one of the scans for the Chinese hair type. The composite image shown here is for the scan that is shown in Figure I.9.

I.4 – Japanese Hair

The scans shown in this appendix all show an estimated fibre width lower than that of the scan shown in Chapter 6; the scans as estimated from the integrated intensity plots as shown in Figures I.11 and I.12 show an estimated fibre width of 110 μm . They also show a more asymmetrical shape to the 1-d trace of the total scattering intensity which may be evidence for heterogeneity in the morphological properties of the hair fibre, but may also be a real effect of the decreasing intensity of the synchrotron; the intensity of the 1-d trace of the total scattering signal falls off more rapidly on the latter side of the scan.

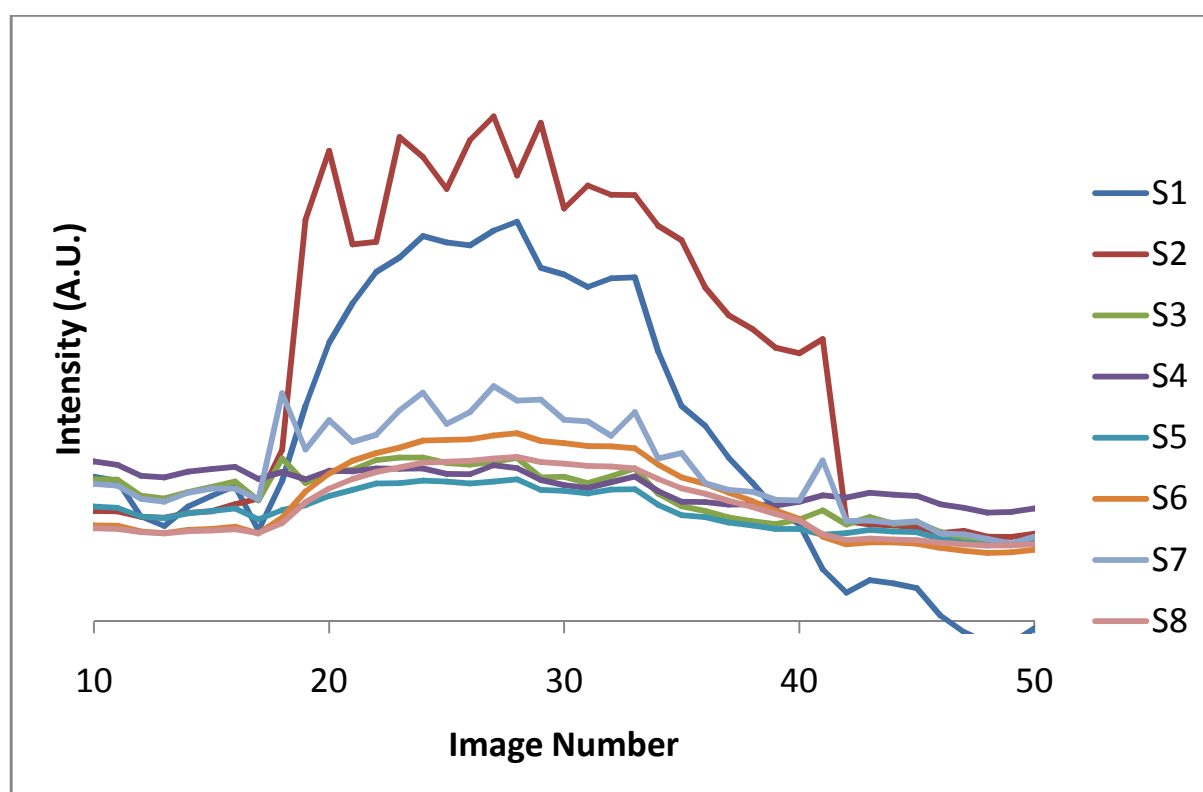


Figure I.11 – The integrated intensity plots for one of the scans of the Japanese hair.

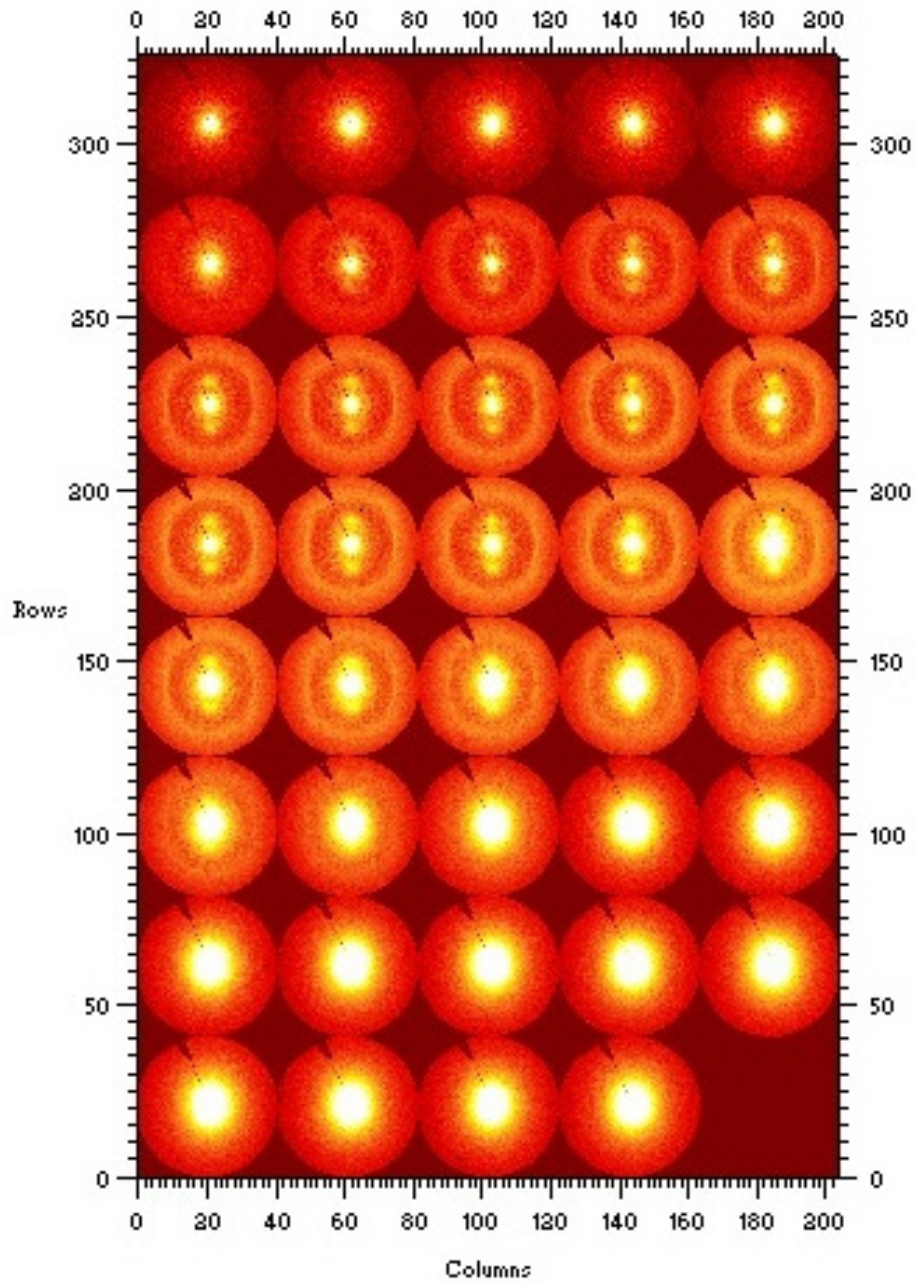


Figure I.12 – Composite image for one of the scans for the Japanese hair type. The scan show here is for the same scan as shown in Figure I.11.

The scan shown in Figure I.11 does not seem to show any notable features as seen in any of the 1-d traces of integrated intensity. There is textural variation across the hair fibre, but there are no significant features to note.

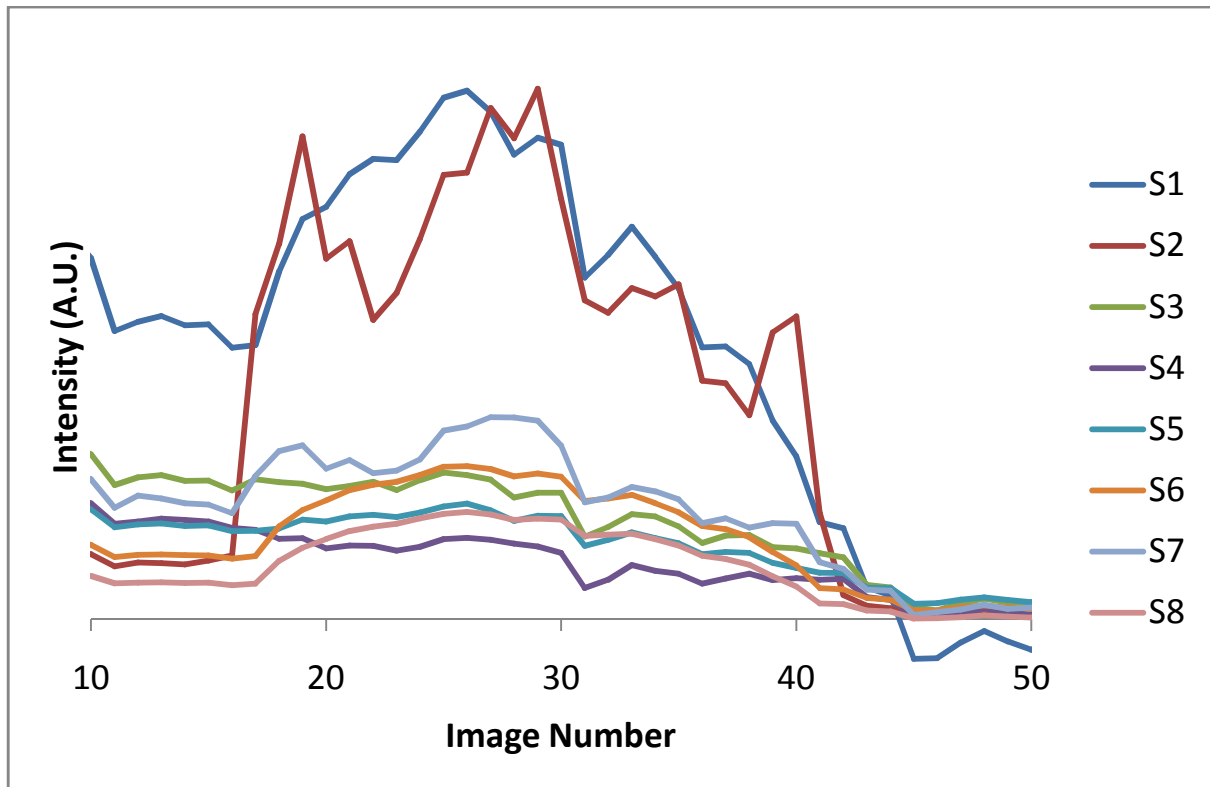


Figure I.13 – The integrated intensity plots for one of the scans of the Japanese hair type.

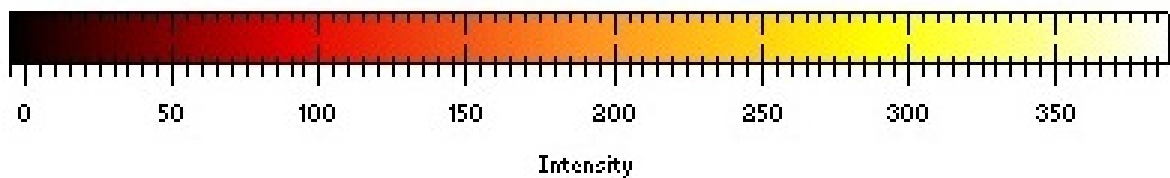
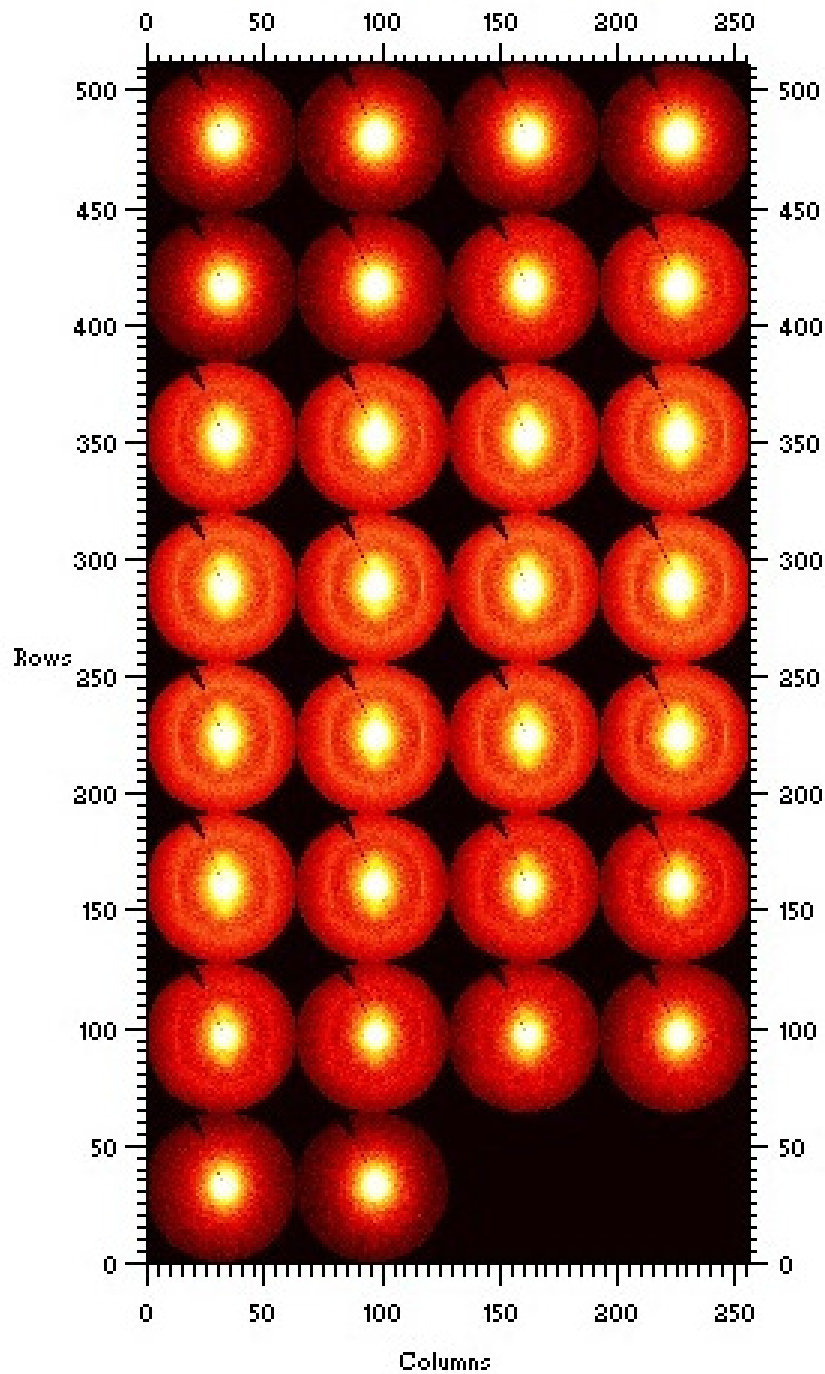


Figure I.14 – Composite image for one of the scans for the Japanese hair type. The scan shown hair is for the same scan as shown in Figure I.13.

The scan shown in Figure I.13 shows a region in the central part of the hair fibre which shows higher intensity for all of the 1-d traces which implies a more ordered central section (see images 25 - 31 of figure I.14) with dimensions of approximately 35 μm . There was no lipid diffraction seen in any of the fibre diagrams in all of the scans.

Appendix II - Gas chromatography Mass spectrometry profiles for lipids

This appendix contains GC/MS profiles for some of the unusual fatty acids that were found in the hair types and for the hydrocarbons that were found in the Afro hair types, specifically the Afro 4 hair sample.

Figure II.1 shows the GC/MS profile for the C14:0 fatty acid.

Figure II.2 shows the GC/MS profile for the C14:1 fatty acid.

Figure II.3 shows the GC/MS profile for the C15:0 fatty acid.

Figure II.4 shows the GC/MS profile for the C21A fatty acid.

Figure II.5 shows the GC/MS profile for the anteiso C15 fatty acid.

Figure II.6 shows the GC/MS profile for the anteiso C17 fatty acid.

Figure II.7 shows the GC/MS profile for the C17 fatty acid.

Figure II.8 shows the GC/MS profile for the C19 fatty acid.

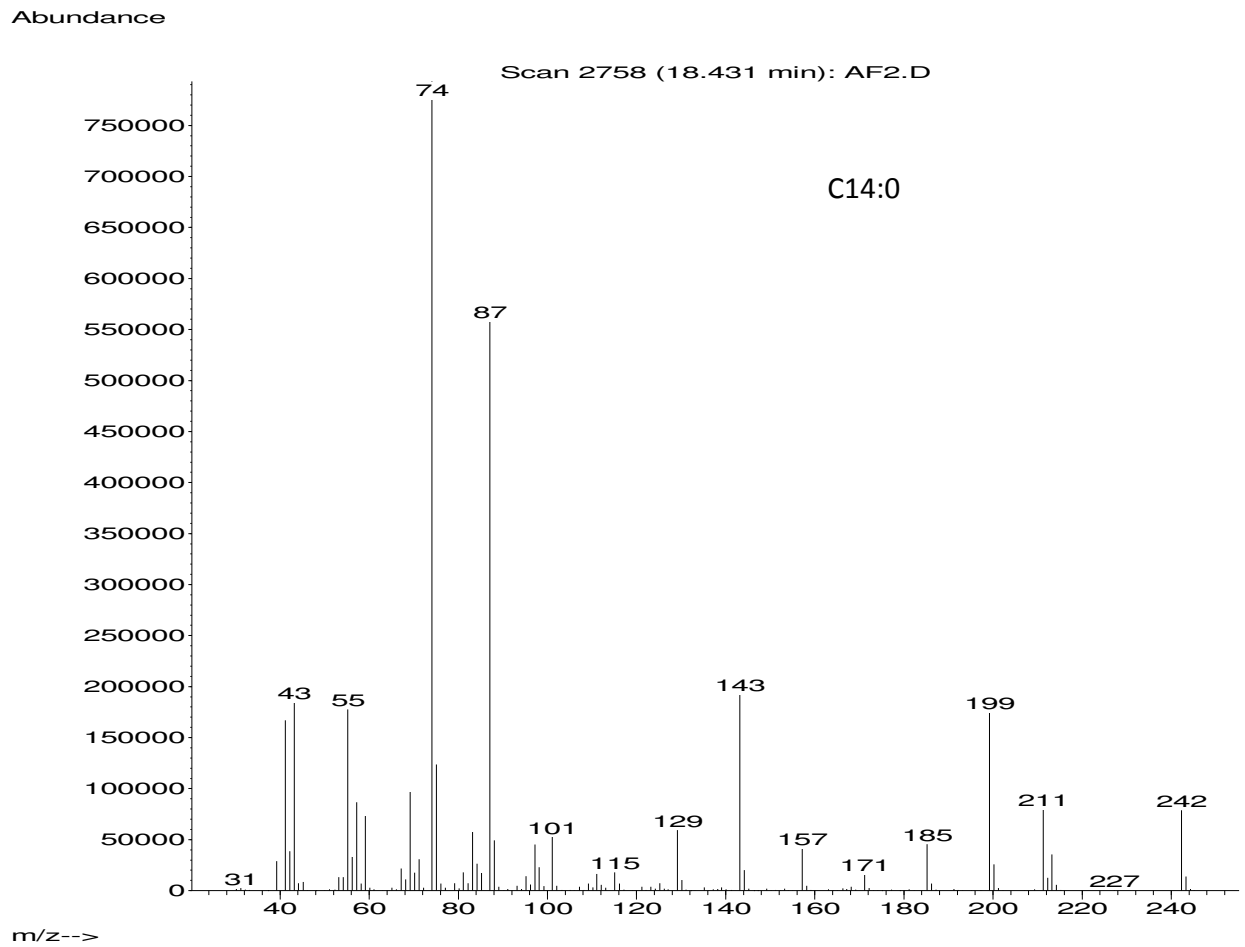


Figure II.1 - GC/MS chromatogram of the C14:0 fatty acid profile. The x axis is the charge to mass ratio (m/z) and the y axis is abundance measured in arbitrary units.

Abundance

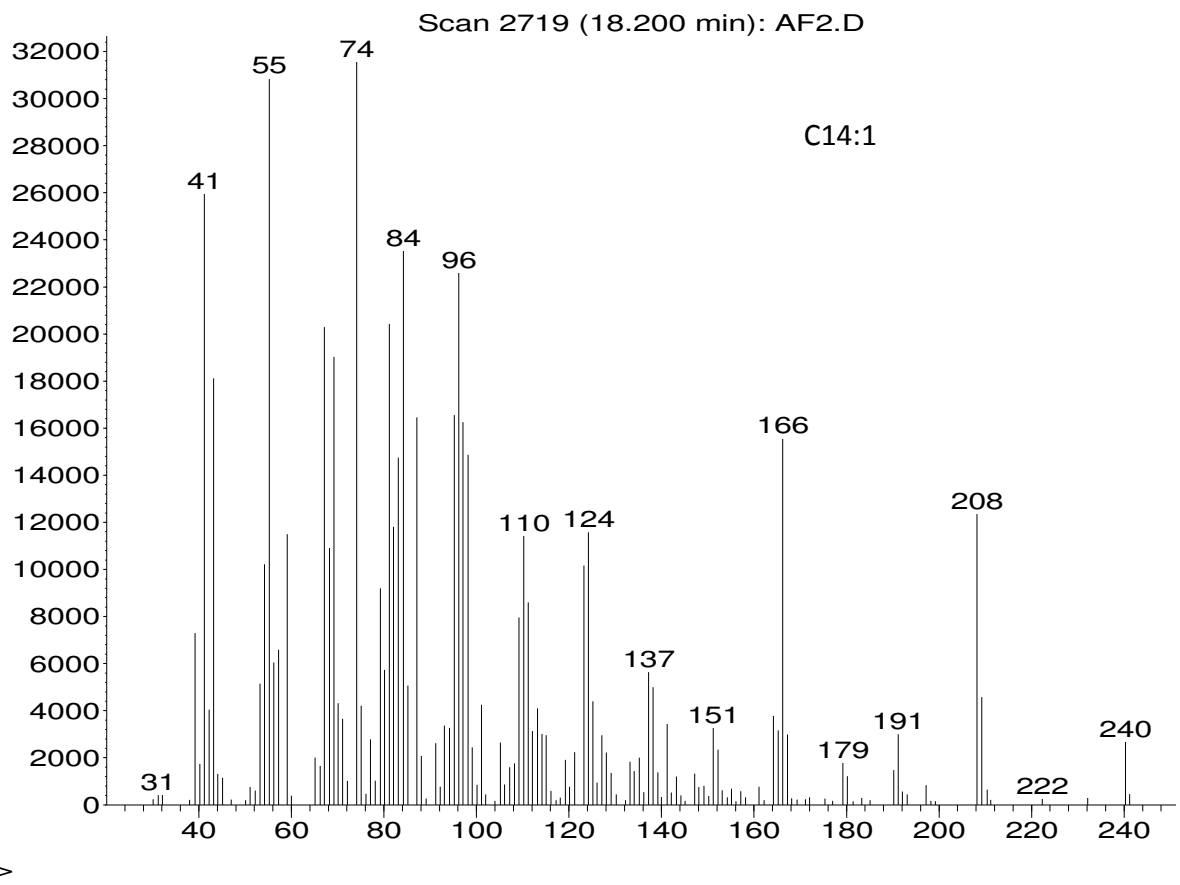


Figure II.2 - GC/MS chromatogram of the C14:1 fatty acid profile. The x axis is the charge to mass ratio (m/z) and the y axis is abundance measured in arbitrary units.

Abundance

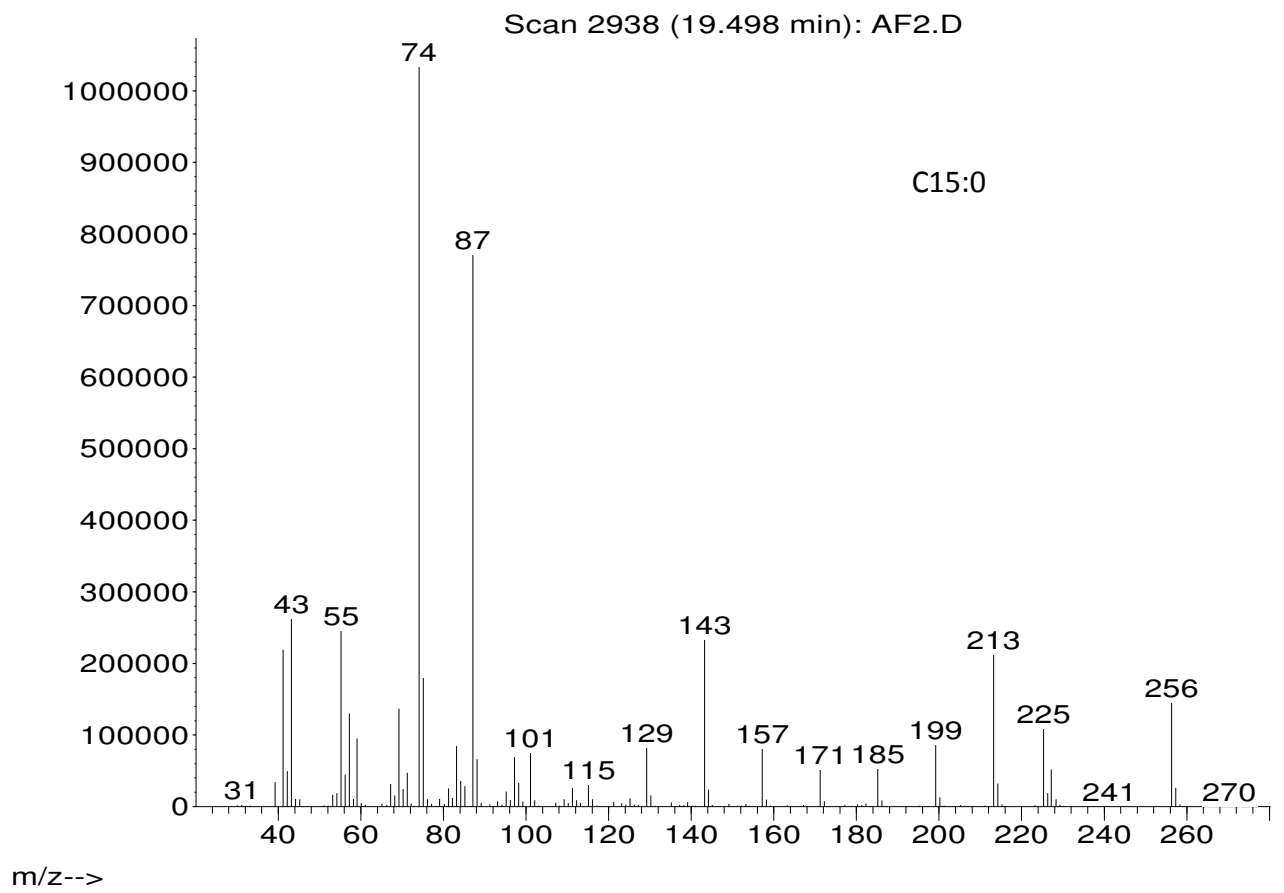


Figure II.3 - GC/MS chromatogram of the C15:0 fatty acid profile. The x axis is the charge to mass ratio (m/z) and the y axis is abundance measured in arbitrary units.

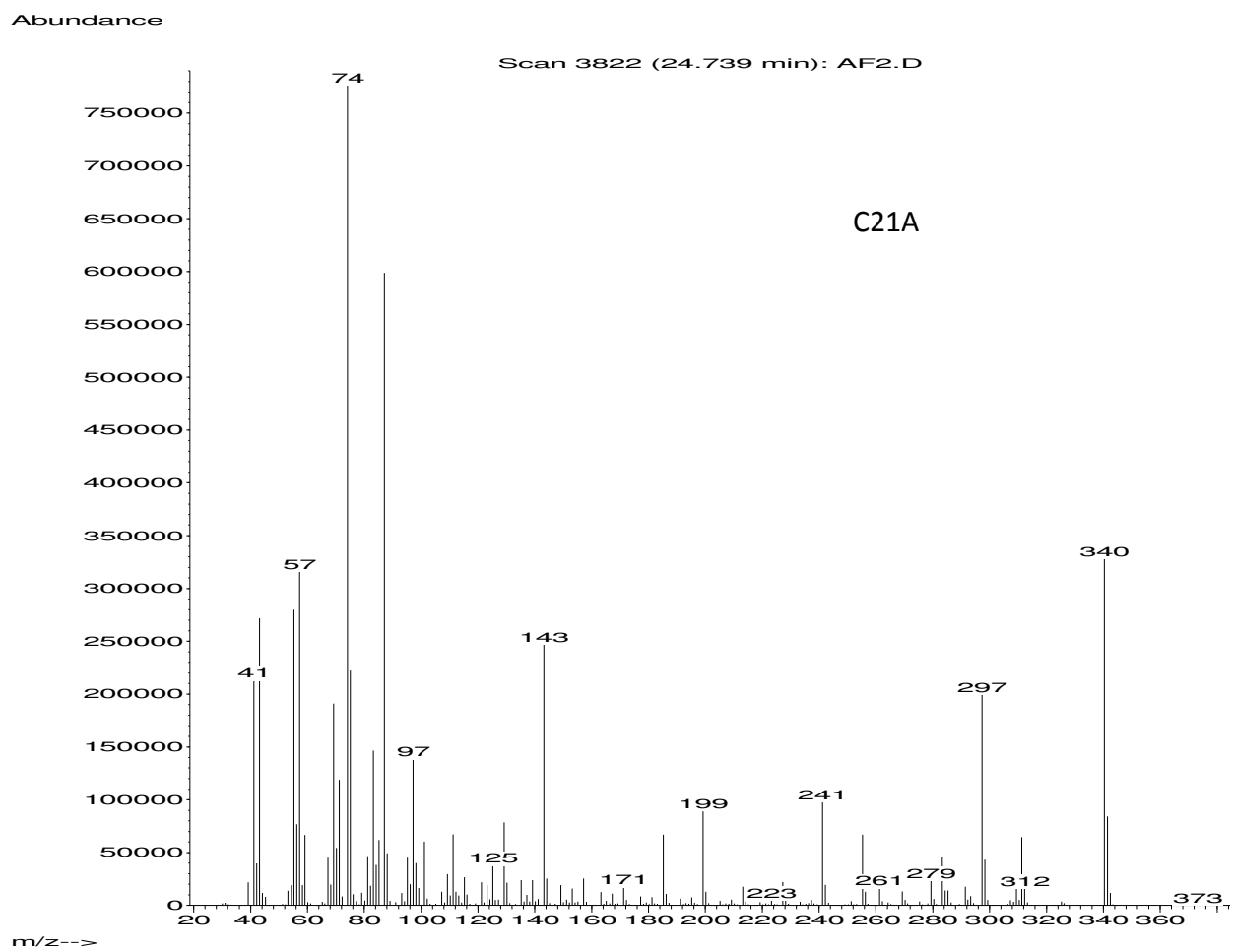


Figure II.4 - GC/MS chromatogram of the C21A fatty acid profile. The x axis is the charge to mass ratio (m/z) and the y axis is abundance measured in arbitrary units.

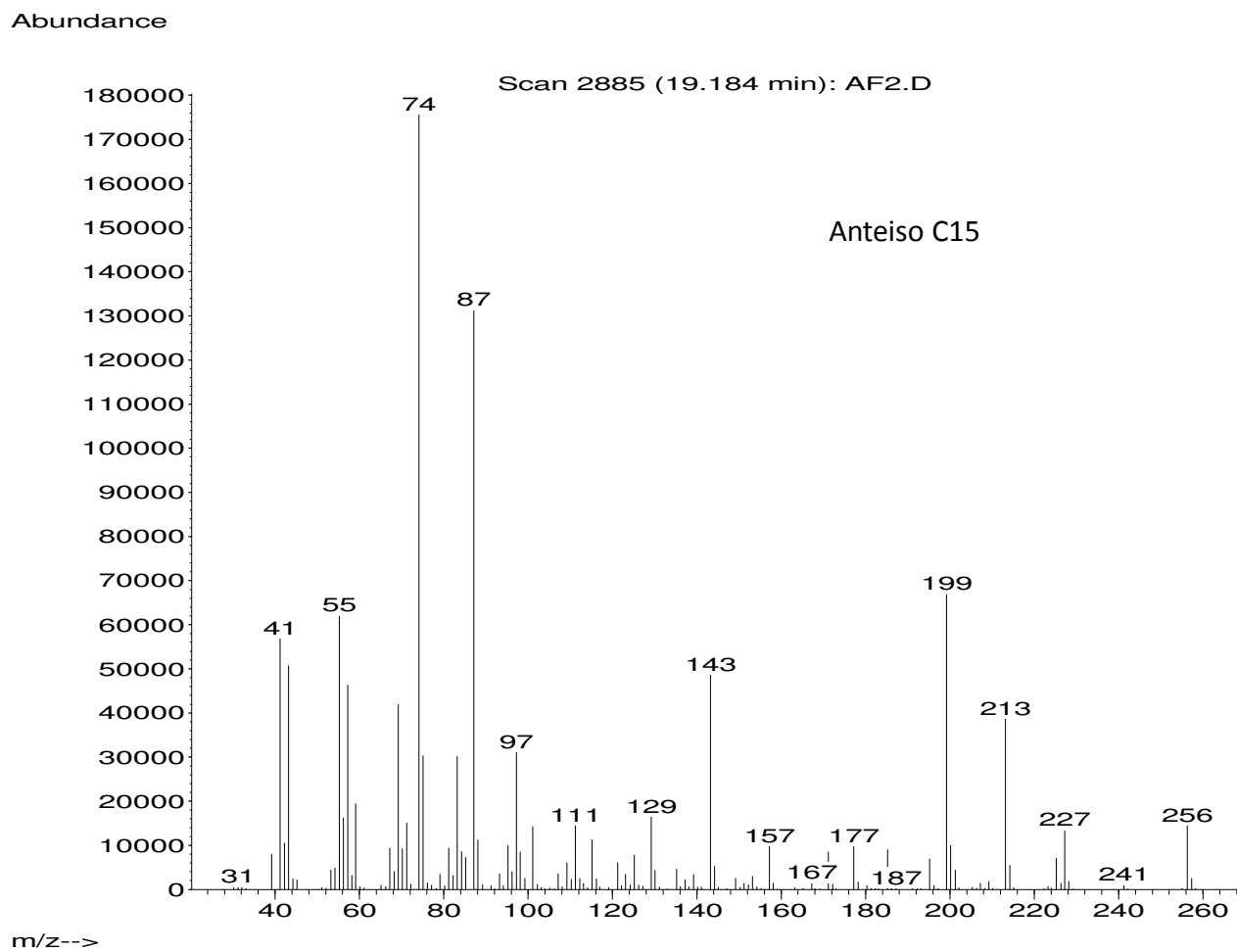


Figure II.5 - GC/MS chromatogram of the anteiso C15 fatty acid profile. The x axis is the charge to mass ratio (m/z) and the y axis is abundance measured in arbitrary units.

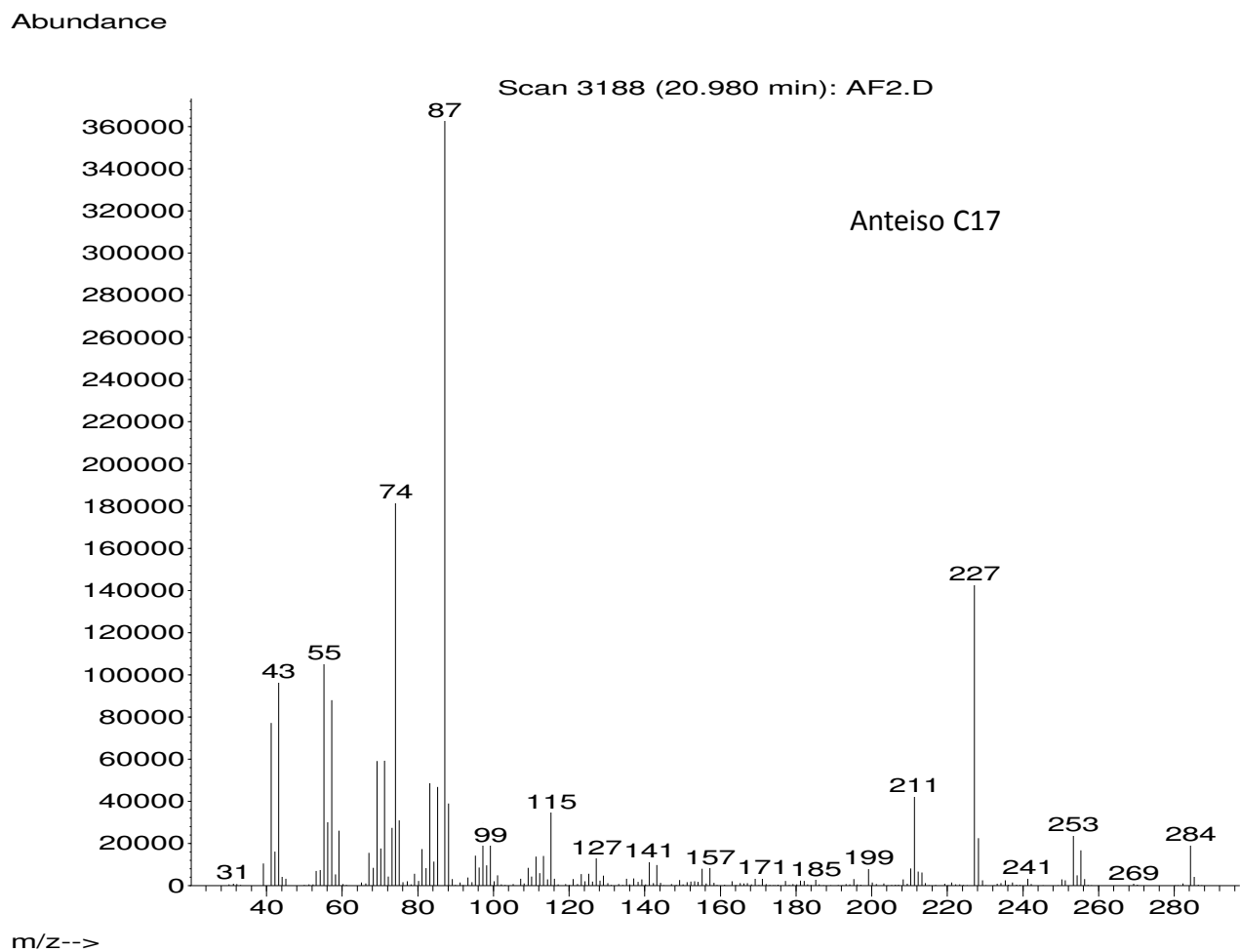


Figure II.6 - GC/MS chromatogram of the anteiso C17 fatty acid profile. The x axis is the charge to mass ratio (m/z) and the y axis is abundance measured in arbitrary units.

Abundance

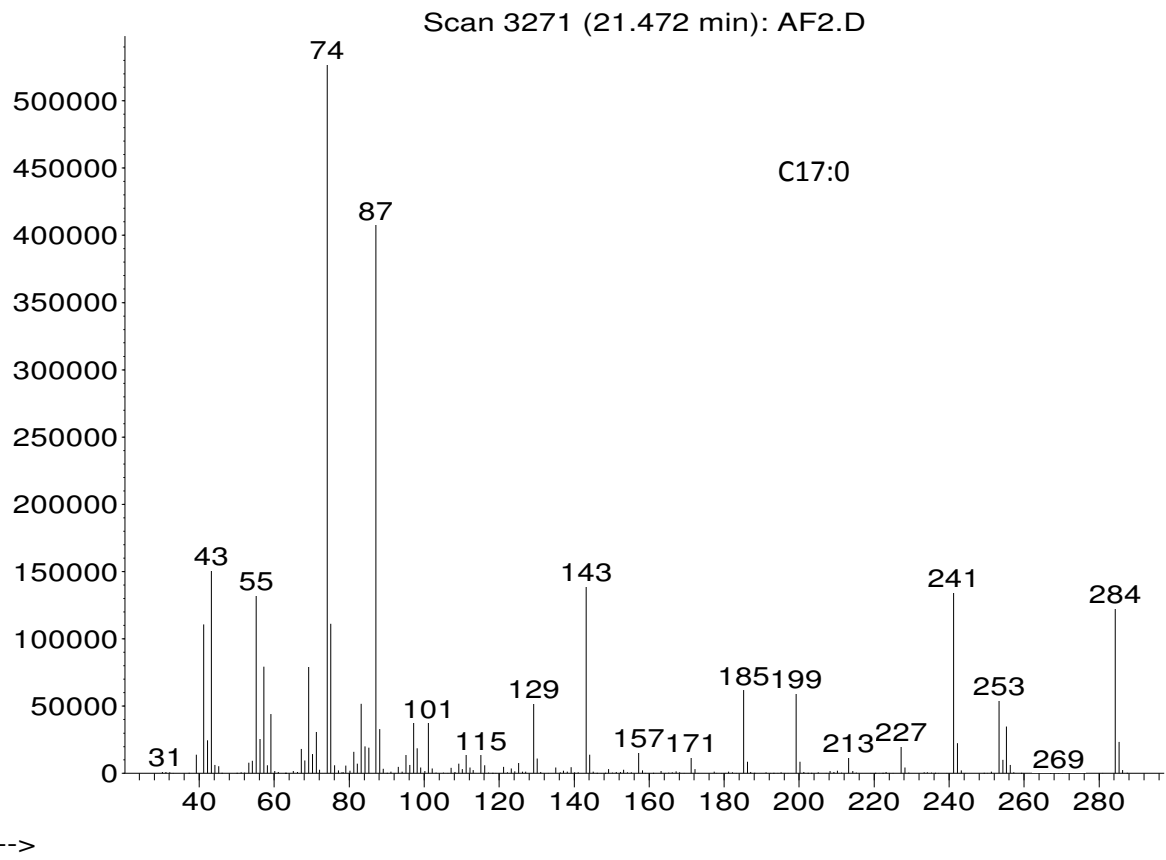


Figure II.7 - GC/MS chromatogram of the C17:0 fatty acid profile. The x axis is the charge to mass ratio (m/z) and the y axis is abundance measured in arbitrary units.

Abundance

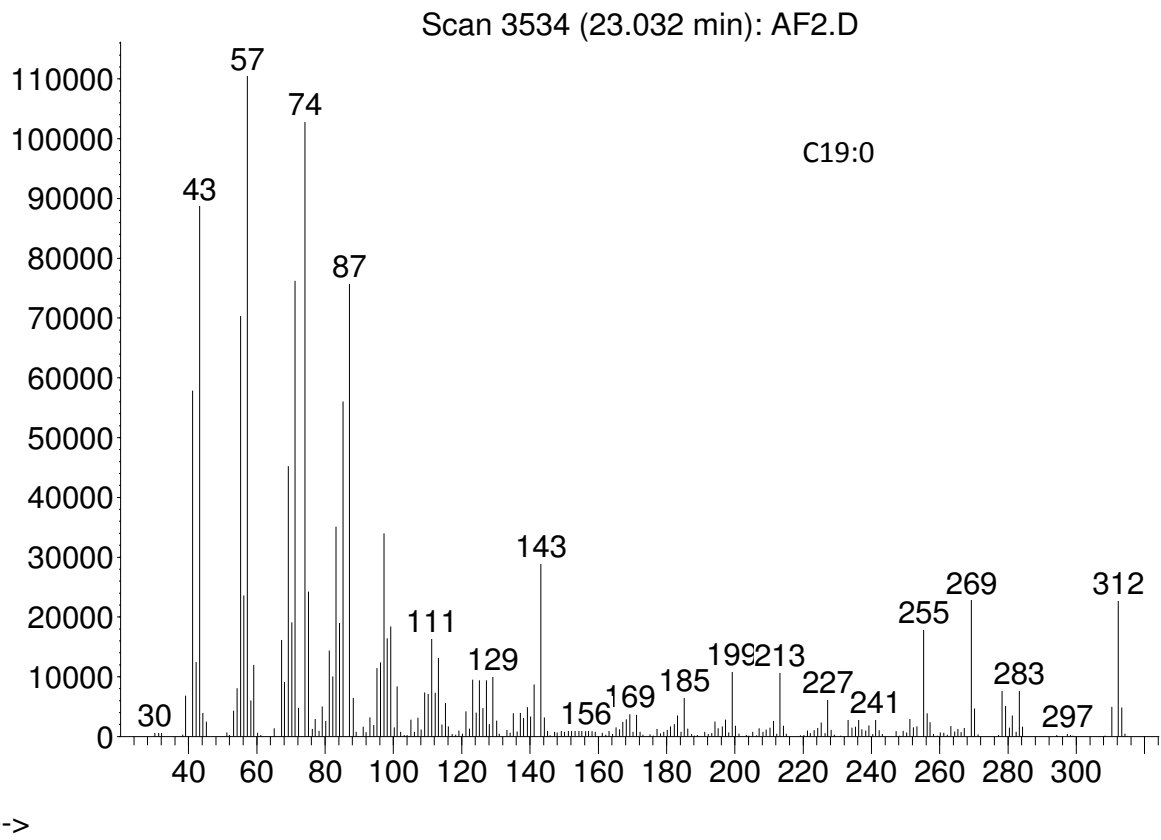


Figure II.8 - GC/MS chromatogram of the C19:0 fatty acid profile. The x axis is the charge to mass ratio (m/z) and the y axis is abundance measured in arbitrary units.

Appendix III – Lipid Tables

This appendix shows tables of information containing the quantified fatty acid methyl ester (FAME) content expressed as an average (mean) percentage for each lipid class by each extraction procedure. The tables shall be presented in extraction procedure order (Hexane wash, solvent extraction, hydrolysis step) and then sub-divided according to lipid class; wax esters (WE), triacylglycerols (TAG), free fatty acids (FFA) and polar lipids (PL).

III.1 Tables of quantified FAME content for the Hexane Wash

Table III.1 shows the FAME content of the WEs that were extracted in the hexane wash expressed as an average (mean) percentage along with its associated standard deviation.

Table III.2 shows the FAME content of the FFAs that were extracted from the hair types in the hexane wash expressed as an average (mean) percentage along with its associated standard deviation.

Table III.3 shows the FAME content of the TAG that were extracted from the hair types in the hexane wash expressed as an average (mean) percentage along with its associated standard deviation.

The TAG content in the hexane wash was variably present among the hair types and samples; most hair samples did not show any TAG content extracted via the hexane wash protocol. In detail, only one of the European samples showed TAG content, four Mullato, two Spanish, one Thai and one Chinese hair type. The Afro and Japanese hair types showed no detectable TAG content. Table III.3 therefore provides the data for the TAG content in the hexane wash, the values for the Mullato and the Spanish hair types are mean values, the values shown for the Chinese, European and Thai are the ones that were able to be detected.

III.2 Lipid tables for the Solvent Extraction

Table III.4 shows the FAME content for the PL extracted in the solvent extraction process expressed as an average (mean) percentage of that lipid class by hair type along with its associated standard deviation.

Table III.5 shows the FAME content for the FFA extracted in the solvent extraction process expressed as an average (mean) percentage of that lipid class by hair type along with its associated standard deviation.

Table III.6 shows the FAME content for the TAG extracted in the solvent extraction process expressed as an average (mean) percentage of that lipid class by hair type along with its associated standard deviation.

Table III.7 shows the FAME content for the WE extracted in the solvent extraction process expressed as an average (mean) percentage of that lipid class by hair type along with its associated standard deviation.

III.3 Lipid tables for the Hydrolysed Fraction

Table III.8 shows the mean content of the FAME extracted from the hydrolysed fraction expressed as an average (mean) percentage along with its associated standard deviation.

	AFRO	CHI	EU	JAP	MU	SPAN	THAI
C12:0 (%)	0.11 ± 0.25	n.d.	n.d.	n.d.	n.d.	n.d.	n.d.
C12:1 (%)	0.06 ± 0.14	n.d.	n.d.	n.d.	n.d.	n.d.	n.d.
C14:0 (%)	2.20 ± 0.92	n.d.	1.35 ± 1.56	n.d.	2.83 ± 1.27	n.d.	1.00 ± 0.68
C14:1i (%)	3.42 ± 1.01	n.d.	2.30 ± 2.83	n.d.	5.33 ± 1.65	n.d.	3.75 ± 2.53
C15:0 (%)	2.52 ± 0.55	1.12 ± 0.56	0.68 ± 0.88	n.d.	1.80 ± 1.06	n.d.	1.48 ± 1.05
C15:1 (%)	1.45 ± 0.54	0.39 ± 0.13	0.74 ± 0.97	n.d.	1.54 ± 0.84	n.d.	1.33 ± 0.90
C15:1i (%)	3.76 ± 1.15	3.21 ± 0.91	2.23 ± 2.62	n.d.	6.28 ± 4.00	n.d.	4.78 ± 5.11
C16:0 (%)	14.27 ± 3.52	17.85 ± 5.36	15.32 ± 2.55	14.38 ± 4.77	18.00 ± 3.52	13.01 ± 3.27	22.73 ± 21.26
C16:1n7 (%)	22.51 ± 6.74	8.97 ± 2.93	10.78 ± 8.82	10.49 ± 6.32	19.21 ± 13.81	8.78 ± 3.47	15.56 ± 9.32
C16:1i (%)	14.70 ± 6.32	6.67 ± 3.07	12.48 ± 7.11	11.94 ± 4.83	8.15 ± 4.28	11.96 ± 3.95	8.22 ± 1.33
C17:0 (%)	1.12 ± 0.46	1.60 ± 0.02	2.01 ± 1.29	2.35 ± 0.61	1.52 ± 0.47	2.13 ± 0.73	1.37 ± 0.58
C17:1 (%)	3.68 ± 0.74	2.30 ± 1.51	1.35 ± 1.35	2.11 ± 0.81	2.42 ± 0.83	1.85 ± 0.16	2.30 ± 1.64
C17:1i (%)	0.94 ± 0.74	1.39 ± 0.84	0.48 ± 0.59	1.88 ± 0.53	0.95 ± 0.63	0.48 ± 0.46	1.02 ± 0.89
C18:0 (%)	2.83 ± 0.88	21.27 ± 20.29	13.75 ± 8.06	11.90 ± 1.34	10.75 ± 8.89	14.60 ± 3.55	6.90 ± 3.88
C18:1n9 (%)	19.74 ± 4.55	25.09 ± 12.55	30.01 ± 11.66	32.62 ± 9.17	13.56 ± 4.07	36.35 ± 4.53	22.10 ± 5.59
C18:2n6 (%)	3.82 ± 4.83	2.21 ± 0.57	3.47 ± 0.88	4.81 ± 4.16	3.00 ± 2.66	3.26 ± 0.53	3.37 ± 2.44
C19:0 (%)	0.53 ± 0.48	0.72 ± 0.15	1.43 ± 1.02	3.17 ± 1.54	0.82 ± 0.69	2.12 ± 0.90	0.85 ± 0.81
C20:0 (%)	0.33 ± 0.17	2.12 ± 1.94	0.25 ± 0.30	0.58 ± 0.68	0.79 ± 0.58	1.72 ± 1.16	0.61 ± 0.26
C20:1 (%)	0.81 ± 0.67	2.13 ± 1.80	0.85 ± 1.01	0.64 ± 0.78	0.64 ± 0.22	0.50 ± 0.79	1.52 ± 1.25
C22:0 (%)	0.21 ± 0.18	1.33 ± 0.20	0.43 ± 0.54	1.18 ± 1.42	1.32 ± 1.11	2.72 ± 1.01	0.48 ± 0.37
C22:1 (%)	0.36 ± 0.49	0.43 ± 0.37	0.12 ± 0.24	0.67 ± 0.79	n.d.	0.16 ± 0.36	0.20 ± 0.40
C24:0 (%)	0.61 ± 0.24	1.19 ± 1.21	n.d.	0.89 ± 1.77	1.06 ± 1.14	0.37 ± 0.83	0.39 ± 0.50

Table III.1 - The FAME content of the WEs that were extracted in the hexane wash expressed as an average (mean) percentage along with its associated standard deviation.

	AFRO	CHI	EU	JAP	MU	SPAN	THAI
C12:0 (%)	0.32 ± 0.46	n.d.	1.55 ± 3.09	n.d.	n.d.	n.d.	n.d.
C12:1 (%)	0.08 ± 0.11	n.d.	n.d.	n.d.	n.d.	n.d.	n.d.
C14:0 (%)	2.51 ± 0.36	0.24 ± 0.42	2.69 ± 3.13	n.d.	1.76 ± 1.19	0.68 ± 0.79	1.11 ± 0.37
C14:1i (%)	4.10 ± 0.71	0.50 ± 0.87	1.90 ± 1.29	n.d.	2.10 ± 1.30	0.54 ± 0.58	2.23 ± 1.55
C15:0 (%)	2.53 ± 0.13	0.54 ± 0.93	1.03 ± 0.92	n.d.	1.07 ± 0.87	0.41 ± 0.38	1.03 ± 0.71
C15:1 (%)	1.13 ± 0.19	0.09 ± 0.15	0.24 ± 0.19	n.d.	0.31 ± 0.26	0.18 ± 0.17	0.42 ± 0.31
C15:1i (%)	2.90 ± 0.28	1.03 ± 1.79	1.23 ± 1.07	n.d.	1.80 ± 1.50	0.52 ± 0.49	2.43 ± 1.79
C16:0 (%)	12.55 ± 0.39	11.76 ± 4.44	16.59 ± 6.79	7.99 ± 0.67	19.61 ± 4.88	11.87 ± 3.29	11.82 ± 1.33
C16:1n7 (%)	18.34 ± 4.73	5.70 ± 4.58	6.25 ± 4.72	3.13 ± 0.15	7.35 ± 6.64	3.51 ± 1.81	12.80 ± 6.10
C16:1i (%)	6.50 ± 1.41	4.77 ± 0.50	4.80 ± 3.60	2.24 ± 0.59	2.93 ± 1.55	1.67 ± 0.54	5.20 ± 1.17
C17:0 (%)	0.91 ± 0.08	1.39 ± 0.26	1.18 ± 0.54	1.16 ± 0.33	1.81 ± 0.74	1.00 ± 0.14	0.92 ± 0.23
C17:1 (%)	5.13 ± 0.42	2.81 ± 0.61	1.45 ± 1.18	2.38 ± 0.03	1.84 ± 1.83	1.45 ± 0.27	2.94 ± 1.35
C17:1i (%)	0.83 ± 0.04	2.23 ± 0.18	0.43 ± 0.44	2.21 ± 0.14	1.04 ± 1.10	0.57 ± 0.05	1.26 ± 0.67
C18:0 (%)	4.60 ± 0.77	13.14 ± 4.71	13.34 ± 8.10	9.09 ± 2.38	14.20 ± 9.12	11.59 ± 1.99	6.77 ± 2.44
C18:1n9 (%)	32.09 ± 4.18	40.75 ± 3.64	37.22 ± 8.04	53.63 ± 0.48	33.28 ± 3.05	54.66 ± 3.98	41.75 ± 10.16
C18:2n6 (%)	1.44 ± 0.75	3.62 ± 1.81	4.05 ± 2.11	6.35 ± 4.52	3.64 ± 0.63	4.60 ± 0.28	4.76 ± 2.51
C19:0 (%)	0.78 ± 0.14	1.22 ± 0.48	0.90 ± 0.34	1.08 ± 0.11	1.36 ± 1.07	0.87 ± 0.31	0.93 ± 0.78
C20:0 (%)	0.34 ± 0.07	1.27 ± 0.63	1.13 ± 0.99	1.02 ± 0.09	1.22 ± 0.71	1.10 ± 0.26	0.45 ± 0.23
C20:1 (%)	1.47 ± 0.17	3.15 ± 0.87	1.09 ± 0.26	3.86 ± 0.11	1.18 ± 0.88	1.58 ± 0.30	1.22 ± 0.51
C22:0 (%)	0.32 ± 0.02	1.54 ± 0.88	1.28 ± 0.99	1.48 ± 0.29	1.69 ± 0.89	1.29 ± 0.27	0.67 ± 0.54
C22:1 (%)	0.37 ± 0.06	1.79 ± 1.39	0.51 ± 1.02	2.39 ± 1.12	0.39 ± 0.41	0.09 ± 0.20	0.57 ± 0.69
C24:0 (%)	0.62 ± 0.13	2.44 ± 1.39	0.72 ± 0.75	1.98 ± 0.02	1.38 ± 0.90	1.85 ± 0.51	0.72 ± 0.32

Table III.2 - The FAME content of the FFAs that were extracted from the hair types in the hexane wash expressed as an average (mean) percentage along with its associated standard deviation.

	CHI 2	EU 1	MU	SPAN	THAI 1
C12:0 (%)	n.d.	3.09	0.21 ± 0.41	n.d.	n.d.
C12:1 (%)	n.d.	n.d.	0.22 ± 0.44	n.d.	n.d.
C14:0 (%)	n.d.	16.16	5.89 ± 4.57	3.05 ± 4.31	n.d.
C14:1i (%)	n.d.	1.90	3.55 ± 2.68	1.00 ± 1.42	n.d.
C15:0 (%)	n.d.	0.43	2.06 ± 1.50	0.14 ± 0.20	n.d.
C15:1 (%)	n.d.	n.d.	0.40 ± 0.43	n.d.	n.d.
C15:1i (%)	n.d.	n.d.	1.37 ± 1.42	n.d.	n.d.
C16:0 (%)	14.65	24.05	25.61 ± 3.83	25.03 ± 2.37	35.01
C16:1n7 (%)	3.32	1.96	8.30 ± 6.23	0.95 ± 0.45	1.37
C16:1i (%)	4.66	4.10	4.36 ± 0.61	11.90 ± 2.40	12.00
C17:0 (%)	1.82	0.69	1.70 ± 0.44	n.d.	n.d.
C17:1 (%)	1.03	0.37	1.65 ± 1.17	n.d.	n.d.
C17:1i (%)	0.89	n.d.	0.58 ± 0.48	n.d.	n.d.
C18:0 (%)	26.80	11.35	16.94 ± 7.48	17.52 ± 3.12	25.07
C18:1n9 (%)	30.85	27.79	19.13 ± 3.52	30.38 ± 0.97	19.99
C18:2n6 (%)	6.51	6.85	3.33 ± 2.91	6.65 ± 0.24	3.24
C19:0 (%)	1.44	1.26	0.93 ± 0.61	2.14 ± 0.50	1.95
C20:0 (%)	1.43	n.d.	0.98 ± 0.25	0.40 ± 0.57	1.34
C20:1 (%)	n.d.	n.d.	0.42 ± 0.29	0.82 ± 1.16	n.d.
C22:0 (%)	1.97	n.d.	0.80 ± 0.55	n.d.	n.d.
C22:1 (%)	2.67	n.d.	0.09 ± 0.18	n.d.	n.d.
C24:0 (%)	1.97	n.d.	1.31 ± 1.19	n.d.	n.d.

Table III.3 - The FAME content of the TAG that were extracted from the hair types in the hexane wash expressed as an average (mean) percentage along with its associated standard deviation.

	AFRO	CHI	EU	JAP	MU	SPAN	THAI
C12:0 (%)	0.59 ± 0.75	0.06 ± 0.10	4.71 ± 6.71	2.38 ± 2.51	3.96 ± 4.13	7.46 ± 2.40	n.d.
C12:1 (%)	1.86 ± 1.89	3.10 ± 3.01	5.55 ± 3.18	5.85 ± 4.61	11.24 ± 5.06	18.21 ± 4.16	0.40 ± 0.56
C14:0 (%)	3.38 ± 1.98	2.33 ± 0.90	5.54 ± 5.49	4.92 ± 3.10	5.83 ± 1.56	8.18 ± 1.07	3.51 ± 1.38
C14:1i (%)	7.28 ± 3.78	0.06 ± 0.10	10.93 ± 5.22	13.15 ± 5.59	15.76 ± 5.19	16.46 ± 2.98	8.38 ± 4.74
C15:0 (%)	2.49 ± 0.92	0.66 ± 0.06	0.59 ± 0.23	1.36 ± 0.51	1.13 ± 1.25	0.49 ± 0.37	0.95 ± 0.39
C15:1 (%)	3.86 ± 2.75	8.48 ± 4.87	9.10 ± 3.42	7.69 ± 6.68	10.48 ± 3.85	5.97 ± 0.25	4.97 ± 3.99
C15:1i (%)	1.88 ± 0.58	1.07 ± 0.21	0.23 ± 0.18	1.88 ± 0.84	1.15 ± 1.20	0.92 ± 0.95	2.45 ± 2.89
C16:0 (%)	15.88 ± 3.31	12.22 ± 2.21	12.93 ± 3.09	12.98 ± 1.45	10.82 ± 4.90	10.24 ± 1.64	14.88 ± 3.07
C16:1n7 (%)	12.04 ± 2.42	4.14 ± 0.74	1.74 ± 1.33	4.58 ± 1.96	5.24 ± 5.82	1.33 ± 0.61	5.58 ± 3.08
C16:1i (%)	0.88 ± 0.64	0.73 ± 1.19	0.38 ± 0.43	0.10 ± 0.12	0.28 ± 0.26	0.53 ± 0.52	0.17 ± 0.08
C17:0 (%)	1.02 ± 0.70	0.41 ± 0.18	0.36 ± 0.24	0.27 ± 0.03	0.35 ± 0.32	0.15 ± 0.07	0.46 ± 0.17
C17:1 (%)	2.10 ± 0.95	5.69 ± 4.35	2.45 ± 2.81	1.94 ± 1.37	5.26 ± 2.95	0.95 ± 0.92	2.95 ± 2.02
C17:1i (%)	6.99 ± 5.70	5.12 ± 1.42	6.61 ± 2.87	4.73 ± 1.55	3.08 ± 0.87	4.41 ± 1.16	6.82 ± 2.71
C18:0 (%)	22.68 ± 6.49	22.31 ± 7.26	17.42 ± 4.77	22.66 ± 4.45	11.67 ± 2.52	14.11 ± 0.97	24.72 ± 5.99
C18:1n9 (%)	1.48 ± 0.49	2.11 ± 1.53	3.26 ± 2.87	2.49 ± 1.14	1.30 ± 0.92	2.24 ± 0.65	2.54 ± 1.31
C18:2n6 (%)	4.05 ± 1.83	9.10 ± 3.26	6.70 ± 5.62	2.66 ± 1.79	8.52 ± 6.89	2.40 ± 1.19	5.30 ± 4.43
C19:0 (%)	0.91 ± 0.14	0.81 ± 0.57	1.85 ± 2.50	1.41 ± 0.91	0.41 ± 0.14	0.46 ± 0.07	2.58 ± 1.29
C20:0 (%)	1.34 ± 0.72	1.07 ± 0.54	0.74 ± 0.20	0.84 ± 0.40	0.68 ± 0.54	0.27 ± 0.13	1.17 ± 0.28
C20:1 (%)	2.49 ± 0.78	2.91 ± 1.40	4.13 ± 5.30	3.35 ± 2.70	0.73 ± 0.66	2.83 ± 4.06	5.25 ± 2.28
C22:0 (%)	1.83 ± 0.24	1.00 ± 0.15	0.94 ± 0.56	0.86 ± 0.43	0.43 ± 0.36	0.64 ± 0.13	1.82 ± 1.10
C22:1 (%)	1.99 ± 1.20	3.55 ± 2.44	1.17 ± 0.90	2.81 ± 3.35	0.76 ± 0.18	0.57 ± 0.35	2.51 ± 2.40
C24:0 (%)	2.95 ± 1.51	2.10 ± 0.46	2.57 ± 1.48	0.98 ± 0.57	0.94 ± 0.38	1.14 ± 0.31	2.57 ± 1.02

Table III.4 - The FAME content for the PL extracted in the solvent extraction process expressed as an average (mean) percentage of that lipid class by hair type along with its associated standard deviation.

	AFRO	CHI	EU	JAP	MU	SPAN	THAI
C12:0 (%)	0.11 ± 0.09	n.d.	2.41 ± 2.80	2.68 ± 3.29	7.89 ± 7.04	17.35 ± 2.83	1.65 ± 2.58
C12:1 (%)	0.67 ± 0.24	0.44 ± 0.18	0.03 ± 0.04	0.81 ± 0.38	0.86 ± 0.60	0.24 ± 0.02	0.72 ± 0.67
C14:0 (%)	5.31 ± 1.97	2.97 ± 1.38	6.94 ± 4.59	6.95 ± 4.56	13.19 ± 4.63	18.23 ± 1.29	5.42 ± 2.31
C14:1i (%)	4.84 ± 0.81	2.97 ± 0.25	1.30 ± 0.49	3.95 ± 0.57	2.26 ± 1.55	1.58 ± 0.33	3.55 ± 1.38
C15:0 (%)	4.39 ± 1.50	3.05 ± 1.16	1.87 ± 1.90	3.69 ± 1.72	3.02 ± 2.96	1.39 ± 0.10	2.50 ± 1.91
C15:1 (%)	1.32 ± 0.30	1.01 ± 0.14	0.36 ± 0.17	0.87 ± 0.24	0.44 ± 0.39	0.41 ± 0.07	0.96 ± 0.36
C15:1i (%)	3.86 ± 1.53	4.77 ± 0.42	1.43 ± 0.93	4.08 ± 0.44	2.20 ± 1.97	0.84 ± 0.11	3.10 ± 1.74
C16:0 (%)	19.17 ± 4.27	18.10 ± 6.20	21.88 ± 10.49	19.42 ± 8.17	21.76 ± 6.76	18.49 ± 1.46	14.62 ± 6.28
C16:1n7 (%)	18.37 ± 3.38	17.66 ± 2.89	6.93 ± 3.04	13.01 ± 3.81	6.83 ± 5.35	5.11 ± 0.62	14.64 ± 5.35
C16:1i (%)	5.52 ± 1.12	4.67 ± 0.91	2.23 ± 1.54	3.93 ± 0.47	2.52 ± 1.75	1.28 ± 0.23	4.03 ± 1.41
C17:0 (%)	1.12 ± 0.28	0.92 ± 0.34	0.82 ± 0.73	0.84 ± 0.43	0.76 ± 0.61	0.41 ± 0.04	0.60 ± 0.41
C17:1 (%)	3.23 ± 0.46	3.12 ± 0.39	1.29 ± 0.45	2.19 ± 0.57	1.23 ± 0.88	0.79 ± 0.12	2.33 ± 0.76
C17:1i (%)	0.94 ± 0.67	1.71 ± 0.37	0.38 ± 0.12	1.21 ± 0.45	0.62 ± 0.38	0.22 ± 0.03	0.79 ± 0.40
C18:0 (%)	3.76 ± 0.86	4.87 ± 1.47	8.11 ± 4.95	4.51 ± 1.67	5.35 ± 1.42	5.13 ± 0.58	3.49 ± 1.39
C18:1n9 (%)	21.75 ± 5.90	26.70 ± 4.43	35.48 ± 14.00	24.67 ± 8.26	24.71 ± 11.98	22.62 ± 2.36	33.66 ± 14.26
C18:2n6 (%)	2.40 ± 1.40	3.16 ± 1.29	4.95 ± 3.55	4.03 ± 3.76	3.91 ± 2.52	4.42 ± 1.46	5.62 ± 3.19
C19:0 (%)	0.34 ± 0.12	0.37 ± 0.05	0.25 ± 0.10	0.27 ± 0.10	0.20 ± 0.07	0.20 ± 0.11	0.17 ± 0.09
C20:0 (%)	0.42 ± 0.05	0.41 ± 0.12	0.49 ± 0.26	0.38 ± 0.09	0.39 ± 0.16	0.30 ± 0.05	0.23 ± 0.10
C20:1 (%)	0.97 ± 0.52	1.25 ± 0.27	1.09 ± 0.31	1.15 ± 0.52	0.73 ± 0.11	0.40 ± 0.07	0.90 ± 0.31
C22:0 (%)	0.31 ± 0.05	0.38 ± 0.11	0.43 ± 0.27	0.32 ± 0.08	0.33 ± 0.15	0.21 ± 0.04	0.18 ± 0.07
C22:1 (%)	0.38 ± 0.26	0.54 ± 0.48	0.73 ± 1.36	0.41 ± 0.25	0.24 ± 0.13	0.06 ± 0.03	0.38 ± 0.53
C24:0 (%)	0.81 ± 0.11	0.80 ± 0.18	0.61 ± 0.43	0.60 ± 0.08	0.58 ± 0.33	0.29 ± 0.07	0.32 ± 0.19

Table III.5 - The FAME content for the FFA extracted in the solvent extraction process expressed as an average (mean) percentage of that lipid class by hair type along with its associated standard deviation.

	AFRO	CHI	EU	JAP	MU	SPAN	THAI
C12:0 (%)	n.d.	n.d.	5.73 ± 9.72	0.17 ± 0.35	6.52 ± 6.46	18.78 ± 9.93	0.06 ± 0.11
C12:1 (%)	n.d.	n.d.	n.d.	n.d.	0.33 ± 0.37	n.d.	n.d.
C14:0 (%)	2.66 ± 1.12	0.57 ± 0.50	9.82 ± 9.53	1.72 ± 2.50	16.63 ± 9.49	19.33 ± 3.17	3.19 ± 6.11
C14:1i (%)	6.50 ± 3.69	0.23 ± 0.40	0.45 ± 0.33	0.20 ± 0.40	1.43 ± 1.08	0.58 ± 0.16	0.15 ± 0.30
C15:0 (%)	2.80 ± 0.70	1.44 ± 0.67	0.43 ± 0.59	0.58 ± 0.16	1.90 ± 1.98	0.29 ± 0.04	0.65 ± 0.42
C15:1 (%)	0.54 ± 0.29	0.59 ± 0.69	0.03 ± 0.04	0.06 ± 0.07	0.49 ± 0.53	0.06 ± 0.01	0.23 ± 0.29
C15:1i (%)	1.70 ± 0.58	1.10 ± 0.95	0.10 ± 0.12	0.80 ± 0.08	1.42 ± 1.36	0.20 ± 0.00	0.78 ± 0.78
C16:0 (%)	17.36 ± 2.65	19.98 ± 1.84	18.55 ± 5.20	16.81 ± 5.11	20.79 ± 4.55	16.39 ± 9.53	17.26 ± 5.60
C16:1n7 (%)	8.49 ± 3.17	7.15 ± 2.67	2.37 ± 2.33	2.51 ± 0.74	7.16 ± 6.75	4.48 ± 8.13	3.46 ± 1.88
C16:1i (%)	3.00 ± 0.52	2.52 ± 2.11	2.39 ± 2.34	2.20 ± 0.84	1.92 ± 1.57	0.41 ± 0.45	1.45 ± 1.87
C17:0 (%)	1.88 ± 0.35	1.20 ± 0.47	0.66 ± 0.65	0.74 ± 0.16	0.65 ± 0.53	1.19 ± 2.36	1.20 ± 0.66
C17:1 (%)	1.94 ± 0.58	1.56 ± 1.27	0.57 ± 0.74	0.81 ± 0.21	1.05 ± 0.96	0.17 ± 0.04	1.41 ± 0.78
C17:1i (%)	0.08 ± 0.19	0.19 ± 0.32	0.16 ± 0.23	0.47 ± 0.12	0.46 ± 0.35	0.07 ± 0.04	0.54 ± 0.64
C18:0 (%)	6.07 ± 1.69	15.32 ± 3.16	9.65 ± 1.28	12.61 ± 1.90	7.58 ± 1.46	8.53 ± 2.10	14.78 ± 5.72
C18:1n9 (%)	14.83 ± 3.23	29.93 ± 1.30	23.51 ± 5.55	36.86 ± 7.91	19.54 ± 7.56	21.33 ± 3.46	30.52 ± 4.55
C18:2n6 (%)	1.47 ± 0.80	4.34 ± 2.71	4.28 ± 2.36	6.24 ± 1.54	3.95 ± 3.11	5.21 ± 1.17	7.07 ± 4.84
C19:0 (%)	1.50 ± 1.06	4.90 ± 5.13	0.73 ± 0.43	0.91 ± 0.49	0.34 ± 0.26	0.54 ± 0.23	1.09 ± 0.69
C20:0 (%)	0.48 ± 0.33	0.20 ± 0.34	0.42 ± 0.31	0.87 ± 0.17	0.50 ± 0.17	0.43 ± 0.13	0.98 ± 0.20
C20:1 (%)	0.90 ± 0.62	1.43 ± 1.38	0.53 ± 0.48	1.62 ± 0.47	0.58 ± 0.27	0.57 ± 0.27	1.55 ± 1.45
C22:0 (%)	0.55 ± 0.77	0.59 ± 0.65	0.15 ± 0.18	1.19 ± 0.41	0.44 ± 0.17	0.46 ± 0.31	1.11 ± 0.49
C22:1 (%)	n.d.	1.19 ± 1.56	0.14 ± 0.27	1.09 ± 0.74	0.07 ± 0.04	0.10 ± 0.17	0.78 ± 1.43
C24:0 (%)	0.45 ± 1.01	0.85 ± 0.95	0.12 ± 0.14	0.99 ± 0.51	0.66 ± 0.43	0.21 ± 0.05	1.42 ± 0.71
C26:0 (%)	26.78 ± 8.30	4.72 ± 1.84	19.17 ± 21.17	10.53 ± 10.04	5.55 ± 3.34	0.54 ± 0.55	10.22 ± 8.38

Table III.6 - The FAME content for the TAG extracted in the solvent extraction process expressed as an average (mean) percentage of that lipid class by hair type along with its associated standard deviation.

	AFRO	CHI	EU	JAP	MU	SPAN	THAI
C12:0 (%)	n.d.	n.d.	1.49 ± 2.67	0.37 ± 0.44	1.05 ± 1.43	3.92 ± 1.94	0.20 ± 0.24
C12:1 (%)	0.19 ± 0.12	0.26 ± 0.23	0.51 ± 0.63	0.37 ± 0.45	0.58 ± 0.50	0.77 ± 0.34	0.29 ± 0.25
C14:0 (%)	2.14 ± 0.67	1.79 ± 0.09	4.09 ± 3.19	1.99 ± 1.01	5.35 ± 2.09	6.64 ± 0.56	2.47 ± 1.34
C14:1i (%)	3.62 ± 0.65	3.40 ± 0.72	3.18 ± 2.10	3.90 ± 1.98	5.66 ± 3.06	4.20 ± 0.63	4.10 ± 1.97
C15:0 (%)	2.66 ± 0.51	8.20 ± 10.42	1.21 ± 0.61	1.81 ± 0.44	1.89 ± 0.79	1.56 ± 0.10	1.74 ± 0.78
C15:1 (%)	1.34 ± 0.58	0.98 ± 0.09	0.82 ± 0.51	1.16 ± 0.63	1.90 ± 1.13	1.45 ± 0.08	1.11 ± 0.50
C15:1i (%)	3.68 ± 0.99	5.03 ± 1.50	3.75 ± 1.98	8.25 ± 1.98	6.84 ± 3.45	3.78 ± 1.02	5.18 ± 3.76
C16:0 (%)	14.33 ± 5.29	15.92 ± 3.76	17.00 ± 2.37	14.88 ± 1.17	13.98 ± 4.01	15.13 ± 0.75	13.35 ± 2.35
C16:1n7 (%)	20.22 ± 6.71	13.59 ± 0.61	12.92 ± 7.26	18.69 ± 5.76	19.94 ± 9.46	13.89 ± 0.76	17.24 ± 5.62
C16:1i (%)	18.44 ± 4.89	5.63 ± 3.74	6.68 ± 3.76	5.90 ± 1.68	7.66 ± 2.53	4.06 ± 2.01	7.50 ± 2.69
C17:0 (%)	1.25 ± 0.72	1.26 ± 0.44	0.81 ± 0.15	0.98 ± 0.22	0.85 ± 0.28	0.71 ± 0.08	0.73 ± 0.08
C17:1 (%)	3.25 ± 0.61	2.11 ± 0.47	1.55 ± 1.05	2.35 ± 0.68	2.23 ± 0.84	1.84 ± 0.20	2.20 ± 0.39
C17:1i (%)	0.81 ± 0.42	1.26 ± 0.17	0.60 ± 0.32	1.59 ± 0.23	0.82 ± 0.13	0.69 ± 0.13	1.16 ± 0.82
C18:0 (%)	3.13 ± 2.00	6.03 ± 2.28	8.01 ± 3.98	4.64 ± 1.00	4.63 ± 3.74	6.19 ± 0.47	4.87 ± 3.04
C18:1n9 (%)	16.26 ± 2.57	23.77 ± 6.57	30.57 ± 10.42	25.46 ± 7.35	17.76 ± 9.94	29.35 ± 1.67	28.43 ± 9.55
C18:2n6 (%)	5.63 ± 7.74	2.15 ± 1.39	3.17 ± 1.53	4.42 ± 4.18	4.24 ± 2.44	2.60 ± 0.54	5.38 ± 2.15
C19:0 (%)	0.23 ± 0.14	0.25 ± 0.10	0.29 ± 0.05	0.49 ± 0.41	0.34 ± 0.30	0.42 ± 0.13	0.37 ± 0.17
C20:0 (%)	0.47 ± 0.42	0.93 ± 0.74	0.40 ± 0.11	0.48 ± 0.08	0.44 ± 0.46	0.54 ± 0.04	0.75 ± 0.30
C20:1 (%)	0.76 ± 0.72	4.81 ± 3.50	0.69 ± 0.23	0.56 ± 0.38	2.30 ± 3.71	0.46 ± 0.08	0.82 ± 0.31
C22:0 (%)	0.27 ± 0.20	0.49 ± 0.11	0.40 ± 0.14	0.39 ± 0.31	0.54 ± 0.47	0.60 ± 0.05	0.55 ± 0.33
C22:1 (%)	0.12 ± 0.11	0.90 ± 1.31	0.20 ± 0.24	0.35 ± 0.24	0.27 ± 0.32	0.20 ± 0.11	0.44 ± 0.58
C24:0 (%)	1.12 ± 1.09	1.19 ± 0.17	0.29 ± 0.33	0.56 ± 0.41	0.65 ± 0.61	0.87 ± 0.08	0.84 ± 0.42
C26:0 (%)	n.d.		1.29 ± 2.57	0.36 ± 0.73	n.d.	n.d.	0.28 ± 0.33

Table III.7 - The FAME content for the WE extracted in the solvent extraction process expressed as an average (mean) percentage of that lipid class by hair type along with its associated standard deviation.

	AFRO	CHI	EU	JAP	MU	SPAN	THAI
C12:0 (%)	0.87 ± 0.89	1.41 ± 1.23	1.74 ± 2.66	0.97 ± 1.46	5.59 ± 6.94	3.55 ± 3.71	1.23 ± 1.87
C14:0 (%)	5.79 ± 1.12	5.93 ± 3.64	10.76 ± 8.89	5.55 ± 3.75	17.08 ± 9.05	13.70 ± 7.14	9.93 ± 6.28
C14:1 (%)	5.36 ± 2.22	4.83 ± 2.12	1.34 ± 0.89	2.28 ± 0.70	2.32 ± 1.29	1.46 ± 0.18	2.38 ± 0.76
C15:0 (%)	4.55 ± 1.25	3.83 ± 2.50	2.04 ± 1.78	3.85 ± 2.33	3.87 ± 3.46	1.63 ± 0.66	4.38 ± 2.44
C15:1 (%)	3.34 ± 1.18	3.17 ± 0.95	1.30 ± 0.83	2.48 ± 0.53	1.92 ± 1.81	0.84 ± 0.25	1.95 ± 1.24
C16:0 (%)	23.41 ± 4.26	30.04 ± 8.83	33.45 ± 5.92	31.29 ± 8.31	35.28 ± 2.93	27.13 ± 8.88	37.11 ± 4.41
C16:1n7 (%)	12.36 ± 4.92	6.19 ± 1.86	2.61 ± 2.13	5.21 ± 0.87	3.95 ± 3.40	2.21 ± 0.29	4.56 ± 2.57
C16:1i (%)	4.30 ± 1.25	2.10 ± 0.62	1.98 ± 1.26	1.83 ± 0.05	1.72 ± 1.29	1.36 ± 0.21	2.08 ± 0.95
C17:0 (%)	1.91 ± 0.42	1.51 ± 0.49	1.30 ± 0.69	1.48 ± 1.08	1.21 ± 0.78	0.96 ± 0.29	1.59 ± 0.68
C17:1 (%)	1.89 ± 0.62	0.90 ± 0.32	0.38 ± 0.29	0.87 ± 0.07	0.60 ± 0.55	0.53 ± 0.12	0.68 ± 0.42
C18:0 (%)	6.62 ± 2.97	8.44 ± 0.91	12.22 ± 1.66	9.40 ± 2.73	8.89 ± 1.56	10.30 ± 1.05	10.78 ± 0.68
C18:1n9 (%)	12.60 ± 2.07	15.08 ± 8.63	15.77 ± 8.00	18.37 ± 10.84	8.55 ± 2.98	15.30 ± 1.78	11.95 ± 3.42
C18:2n6 (%)	1.97 ± 2.97	2.71 ± 3.25	1.97 ± 1.15	2.99 ± 3.59	1.41 ± 0.97	7.06 ± 10.67	2.00 ± 1.14
C19:0 (%)	0.81 ± 0.21	0.63 ± 0.27	0.62 ± 0.30	0.59 ± 0.16	0.36 ± 0.19	0.90 ± 0.93	0.43 ± 0.13
C20:0 (%)	1.55 ± 0.68	1.42 ± 0.66	1.54 ± 0.50	1.52 ± 0.34	0.90 ± 0.34	1.52 ± 0.41	1.15 ± 0.08
C20:1 (%)	1.91 ± 2.33	1.32 ± 0.89	1.42 ± 0.85	2.24 ± 1.89	0.88 ± 0.64	4.20 ± 6.68	0.89 ± 0.52
C21A (%)	6.39 ± 3.77	6.50 ± 4.53	6.20 ± 5.18	3.88 ± 1.16	1.97 ± 0.81	4.71 ± 2.89	2.89 ± 1.06
C22:0 (%)	1.40 ± 0.39	0.99 ± 0.45	1.18 ± 0.30	1.25 ± 0.29	0.66 ± 0.28	1.00 ± 0.27	1.01 ± 0.15
C22:1 (%)	1.31 ± 0.93	1.21 ± 1.33	0.57 ± 0.80	1.06 ± 0.62	0.31 ± 0.22	0.44 ± 0.22	0.62 ± 0.54
C24:0 (%)	1.03 ± 0.37	0.98 ± 0.36	1.26 ± 0.84	1.51 ± 0.53	0.88 ± 0.48	0.81 ± 0.17	1.22 ± 0.37

Table III.8 - The mean content of the FAME extracted from the hydrolysed fraction expressed as an average (mean) percentage along with its associated standard deviation.